Assessing the heterogeneous source of the Azores mantle plume

by

BSc, MSc Felix S. Genske

Australian Research Council Centre of Excellence for Core to Crust Fluid Systems/GEMOC, Department of Earth and Planetary Sciences, Faculty of Science, Macquarie University Sydney, Australia

GeoZentrum Nordbayern, Friedrich-Alexander-Universität Erlangen-Nürnberg, Schlossgarten 5, 91054 Erlangen, Germany

This thesis is presented for fulfilment of the degree of Doctor of Philosophy,

August 2012

TABLE OF CONTENT

ABSTRACT

The Azores islands in the central North-Atlantic are the subaerial parts of a large oceanic plateau that is best explained by the presence of a mantle plume that arrived in the vicinity of the Mid-Atlantic ridge (MAR) some 40 Ma ago. Recent volcanic activity either side of the MAR implies that this plume is still feeding volcanism on the islands today. Much work has therefore focused on the nature of the magmatism on both the islands and the MAR. Significant geochemical heterogeneity is observed in the ocean islands basalts (OIB) from the eastern islands implying similar heterogeneity in the plume itself. However, there has, to date, been little information available from the islands situated to the west of the MAR.

This thesis has two foci and associated aims. The first encompasses the petrology and geochemistry of lavas from the western Azores islands of Flores and Corvo and forms the basis of the second chapter. Subsequently, the data obtained from these islands is incorporated with published data from the eastern islands and MAR into a broader assessment of the mantle source composition across the plateau. This second focus encompasses perspectives from both radiogenic and stable isotopes. Across plateau variations of Sr-Nd-Hf-Pb-Os and B-O-Li isotope ratios are assessed. Chapter three reveals important clues for the characterization of the mantle source of OIB from oxygen isotopes from olivine phenocrysts. In chapter four, the light elements lithium and boron and their isotopic composition are investigated in primitive lavas that are otherwise well characterized. The processes of assimilation fractional crystallization (AFC) show to be important in accounting for the variability that is observed on each island. Stripping-off these effects is crucial for characterization of the primary mantle signal of these OIB. Chapter five combines this information with Hf-Pb-Os isotopes and trace-element variations across the plateau. Evidence for melting of carbonated peridotite on Santa Maria Island, which is the eastern most island on the plateau, is presented in the final chapter six. The distribution and characterization of distinct sources beneath the Azores plateau conforms to a geodynamic scenario of a slow upwelling plume that most likely entrained Archaean oceanic lithosphere, yet the true dimensions of the plume and the relative contributions of recycled components remains complex.

ABSTRACT (DEUTSCH)

Die Inselgruppe der Azoren im Nordatlantik repräsentieren den subaerischen Teil eines großen ozeanischen Plateaus dessen Entstehung am besten durch einen Mantel Plume erklärt werden kann. Dieser Plume erreichte die Erdoberflaeche vermutlich vor bereits 40 Ma und wurde erstmals am Mittelantlatischen Rücken (MAR) beobachtet. Rezente vulkanische Aktivität zu beiden Seiten des MAR bezeugt, dass dieser Plume auch heute noch den Vulkanismus der Inseln fördert. Daher haben sich viele geochemische Studien auf die Gründe und Herkunft des hier auftretenden Magmatismus konzentriert. Hierbei ist eine signifikante geochemische Heterogenität in den Ozean Insel Basalten (OIB) der östlichen Inseln beobachtbar, die direkt auf den Plume zurückgeführt werden kann. Allerdings gibt es hierzu relativ wenige Informationen von den einzigen zwei Inseln westlich des MAR, Flores und Corvo.

Diese These konzentriert sich auf zwei Aspekte. Der erste umfasst die Petrologie und Geochemie der Laven von Flores und Corvo und bildet die Basis des zweiten Kapitels. Folglich werden die hier neu ermittelten Daten mit bereits verfügbaren Daten der östlichen Inseln und des MAR kombiniert, um neue Schlussfolgerungen über den Azoren Plume und seiner Quellen zu ermöglichen. Der zweite Kernaspekt fokussiert daher Perspektiven, die durch radiogene und stabile Isotopendaten möglich sind. Variationen der Sr-Nd-Hf-Pb-Os und B-O-Li Isotopensysteme entlang eines west-ost-gerichteten Transekts können hierbei ausgwertet werden. Kapitel drei dieser Arbeit zeigt mit Hilfe von Sauerstoffisotopen auf, dass Assimilationsprozesse wichtig sind um korrekte Aussagen über die Mantelquellensignatur zu treffen. Im vierten Kapitel wird dies anhand von Lithium und Bor Isotopendaten verdeutlicht. Kapitel fünf kombiniert dann diese Information mit Hf-Pb-Os Isotopen- und Spurenelementdaten in der Betrachtung der Unterschiedlichen Azoren Mantelquellen. Im finalen Kapitel sechs wird erstmals in den Azoren das Schmelzen eines karbonatisierten Peridotits auf der Insel Santa Maria nachgewiesen.

Die Verteilung und Charakerisierung unterschiedlicher Quellen unter dem Azoren Plateau bestätigt das geodynamisches Szenario eines langsam aufsteigenden Plumes der sehr wahrscheinlich archaische Ozeanlithosphäre mit sich führt, allerdings bleiben die tatsächlichen Dimensionen dieses Plumes sowie die relativen Anteile recycelter Komponenten weiterhin komplex und daher schwer zu bestimmen.

STATEMENT OF CANDIDATE

I certify that the work in this thesis entitled "**Assessing the heterogeneous source of the Azores mantle plume**" has not previously been submitted for a degree nor has it been submitted as part of requirements for a degree to any other university or institution other than Macquarie University and the Friedrich-Alexander-University Erlangen-Nürnberg and is presented here under a cotutelle agreement between these two Universities.

I also certify that the thesis is an original piece of research and it has been written by me. Any help and assistance that I have received in my research work and the preparation of the thesis itself have been appropriately acknowledged.

In addition, I certify that all information sources and literature used are indicated in the thesis.

This thesis contains material that has been published, accepted, submitted or prepared for publication, as follows:

Chapter 2

Genske, F.S., Turner, S.P., Beier, C., Schaefer, B.F., 2012. The Petrology and Geochemistry of Lavas from the Western Azores Islands of Flores and Corvo. *Journal of Petrology* 53, 1673–1708.

My contribution to the research and paper: Concept - 85%; Data collection - 95%; Analysis - 95%; Writing - 85%; Total - 90%

Chapter 3

Genske, F.S., Beier, C., Haase, K.M., Turner,S.P., Krumm, S., Brandl, P.A.. Oxygen isotopes in the Azores islands: Crustal assimilation recorded in olivine. (*Geology*, doi: 10.1130/G33911.1)

My contribution to the research and paper: Concept - 95%; Data collection - 85%; Analysis - 95%; Writing - 90%; Total - 90%

Chapter 4

Genske, F.S., Turner, S.P., Beier, C., Chu, M.-F., Tonarini, S., Pearson, N.J., Haase, K.M. (submitted to *Chemical Geology*). Lithium and boron isotopic constraints on the source of magmas in the Azores islands

My contribution to the research and paper: Concept - 85%; Data collection - 75%; Analysis - 95%; Writing - 90%; Total - 85%

Chapter 5

Genske, F.S., Turner, S.P., Beier, C., Haase, K.M., Pearson, N.J., Schaefer, B.F, Hauff, F. (presented at the Goldschmidt conference, Florence, Italy, 2013 and to be submitted to *Earth and Planetary Science Letters*). Constraining the nature of the western Azores mantle source using Pb-Hf-Os isotope systematics and high field strength elements

My contribution to the research and paper: Concept - 80%; Data collection - 75%; Analysis - 85%; Writing - 90%; Total - 85%

Chapter 6

Beier, C., Mata, J., Stöckhert, F., Mattielli, N., Brandl, P.A., Madureira, P., Genske, F.S., Martins, S., Madeira, J., Haase, K.M. Geochemical evidence for melting of carbonated peridotite on Santa Maria Island, Azores. (*Contributions to Mineralogy and Petrology*)

My contribution to the research and paper: Concept - 10%; Data collection - 0%; Analysis - 5%; Writing - 15%; Total - 15%

Felix S. Genske MQ Student ID: 41256603

20.08.2012

ACKNOWLEDGEMENTS

First and foremost I want to thank all of my supervisors, Simon Turner, Christoph Beier, Bruce Schaefer and Karsten Haase who have supported me throughout this thesis, and made the printed piece of work possible after all.

Second, I want to thank all of the people that have accompanied me along this very exciting path. There are many colleagues, friends and family members that have supported me in so many ways.

Especially though I would like to express special thanks to Norm Pearson and Peter Wieland who *always* lend an ear and who taught me so many aspects of analytical geochemistry. Mei-Fei Chu is highly appreciated for her patience while teaching me everything I now know about Li isotope analytics.

Dick Flood is thanked for his continued interest in my work and my well being.

This thesis is decicated to K, K and L!

I also acknowledge the support from Macquarie University in form of a scholarship. The Australian Research Council and Deutsche Forschungs Gemeinschaft provided funding that was essential for carying out this research.

CHAPTER 1: INTRODUCTION AND EXPOSITION

1.1. OCEAN ISLAND BASALTS AND MANTLE PLUMES

Ocean Island Basalts (OIB) provide important information on mantle convection and recycling of crustal material (Gast et al., 1964; Hofmann, 1997). The presence of OIB have generally been linked to the presence of dominantly thermally induced melting ("hotspots", *cf.* (Ritsema and Allen, 2003; Montelli et al., 2004)), but heterogeneity, in the location of the mantle solidus due to the presence of enriched, volatile-rich material has also been discussed (e.g. "wetspot" (Bonatti, 1990)). Heterogeneous thermochemical piles have been proposed to result from a combination of subduction related effects (e.g. (Farnetani and Samuel, 2005; Sobolev et al., 2005)). Fluid dynamic models suggest that most mantle plumes will be radially symmetric (White et al., 1979; 1979; Campbell, 1990; 1990; Shorttle et al., 2010; 2010). For example, radiogenic isotopes from the Galápagos OIB exhibit a horseshoe shaped pattern thought to reflect a cross-section through a toroid plume head that is enfolding shallow mantle material (White et al., 1993). The chemical and physical perspectives of mantle plumes in general are nicely summarized in recent reviews by White (2010) and Campbell (2007). However, plumes that similarly rise close to Mid-Ocean Ridges (MOR), or OIB near ridges in general, appear even more complex.

Chain	Location	Oceanic crust age	Youngest volcanism	Oldest volcanism	Flux (Mg s^{-1})	Seismic depth[3] (km)	Large igneous province
Azores	38° N 28° W	0 Ma	0 Ma	36 Ma[4]	1.1[1]	2800	Azores Plateau?
Galapagos	1° S 92° W	5 Ma	0 Ma	~ 100 Ma[5]	1[1]	≤ 1000	Caribbean[6]
Hawaii	19° N 155° W	93 Ma	0 Ma	> 80 Ma	8.7[1] 6.2[2]	≥ 2350	?
Iceland	65° N 10° W	0 Ma	0 Ma	61 Ma	1.4[1]	≤ 1000	North Atlantic Tertiary
Samoa	15° S 168° W	100 Ma	0 Ma	24 Ma[7]	1.6[1]	~ 2800	No

[1]Sleep (1990). [2]Davies (1988). [3]Montelli et al. (2004). [4]Cannat et al. (1999). [5]Courtillot et al. (2003). [6]Duncan & Hargraves (1984). [7]Hart et al. (2004).

Table 1: Modified after White (2010), summarising key parameters of selected ocean island chains thought to be generated by mantle plumes.

Volcanic systems on young intraplate ocean islands have been widely studied to gain insights into the composition of the upper, and possibly lower, mantle and therefore into the recycling of lithosphere-derived components (*cf.* Fig. 1). Some of the best-studied OIB include those from Hawaii (e.g. (Macdonald, 1968; Clague, 1987; Watson and McKenzie, 1991; Sobolev et al., 2007; Wang and Eiler, 2008)), Iceland (e.g. (Chen and Frey, 1983; Eiler et al., 2000; Gudmundsson, 2000; Skovgaard et al., 2001; Kokfelt et al., 2003; Thirlwall et al., 2004; Kokfelt et al., 2006)) and Samoa (e.g. (Johnson et al., 1986; Wright and White, 1987; Farley et al., 1992; Hart et al., 2004; Workman et al., 2004; Koppers et al., 2008)).

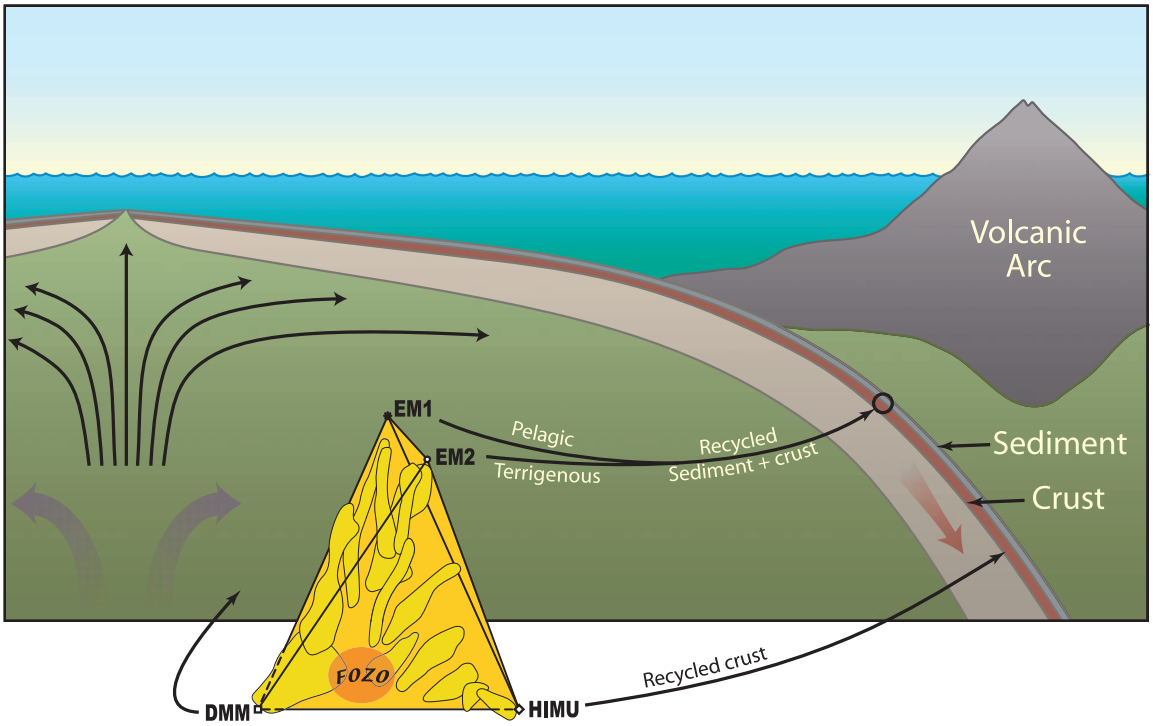

Fig. 1: Taken from (Workman et al., 2004), showing the Standard Model describing distinct mantle components and their origin based on defined isotopic compositions. Major inputs to the model are from (Armstrong, 1968; Chase, 1981; Cohen and O'Nions, 1982; Hofmann and White, 1982; Zindler and Hart, 1986; Weaver, 1991; Hart et al., 1992). Recent studies by Stracke and Hart (2005) and Willbold and Stracke (2006) review and further refined this model in terms of radiogenic isotope and trace element compositions.

Clague (1987) reviewed Hawaiian alkaline volcanism and he indicated that the erupted lavas were generated from a heterogeneous mantle source, based on trace-element and radiogenic isotope data. It has been proposed that this source consists of at least three distinct components. Subsequent studies aimed at defining these components, not only in Hawaii, but also in numerous other OIB settings. Recently however it was shown for the

Hawaiian mantle plume that it is distinctly chemically zoned (Xu et al., 2005; Huang et al., 2011; Weis et al., 2011), based on the differences observed between the Kea trend in the north and Loi trend in the south. Chemical zoning may be a common feature for mantle plumes, as this is also observed in the Galapagos plume (e.g. White et al., 1993; Hoernle et al., 2000) and Marquesas (e.g. Chauvel et al., 2012). The rapidly increasing amount of data from geochemical studies eventually lead to what is referred to be the mantle zoo. The following paragraph will now provide links between the mantle zoo and associated OIB.

Hart (1992) described the mantle end members to directly reflect recycled lithospheric components that were delivered to the mantle via subduction. The definition of the various species of the mantle zoo mainly focused on the radiogenic isotope composition of OIB, and these were recently redefined by Stracke et al. (2005) using a compilation of global OIB and MORB data (Fig. 2). Willbold and Stracke (2006) redefined the trace-element characteristics of mantle end members, allowing for more precise constraints on the nature of the different mantle reservoirs. A subsequent study by Jackson and Dasgupta (2008) assigned distinct major element characteristics to the HIMU, EM1 and EM2 end members, based on the relationships observed between major elements and isotope data. This study accordingly examined the different lithological characteristics of mantle end members.

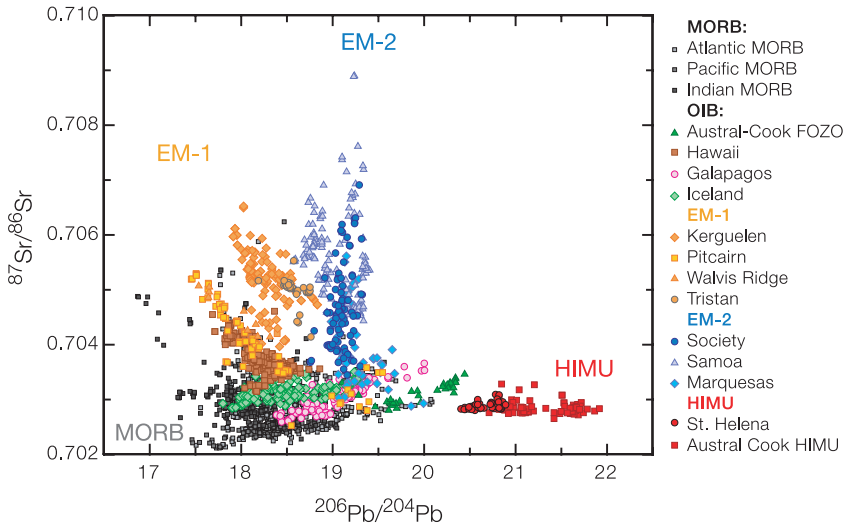

Fig. 2: Taken from Willbold and Stracke (2006). Variation trends in Sr-Pb space of lavas from MORB and global OIB settings, defining distinct mantle end member compositions. Data were originally compiled in Stracke et al. (2003).

HIMU-type mantle is most strongly identified in lavas from the Cook Austral chain volcanics (e.g. (Chauvel et al., 1997; Lassiter et al., 2003; 2008; Chan et al., 2009; Parai et al., 2009) or from St. Helena (e.g. (Weaver et al., 1987; Willbold and Stracke, 2006)). HIMU stands for „high-μ" with μ being defined as $\mu = (^{238}U/^{204}Pb)_{t=0}$. The origin of the HIMU signature however has been greatly debated. Recycled oceanic crust (e.g. (Hofmann and White, 1982; Chauvel et al., 1992; Hauri and Hart, 1993; Schiano et al., 2001)) or mantle metasomatism (e.g. (Nakamura and Tatsumoto, 1988; Halliday et al., 1995)) could both explain chemical characteristics of the HIMU mantle.

In contrast, the enriched mantle end members EM1 and EM2 are widely believed to carry signatures of recycled pelagic and terrigenous sediments, respectively (Fig. 1). The Kerguelen (e.g. (Gautier et al., 1990; Weis et al., 1993; Frey, 2002)) and Pitcairn (e.g. (Woodhead and Devey, 1993; Eisele et al., 2002; Saal et al., 2005)) hotspot lavas, for example, reflect the EM1 mantle. However, there has been much discussion about the amount of subducted sediment that is involved in generating their observed trace-element and (stable) isotope characteristics (e.g. (Eiler et al., 1995; Eisele et al., 2002)).

The lavas from Samoa (e.g. (Wright and White, 1987; Farley et al., 1992; Workman et al., 2004)) or the Society islands (e.g. (Hémond et al., 1994)) are classic examples for EM2 mantle. The presence of recycled sediments in the source of this end member was mainly derived from Sr-Nd-Pb isotope ratios, and further supported by O isotopes (Eiler et al., 1997) yet again, the origin of the terrigenous-indicative chemical signal remain a matter of debate (e.g. (Jackson et al., 2007; Koppers et al., 2008) and (Workman et al., 2004)).

In addition to the end-members described above there remain two reservoirs that are thought to be common to (almost) all OIB. The first is called FOZO (i.e. focal zone) - and similar to "C" (Hofmann and White, 1982; Chauvel et al., 1992; Hauri and Hart, 1993; Hanan and Graham, 1996; Schiano et al., 2001) - and was first defined by Hart and co-workers (1992). The ubiquitous presence and distinct composition of the FOZO reservoir has lead Stracke et al. (2005), who also redefined this end member, to conclude that the isotopic arrays, which it forms with the MORB reservoir, are most simply explained by normal mantle melting and continuous subduction (and subsequent aging) of the crust.

The second reservoir common to (most) OIB and MORB is the depleted (MORB) mantle (i.e. DMM). Its nature has been studied intensively in MORB settings due to its global

presence (e.g. (Saunders et al., 1988; White, 1993; Michael, 1995; Rudnick, 2000; Weyer et al., 2003; Workman and Hart, 2005; Cooper et al., 2009)). However, small-scale studies at individual locations have also shown that the depleted mantle may indeed carry signatures indicating enrichment from various sources. A most recent study, describing processes involved in E-MORB generation in more detail, is given by Ulrich et al. (2012).

In the following section an introduction to the Azores islands in the context of the Azores mantle plume will summarize studies dealing with the generation of this intraplate volcanism.

1.2. THE AZORES ISLANDS

Early geological studies on the Azores islands date back to the beginning of the last century (e.g. (Esenwein, 1929; Acostinho, 1936)), prior to the plate tectonic theory and subsequent debates on mantle plumes and the role of recycled components in the mantle. Since then there have been major advances both theoretically and analytically. Due to the remoteness of the Azores islands (as is the case for most OIB), advances in our understanding of the generation of these islands may sometimes be hindered simply because no samples are accessible for chemical and/or physical studies. In the Azores, this has been especially true for the islands of Flores and Corvo, where only limited sample sets (i.e. (White, 1977) and (França, Lago, et al., 2006)) for geochemical studies were available. Thus, one major aim for undertaking this thesis was to collect and study new samples from these two islands in order to complement the available data sets from the eastern side of the Azores plateau.

The submarine Azores plateau in the central North-Atlantic ocean sits astride the Mid-Atlantic Ridge (MAR) for about 300 km from 37°30’ and 40°00’ N and extends 700 km from its south-eastern to its north-western edge (Fig. 3). The ultraslow spreading Terceira axis (Searle, 1980; Vogt & Jung, 2004) is situated at on eastern plateau and strikes in a NW-SE direction towards the Mid-Atlantic Ridge. A total of nine volcanic islands emerge from this plateau. There are three islands (Graciosa, Terceira, and São Miguel) directly located on the Terceira axis (Fig. 4), which indicates the importance of the spreading movement for magma generation (Beier et al., 2008). The islands of Faial, Pico and São Jorge are elongated and align parallel just south of the Terceira rift axis (Fig. 3). The islands of Flores and Corvo are the only two volcanic edifices west of the MAR, but

a subsided island ~50 km west of Flores has been reported (Ryall et al., 1983). In contrast to the eastern islands, which are dominated by NW-SE-striking structures, the two western islands lie on a NNE-SSW-trending ridge that is subparallel to the MAR (Fig. 3).

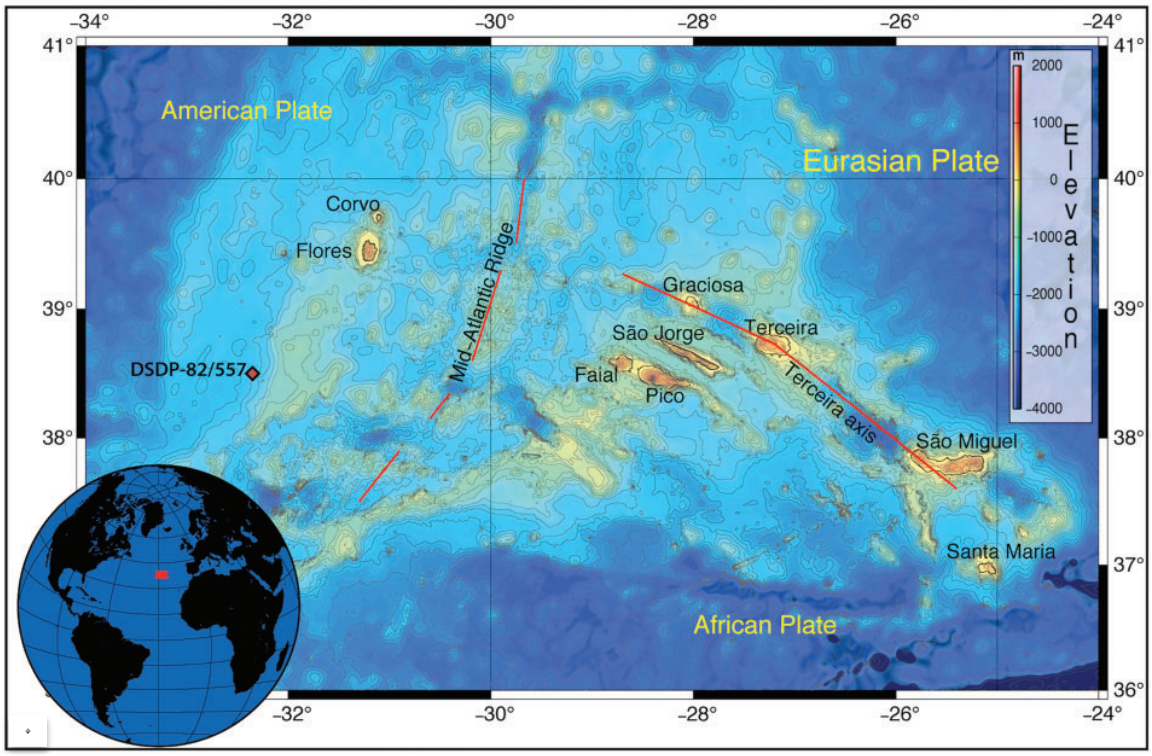

Fig. 3: From Genske et al. (2012). Bathymetric map showing the location of the Azores archipelago in the central North-Atlantic, as well as the two spreading axes of the MAR and the Terceira Rift.

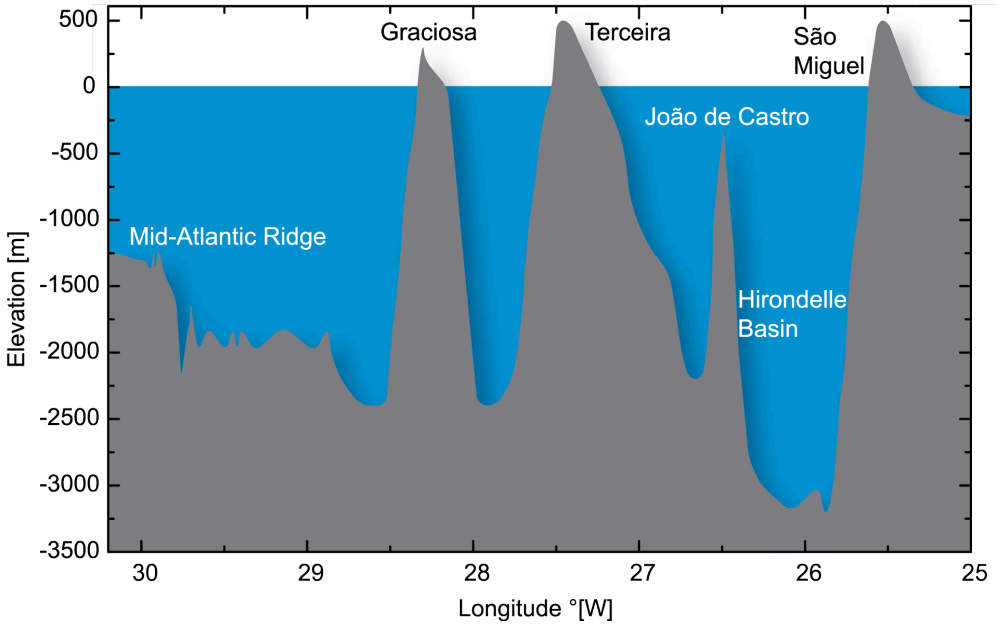

Fig. 4: Schematic cross section along the Terceira Rift axis, taken from Beier et al. (2008).

The island of Santa Maria is located at the easternmost edge of the Azores plateau where most published works have focused on the occurrence of fossiliferous sediments and carbonates (e.g. (Madeira et al., 2007)).

Geodynamically, the Azores plateau reflects the surface expression of a low buoyancy flux mantle plume (Sleep, 1990) which is characterised by a slow upwelling rate of ~3-4 cm a^{-1} (Sleep, 1990; Bourdon et al., 2005). However, numerous workers have emphasized the potential that lies in these nine islands and the nearby Mid-Atlantic Ridge (MAR) to study the dynamics associated with plume-ridge interaction (e.g. Bourdon et al., 1996; Gente et al., 2003; Madureira et al., 2005; Shorttle et al., 2010). Additionally, the Azores basalts may provide evidence for the recycling of ancient, perhaps even Archaean, lithosphere (Schaefer et al., 2002; Turner et al., 2007). The MORB along the adjacent Mid-Atlantic Ridge (MAR) have trace element and isotopic signatures believed to reflect an enriched mantle plume (e.g. (Schilling, 1975)). This section of the MAR is also the place where Bonatti (1990) and more recently Dixon et al. (2002) suggested wetspots (in contrast to hotspots) in the mantle.

Current models for the Azores mantle plume are based mainly on interpretations arising from geochemical and geophysical studies of the islands to the east of the Mid-Atlantic Ridge (e.g. (Abdel-Monem et al., 1975; Flower et al., 1976; White et al., 1979; Dupré et al., 1982; Madeira and Ribeiro, 1990; Turner et al., 1997; Claude-Ivanaj et al., 2001; Haase and Beier, 2003; França, Tassinari, et al., 2006; Beier et al., 2008; Millet et al., 2009; Prytulak and Elliott, 2009; Beier et al., 2010) and the nearby MAR (e.g. (Abdel-Monem et al., 1975; Flower et al., 1976; White et al., 1979; Dupré et al., 1982; Madeira and Ribeiro, 1990; Kingsley and Schilling, 1995; Bourdon et al., 1996; Turner et al., 1997; Yu et al., 1997; Cannat et al., 1999; Charlou et al., 2000; Claude-Ivanaj et al., 2001; Haase and Beier, 2003; França, Tassinari, et al., 2006; Beier et al., 2008; Millet et al., 2009; Prytulak and Elliott, 2009; Beier et al., 2010). The plume has been imaged to depths greater than ~ 240 km by seismic tomography (Montelli et al., 2004) and is suggested to be centred either to the NE of the island of Terceira (Moreira et al., 1999) or potentially in the vicinity of the island of Faial (Cannat et al., 1999; Shorttle et al., 2010), but in either case on the eastern plateau, 150-200 km away from the MAR.

Even though there have been great advances over the years in deciphering the nature of the Azores mantle plume, there still remain discrepancies between models that may not

easily be resolved. For example, early studies by Shirey et al. (1987) and Hawkesworth et al. (1979) claimed that lavas in the Azores region show evidence for recycled sediments to the mantle source, thus making the islands examples of EM2 (see above). Their arguments are mainly based on distinct neodymium-strontium-lead isotope arrays, however in terms of the islands this has been demonstrated only for São Miguel, hence Snyder et al. (2004) and Widom et al. (1993) developed models of syenite contamination to explain the unusual chemical signature. Arguably, this island shows the most enriched compositions in the Azores, but these have not been found elsewhere. Thus, for this single island alone there has been a great debate as to its source signatures. Numerous authors have suggested different origins of the peculiar geochemical signature observed here. Widom et al. (1997) proposed a model of delaminated subcontinental lithospheric mantle (SCLM) that originates from the opening of the Atlantic ocean. This SCLM is then a contaminant of the rising mantle plume and subsequently imprints a characteristic trace-element and isotopic signature into the magmas during melting.

This model is in contrast to studies by Beier et al. (2007) and Elliott et al. (2007) both of which argue, based on modern day observations of subduction-related crustal alteration and associated arc basalt genesis, that the unusual signatures of São Miguel lavas can readily be explained by simple recycling models, however remelting and mixing processes during magma generation are also invoked. The relatively distant location of São Miguel to the MAR, in contrast to the island of Pico, allowed Prytulak and Elliott (Prytulak and Elliott, 2007) to address the origin of titanium enrichment, which is observed in many OIB as is the case in the Azores. São Miguel erupted on thicker crust than Pico, thus during their study they were able to monitor melting pressure and fraction. Subsequently, titanium enrichments are invoked to reflect contributions from recycled mafic crust to the source of OIB. The contribution of recycled MORB crust to the source of the Azores mantle plume was further refined by Prytulak and Elliott (Prytulak and Elliott, 2009), where it was suggested that eclogitic melts are dispersed into the peridotite mantle before remelting, to account for the discrepancy between low melt productivity (as deduced from U-series disequilibria) and independent evidence for mafic lithologies. In summary, these more recent studies would make the Azores more HIMU-like (see above for definition).

The question now rises if there are other means of testing between these competing models (i.e. sediment contribution to the source - yes or no?). Additional means in terms

of geochemical analyses can be found in the application of stable isotopes, more specifically of lithium, boron and oxygen isotopes, as these are most efficiently fractionated during low-temperature processes that ultimately occur near the surface. If these surface fractionated signatures are delivered back into the mantle during recycling they should be evident in OIB, thus making stable isotopes a potentially powerful tool in discriminating between different source origins. However, processes such as contamination in the form of assimilation may equally impart on the stable isotope signals. This challenge forms the base for the second major aim of this thesis and will be addressed specifically in chapters 3 and 4. To further constrain the source of the Azores mantle plume, age information is crucial in understanding when and where the different recycled contributions originate from and this ultimately has consequences on time scales of mantle convection. Newly available samples from the western islands are thus analysed for osmium isotopes to test whether recycled MORB crust may be evident in the source, but also new hafnium and lead isotope data will allow for a full assessment of the source underneath Flores and Corvo and across the entire plateau. The western island lavas allow for further constraints on the source distribution in the Azores region, and across the MAR. Data from the latter, including so far unpublished Os isotopes, are incorporated during this investigation and are presented in chapter five.

1.3. THE WESTERN AZORES ISLANDS - FLORES AND CORVO: CHAPTER TWO

In the second chapter of this thesis, the first detailed geochemical and petrological study of Flores and Corvo is presented to facilitate a better overall understanding of the Azores plume. A continuous polybaric fractional crystallization model appears to best describe the petrological and geochemical evolution of the volcanic suites, which is in contrast to studies from the eastern islands, where storage in discrete magma chambers at various depths was invoked beneath the volcanic centres (e.g. (Beier et al., 2006; França et al., 2006). Further, a unique mantle source with respect to the eastern islands is identified on the basis of the trace-element and Nd-Sr isotope data.

These newly available data now allow for full across island assessments of chemical parameters to further inform current models of the Azores plume source. The following two chapters (three and four) investigate the respective behaviour of Li-B-O in the primitive Azores lavas.

1.4. OXYGEN ISOTOPES IN THE AZORES: CHAPTER THREE

In chapter three, oxygen isotopes of selected well-characterised samples are presented. Oxygen isotopes have been widely used as a petrogenetic tool to decipher the source of igneous rocks (e.g. (Magaritz et al., 1978; Harris et al., 2000; Bindeman and Valley, 2001; Garcia et al., 2007; Day et al., 2009; Gurenko et al., 2011; Huang et al., 2011)). This is because isotopic fractionation of oxygen associated with low-temperature weathering and water-rock interaction fingerprints many crustal rocks, thus their role in the generation of OIB via recycling processes and/or contamination may be studied (Eiler, 2001). Over the last two decades, advances in analytical techniques from conventional fluorination to laser fluorination and more recently ion microprobe analysis have increased the amount and quality of data from natural and synthetic samples (Eiler, 2001; Bindeman, 2008; Eiler et al., 2011). This has afforded more precise determination of oxygen isotopic variability in basaltic rocks, which in turn may provide tighter constraints on the nature of their mantle source regions (e.g. (Magaritz et al., 1978; Kyser et al., 1982; Thirlwall et al., 2006)).

The main objective in this chapter is therefore to constrain the primary (i.e. source) oxygen isotope composition of the Azores islands, including, for the first time, the islands west of the Mid-Atlantic Ridge (MAR). For this purpose olivine separates were prepared from primitive Azores lavas. It is shown that, despite the fact that most olivines have forsterite and $\delta^{18}O$ compositions very close to mantle values, reaction with hydrothermally altered crust was nearly ubiquitous. The conclusions are that the range in mantle oxygen composition beneath the Azores region is significantly smaller than previously inferred and that, in order to better constrain the oxygen isotope composition of the mantle, the effects of assimilation need to be appraised more closely. These conclusions may apply widely.

Knowing that ubiquitous assimilation takes place underneath the volcanic centres of the Azores islands is important, as this will potentially be reflected in the light elements of B and Li and their isotopic compositions. Thus, in order to further assess mantle source composition, the newly established assimilation model needs to be accounted for and can be tested in the following chapter.

1.5. LITHIUM AND BORON ISOTOPES IN THE AZORES: CHAPTER FOUR

To further assess the source heterogeneity across the Azores islands new analytical data from the stable isotopes of lithium (Li) and boron (B) are presented in chapter four of this thesis. In detail, primitive lavas from seven Azores islands that are otherwise well characterised were selected for the Li-B analyses, for reasons given above. Studies of these two light elements and their isotopic composition may further decipher the nature of individual mantle components, as they provide a powerful proxy for the recycling of crustal material that underwent low temperature alteration near the surface (e.g. (Tomascak et al., 2002; Kobayashi et al., 2004; Elliott et al., 2006; Turner et al., 2007; Chan et al., 2009)). In the case of Li however it was shown in more recent studies that most OIB lavas conform to a range of δ^7Li that is indistinguishable from MORB and thus depleted upper mantle (Ryan and Kyle, 2004; Magna et al., 2011).

In terms of the new data from the Li and B stable isotope systems, we can constrain a relatively narrow source signature underneath the entire archipelago, which appears to be decoupled from the radiogenic isotope systems. Heavy boron is observed on Flores and Corvo consistent with assimilation fractional crystallization processes that differ slightly from those occurring underneath the eastern volcanic centres.

In summary, the stable isotopes reveal that assimilation was an important process in the evolution of the Azores lavas. However, what is also important is the fact that these processes cannot explain the variability that is observed in the traditional radiogenic isotope systems, thus they reflect intra mantle processes. The role of recycling in generating OIB has commonly been accepted, but the nature of the enriched components within the Azores mantle plume remain a matter of debate. In the next chapter, newly collected Hf-Pb-Os data are presented along with key trace element data (i.e. high-field strength elements (HFSE) to further constrain the nature of the Azores mantle source.

1.6. CONSTRAINTS ON THE MANTLE SOURCE FROM SR-ND-PB-HF-OS ISOTOPES: CHAPTER FIVE

The nature and origin of the Azores mantle source is assessed across the islands, which makes it possible to address the plume-ridge interaction with the MAR by comparing new and published data from the islands with those published for the Azores MAR. This east-west directed assessment also places spatial constraints on the distribution of the

Azores mantle plume. In this chapter, the first comprehensive Pb-Hf-Os isotope dataset along with published major element, trace element and Sr-Nd isotope data for the western two islands of Corvo and Flores is presented. It is shown that all radiogenic isotope systems determined on lavas from the western islands are comparable to the ancient (>> 1Ga inferred from Os isotopes), enriched (Sr-Nd-Pb) mantle sources commonly present underneath the eastern Azores islands. Yet the high-field-strength elements in Flores and Corvo lavas seem to be decoupled from this common source component as Nb and Ta are more fractionated from Zr and Hf, respectively, when compared to the eastern islands (Genske et al. 2012, chapter 2). The higher ratios of Nb/Zr and Ta/Hf may thus reflect either a different, distinct source component or, alternatively, a different process involved in magma generation.

Mixing models involving recycled ancient (2.5 Ga) MORB, sediment and DMM (i.e. the ambient mantle beneath the plateau) fail to explain the unusual trace element characteristics. Sediments are ruled out because their expected contribution to the Nd-Hf isotope systematics is not observed in the data. The contribution from sediments is further ruled out by the stable isotope data (chapters 3 & 4). In contrast, the MORB-DMM mixing model may confirm previous suggestions of up to 10% contribution from recycled mafic crust to the plume source however this cannot explain the full range of the HFSE ratios observed in the Azores either. The age constraint on the origin of the Azores mantle plume is derived from Os isotope ratios across the islands, but furthermore the mixing of modern N-MORB with DMM cannot explain the isotopic and trace element range that is present in the Azores lavas. Instead, ancient (up to 2.5 Ga) MORB is required in this model, consistent with previous suggestions for the Azores plume source.

The nature of the mantle source has not been determined so far for the island of Santa Maria. Thus, the final chapter will provide new insights on this easternmost Azores Island from rmajor and trace elements and Sr-Nd-Pb isotopes.

1.7. THE EASTERNMOST ISLAND - SANTA MARIA: CHAPTER SIX

For Santa Maria most studies have focused on the occurrence of fossiliferous sediments and carbonates (Madeira, et al. 2007) and, along with selected petrographical/geochemical data, few K-Ar age data are available (Abdel Monem, et al. 1975; Anderson and Flower 1982; Esenwein 1929; Féraud, et al. 1980; Féraud, et al. 1981). The higher alkalinity of lavas from Santa Maria, compared to the other Azores

islands, was first observed by White et al. (1979). The position of Santa Maria at the eastern edge of the submarine Azores Plateau (Fig.1) affords a different perspective on the conditions of melting at the edge of the Azores melting anomaly some 5-8 Ma ago (Abdel Monem, et al. 1975; Féraud, et al. 1981). In addition, by comparing Santa Maria with the much younger neighbouring islands, we can constrain the evolution of the Azores islands mantle sources from their earliest formation stages 5-8 Ma ago to the younger stages observed today.

Here, we present the first comprehensive major element, trace element and Sr-Nd-Pb radiogenic isotope data for basalts of Santa Maria, the easternmost island in the Azores. We show that the Sr-Nd-Pb isotope ratios of Santa Maria lavas are comparable to those of islands closer to the MAR and the magmas thus originate from isotopically similar mantle. However, the trace element ratios of Santa Maria lavas are both more enriched and more variable than those observed in islands erupted closer to the MAR. We explain this discrepancy by smaller degrees of partial melting beneath Santa Maria compared to the other Azores islands, in agreement with the higher alkalinity (White, et al. 1979).

We can show that the geochemical signatures from Santa Maria lavas provide evidence for melting of a CO2-rich peridotite lithology. While this carbonatite signal is weakened underneath the other islands due to larger degrees of partial melting and mixing between melts of carbonated peridotite and volatile-free garnet-peridotite, the thicker lithosphere during eruption and smaller degrees of partial melting preserve this signature underneath Santa Maria. At larger degrees of partial melting or a longer melting column this carbonatite source fingerprint may be obscured.

1.8. THESIS FRAMEWORK

This thesis was undertaken under a cotutelle agreement between Macquarie University, Sydney and the Friedrich-Alexander-University Erlangen-Nürnberg, Germany. The thesis is submitted at both Universities for consideration to award the combined academic degree of Doctor of Philosophy (PhD) and Doctor rerum naturalium (Dr. rer. nat.), respectively. Professor Simon P. Turner and Dr. Bruce F. Schaefer in Sydney, and Professor Karsten M. Haase and Dr. Christoph Beier in Erlangen supervised the work. It was written as a series of papers either published, submitted or in preparation.

The new samples collected for a major part of this study stem from the western Azores islands of Flores and Corvo. The fieldwork to obtain these samples immediately followed the 2009 Penrose conference of the Geological Society of America: "Plumes and Their Role in Whole Mantle Convection and Recycling". This conference provided an ideal opportunity to visit and study these unique islands in the central North-Atlantic, but further allowed for insightful discussions on the nature of the Azores mantle plume. This timely introduction to the topic on both a regional and global scale provided a good base for the further thesis layout.

1.9. ANALYTICAL TIME LINE

Upon collection and shipping of two splits of the samples to Germany and Australia, respectively, initial preparation was carried out at Macquarie University in 2009. This included inspection and characterization of the lavas macro- and microscopically. Subsequently, fresh samples where chosen for analytical work. First, thin sections where inspected to estimate modal abundances and mineral chemical compositions, and whole-rock chemistry was determined on prepared powders at the Geochemical Analysis Unit, Macquarie University. This work carried on in 2010, when based on the preliminary chemical composition, selected samples have been analysed for strontium and neodymium isotopic compositions. In June of 2010 a first travel to Europe was undertaken to visit the cotutelle partner University, but also to analyse new samples from Flores and Corvo together with previously well-characterised samples from the eastern islands for boron contents and boron isotopic composition at the Institute of Geosciences and Earth Resources of the Consiglio Nazionale delle Ricerche in Pisa, Italy, under the supervision of Dr. Sonia Tonarini.

The remainder of that year was used to fill in data gaps of trace elements and radiogenic isotopes, which included the whole-rock hafnium isotopic composition of lavas across the Azores islands. The latter carried over to 2011. In 2011, it was anticipated to analyse well-characterised samples for osmium, oxygen and lithium isotopes. The sophisticated techniques to collect the Os and Li isotope data however required more time than initially set out in the planning of the thesis, in order to assure data quality. Therefore, chapters 4 and 5 require further work before these will be suitable for publication in international journals.

From June 2011 to August 2012, during the second stay in Erlangen, oxygen isotopes on silicate phases from selected primitive Azores lavas were determined. In order to finish the Li and Os isotope data collection, an additional visit back to Macquarie University was scheduled for October/November 2011; however, due to analytical problems encountered during the Os analyses, not all the initially anticipated samples could be successfully analysed and further work is needed to complement the data set accordingly.

REFERENCES

Abdel-Monem, A.A., Fernandez, L.A., Boone, G.M., 1975. K-Ar ages from the eastern Azores group (Santa Maria, S„o Miguel and the Formigas Islands). Lithos 8, 247–254.

Acostinho, J., 1936. The Volcanoes of the Azores Islands, 8th ed. Bulletin Volcanologique.

Beier, C., Haase, K.M., Abouchami, W., Krienitz, M.S., Hauff, F., 2008. Magma genesis by rifting of oceanic lithosphere above anomalous mantle: Terceira Rift, Azores. Geochem. Geophys. Geosyst. 9.

Beier, C., Stracke, A., Haase, K.M., 2007. The peculiar geochemical signatures of São Miguel (Azores) lavas: Metasomatised or recycled mantle sources? Earth and Planetary Science Letters 259, 186–199.

Beier, C., Turner, S.P., Plank, T., White, W.M., 2010. A preliminary assessment of the symmetry of source composition and melting dynamics across the Azores plume. Geochem. Geophys. Geosyst. 11, Q02004.

Bonatti, E., 1990. Not So Hot "Hot Spots" in the Oceanic Mantle. Science 250, 107–111.

Bourdon, B., Langmuir, C.H., Zindler, A., 1996. Ridge-hotspot interaction along the Mid-Atlantic Ridge between 37°30" and 40°30" N: the U-Th disequilibrium evidence. Earth and Planetary Science Letters 142, 175–189.

Campbell, I.H., 1990. Implications of mantle plume structure for the evolution of flood basalts 10.1016/0012-821X(90)90072-6 : Earth and Planetary Science Letters | ScienceDirect.com. Earth and Planetary Science Letters.

Campbell, I.H., 2007. Testing the plume theory. Chemical Geology 241, 153–176.

Cannat, M., Briais, A., Deplus, C., Escartín, J., Georgen, J.E., Lin, J., Mercouriev, S., Meyzen, C., Muller, M., Pouliquen, G., Rabain, A., da Silva, P., 1999. Mid-Atlantic Ridge-Azores hotspot interactions: along-axis migration of a hotspot-derived event of enhanced magmatism 10 to 4 Ma ago. Earth and Planetary Science Letters 173, 257–269.

Chan, L.-H., Lassiter, J.C., Hauri, E.H., Hart, S.R., Blusztajn, J., 2009. Lithium isotope systematics of lavas from the Cook–Austral Islands: Constraints on the origin of HIMU mantle. Earth and Planetary Science Letters 277, 433–442.

Charlou, J.L., Donval, J.P., Douville, E., Jean-Baptiste, P., Radford-Knoery, J., Fouquet, Y., Dapoigny, A., Stievenard, M., 2000. Compared geochemical signatures and the evolution of Menez Gwen (37°50“ N) and Lucky Strike (37°17” N) hydrothermal fluids, south of the Azores Triple Junction on the Mid-Atlantic Ridge. Chemical Geology 171, 49–75.

Chauvel, C., Hofmann, A.W., Vidal, P., 1992. HIMU-EM: The French Polynesian connection. Earth and Planetary Science Letters 110, 99–119.

Chauvel, C., McDonough, W., Guille, G., Maury, R., Duncan, R., 1997. Contrasting old and young volcanism in Rurutu Island, Austral chain. Chemical Geology 139, 125–143.

Chauvel, C., Maury, R.C., Blais, S., Lewin, E., Guillou, H., Guille, G., Rossi, P., Gutscher, M.-A., 2012. The size of plume heterogeneities constrained by Marquesas isotopic stripes. Geochem. Geophys. Geosyst. 13, Q07005.

Chen, C.-Y., Frey, F.A., 1983. Origin of Hawaiian tholeiite and alkalic basalt. Nature 302, 785–789.

Clague, D.A., 1987. Hawaiian alkaline volcanism. Geological Society, London, Special Publications 30, 227–252.

Claude-Ivanaj, C., Joron, J.-L., Allègre, C.J., 2001. 238U-230Th-226Ra fractionation in historical lavas from the Azores: long-lived source heterogeneity vs. metasomatism fingerprints. Chemical Geology 176, 295–310.

Cooper, K.M., Eiler, J.M., Sims, K.W.W., Langmuir, C.H., 2009. Distribution of recycled crust within the upper mantle: Insights from the oxygen isotope composition of MORB from the Australian-Antarctic Discordance. Geochem. Geophys. Geosyst. 10, Q12004.

Dixon, J.E., Leist, L., Langmuir, C.H., Schilling, J.-G., 2002. Recycled dehydrated lithosphere observed in plume-influenced mid-ocean-ridge basalt. Nature.

Dupré, B., Lambret, B., Allègre, C.J., 1982. Isotopic variations within a single oceanic island: the Terceira case. Nature 299, 620–622.

Eiler, J.M., 2001. Oxygen Isotope Variations of Basaltic Lavas and Upper Mantle Rocks. Reviews in Mineralogy and Geochemistry 43, 319–364.

Eiler, J.M., Farley, K.A., Valley, J.W., Hauri, E.H., Craig, H., Hart, S.R., Stolper, E.M., 1997. Oxygen isotope variations in ocean island basalt phenocrysts. Geochimica et Cosmochimica Acta 61, 2281–2293.

Eiler, J.M., Farley, K.A., Valley, J.W., Stolper, E.M., Hauri, E.H., Craig, H., 1995. Oxygen isotope evidence against bulk recycled sediment in the mantle sources of Pitcairn Island lavas. Nature 377, 138–141.

Eiler, J.M., Grönvold, K., Kitchen, N., 2000. Oxygen isotope evidence for the origin of chemical variations in lavas from Theistareykir volcano in Iceland's northern volcanic zone. Earth and Planetary Science Letters 184, 269–286.

Eisele, J., Sharma, M., Galer, S.J.G., Blichert-Toft, J., Devey, C.W., Hofmann, A.W., 2002. The role of sediment recycling in EM-1 inferred from Os, Pb, Hf, Nd, Sr isotope and trace element systematics of the Pitcairn hotspot. Earth and Planetary Science Letters 196, 197–212.

Elliott, T., Blichert-Toft, J., Heumann, A., Koetsier, G., Forjaz, V.H., 2007. The origin of enriched mantle beneath São Miguel, Azores. Geochimica et Cosmochimica Acta 71, 219–240.

Esenwein, P., 1929. Zur Petrographie der Azoren, 12th ed. Zeitschrift für Vulkanologie.

Farley, K.A., Natland, J.H., Craig, H., 1992. Binary mixing of enriched and undegassed (primitive?) mantle components (He, Sr, Nd, Pb) in Samoan lavas. Earth and Planetary Science Letters 111, 183–199.

Farnetani, C.G., Samuel, H., 2005. Beyond the thermal plume paradigm. Geophys. Res. Lett. 32, L07311.

Flower, M.F.J., Schmincke, H.-U., Bowman, H., 1976. Rare earth and other trace elements in historic azorean lavas. Journal of Volcanology and Geothermal Research

1, 127–147.

França, Z.T.M., Lago, M., Nunes, J.C., Gale, C., Forjaz, V.H., Pueyo, O., Arranz, E., 2006. Geochemistry of alkaline basalts of Corvo Island (Azores, Portugal): preliminary data. Geogaceta. 40.

França, Z.T.M., Tassinari, C.C.G., Cruz, J.V., Aparicio, A.Y., Araña, V., Rodrigues, B.N., 2006. Petrology, geochemistry and Sr-Nd-Pb isotopes of the volcanic rocks from Pico Island--Azores (Portugal). Journal of Volcanology and Geothermal Research 156, 71–89.

Frey, F.A., 2002. Involvement of Continental Crust in the Formation of the Cretaceous Kerguelen Plateau: New Perspectives from ODP Leg 120 Sites. J Petrology 43, 1207–1239.

Gautier, I., Weis, D., Mennessier, J.-P., Vidal, P., Giret, A., Loubet, M., 1990. Petrology and geochemistry of the Kerguelen Archipelago basalts (South Indian Ocean): evolution of the mantle sources from ridge to intraplate position. Earth and Planetary Science Letters 100, 59–76.

Gudmundsson, A., 2000. Dynamics of Volcanic Systems in Iceland: Example of Tectonism and Volcanism at Juxtaposed Hot Spot and Mid-Ocean Ridge Systems. Annual Review of Earth and Planetary Sciences 28, 107–140.

Haase, K.M., Beier, C., 2003. Tectonic control of ocean island basalt sources on São Miguel, Azores? Geophys. Res. Lett. 30.

Halliday, A.N., Lee, D.-C., Tommasini, S., Davies, G.R., Paslick, C.R., Godfrey Fitton, J., James, D.E., 1995. Incompatible trace elements in OIB and MORB and source enrichment in the sub-oceanic mantle. Earth and Planetary Science Letters 133, 379–395.

Hanan, B.B., Graham, D.W., 1996. Lead and Helium Isotope Evidence from Oceanic Basalts for a Common Deep Source of Mantle Plumes. Science 272, 991–995.

Hart, S.R., Coetzee, M., Workman, R.K., Blusztajn, J., Johnson, K.T.M., Sinton, J.M., Steinberger, B., Hawkins, J.W., 2004. Genesis of the Western Samoa seamount province: age, geochemical fingerprint and tectonics. Earth and Planetary Science

Letters 227, 37–56.

Hart, S.R., Hauri, E.H., Oschmann, L.A., Whitehead, J.A., 1992. Mantle Plumes and Entrainment: Isotopic Evidence. Science 256, 517–520.

Hauri, E.H., Hart, S.R., 1993. ReOs isotope systematics of HIMU and EMII oceanic island basalts from the south Pacific Ocean. Earth and Planetary Science Letters 114, 353–371.

Hawkesworth, C.J., Norry, M.J., Roddick, J.C., Vollmer, R., 1979. 143Nd/144Nd and 87Sr/86Sr ratios from the Azores and their significance in LIL-element enriched mantle. Nature 280, 28–31.

Hémond, C., Devey, C.W., Chauvel, C., 1994. Source compositions and melting processes in the Society and Austral plumes (South Pacific Ocean): Element and isotope (Sr, Nd, Pb, Th) geochemistry. Chemical Geology 115, 7–45.

Hoernle, K.A., Werner, R., Morgan, J.P., Garbe-Schönberg, D., Bryce, J., Mrazek, J., 2000. Existence of complex spatial zonation in the Galápagos plume. Geol 28, 435–438.

Hofmann, A.W., White, W.M., 1982. Mantle plumes from ancient oceanic crust. Earth and Planetary Science Letters 57, 421–436.

Huang, S., Hall, P.S., Jackson, M.G., 2011. Geochemical zoning of volcanic chains associated with Pacific hotspots. Nature Geoscience 4, 874–878.

Jackson, M.G., Dasgupta, R., 2008. Compositions of HIMU, EM1, and EM2 from global trends between radiogenic isotopes and major elements in ocean island basalts. Earth and Planetary Science Letters 276, 175–186.

Jackson, M.G., Hart, S.R., Koppers, A., Staudigel, H., 2007. The return of subducted continental crust in Samoan lavas : Article : Nature. Nature.

Johnson, K.T.M., Sinton, J.M., Price, R.C., 1986. Petrology of seamounts northwest of Samoa and their relation to Samoan volcanism. Bull Volcanol 48, 225–235.

Kingsley, R.H., Schilling, J.-G., 1995. Carbon in Mid-Atlantic Ridge basalt glasses from 28° N to 63° N: Evidence for a carbon-enriched Azores mantle plume. Earth and

Planetary Science Letters 129, 31–53.

Kokfelt, T.F., Hoernle, K.A., Hauff, F., 2003. Upwelling and melting of the Iceland plume from radial variation of 238U-230Th disequilibria in postglacial volcanic rocks. Earth and Planetary Science Letters 214, 167–186.

Kokfelt, T.F., Hoernle, K.A., Hauff, F., Fiebig, J., Werner, R., Garbe-Schönberg, D., 2006. Combined Trace Element and Pb-Nd-Sr-O Isotope Evidence for Recycled Oceanic Crust (Upper and Lower) in the Iceland Mantle Plume. J Petrology 47, 1705–1749.

Koppers, A.A.P., Russell, J.A., Jackson, M.G., Konter, J., Staudigel, H., Hart, S.R., 2008. Samoa reinstated as a primary hotspot trail. Geol 36, 435.

Lassiter, J.C., Blichert-Toft, J., Hauri, E.H., Barsczus, H.G., 2003. Isotope and trace element variations in lavas from Raivavae and Rapa, Cook–Austral islands: constraints on the nature of HIMU- and EM-mantle and the origin of mid-plate volcanism in French Polynesia. Chemical Geology 202, 115–138.

Lassiter, J.C., Hauri, E.H., Hart, S.R., Blusztajn, J., Chan Deceased, L., 2008. Lithium isotope variations in lavas and olivine phenocrysts from the Cook-Austral Islands: Constraints on sample alteration and the true Li-isotope signature of HIMU mantle. AGU Fall Meeting Abstracts -1, 02.

Macdonald, G.A., 1968. Composition of Hawaiian lavas, in: Coats, R.R., Hay, R.L., Anderson, C.A. (Eds.), Studies in Volcanology: a Memoir in Honor of Howel Williams. Geological Society of America (GSA), Boulder, CO, pp. pp. 477–522.

Madeira, J., Ribeiro, A., 1990. Geodynamic models for the Azores triple junction: A contribution from tectonics. Tectonophysics 184, 405–415.

Madeira, P., Kroh, A., Martins, A.M. de F., Ávila, S.P., 2007. The marine fossils from Santa Maria Island. An Historical overview. AÇOREANA.

Michael, P., 1995. Regionally distinctive sources of depleted MORB: Evidence from trace elements and H2O. Earth and Planetary Science Letters 131, 301–320.

Millet, M.-A., Doucelance, R., Baker, J.A., Schiano, P., 2009. Reconsidering the origins

of isotopic variations in Ocean Island Basalts: Insights from fine-scale study of São Jorge Island, Azores archipelago. Chemical Geology 265, 289–302.

Montelli, R., Nolet, G., Dahlen, F.A., Masters, G., Engdahl, E.R., Hung, S.-H., 2004. Finite-Frequency Tomography Reveals a Variety of Plumes in the Mantle. Science 303, 338–343.

Moreira, M., Doucelance, R., Kurz, M.D., Dupré, B., Allègre, C.J., 1999. Helium and lead isotope geochemistry of the Azores Archipelago. Earth and Planetary Science Letters 169, 189–205.

Nakamura, Y., Tatsumoto, M., 1988. Pb, Nd, and Sr isotopic evidence for a multicomponent source for rocks of Cook-Austral Islands and heterogeneities of mantle plumes. Geochimica et Cosmochimica Acta 52, 2909–2924.

Parai, R., Mukhopadhyay, S., Lassiter, J.C., 2009. New constraints on the HIMU mantle from neon and helium isotopic compositions of basalts from the Cook–Austral Islands. Earth and Planetary Science Letters 277, 253–261.

Prytulak, J., Elliott, T., 2007. TiO2 enrichment in ocean island basalts. Earth and Planetary Science Letters 263, 388–403.

Prytulak, J., Elliott, T., 2009. Determining melt productivity of mantle sources from 238U-230Th and 235U-231Pa disequilibria; an example from Pico Island, Azores. Geochimica et Cosmochimica Acta 73, 2103–2122.

Ritsema, J., Allen, R.M., 2003. The elusive mantle plume. Earth and Planetary Science Letters 207, 1–12.

Rudnick, R.L., 2000. Rutile-Bearing Refractory Eclogites: Missing Link Between Continents and Depleted Mantle. Science 287, 278–281.

Ryall, P.J.C., Blanchard, M.-C., Medioli, F., 1983. A subsided island west of Flores, Azores. Canadian Journal of Earth Sciences 20, 764–775.

Saal, A.E., Hart, S.R., Shimizu, N., Hauri, E.H., Layne, G.D., Eiler, J.M., 2005. Pb isotopic variability in melt inclusions from the EMI-EMII-HIMU mantle end-members and the role of the oceanic lithosphere. Earth and Planetary Science Letters

240, 605–620.

Saunders, A.D., Norry, M.J., Tarney, J., 1988. Origin of MORB and chemically-depleted mantle reservoirs: trace element constraints. J Petrology.

Schiano, P., Burton, K.W., Dupre, B., Birck, J.-L., Guille, G., Allègre, C.J., 2001. Correlated Os–Pb–Nd–Sr isotopes in the Austral–Cook chain basalts: the nature of mantle components in plume sources. Earth and Planetary Science Letters 186, 527–537.

Schilling, J.-G., 1975. Azores mantle blob: Rare-earth evidence. Earth and Planetary Science Letters 25, 103–115.

Shirey, S.B., Bender, J.F., Langmuir, C.H., 1987. Three-component isotopic heterogeneity near the Oceanographer transform, Mid-Atlantic Ridge. Nature.

Shorttle, O., Maclennan, J., Jones, S.M., 2010. Control of the symmetry of plume-ridge interaction by spreading ridge geometry. Geochem. Geophys. Geosyst. 11, Q0AC05.

Skovgaard, A.C., Storey, M., Baker, J.A., Blusztajn, J., Hart, S.R., 2001. Osmium-oxygen isotopic evidence for a recycled and strongly depleted component in the Iceland mantle plume. Earth and Planetary Science Letters 194, 259–275.

Snyder, D.C., Widom, E., Pietruszka, A.J., Carlson, R.W., 2004. The Role of Open-System Processes in the Development of Silicic Magma Chambers: a Chemical and Isotopic Investigation of the Fogo A Trachyte Deposit, São Miguel, Azores. J Petrology 45, 723–738.

Sobolev, A.V., Hofmann, A.W., Kuzmin, D., Yaxley, G.M., 2007. The amount of recycled crust in sources of mantle-derived melts. Science.

Sobolev, A.V., Hofmann, A.W., Sobolev, S.V., Nikogosian, I.K., 2005. An olivine-free mantle source of Hawaiian shield basalts. Nature 434, 590–597.

Thirlwall, M.F., Gee, M.A.M., Taylor, R.N., Murton, B.J., 2004. Mantle components in Iceland and adjacent ridges investigated using double-spike Pb isotope ratios. Geochimica et Cosmochimica Acta 68, 361–386.

Turner, S.P., Hawkesworth, C.J., Rogers, N., King, P., 1997. U---Th isotope disequilibria

and ocean island basalt generation in the Azores. Chemical Geology 139, 145–164.

Ulrich, M., Hémond, C., Nonnotte, P., Jochum, K.P., 2012. OIB/seamount recycling as a possible process for E-MORB genesis. Geochem. Geophys. Geosyst. 13, Q0AC19–.

Wang, Z., Eiler, J.M., 2008. Insights into the origin of low-[delta]18O basaltic magmas in Hawaii revealed from in situ measurements of oxygen isotope compositions of olivines. Earth and Planetary Science Letters 269, 377–387.

Watson, S., McKenzie, D., 1991. Melt Generation by Plumes: A Study of Hawaiian Volcanism. J Petrology 32, 501–537.

Weaver, B., Wood, D., Tarney, J., 1987. Geochemistry of ocean island basalts from the South Atlantic: Ascension, Bouvet, St. Helena, Gough and Tristan da Cunha. Geological Society.

Weis, D., Frey, F.A., Leyrit, H., Gautier, I., 1993. Kerguelen Archipelago revisited: geochemical and isotopic study of the Southeast Province lavas. Earth and Planetary Science Letters 118, 101–119.

Weis, D., Garcia, M.O., Rhodes, J.M., Jellinek, M., Scoates, J.S., 2011. Role of the deep mantle in generating the compositional asymmetry of the Hawaiian mantle plume. Nature Geoscience 4, 831–838.

Weyer, S., Münker, C., Mezger, K., 2003. Nb/Ta, Zr/Hf and REE in the depleted mantle: implications for the differentiation history of the crust–mantle system. Earth and Planetary Science Letters 205, 309–324.

White, W.M., 1977. Geochemistry of igneous rocks from the central North Atlantic: The Azores and the Mid-Atlantic Ridge. Ph.D. Thesis Rhode Island Univ., Kingston.

White, W.M., 1993. 238U/204Pb in MORB and open system evolution of the depleted mantle. Earth and Planetary Science Letters 115, 211–226.

White, W.M., McBirney, A.R., DUNCAN, R.A., 1993. Petrology and Geochemistry of the Galápagos Islands: Portrait of a Pathological Mantle Plume. J. Geophys. Res. 98, 19533–19563.

White, W.M., 2010. Oceanic Island Basalts and Mantle Plumes: The Geochemical

Perspective. Annual Review of Earth and Planetary Sciences 38, 133–160.

White, W.M., Tapia, M.D.M., Schilling, J.-G., 1979. The petrology and geochemistry of the Azores Islands. Contributions to Mineralogy and Petrology 69, 201–213.

Widom, E., Carlson, R.W., Gill, J.B., Schmincke, H.-U., 1997. Th-Sr-Nd-Pb isotope and trace element evidence for the origin of the Sao Miguel, Azores, enriched mantle source. Chemical Geology 140, 49–68.

Widom, E., Gill, J.B., Schmincke, H.-U., 1993. Syenite Nodules as a Long-Term Record of Magmatic Activity in Agua de Pao Volcano, Sao Miguel, Azores. J Petrology 34, 929–953.

Willbold, M., Stracke, A., 2006. Trace element composition of mantle end-members: Implications for recycling of oceanic and upper and lower continental crust. Geochem. Geophys. Geosyst. 7, Q04004.

Woodhead, J.D., Devey, C.W., 1993. Geochemistry of the Pitcairn seamounts, I: source character and temporal trends. Earth and Planetary Science Letters 116, 81–99.

Workman, R.K., Hart, S.R., 2005. Major and trace element composition of the depleted MORB mantle (DMM). Earth and Planetary Science Letters 231, 53–72.

Workman, R.K., Hart, S.R., Jackson, M.G., Regelous, M., Farley, K.A., Blusztajn, J., Kurz, M.D., Staudigel, H., 2004. Recycled metasomatized lithosphere as the origin of the Enriched Mantle II (EM2) end-member: Evidence from the Samoan Volcanic Chain. Geochem. Geophys. Geosyst. 5.

Wright, E., White, W.M., 1987. The origin of Samoa: new evidence from Sr, Nd, and Pb isotopes. Earth and Planetary Science Letters 81, 151–162.

Xu, G., Frey, F.A., Clague, D.A., Weis, D., Beeson, M.H., 2005. East Molokai and other Kea-trend volcanoes: Magmatic processes and sources as they migrate away from the Hawaiian hot spot. Geochem. Geophys. Geosyst. 6, Q05008.

Yu, D., Fontignie, D., Schilling, J.-G., 1997. Mantle plume-ridge interactions in the Central North Atlantic: A Nd isotope study of Mid-Atlantic Ridge basalts from 30° N to 50° N. Earth and Planetary Science Letters 146, 259–272.

CHAPTER 2: THE PETROLOGY AND GEOCHEMISTRY OF LAVAS FROM THE WESTERN AZORES ISLANDS OF FLORES AND CORVO

Felix S. Genske[1, 2]*, Simon P. Turner[1], Christoph Beier[1, 2] and Bruce F. Schaefer[1]

[1]GEMOC, Department of Earth and Planetary Sciences, Macquarie University, Sydney, NSW 2109, Australia

[2]GeoZentrum Nordbayern, Universität Erlangen-Nürnberg, Schlossgarten 5, D-91054 Erlangen, Germany

ABSTRACT

The islands of Flores and Corvo in the Azores archipelago are the only two of nine subaerial volcanic edifices lying west of the Mid-Atlantic Ridge (MAR). This makes them important for constraining the evolution of this young (540 Ma) oceanic plateau. The alkalic basalt suites from Flores and Corvo lie on a single liquid line of descent. Ankaramitic cumulates, with MgO contents up to ~18 wt %, result from clinopyroxene-dominated polybaric crystallization. The parental magmas (MgO ~ 11 wt %) are inferred to be low-degree partial melts (F = 3-5%) of enriched peridotite generated at depths of ~ 80-90 km. These primary magmas commenced crystallizing at the lithosphere-asthenosphere boundary and this continued in conduits over a pressure range of ~ 0.6-1.2 GPa. Only lavas with MgO < 3 wt % fractionated at shallow crustal levels. Nd and Sr isotope data reveal variations in the source of both magmatic systems, suggesting variable contributions from both enriched (E-) and depleted (D-) mid-ocean ridge basalt (MORB)-source mantle components. This is supported by the greater variability of incompatible trace-element ratios within the Flores lavas (e.g. Ba/Nd, La/Sm, Th/Nd), whereas those from Corvo exhibit a good correlation between key trace-element ratios

[e.g. $(La/Sm)_N$, Th/Nd] and Sr isotope ratios. Lavas from Flores display a greater variability in Sr and Nd isotope compositions and define a mixing array between an E-MORB source and a common Azores mantle source. The latter signature is restricted to lava suites from the north and east of Flores. We concur with the generally accepted notion that Flores and Corvo are derived from the same mantle plume as is responsible for the eastern Azores islands. However, there is evidence (different Nb/Zr, Ta/Hf and La/Sm, but homogeneous Sr and Nd isotopic composition) that these two islands are dominated by a source component that is not as evident in the eastern archipelago.

KEY WORDS: *Azores plateau; magmatic differentiation; polybaric fractionation; oceanic lithosphere; OIB*

2.1 INTRODUCTION

Volcanic systems on young intraplate ocean islands have been widely studied to gain insights into the composition of the upper, and possibly lower, mantle and therefore into the recycling of lithosphere-derived components. Some of the best-studied ocean island basalts (OIB) include those from Hawaii (e.g. Macdonald, 1968; Chen & Frey, 1983; Clague, 1987; Watson & McKenzie, 1991; Sobolev et al., 2005) and Iceland (e.g. Gudmundsson, 2000; Skovgaard et al., 2001; Kokfelt et al., 2009), which are both inferred to represent the surface expressions of deep-rooted mantle plumes (Woodhead, 1992; Sleep, 2006; Zhao, 2007). Given its lower buoyancy flux, the Azores archipelago may not necessarily reflect the surface expression of a typical mantle plume (Sleep, 1990). However, numerous workers have emphasized the potential that lies in these nine islands and the nearby Mid-Atlantic Ridge (MAR) to study the dynamics associated with plume-ridge interaction (e.g. Bourdon et al., 1996; Gente et al., 2003; Madureira et al., 2005; Shorttle et al., 2010). Additionally, the Azores basalts may provide evidence for the recycling of ancient, perhaps even Archaean, lithosphere (Schaefer et al., 2002; Turner et al., 2007).

Current models for the Azores mantle plume are based mainly on interpretations arising from geochemical and geophysical studies of the islands to the east of the Mid-Atlantic Ridge (e.g. Abdel-Monem et al., 1975; Flower et al., 1976; White et al., 1979; Dupré et al., 1982; Madeira & Ribeiro, 1990; Turner et al., 1997; Claude-Ivanaj et al., 2001; Haase & Beier, 2003; França et al., 2006b; Beier et al., 2008; Beier et al., 2010; Millet et al., 2009; Prytulak & Elliott, 2009) and the nearby MAR (e.g. Kingsley & Schilling, 1995;

Bourdon et al., 1996; Yu et al., 1997; Cannat et al., 1999; Charlou et al., 2000). The plume has been imaged to depths greater than ~ 240 km by seismic tomography (Montelli et al., 2004) and is suggested to be centred either to the NE of the island of Terceira (Moreira et al., 1999) or potentially in the vicinity of the island of Faial (Cannat et al., 1999; Gente et al., 2003; Shorttle et al., 2010), but in either case on the eastern plateau, 150-200 km away from the MAR. The remote islands of Flores and Corvo to the west of the MAR have been much less well studied and afford a different perspective for models for the interaction of the Azores mantle plume with the MAR. Here, we present the first detailed geochemical and petrological study of Flores and Corvo to facilitate a better overall understanding of the Azores plume. A continuous polybaric fractional crystallization model appears to best describe the petrological and geochemical evolution of the volcanic suites and a unique source is identified on the basis of the trace-element and Nd-Sr isotope data.

2.2 BACKGROUND

2.2.1 Geological Setting

The Azores islands are situated on a submarine plateau that is subdivided by the MAR into eastern and western parts. Seven of the nine islands are located to the east of the MAR on the Eurasian and African plates and only the islands of Flores and Corvo (Fig. 2.1) emerge from the American plate.

In contrast to the eastern islands, which are dominated by NW-SE-striking structures parallel to the ultraslow Terceira Rift axis (Searle, 1980; Vogt & Jung, 2004), the two western islands lie on a NNE-SSW-trending ridge that is subparallel to the MAR (Fig. 1). The Azores archipelago is located in the vicinity of a triple junction (Krause & Watkins, 1970; Searle, 1980; Madeira & Ribeiro, 1990; Fernandes et al., 2006), and there are no obvious extensional structures on the western plateau similar to those found on the eastern plateau (e.g. the Terceira Rift Axis; Vogt & Jung, 2004; Georgen, 2008; Georgen & Sankar, 2010). The geometric shape of the western plateau is clearly influenced by the MAR, resulting in predominantly north-south-striking tectonic structures. The structural influence of MAR transform faults is reflected by the linear, east-west-striking northern and southern coastal areas of Flores and Corvo (Fig. 2) together with a relative sinistral displacement of Corvo at ~1cm a^{-1} (Baptista et al., 1999). The motion of the North

American plate relative to a fixed triple junction point is in a SW direction with a velocity equivalent to a 1.2 cm a^{-1} half spreading rate (Georgen & Sankar, 2010).

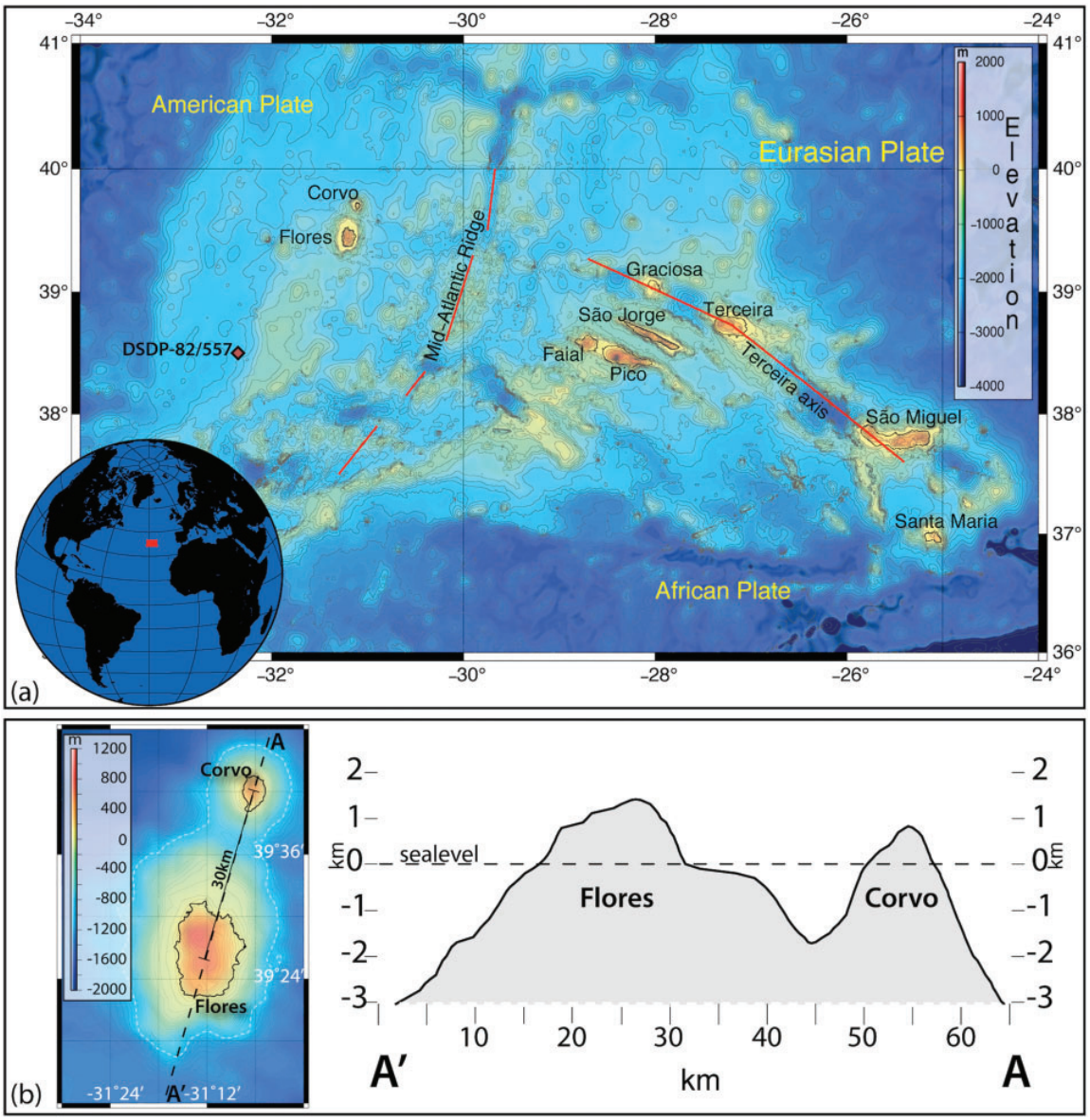

Fig. 1. (a) Bathymetric map of the Azores plateau showing the nine islands east and west of the Mid-Atlantic Ridge. (b) Bathymetric map of Flores and Corvo highlighting the emerging topography above the ocean floor. The erosion platforms on the west and NW of both volcanoes in- dicate the original size of both islands prior to erosion. The profile A-A' highlights the submarine parts of the volcanic systems, which extend to depths of around 3000 m below present-day sea level. Map produced using GMT (Wessel & Smith, 1991, 1995). Vertical exaggeration is 4·75 times the horizontal.

To date, only one submarine volcanic edifice has been identified on the western plateau and this has basalts dated at around 4.8 Ma (Ryall et al., 1983). However, Gente et al. (2003) identified several ridges parallel to the MAR. The subsidence-corrected

topography (Gente et al., 2003) suggests at least one set of two seamounts roughly 50 km west of Flores and Corvo. The spatial dimensions of these appear very similar to those of the emergent islands and may be observed again on the magnetic Chron 6 ridge (~20 Ma). Gente et al. (2003) also showed that the Chron 6 ridge defines the westernmost boundary of the Azores plateau as suggested by east-west-directed seismic profiles and the bathymetry, both of which define a sharp drop off towards older oceanic crust (Fig. 1a, -32° to -33°W).

The overall dimensions of the western Azores plateau are ~300 km from east to west and ~400 km from north to south. The thickened oceanic crust on each flank of the MAR has a similar thickness (~8-10 km) across the plateau (Krause & Watkins, 1970; Searle, 1980; Gente et al., 2003; Nunes et al., 2006; Beier et al., 2008; Georgen & Sankar, 2010). The top 2-3 km can be attributed to the plume, and the normal crustal thickness in this area is of the order of 7-8 km. Maximum thicknesses of ~12 km are found in the vicinity of the emergent volcanoes (Luis et al., 1998; Gente et al., 2003).

Flores, which is the larger of the two islands (Fig. 1b), is characterized by a group of connected and overlapping stratovolcanoes with small independent caldera systems. The lack of extended fissure systems (compare the Terceira axis and the Faial horst-and-graben system), combined with the absence of a large caldera, give Flores a unique geological character in the Azores archipelago. Current constraints from K/Ar dating of the subaerial base of Flores suggest a maximum age of ~2 Ma (Azevedo & Ferreira, 1999). The major volcanic and tectonic features on Flores have been described by Azevedo & Ferreira (2006). Corvo's dominant feature is one large caldera with a diameter of around 2 km and a maximum height of 300 m. Published ages for Corvo are somewhat ambiguous. The oldest lavas at the base of the island are re- ported to be 1-1.5 Ma whereas the youngest ages place the Vila do Corvo flank eruption at 80 ka (França a et al., 2006a); no historical record of volcanic activity exists. Both islands represent the subaerial expressions of volcanic systems with a base as deep as 3000 m below the present-day sea level (Fig. 1b). The bathymetric map and the NE-SW profile indicate a relative distance of 30 km between the volcanic centres and also show the erosion platforms of both islands at the eastern and northern shore at ~100 m below sea level (Fig. 1).

The thick submarine volcanic packages of both islands lead to the conclusion that the age of initial volcanism must be older than 2 Ma. The magnetic stripes on the ocean floor north and south of the Azores plateau suggest that Flores and Corvo emerged from oceanic crust that is slightly younger than 10 Ma (Gente et al., 2003). These age constraints, combined with plate motion of 1-1.5 cm a^{-1}, imply that the initial volcanism of the western Azores islands may have commenced when they were between 70 and 90 km from the MAR.

2.2.2 Stratigraphy of Flores and Corvo

The stratigraphy of Flores has previously been described by Azevedo & Ferreira (2006), and we use their stratigraphic characterization herein. Because of the complexity of the volcanic system and the different styles of eruption that characterize the island, the finer strati- graphic units cannot always be ascertained, but the division into Base Volcanic Complex (BVC) and Upper Volcanic Complex (UVC1-3) is readily identifiable in the field and is illustrated in Fig. 2a.

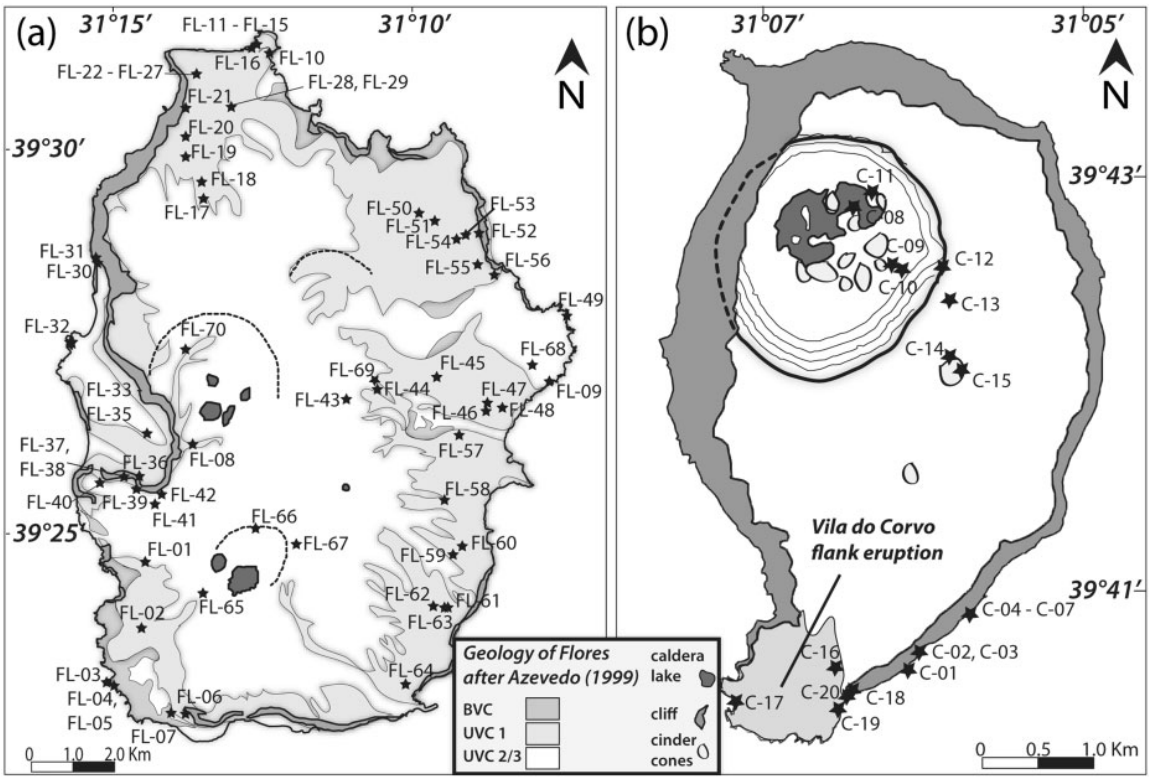

Fig. 2. Geological maps of Flores (a) and Corvo (b) indicating the sample localities from this study. The stratigraphic classification for Flores (BVC, base volcanic complex; UVC 1-3, upper volcanic complex) is taken from Azevedo & Ferreira (1999). (See text for a full description of these units.) The difference in scale between the two maps should be noted.

The upper complex comprises all units resulting from subaerial volcanism, whereas the BVC includes units from both submarine and emergent stages, which are largely observed in outcrops at sea level along the north and south coast. Owing to the possible interaction with seawater, the BVC rocks are mostly altered, making them mostly unsuitable for petrological and geochemical analysis. The only location where the BVC was sampled during this study was the SW coast of the island, where samples appear to be relatively unweathered and unaltered. The rocks belonging to the UVC are generally better preserved, as they form the upper section of the volcanic pile. The stratovolcanic cycles resulted in extrusive flow and fall deposits that range from basaltic lavas to trachytic scoria cones and ash layers. The eruptive styles on Flores became more explosive towards the later stages (Azevedo & Ferreira, 2006).

França et al. (2006a) have established a stratigraphic record for Corvo. Similar to Flores, it can be subdivided into a Basal (proto-island) Complex and an Upper Complex. The latter includes pre-, syn- and postcaldera deposits. The syncaldera episode is characterized by more explosive, pyroclastic flow deposits. The youngest rocks on Corvo may be associated with the Vila Nova do Corvo flank eruption. However, there are no age constraints.

2.3 ANALYTICAL METHODS

2.3.1 Sampling and sample treatment

The islands of Flores and Corvo were sampled in May 2009 (Fig. 2). The sampling campaign was based on observations in the field and previous stratigraphic work on Flores (Azevedo & Ferreira, 1999, 2006; França et al., 2008) and Corvo (França et al., 2006a). The aim was to sample stratigraphic profiles, two for Flores and one for Corvo, to encompass as much of the magmatic evolution of both islands as possible. Whenever possible, visibly fresh material was recovered; however, some samples collected near the shoreline show evidence of surficial seawater alteration. These latter samples were only investigated microscopically. For analytical work, fresh cores were cut from the unaltered samples and these were then washed and ultrasonicated in deionized water.

2.3.2 Electron microprobe analysis (EMPA)

Representative samples were selected for macro- and microscopical studies before electron microprobe analyses were conducted. Major-element compositions of silicate minerals were obtained using a CAMECA SX100 electron microprobe (EMP) with five fixed wavelength-dispersive spectrometers and one energy-dispersive X-ray detector at the Geochemical Analysis Unit (GAU), Macquarie University, Sydney. Cr2O3 and NiO concentrations were also determined for opaque phases and iron-magnesium silicates. Analyses were obtained using a focused beam, with an accelerating voltage of 15 kV and a beam current of 20 nA. Calibration standards used were albite (Na), Fe_2O_3 (Fe), kyanite (Al), olivine (Mg), chromite (Cr), spessartine (Mn), orthoclase (K), wollastonite (Ca, Si), and rutile (Ti).

2.3.3 Major- and trace-element analysis

Sample cores were crushed using a hydraulic press and then powdered using an agate mill to obtain a fine powder (~50 mm grain size). Thorough care was taken when cleaning the mill with Milli-Q® water and ethanol between samples to avoid cross-contamination.

Standard techniques (e.g. Potts et al., 1984) were used for the major-element analysis. Glass discs for X-ray fluorescence (XRF) analysis were prepared by homogeneously fusing 0·4 g of sample with 2.5 g lithium tetraborate-metaborate flux (12:22 mixture) and ammonium iodide in a Pt crucible at 1050°C. The discs were analysed using a Spectro XEPOS energy-dispersive XRF spectrometer at the School of Earth and Environmental Sciences, University of Wollongong. Loss on ignition was determined for each sample at 1050°C for 1.5 h. Analyses of international rock standards and the samples are listed in Table 1. Accuracy of the measured values was generally better than 0·9%.

For the trace-element analyses standard methods (e.g. Eggins et al., 1997) were employed. Approximately 100 mg of sample (n = 37) was weighed into clean 15 ml Savillex® Teflon beakers. Samples were digested using a 1:1 mixture of HF (Merck, suprapur grade) and HNO_3 (Ajax) at 160°C for 24 h, then dried down and repeated. To fully dissolve any spinel in the samples, a HF-HCl-$HClO_4$ mix was added to the digestion procedure for 2 days at 160°C. This step was repeated when necessary. After drying down at 200°C the samples were then further digested in 6N HNO_3 for 24h, dried down

again, and diluted to 10 ml in 2% HNO_3 with trace HF. Then 1:1000 dilutions of each sample were individually spiked with a 15 µl aliquot of a solution of Li, As, Rh, In, Tm and Bi in 2% HNO_3.

Samples and standards were analysed by quadrupole inductively coupled plasma mass spectrometry (ICP-MS) on an Agilent 7500c/s system at the GAU, Macquarie University, Sydney. BCR-2 was used as a calibration standard to correct for instrument sensitivity and run drift. The background was measured on a 2% HNO_3 rinse solution. Measured values and the deviation from reference values from GeoReM (Jochum & Nohl, 2008) for standards BIR-1 and BHVO-2 are given in Table 1. The full dataset for the analysed samples (including Sr and Nd isotopes) is given in Electronic Appendix 1 (and in the printed Appendix 1 of this thesis), which is available for downloading at: http://www.petrology.oxfordjournals.org.

2.3.4 Sr and Nd isotopes

Purification of Sr and Nd was carried out for whole-rock samples (n = 17) and international rock standards (~140 mg) using powders digested in Teflon beakers with concentrated HF and HNO3. Samples were then dried down and ~1ml of concentrated $HClO_4$ was added, followed by 4 ml 6N HCl and H_2O_2. These were dried down once again, dissolved in 6N HCl, dried, dissolved in HCl and HF, and centrifuged to remove any undissolved residue. The samples were then loaded onto Teflon columns using Biorad® AG50W-X8 (200-400 mesh) cation exchange resin and eluted using a 2·5N HCl-0·1N HF solution. Sr was collected from the column followed by Nd. Neodymium was further purified from Sm, Ba, La and Ce using a second column [Eichrom® Ln spec resin (50-100 µm)] following the methods described by Pin & Zalduegui (1997).

Isotopic analyses of Sr and Nd were obtained by thermal ionization mass spectrometry (TIMS) using a Thermo Finnigan Triton system at the GAU, Macquarie University, Sydney. Sr was loaded onto single rhenium filaments with a Ta activator and analysed between 1380 and 1430°C in a static measurement mode with rotating amplifiers. Measured $^{87}Sr/^{86}Sr$ ratios for BHVO-2 are listed in Table 1. NIST SRM 987 was analysed for instrument sensitivity during times of the analyses (n= 17) and gave a long-termreproducibility of $^{87}Sr/^{86}Sr$ = 0·710250 (2SD = 0·000034). Ratios were normalized to $^{86}Sr/^{88}Sr$ = 0·1194 to correct for mass fractionation.

Table 1: Major-element, trace-element and Nd-Sr isotope date for selected lavas from Flores and Corvo and international rock standards.

Sample no.:	C-09-01	C-09-02	C-09-06	C-09-07	C-09-08	C-09-10	C-09-13	C-09-17.1	C-09-17.2	C-09-18	C-09-19	C-09-20
Island:	Corvo	Corvo	Corvo	Corvo	Corvo	Corvo	Corvo	Corvo	Corvo	Corvo	Corvo	Corvo
Lat. (°N):	39·6752	39·6766	39·6802	39·6802	39·7128	39·7081	39·7051	39·6727	39·6727	39·6736	39·6718	39·6718
Long. (°W):	31·1036	31·1025	31·0963	31·0963	31·1079	31·1029	31·0982	31·1215	31·1215	31·1089	31·1108	31·1108
Elevation (m):	2	2	2	5	412	460	546	5	5	5	5	5
Volcano-stratigraphy:	pre-caldera	caldera	pre-caldera	pre-caldera	caldera	caldera	caldera	VDC	VDC	pre-caldera	VDC	pre-caldera
TAS classification:	Alkali basalt	Tephrite	Alkali basalt	Tephrite	trachy-andesite	Tholeiite basalt	Tholeiite basalt	Trachy-andesite	Picro-basalt	Tephrite	Tephrite	Tephrite
wt %												
SiO_2	45·54	47·06	45·15	45·18	48·50	46·55	46·07	56·08	41·05	44·56	46·82	45·52
TiO_2	2·43	3·10	2·66	1·98	2·97	1·33	1·50	1·03	2·99	2·58	3·13	2·30
Al_2O_3	13·99	16·33	13·79	12·48	16·34	7·60	10·12	18·85	11·76	14·90	16·46	12·74
Fe_2O_3	11·33	12·02	12·12	10·71	11·33	9·10	9·31	7·99	14·13	12·05	11·77	11·32
MnO	0·18	0·22	0·18	0·16	0·19	0·15	0·14	0·24	0·17	0·19	0·22	0·17
MgO	9·27	4·23	8·76	11·49	3·27	18·18	15·52	1·23	10·67	8·08	4·29	10·74
CaO	12·06	8·61	11·94	13·90	6·34	14·92	14·61	4·16	15·29	12·04	8·35	13·21
Na_2O	3·12	5·10	3·28	2·89	4·16	1·08	1·51	6·48	1·67	3·55	5·59	2·32
K_2O	1·17	1·97	1·12	0·45	2·67	0·37	0·48	2·99	0·13	1·18	1·86	0·88
P_2O_5	0·49	0·84	0·49	0·30	0·94	0·20	0·25	0·50	0·17	0·45	1·11	0·39
LOI	0·41	0·77	0·35	0·80	2·98	0·70	0·75	0·43	2·01	0·75	0·05	0·40
Total	99·99	100·25	99·82	100·34	99·69	100·18	100·26	99·98	100·04	100·33	99·65	99·99
ppm												
Sc	32·2	12·8	30·3	42·7	14·3	66·5	55·9	2·71	58·9	28·8	12·6	41·7
V	268	213	327	297	172	282	264	11·7	625	338	184	321
Cr	456	21·9	418	697	24·0	2530	1414	2·04	716	226	3·71	625
Co	49·1	28·8	51·0	55·0	25·3	77·0	59·4	7·45	72·5	52·5	26·8	57·9
Ni	182	11·3	186	190	17·1	595	356	0·89	95·9	151	3·44	235
Cu	161	35·1	127	95·9	42·0	172	114	7·73	53·8	121	19·3	91·9
Zn	81·0	105	82·5	67·6	121	64·3	53·6	131	115	83·0	111	78·8
Mo	1·54	2·61	1·76	0·97	2·20	0·51	0·70	3·31	4·67	1·93	3·07	1·41
Rb	26·5	48·0	28·9	10·9	61·5	7·10	9·66	54·1	2·59	28·7	56·2	23·9
Sr	541	738	560	426	694	272	293	770	573	593	949	499
Y	24·9	38·9	26·0	20·0	38·6	17·0	16·4	41·7	20·2	24·9	42·9	24·8
Zr	185	306	181	126	347	94·6	98·4	591	84·8	177	325	166
Nb	64·8	109	60·2	35·9	124	31·2	30·2	200	11·6	61·8	131	56·4
Cs	0·28	0·40	0·26	0·37	0·40	0·14	0·09	0·13	0·03	0·29	0·69	0·23
Ba	380	629	384	245	573	182	191	1158	110	381	613	349
La	38·0	63·6	36·2	23·5	63·4	17·6	19·3	106	18·4	36·2	74·3	37·0
Ce	73·0	122	69·1	46·4	119	36·6	37·1	191	29·4	69·7	144	67·3
Pr	8·62	15·3	8·38	5·82	14·2	4·50	4·65	20·6	4·45	8·27	17·6	8·42
Nd	32·8	54·7	32·3	23·3	52·1	18·3	18·5	65·5	19·4	31·4	62·4	32·0
Sm	6·36	10·2	6·38	4·90	9·78	3·95	3·89	10·6	4·67	6·09	11·8	6·28
Eu	2·02	3·14	2·03	1·53	2·88	1·22	1·21	3·34	1·51	1·95	3·49	2·00
Gd	5·71	8·89	5·73	4·62	8·52	3·66	3·65	8·30	4·53	5·45	10·38	5·71
Tb	0·80	1·26	0·81	0·68	1·20	0·47	0·50	1·28	0·62	0·76	1·51	0·82
Dy	4·36	6·67	4·42	3·60	6·31	2·85	2·87	6·64	3·60	4·17	7·75	4·37
Ho	0·79	1·25	0·82	0·69	1·19	0·47	0·50	1·34	0·59	0·76	1·49	0·81
Er	2·14	3·35	2·17	1·78	3·14	1·31	1·36	3·73	1·59	2·04	3·84	2·12
Yb	1·71	2·68	1·72	1·40	2·54	0·98	1·06	3·58	1·14	1·61	3·15	1·67
Lu	0·19	0·34	0·20	0·19	0·33	0·12	0·09	0·57	0·14	0·18	0·45	0·19
Hf	3·81	5·81	3·66	2·97	6·52	2·31	2·30	10·6	2·92	3·52	7·03	3·62
Ta	3·95	6·69	3·64	1·93	7·42	2·20	1·69	18·7	0·62	3·58	11·24	4·08
Pb	2·36	3·30	1·62	1·35	5·10	0·83	0·85	7·38	0·47	1·68	3·89	1·58
Th	4·67	7·71	4·22	2·62	8·59	1·90	2·05	16·7	0·65	4·05	10·54	4·01
U	1·25	1·94	1·02	0·65	2·13	0·52	0·55	4·21	0·44	1·10	2·63	1·01
$^{87}Sr/^{86}Sr$	0·70335	0·70339	0·70343		0·70334		0·70350			0·70337	0·70330	0·70341
$^{143}Nd/^{144}Nd$	0·51292	0·51293	0·51292		0·51293		0·51294			0·51292	0·51292	0·51292

Sample no.:	FL-09-01	FL-09-07	FL-09-09	FL-09-19	FL-09-20	FL-09-23	FL-09-26	FL-09-32	FL-09-38	FL-09-41	FL-09-42	FL-09-58	FL-09-59
Island:	Flores	Flores	Flores	Flores	Flores	Flores	Flores	Flores	Flores	Flores	Flores	Flores	Flores
Lat. (°N):	39·4100	39·3769	39·4480	39·4985	39·5023	39·5149	39·5149	39·4581	39·4285	39·4226	39·4244	39·4224	39·4094
Long. (°W):	31·2451	31·2373	31·1308	31·2317	31·2316	31·2281	31·2281	31·2645	31·2512	31·2417	31·2399	31·1634	31·1602
Elevation (m):	356	151	59	359	303	100	95	6	284	460	472	350	278
Volcano-stratigraphy:*	UVC1	BVC	UVC2/3	UVC1	UVC1	UVC1	UVC1	UVC2/3	UVC1	UVC2/3	UVC2/3	UVC1	UVC1
TAS classification:	Trachy-basalt	Trachyte	(altered basalt)	Tephrite	Alkali basalt	Alkali basalt	Alkali basalt	Trachy-basalt	Trachy-basalt	Alkali basalt	Alkali basalt	Alkali basalt	Tephrite
wt %													
SiO_2	47·64	62·11	41·74	46·90	44·03	46·71	47·42	44·89	46·70	46·35	44·80	45·13	44·53
TiO_2	2·21	0·62	3·12	3·11	3·61	1·76	1·82	2·79	2·50	1·82	2·24	2·97	3·47
Al_2O_3	16·31	17·95	17·83	16·61	16·19	15·74	16·00	15·30	16·30	13·59	14·63	15·49	15·80
Fe_2O_3	10·46	3·97	13·84	11·24	13·18	11·11	11·14	12·09	11·55	10·74	11·42	11·85	12·68
MnO	0·19	0·19	0·27	0·20	0·19	0·17	0·17	0·18	0·20	0·17	0·18	0·19	0·19
MgO	6·67	0·50	3·36	4·22	5·52	8·79	7·57	7·91	5·76	10·50	9·30	6·42	6·45
CaO	9·81	1·35	5·57	7·88	10·27	11·15	11·80	10·02	10·36	11·61	10·77	10·38	10·75
Na_2O	3·74	6·14	4·32	4·51	2·58	2·61	2·77	4·36	4·08	3·16	2·78	2·78	3·34
K_2O	1·45	5·35	1·63	2·06	1·27	0·61	0·62	1·30	1·45	1·14	1·09	0·78	1·37
P_2O_5	0·61	0·14	1·67	1·33	0·86	0·43	0·43	0·70	0·76	0·46	0·64	0·65	1·01
LOI	1·15	1·69	6·36	1·79	2·00	1·09	0·38	0·31	0·38	0·01	1·92	3·11	0·67
Total	100·24	100·01	99·71	99·85	99·70	100·17	100·12	99·85	100·04	99·55	99·77	99·75	100·26
ppm													
Sc	25·4	1·56	12·9	16·7	23·3	30·8	33·0	22·9	23·0	35·5	33·0	29·2	27·0
V	216	8·56	100	211	336	207	219	249	253	252	253	327	310
Cr	255	1·86	3·03	13·0	42·1	367	232	419	141	671	572	197	116
Co	39·0	1·92	22·6	22·7	40·6	46·2	43·8	45·6	35·4	51·7	48·6	43·5	42·0
Ni	106	0·56	2·57	7·18	30·6	175	113	147	66·5	246	209	82·4	56·9
Cu	64·3	5·67	18·7	27·5	46·7	63·9	80·5	54·3	56·3	96·1	93·5	95·4	56·6
Zn	94·2	84·9	103	100	104	74·3	77·6	90·5	93·2	68·0	76·4	89·8	103
Mo	2·12	0·50	1·09	2·23	1·87	0·82	0·97	2·35	2·43	1·89	1·35	1·98	0·41
Rb	36·4	50·2	28·1	46·9	27·4	10·1	11·0	29·0	34·4	32·6	27·7	5·40	32·3
Sr	666	99·7	654	956	866	446	484	768	698	556	627	726	915
Y	49·8	14·7	41·6	42·5	33·6	21·8	25·1	26·8	30·1	24·0	25·5	30·6	34·4
Zr	246	521	304	322	225	118	120	221	200	158	160	249	228
Nb	81·2	151	104	97·0	66·4	33·4	34·7	72·4	77·4	57·9	61·2	85·2	72·7
Cs	0·39	0·36	0·22	0·20	0·19	0·04	0·10	0·30	0·47	0·43	0·20	0·17	0·16
Ba	615	1061	1079	755	464	310	307	495	585	467	528	490	540
La	72·9	24·5	53·3	68·4	44·7	22·3	24·5	42·1	42·8	33·2	36·9	50·6	46·9
Ce	95·5	46·9	111	139	87·1	45·6	47·9	80·5	84·0	64·3	70·7	98·4	95·1
Pr	14·3	5·39	15·5	18·0	11·2	5·93	6·22	9·71	10·3	7·75	8·67	12·3	12·5
Nd	51·9	18·6	60·8	68·3	44·8	23·9	24·9	36·8	39·6	29·4	33·1	43·9	48·5
Sm	9·26	3·31	12·4	13·0	9·05	4·95	5·15	7·09	7·55	5·65	6·33	8·10	9·64
Eu	3·08	1·19	4·63	4·43	3·16	1·82	1·87	2·40	2·63	1·90	2·17	2·55	3·39
Gd	9·10	2·84	11·05	11·05	8·08	4·66	4·94	6·12	6·57	5·08	5·62	6·97	8·26
Tb	1·30	0·44	1·59	1·57	1·15	0·67	0·72	0·85	0·93	0·74	0·81	1·01	1·16
Dy	6·74	2·75	7·91	7·75	5·75	3·74	4·03	4·54	4·93	3·95	4·20	5·12	5·67
Ho	1·37	0·55	1·48	1·43	1·06	0·69	0·76	0·81	0·90	0·75	0·79	0·97	1·00
Er	3·51	1·66	3·66	3·47	2·63	1·84	2·03	2·16	2·43	1·99	2·07	2·46	2·49
Yb	2·66	1·62	2·80	2·57	1·90	1·46	1·61	1·68	1·91	1·64	1·67	1·97	1·71
Lu	0·39	0·21	0·39	0·35	0·25	0·16	0·18	0·22	0·26	0·21	0·21	0·26	0·22
Hf	5·12	9·78	5·96	6·19	4·59	2·43	2·48	4·26	3·73	3·08	3·10	4·85	4·20
Ta	6·59	11·97	7·72	7·47	5·76	2·30	2·28	5·97	6·18	4·06	4·30	6·26	5·64
Pb	2·17	5·19	3·21	2·91	1·99	0·94	0·92	2·15	1·88	1·51	1·60	2·09	1·84
Th	5·44	6·67	7·39	6·49	4·04	1·89	1·92	4·59	4·16	3·58	3·55	5·24	3·52
U	1·62	1·03	1·90	1·73	0·91	0·55	0·54	1·24	1·16	0·97	0·94	1·12	0·78
$^{87}Sr/^{86}Sr$	0·70339		0·70351	0·70350	0·70355	0·70326	0·70331	0·70343	0·70337	0·70333	0·70337	0·70353	0·70350
$^{143}Nd/^{144}Nd$	0·51294		0·51291	0·51290	0·51290	0·51295	0·51294	0·51292	0·51292	0·51292	0·51293	0·51291	0·51290

Table 1 continued

Sample no.:	BHVO-1	Deviation	BIR-1	Deviation	BHVO-2	Deviation
wt %						
SiO_2	50·06	0·12	48·09	0·13	49·32	0·58
TiO_2	2·79	0·08	0·97	0·01	2·67	0·06
Al_2O_3	13·77	0·03	15·76	0·26	13·53	0·03
Fe_2O_3	12·34	0·11	11·51	0·21	12·03	0·27
MnO	0·17	0	0·17	0·01	0·16	0·01
MgO	7·25	0·02	9·69		7·17	
CaO	11·57	0·17	13·58	0·28	11·23	0·17
Na_2O	2·27	0·01	1·79	0·03	2·71	0·49
K_2O	0·52	0	0·02	0·01	0·51	0·01
P_2O_5	0·29	0·02	0·03	0·01	0·29	0·02
LOI						
Total	101·03		101·61		99·62	

Sample no.:	*n*	BHVO-2	2SD
$^{87}Sr/^{86}Sr$	22	0·703480	0·000034
$^{143}Nd/^{144}Nd$	19	0·512976	0·000015

Sample no.:	BHVO-1	Deviation†	BIR-1 ($n=3$)	Deviation†	BHVO-2 ($n=3$)	Deviation
ppm						
Sc			47·4	4·41	35·0	2·97
V			329	10·1	324	7·13
Cr			391	0·43	303	23·3
Co			54·5	2·49	46·3	1·34
Ni			197	31·1	137	17·6
Cu			152	33·5	168	40·8
Zn			68·2	3·77	102	0·82
Mo			0·04	0·03	4·31	0·31
Rb			0·22	0·02	9·39	0·28
Sr			109	0·38	402	5·80
Y			17·3	1·72	29·0	3·00
Zr			14·9	0·86	185	12·5
Nb			0·55	0·00	19·9	1·83
Cs			0·00	0·00	0·10	0·00
Ba			6·43	0·71	132	1·39
La			0·58	0·03	15·5	0·35
Ce			1·88	0·04	38·0	0·48
Pr			0·34	0·03	5·44	0·09
Nd			2·35	0·03	24·7	0·19
Sm			1·07	0·05	6·23	0·16
Eu			0·46	0·07	2·03	0·04
Gd			1·88	0·01	6·34	0·10
Tb			0·32	0·04	0·95	0·03
Dy			2·50	0·01	5·28	0·03
Ho			0·55	0·01	0·99	0·01
Er			1·68	0·02	2·54	0·00
Yb			1·57	0·08	1·93	0·07
Lu			0·18	0·07	0·20	0·08
Hf			0·57	0·01	4·35	0·01
Ta					1·25	0·11
Pb			2·99	0·11	1·61	0·01
Th			0·03	0·00	1·24	0·02
U			0·01	0·00	0·41	0·01

*Volcano-stratigraphy from Azevedo & Ferreira (1999).
†Deviation refers to preferred GeoRem values (Jochum & Nohl, 2008).

Nd was loaded as a nitrate onto double rhenium filaments and analysed with an evaporation filament current of 1200-1600 mA and a signal of 0·5-10 V. Reference

materials BHVO-2 and JMC 321 (n = 15) were also analysed, yielding $^{143}Nd/^{144}Nd$ ratios close to published values (Table 1). External precision was determined using JMC 321, which gave $^{143}Nd/^{144}Nd$ = 0·511115 (2SD = 0·000047) during the time of the analyses. Ratios were normalized to $^{146}Nd/^{144}Nd$ = 0·7219 to correct for mass fractionation.

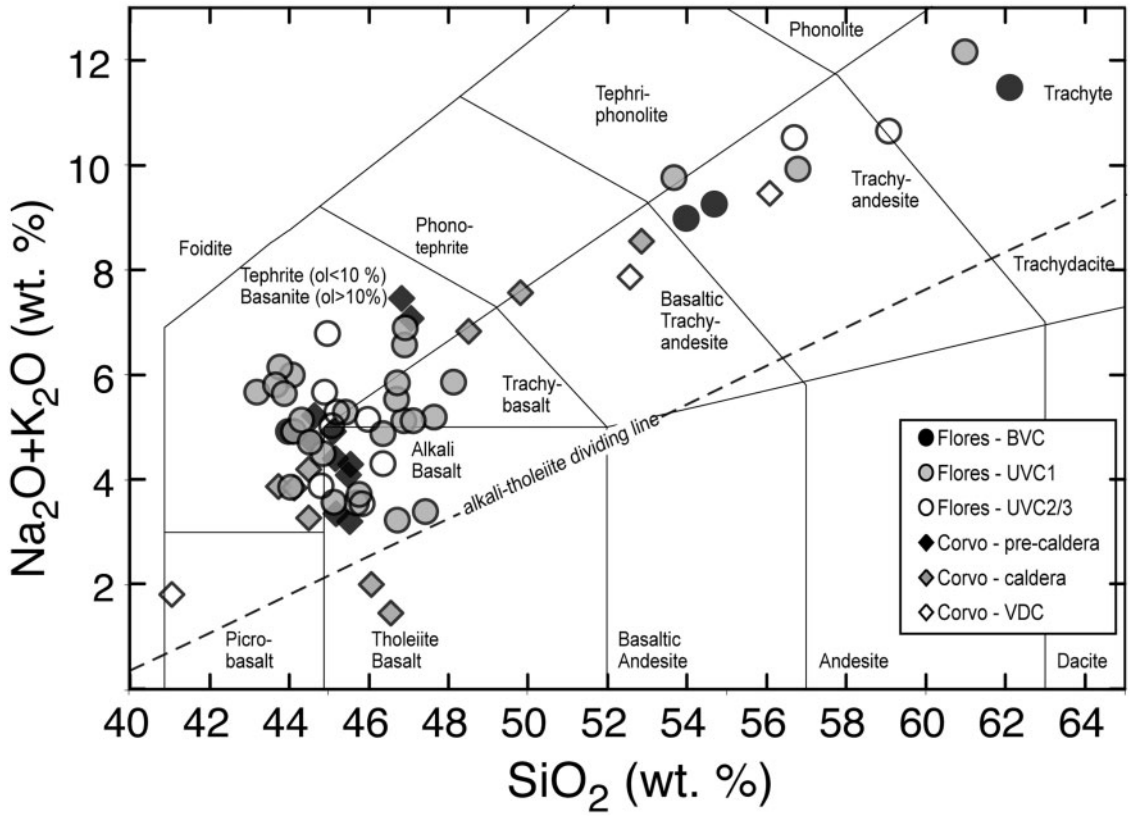

Fig. 3. Volatile-free total alkalis vs SiO2 (TAS) diagram with the IUGS classification after Le Maitre et al. (1989). The stratigraphic subdiv- isions for Flores are adopted from Azevedo & Ferreira (2006). The dividing line between alkaline and tholeiitic compositions is from Macdonald (1968).

2.4 RESULTS

2.4.1 Petrography

The rocks analysed from both islands range in composition from alkali basalt to trachyte following the TAS classification of Le Maitre et al. (1989) (Fig. 3). However, three basalts plot in the tholeiitic basalt field and were identified in the field as clinopyroxene-dominated cumulate rocks. The broad trend that characterizes the more primitive rocks narrows in TAS compositional space towards the more evolved trachyte compositions (Fig. 3). No compositional gap is observed on either island. A summary of the petrography of representative samples is given in Table 2.

Table2: Summarized petrography of selected samples from Flores (FL-09-xx) and Corvo (C-09-xx).

Sample	Rock type	Description of lavas
Pre-caldera stage		
C-09-01	Alkali basalt	Fresh lava flow with ~15% cpx (pheno- and xenocrystals up to 7 mm), ~5% altered Ol (<2 mm), 15% Pl phenocrysts (<3 mm), <1% Fe-Ti oxides
C-09-02	Tephrite	Highly vesicular (20%, up to 2 cm) lava, cryptocrystalline matrix with <2% Pl (<1 mm)
C-09-18	Tephrite	Lower flow of an eruption sequence, up to 1 cm sized vesicles (15%), Cpx up to 7 mm (10%), ~15% Pl phenocrysts (<1 mm) and xenocrystals (<3 mm), ~3% altered Ol, dense matrix
C-09-20	Alkali basalt	Ankaramitic basalt, fine-grained dense matrix, large vesicles (5%, <7 mm), ~10% Cpx (xenocrystals up to 2 cm), ~2% Ol, <1% Fe-Ti oxides
Caldera related		
C-09-08	Basaltic trachyandesite	Scoriaceous vesicular trachyandesite, weathered surface, glassy pumice (<2%), ~2% Pl xenocrystals
C-09-09	Alkali basalt	Fresh dense lava flow, evenly distributed Ol and Cpx (10%) up to 7 mm in size
C-09-13	Ankaramite basalt	Fresh ankaramitic flow, ~20% large idiomorphic Cpx (<1 cm), 5% altered Ol, Fe-Ti oxides disseminated in matrix (<1%)
*BVC**		
FL-09-06	Alkali basalt	Altered medium- to coarse-grained mafic composition, ~20% Pl up to 7 mm, ~20% weathered Cpx (<5 mm), relics of altered Ol (<2%)
FL-09-07	Trachyte	Massive intermediate flow, dense, ~30% Pl pheno- and xenocrystals, ~1% Bt (<1 mm)
UVC1		
FL-09-23	Alkali basalt	Fresh, vesiculated but dense basalt flow, occasional mafic cumulates (<1%), ~3% Cpx, ~3% Pl, <1% Ol, Fe-Ti oxides disseminated (≪1 mm)
FL-09-26	Alkali basalt	Fresh basaltic flow at the base of a sequence, fine-grained, ~3% Cpx (<2 mm), ~5% Pl <2 mm), ~1% Ol (<1 mm)
FL-09-59	Tephrite basanite	Scoriaceous flow, ~20% vesicles, fine-grained dense matrix, ~3% Pl, ~2% Cpx phenocrystals
UVC2-3		
FL-09-32	Trachybasalt	Fresh mafic composition, ~4% Ol xenocrystals up to 3 mm, ~2% Cpx (<3 mm), occasional (~1%) Pl laths up to 2 mm
FL-09-41	Alkali basalt	Fresh porous basalt, cm-sized Cpx ~2%, vesicular matrix, ~1% large Pl (<8 mm) xenocrystals enclosing small Cpx, ~1% Ol phenocrystals (<1 mm)
FL-09-42	Alkali basalt	Vesicular fresh basalt, ~5% Cpx up to 5 mm, ~3% Pl crystals (<3 mm), ~1% altered Ol, occasional Fe-Ti oxides

*Stratigraphy after Azevedo & Ferreira (1999).

2.4.1.1 Primitive lavas and ankaramitic cumulates

The primitive rocks from both islands are alkali-basalts, with the exception of three tholeiitic basalts (two from Corvo and one from Flores), which are characterized by megacrysts of clinopyroxene and olivine. The basalts en- compass a range in MgO contents between 5 and 18 wt %, though the rocks from Corvo are generally more primitive than those from Flores. The xeno- and phenocrysts of olivine, clinopyroxene and plagioclase are notably larger (up to 2 cm) in the Corvo basalts (Table 2). The matrix of all the basalts is cryptocrystalline to finely crystalline and plagioclase-dominated. Glass is absent in the groundmass, but small melt inclusions can be found in the iron-magnesium silicate phases. However, these melt inclusions cannot be linked to any specific generation of these minerals (i.e. xeno- or phenocryst). Olivines and clinopyroxene are usually normally zoned. The Corvo samples with MgO concentrations higher than 12 wt % (e.g. samples C-09-03, -05, -10 and -13) show evidence, such as

aggregation and the xenomorphic shape of the crystals (Fig. 4e), for accumulation of olivine and clinopyroxene. Xenocrystic olivines have corroded cores and are often overgrown by clinopyroxene. Large xenocrysts of olivine and clinopyroxene are also found in the lower MgO Corvo basalts, but their abundance is more restricted (Fig. 4e-g).

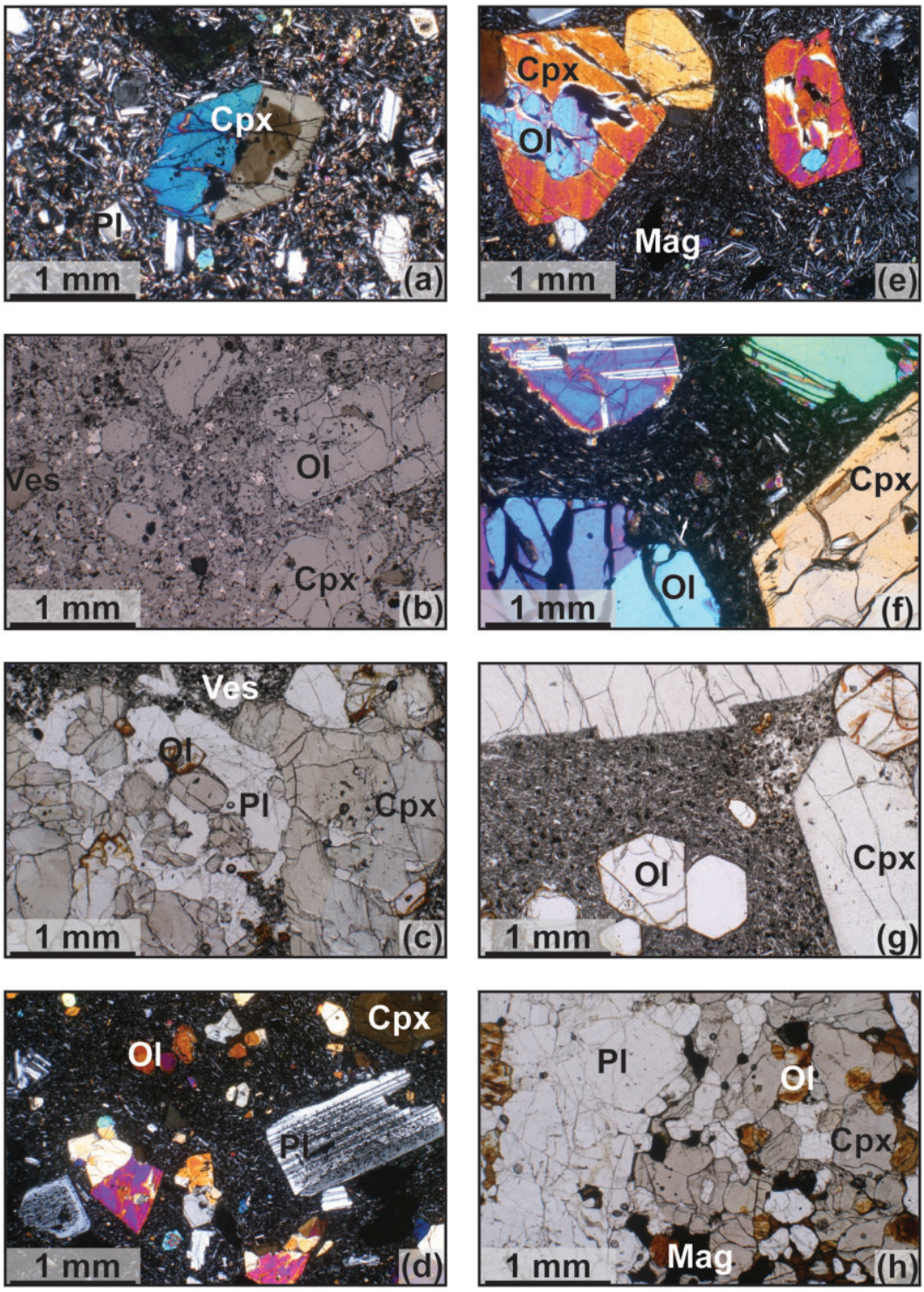

Fig. 4. Representative photomicrographs from Flores (left) and Corvo (right): (a) zoned clinopyroxene (Cpx) under crossed polars, FL-09-08; (b) opaque phases surrounding olivine (Ol) and disseminated in the

matrix, reflected light, FL-09-23; (c) plagioclase (Pl), Cpx and Ol aggre- gate in FL-09-26; (d) inclusions in plagioclase, crossed polars, FL-09-41; (e) Ol overgrown by Cpx; magnetite (Mag) appears opaque; C-09-06; (f) Ol and hour-glass sector zoned Cpx crystals, crossed polars C-09-07; (g) ankaramitic cumulate with megacrysts of Cpx and cor- roded Ol C-09-13; (h) gabbroic cumulate enclave with hypidiomorphic plagioclase, olivine and clinopyroxene crystals C-09-17.2.

2.4.1.2 Intermediate rocks and trachytes

The more evolved rocks from Flores and Corvo tend to belong to the younger volcanic cycles and, compared with the basalts, show greater evidence for explosive eruption styles, such as fragmented crystals and higher vesicularity (up to 30 vol. %). Using the TAS classification they range from trachybasalt to trachyte in composition (Fig. 3, Table 1). These rocks typically contain olivine, clinopyroxene, magnetite and plagioclase as abundant phenocrysts. A small amount of reversely zoned clinopyroxene is present in some of the trachytic lavas, but the majority (>90%) of the crystals are normally zoned, similar to the basaltic lavas. Apatite is an accessory phase in the more evolved rocks and can be found together with plagioclase and clinopyroxene phenocrysts. Olivine crystals often have iddingsitized rims and cracks that are usually filled with iron oxides. As the rocks evolve to higher silica content, plagioclase becomes more dominant (Fig. 4). Hydrous phases are observed only as alteration products of clinopyroxene in the form of kaersutitic amphiboles (Table 3) in young scoriaceous rocks in the caldera of Corvo and as pseudomorphs in young trachytic basalts on Flores.

2.4.1.3 The Vila do Corvo flank eruption and hosted cumulates

The Vila do Corvo flank eruption is thought to represent the most recent volcanic activity on Corvo (Fig. 2). Age estimates place this eruption at 580 ka (França et al., 2006a). Based on the TAS classification, the most primitive rock analysed here is a gabbroic enclave from this flank eruption. The host lava is altered and finely crystalline to aphyric, whereas the enclave is characterized by xenomorphic crystal shapes (Fig. 4h) and is interpreted to be a cumulate. Relatively unaltered samples of the host lava have evolved trachyandesite compositions, making this one of the most evolved rocks on Corvo. This flow carries abundant ovoid enclaves that vary in size from roughly fist-sized to ~30 cm. The chemical characteristics of the host lava and the enclave are summarized in Table 1.

Table 3: Representative mineral compositions determined by EMPA.

Sample no.:	LLD (wt %	C-09-01	C-09-07	C-09-10	C-09-17.2	C-09-01		C-09-07		C-09-10		C-09-17.2	C-09-08	C-09-01	C-09-07	C-09-06
Island:	oxide)	Corvo	Corvo	Corvo	Corvo	Corvo		Corvo		Corvo		Corvo	Corvo	Corvo	Corvo	Corvo
Volcano-stratigraphy:		Pre-caldera	Pre-caldera	Caldera	VDC	Pre-caldera		Pre-caldera		Caldera		VDC	Caldera	Pre-caldera	Pre-caldera	Pre-caldera
Mineral:		Ol	Ol	Ol	Ol	Cpx core	Cpx rim	Cpx core	Cpx rim	Cpx core	Cpx rim	Cpx	Kaer	Pl	Pl	Pl
SiO_2	0·08	40·01	40·81	40·21	37·52	51·92	49·63	48·88	49·29	51·73	49·47	48·32	41·25	46·95	46·67	51·74
TiO_2	0·03				0·04	0·52	1·29	1·89	1·34	0·68	1·12	2·06	5·09	0·05	0·05	
Al_2O_3	0·03		0·04	0·08	0·05	2·73	6·03	6·27	6·01	3·02	5·14	5·33	10·92	33·31	32·61	29·66
Cr_2O_3	0·06			0·08		0·98	0·39	0·10	0·70	0·40	0·62	0·06				
FeO	0·08	14·40	11·48	9·67	25·92	1·74	3·09	4·77	3·97	1·81	2·32	4·48	3·08	0·53	0·51	0·71
Fe_2O_3						2·03	1·84	1·66	1·62	2·14	2·38	2·98	14·33			
MgO	0·11	45·25	47·32	49·11	36·31	17·01	14·68	13·88	14·32	16·68	15·33	13·42	10·73			
MnO	0·06	0·23	0·21	0·17	0·50	0·07	0·09	0·12	0·12	0·11	0·07	0·21	0·43			
CaO	0·03	0·34	0·36	0·41	0·06	22·59	23·09	22·54	22·46	23·06	22·56	22·25	11·19	17·42	17·28	13·00
Na_2O	0·03				0·03	0·31	0·33	0·35	0·37	0·26	0·33	0·54	2·97	1·73	1·75	4·04
K_2O	0·03												1·21	0·08	0·08	0·25
NiO	0·09	0·09	0·21	0·30												
Total		100·38	100·47	100·06	100·43	99·94	100·51	100·47	100·24	99·93	99·37	99·65	101·20	100·08	98·98	99·46
Mg#		85	88	90	71	95	89	84	87	94	92	84				

Sample no.:	LLD (wt	C-09-08		C-09-17.2	C-09-01	C-09-05	C-09-10	C-09-08	C-09-01	C-09-05		C-09-08	
Island:	% oxide)	Corvo		Corvo	Corvo	Corvo	Corvo	Corvo	Corvo	Corvo		Corvo	
Volcano-stratigraphy:		Caldera		VDC	Pre-caldera	Pre-caldera	Caldera	Caldera	Pre-caldera	Pre-caldera		Caldera	
Mineral:		Pl	Pl	Pl	Mag-Chr	Mag-Chr	Mag	Ti-Mag	Ilm	Ilm	Ilm	Ilm	Ilm
SiO_2	0·08	61·24	54·87	47·71	0·07	0·05	0·10	0·06	0·06	0·98	0·94	0·06	0·01
TiO_2	0·03	0·04	0·09	0·04	2·16	1·30	1·92	17·19	14·00	48·41	47·82	20·65	50·38
Al_2O_3	0·03	23·61	27·98	32·24	25·58	18·65	42·05	3·50	0·94	0·50	0·32	1·82	0·06
Cr_2O_3	0·06				31·08	32·52	14·86	1·90	0·41				
FeO	0·08	0·26	0·32	0·33	19·90	22·73	13·68	41·92	8·57	36·05	35·27	11·65	32·65
Fe_2O_3					10·11	16·33	9·93	30·10	71·60	7·73	7·69	59·64	7·54
MgO	0·11				12·10	8·73	17·35	3·05	1·95	4·88	5·17	3·60	6·66
MnO	0·06							0·85	0·70	0·86	0·79	0·93	0·80
CaO	0·03	4·91	10·47	15·80	0·04			0·05	0·05	0·15	0·26	0·03	
Na_2O	0·03	8·32	5·98	2·56						0·17	0·15	0·12	
K_2O	0·03	1·46	0·35	0·10						0·10	0·10		
NiO	0·09				0·10	0·09	0·23						
Total		99·89	100·16	98·86	101·13	100·40	100·12	98·63	98·28	99·83	98·51	98·51	98·10

Sample:	LLD (wt	FL-09-23	FL-09-26	FL-09-41	FL-09-42	FL-09-23	FL-09-26		FL-09-41	FL-09-42	FL-09-06	FL-09-44		FL-09-23	FL-09-26
Island:	% oxide)	Flores	Flores	Flores	Flores	Flores	Flores		Flores	Flores	Flores	Flores		Flores	Flores
Stratigraphy		UVC1	UVC1	UVC2/3	UVC2/3	UVC1	UVC1		UVC2/3	UVC2/3	BVC	UVC2/3		UVC1	UVC1
Mineral:		Ol	Ol	Ol	Ol	Cpx	Cpx core	Cpx rim	Cpx	Cpx	Cpx	Kaer		Pl	Pl
SiO_2	0·08	40·74	40·33	40·25	40·60	48·70	48·11	46·82	45·30	48·89	52·26	41·30	40·48	55·39	56·79
TiO_2	0·03					1·51	2·21	2·63	2·59	1·49	0·83	5·52	5·51		
Al_2O_3	0·03	0·06	0·06	0·08	0·03	6·89	5·58	6·72	10·44	4·89	3·09	11·03	10·84	27·37	26·11
Cr_2O_3	0·06			0·06	0·09	0·36	0·09		0·10	0·18	0·23				
FeO	0·08	12·78	13·83	11·80	9·71	3·39	4·73	5·24	3·95	3·66	3·19	0·68	12·70	0·35	0·21
Fe_2O_3						2·85	2·84	3·41	3·15	3·77	0·94	13·51	0·00		
MgO	0·11	46·35	45·65	47·99	49·11	14·24	13·44	12·49	12·26	13·75	16·27	12·51	12·66		
MnO	0·06	0·16	0·18	0·14	0·14	0·15	0·19	0·19	0·17	0·16	0·08	0·47	0·45		
CaO	0·03	0·33	0·34	0·36	0·31	22·39	22·08	21·98	22·50	22·60	23·26	11·49	11·35	10·33	9·31
Na_2O	0·03					0·41	0·51	0·54	0·36	0·53	0·25	2·92	2·98	5·37	6·09
K_2O	0·03											1·03	1·02	0·32	0·42
NiO	0·09	0·20	0·22	0·19	0·19										
Total		100·69	100·71	100·89	100·19	100·93	99·78	100·02	100·84	99·94	100·41	100·48	97·98	99·14	98·93
Mg#		87	85	88	90	88	83	81	85	87	90				

Sample:	LLD (wt	FL-09-41	FL-09-42	FL-09-07		FL-09-23	FL-09-23	FL-09-26	FL-09-41	FL-09-41	FL-09-42	FL-09-42	FL09-44	FL-09-11	FL-09-69
Island:	% oxide)	Flores	Flores	Flores		Flores	Flores	Flores	Flores	Flores	Flores	Flores	Flores	Flores	Flores
Stratigraphy:		UVC2/3	UVC2/3	BVC		UVC1	UVC1	UVC1	UVC2/3	UVC2/3	UVC2/3	UVC2/3	UVC2/3	UVC1	UVC2/3
Mineral:		Pl	Pl	Kfs		Mag	Mag-Chr	Ti-Mag	Ti-Mag	Mag-Chr	Ti-Mag	Mag-Chr	Ilm	Ilm	Ilm
SiO_2	0·08	50·72	49·55	64·64	62·02	0·08	0·04	0·07	0·13	0·13	0·13	0·12	0·00	0·01	0·43
TiO_2	0·03			0·05	0·04	23·44	15·34	17·59	22·87	0·94	17·62	0·81	48·92	49·84	36·30
Al_2O_3	0·03	30·81	31·23	20·30	21·98	2·95	6·54	5·54	2·93	20·91	3·75	22·13	0·06	0·15	2·40
Cr_2O_3	0·06					4·82	17·74	0·08		41·74	0·11	41·99			
FeO	0·08	0·57	0·58	0·14	0·25	47·85	40·31	41·55	48·24	16·01	43·87	12·91	36·24	28·83	23·76
Fe_2O_3						16·98	16·04	30·27	21·80	7·20	30·11	7·10	9·33	13·21	32·38
MgO	0·11	0·14	0·12			3·40	3·94	4·18	2·58	13·04	2·47	15·17	3·56	8·49	5·33
MnO	0·06					0·73	0·66	0·49	0·94	0·44	0·70	0·38	1·60	0·81	
CaO	0·03	14·57	14·62	2·15	4·54	0·10	0·04		0·09		0·20		0·05		0·05
Na_2O	0·03	3·20	3·02	7·98	8·12				0·05				0·04		
K_2O	0·03	0·20	0·19	3·81	1·59										
NiO	0·09					0·10				0·14		0·16			
Total		100·21	99·29	99·07	98·53	100·45	100·65	99·78	99·63	100·55	98·96	100·75	99·81	101·34	100·64

Fe_2O_3 calculated assuming stoichiometry; for amphiboles after Droop (1987). LLD, lower limit of detection. VDC corresponds to Vila do Corvo flank. Stratigraphy for Flores is according to Azevedo & Ferreira (2006).

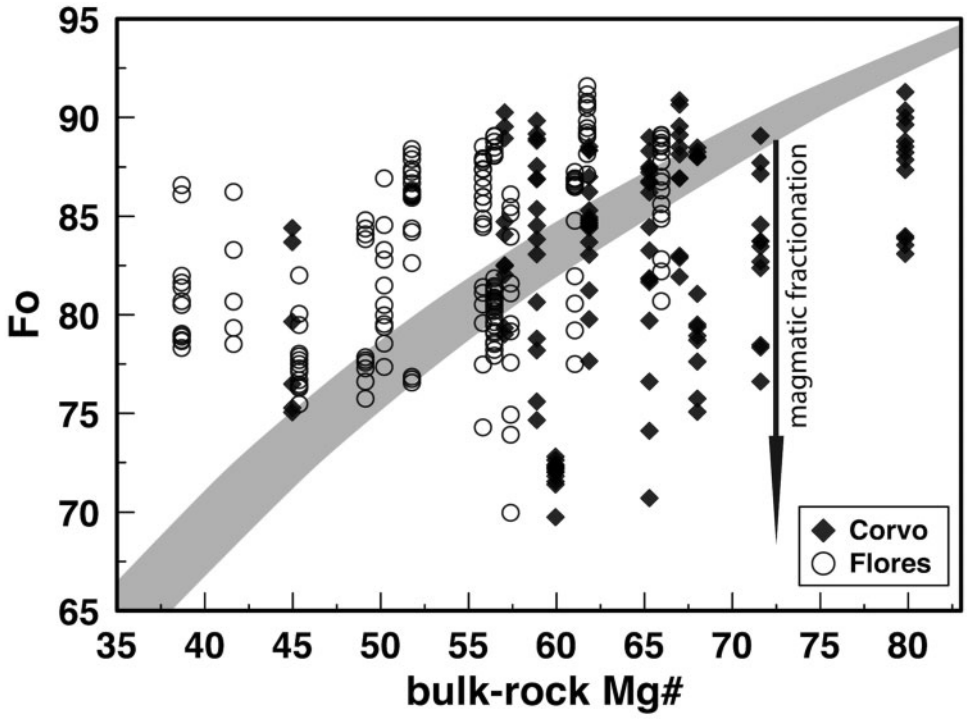

Fig. 5. Variation of the forsterite content of olivine versus bulk-rock Mg# (after Rhodes et al., 1979) in single lavas from Flores and Corvo. Olivines that are in equilibrium with the host lavas plot in the grey field, where equilibrium is based on the Fe^Mg exchange coefficient between the olivine and the host lava. The K_D value used here is 0·3 (±0·03).

2.4.2 Mineral chemistry

2.4.2.1 Olivine

A predominance of forsteritic olivines is characteristic of lavas from both islands (Table 3). The analysed olivine cores from Flores range from Fo_{69} to Fo_{91} (Fig. 5). The Corvo olivines range from Fo_{68} to Fo_{91}, whereas Fo_{68-73} is typical for the olivines in the gabbroic enclave (C-09-17.2) in the Vila do Corvo flank eruption (C-09-17.1). The lavas on Corvo contain only olivines between Fo_{71} and Fo_{91}, and are characterized by normal chemical zoning. Olivine rims from both islands extend to $Fo_{\sim 64}$. In summary, the olivines from Corvo are, on average, slightly more primitive. The highest abundance of olivine crystals that are in chemical disequilibrium with the host lavas is observed for lavas with bulk-rock Mg# between 55 and 67 (Fig. 5). NiO contents increase with increasing Fo content and whole-rock Mg#. However, the NiO concentration in the most primitive olivine cores (Fo_{89-91}) ranges from ~1000 to 2500ppm, which may be indicative of mixing between evolved and primitive magmas, as has also been observed in the eastern island of Sao Miguel (e.g. Beier et al., 2006).

2.4.2.2 Clinopyroxene

The clinopyroxenes from both islands are Ti-augites (Table 3). Like the olivines, their chemical composition is very restricted and they seem to be slightly more evolved in the lavas from Flores ($Wo_{38-46}En_{41-55}Fs_{03-16}$) compared with those from Corvo ($Wo_{40-46}En_{45-55}Fs_{02-11}$). However, this compositional distinction is very subtle (Fig. 6). Most crystals are slightly zoned with decreasing MgO and increasing TiO_2 and FeO contents from core to rim, but occasionally some crystals show reverse zoning. Faint hour-glass (or sector) zoning (e.g. Vernon, 2004) is observed occasionally (Fig. 4f) but is not reflected in the composition.

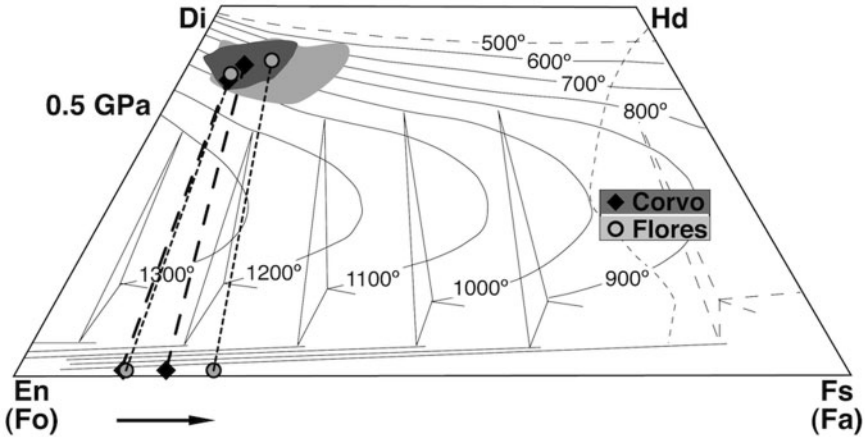

Fig. 6. Clinopyroxene compositions projected into the pyroxene quadrilateral with temperature contours after Lindsley (1983). The 0·5 GPa projection was chosen according to the pressure range obtained from samples with whole-rock MgO contents of around 5 wt %. Coexisting olivines are plotted on the En-Fs (Fo-Fa) base line for both primitive and evolved samples from both islands.

2.4.2.3 Feldspar

The feldspars from both islands are predominantly plagioclase; those from Flores have a total compositional range of $Ab_{12-66}An_{41-88}Or_{0-3}$. However, the basalts with the lowest whole-rock alkali contents contain two distinct plagioclase compositions: a more primitive plagioclase generation with An_{64-77} and a more evolved one with An_{41-51}. Only the trachytic lavas on Flores contain anorthoclase $Ab_{67-70}An_{10-13}Or_{19-23}$ (Table 3, Fig. 7). Corvo's feldspar compositional range is more restricted (bytownite-labradorite) and also more primitive ($Ab_{10-40}An_{60-90}Or_{0-2}$).

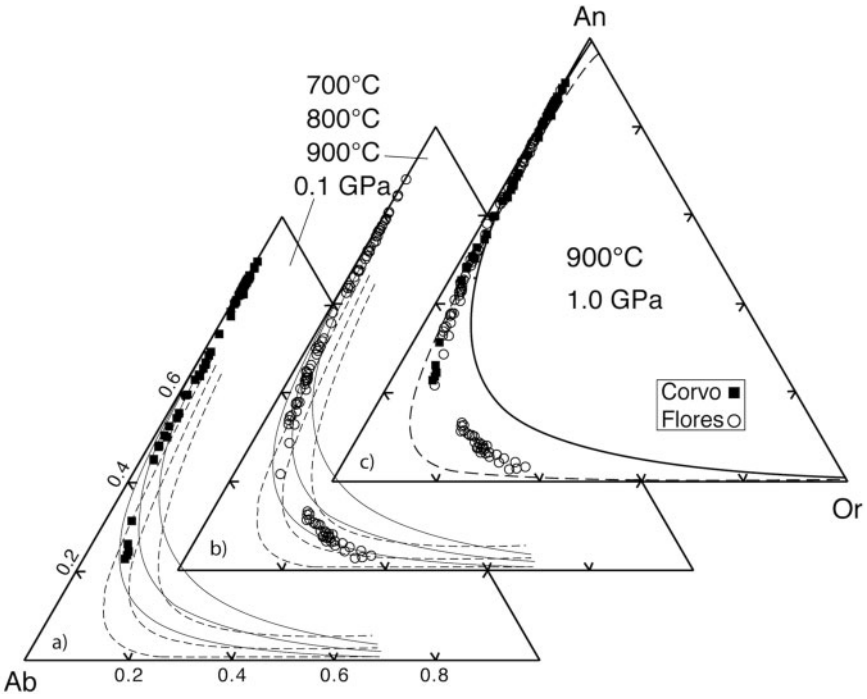

Fig. 7. Feldspar ternary diagram with temperature curves from the models of Benisek et al. (2010) (continuous lines) and Fuhrman & Lindsley (1988) (dashed lines). The 0·1 GPa projection reflects minimum pressure conditions, as the magmas most probably crystallize early plagioclase at greater depths and higher temperatures.

2.4.2.4 Fe-Ti oxides and spinels

Ilmenite, titanomagnetite and chrome-spinel are the opaque phases found in the matrix of the lavas from Flores and Corvo. They also occur around the rims of, and as inclusions in, the Fe-Mg silicates. The more mafic rocks contain proportionally more spinel (1-2%), whereas the trachytic lavas show a dominance of ilmenite (~1%) over titanomagnetite and chrome-spinel (<0.5%) (Tables 2 and 3).

2.4.2.5 Amphibole

Idiomorphic to hypidiomorphic Ti-rich kaersutitic amphiboles were observed in one basaltic trachyandesite on Corvo and in one trachyte on Flores (C-09-08, FL-09-44; Table 3). These partially to completely replace original Ti-augite, which is most clearly identified by the skeletal (pseudomorphic) clinopyroxene crystal shape; however, some cores of the original augite are also occasionally preserved. The kaersutites typically exhibit opaque rims of magnetite (e.g. Deer et al., 1992).

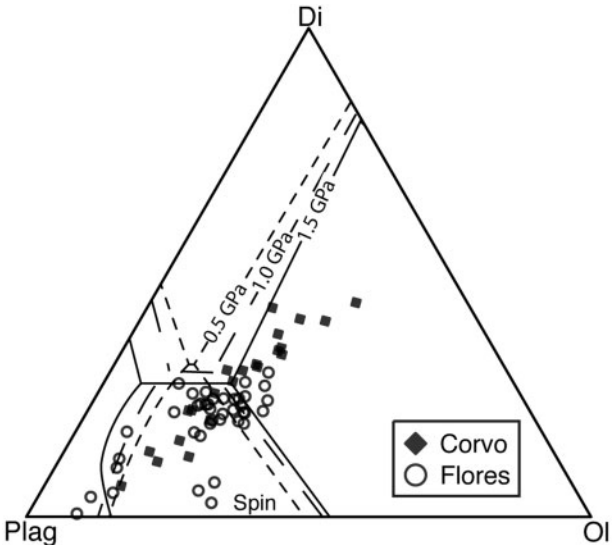

Fig. 8. Olivine-clinopyroxene-plagioclase phase diagram redrawn after Presnall et al. (1978), showing the calculated mineral proportions in the lavas from Flores and Corvo, determined using the method of Stolper (1980). The evolution of the lavas towards the plagioclase corner follows the change of liquidus boundaries with decreasing pressure. The three Corvo samples in the olivine field furthest away from the 1·5 GPa line represent the ankaramitic cumulates.

2.4.2.6 Biotite

Biotite was observed only in one mildly altered trachyte sample of the BVC unit of Flores (FL-09-07). The crystals occur in small (2-3mm) patches around the feldspars and in the matrix. They are brown to dark brown in colour with strong pleochroism. Smaller (51mm) single crystals are also disseminated throughout the matrix.

2.4.2.7 Accessory phases

Apatite needles with a maximum length of 1mm occur in the matrix and as inclusions in clinopyroxene and plagioclase, with increasing modal abundance in the intermediate to evolved rocks (1-5wt % MgO). A few larger apatite crystals were found in the caldera scoria cones of Corvo with sizes up to 5 mm (C-09-08).

2.4.3 Whole-rock geochemistry

2.4.3.1 Major and trace elements

Representative whole-rock major-element data are given in Table 1. The modal olivine-clinopyroxene-plagioclase abundance in all of the lavas was calculated using the method of Stolper (1980). The results are projected onto a phase diagram (Fig. 8), after Presnall

et al. (1978), and demonstrate a good agreement with the observed petrography. The lavas from Flores show a more variable trend when compared with those from Corvo; their average composition appears slightly more evolved.

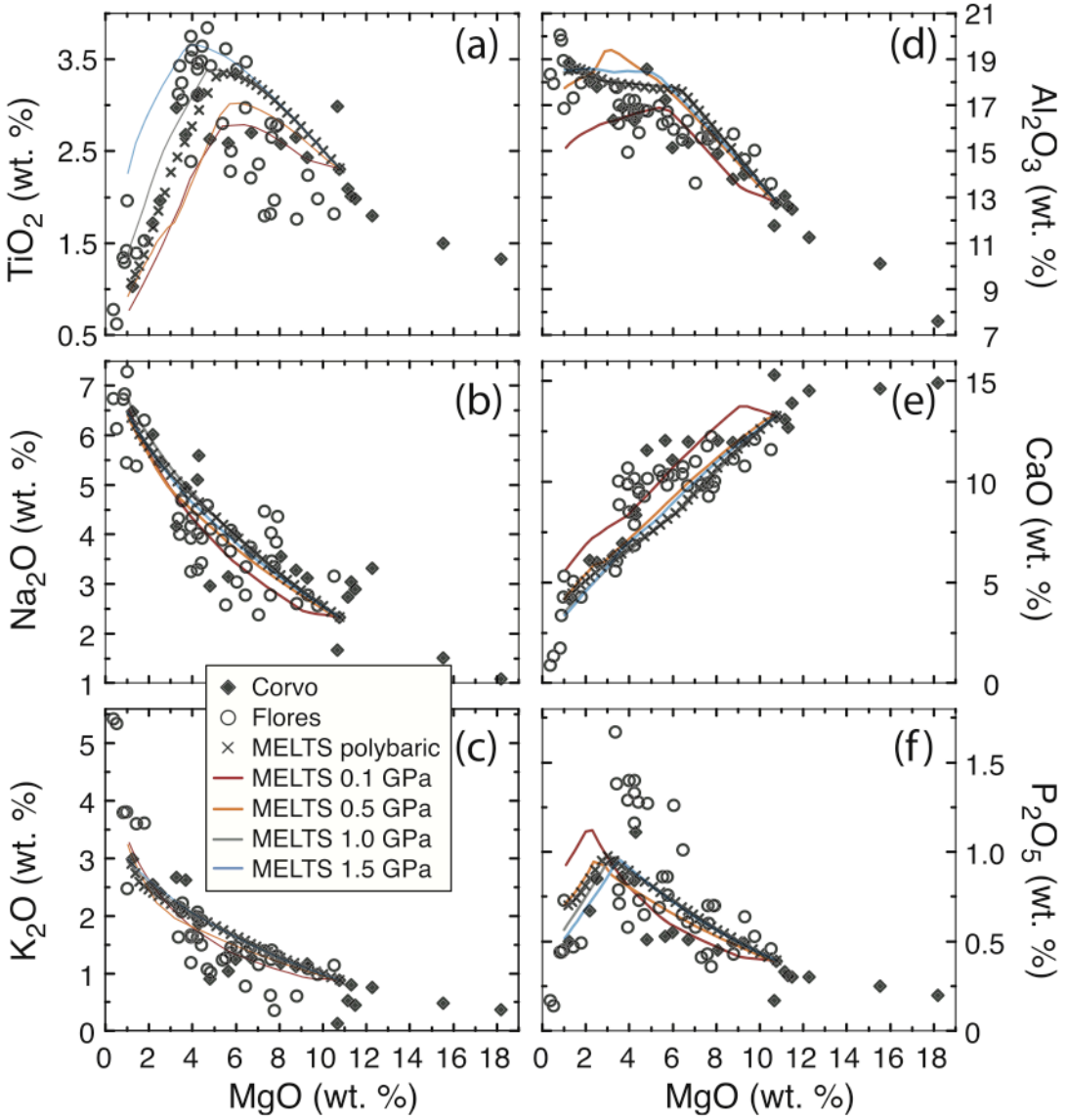

Fig. 9. Major-element contents versus MgO (wt %) for lavas from Flores and Corvo. Continuous lines represent the evolution of the liquid at different pressures modelled using the MELTS algorithm (Ghiorso & Sack, 1995; Asimow & Ghiorso, 1998), whereas the crosses represent a polybaric MELTS model. It should be noted that for all models shown, C-09-20 is the parental starting magma composition chosen for the calculations. Tick marks on the polybaric model represent 108C intervals. (See text for full details and model parameters.)

Bivariate plots of selected major-element oxides versus MgO wt % are used to investigate the evolutionary trends for the lavas from Flores and Corvo in Fig. 9. The two islands are comparable in their overall compositional range as MgO decreases from 12 to

4 wt %. Across this range SiO2 decreases slightly, from ~47 to 44 wt %, but then abruptly increases (up to 63 wt %) in lavas with 53 MgO (wt %) (not shown; refer to Table 1 and Fig. 3). CaO decreases over the entire MgO range with a slight positive inflection between 4 and 6 MgO wt %. P2O5 and TiO2 first increase to a maximum at 4-4·5wt % MgO, after which they decrease significantly as the com- positions evolve to lower MgO (Fig. 9a and f). FeOT (FeOT = 0·8998 x Fe2O3) shows a similar trend to TiO2; however, it does not increase as strongly between 4·5 and 12 MgO wt %. Al2O3 and alkali contents (Fig. 9b-d) increase towards lower MgO. A good correlation between Al2O3 and CaO is observed (Fig. 10a). The lavas from Flores form a dominant cluster at around 10 wt % CaO.

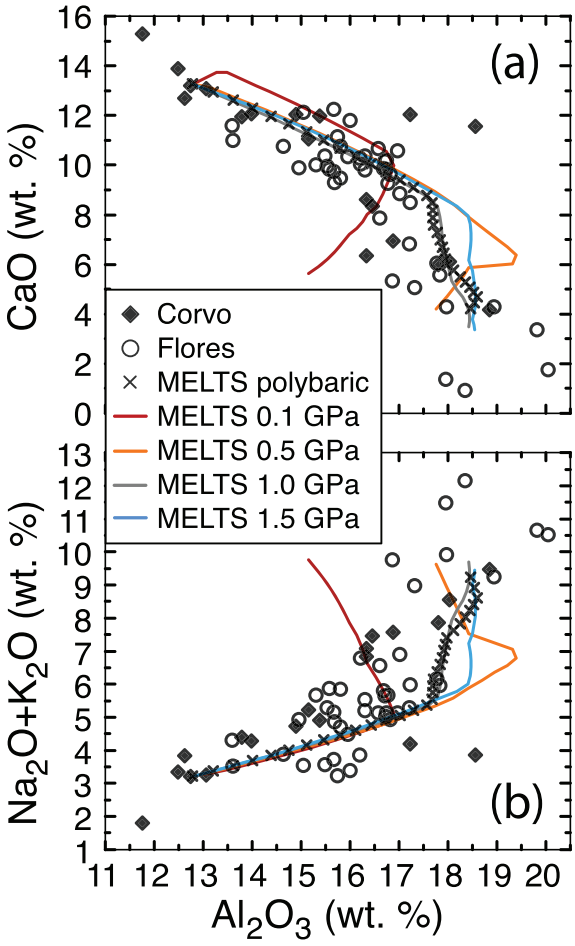

Fig. 10. Total alkalis and calcium contents versus Al2O3 (wt %) of Flores and Corvo lavas. Shown for comparison are model MELTS curves (see Fig. 9) at 0·1, 0·5, 1·0 and 1·5 GPa. Only samples with MgO <13 (wt %) are plotted to illustrate the models better.

Both lava suites show a positive correlation between MgO and Ni and Cr concentrations at MgO higher than 4 wt % (Fig. 11a and b). Maximum Ni concentrations of 250 and 300

ppm correspond to 10·5 and 11·1wt % MgO respectively (Table 1). Incompatible trace-element variations (La, Sr, Y, Zr) are shown in panels (c)-(e) of Fig. 11. These form negative correlations with MgO and the lowest concentrations are observed in the ankaramitic cumulate rocks from Corvo at ~15 and 18 wt % MgO. The observed trends for Corvo are better defined than the more scattered ones from the Flores suite. On Corvo, only sample C-09-17.2 deviates from the trends, and this can be explained by its gabbroic nature. The scatter in the Flores lavas cannot be attributed to relative age or location of the samples; this is discussed further below.

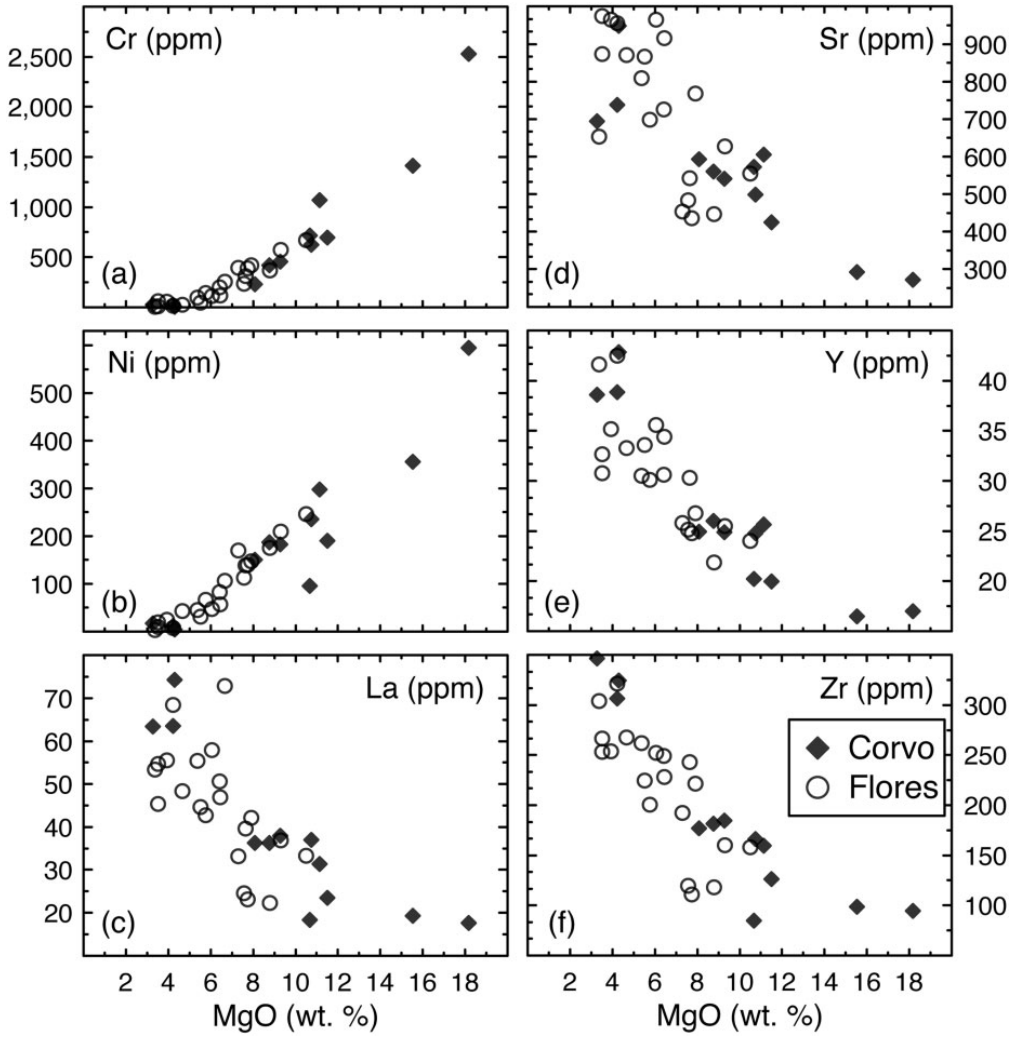

Fig. 11. Compatible (a, b) and incompatible (c-f) trace-element variations versus MgO (wt %) in the lavas from Corvo and Flores. The highest Cr and Ni contents correlate with the ankaramitic samples (C-09-10 and C-09-13). These two samples are also characterized by the lowest incompatible trace-element concentrations.

The same trace elements illustrated in Fig. 11 are plotted against the highly incompatible element Nb in Fig. 12. It should be noted that the x-axis is log-scaled to highlight the

differences between the Flores and Corvo trends and to emphasize the deviation of the most primitive cumulate rocks at the lowest Nb contents. Again, relatively clean trends are observed for the Corvo suite, whereas the Flores lavas show scatter, which is greatest for Sr and Y.

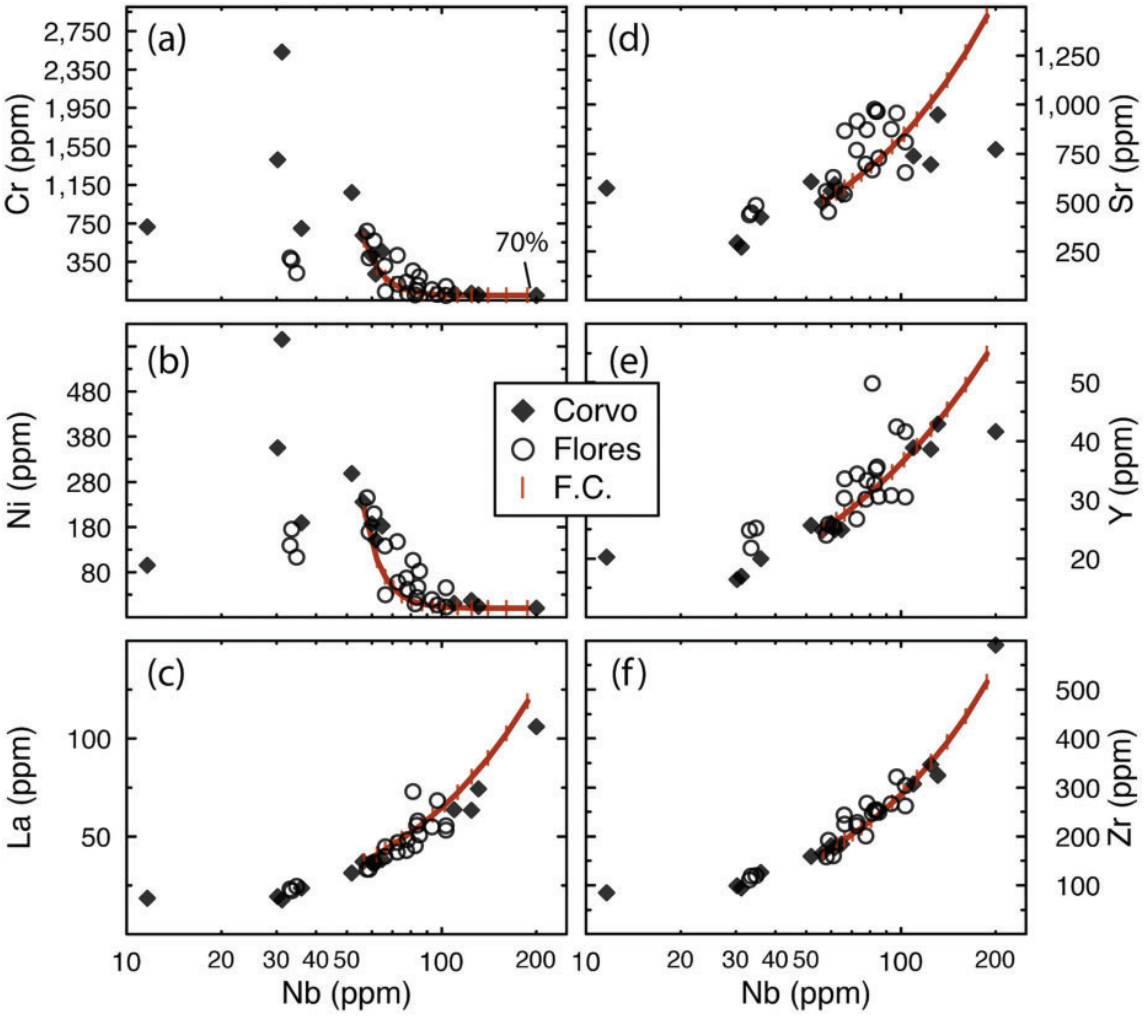

Fig. 12. Variation of Cr, Ni, La, Sr, Y and Zr versus Nb (ppm), where Nb is selected as a highly incompatible element to constrain the crystal fractionation history. A Rayleigh-fractionation model is represented by the continuous line with sample C-09-20 as the starting composition, stopping at 70% fractionation. Tick marks represent 5% increments of fractional crystallization. The fractionating assemblage used here is based on the petrographic observations and is composed of cpx-ol-plag-mag (modal %: ~30-3-5-1). Partition coefficients used to calculate the model are given in Table 7.

In terms of their primitive-mantle normalized incompatible trace-element patterns (Fig. 13), the lavas from both islands are enriched in Nb-Ta and La-Ce, whereas Zr and Hf show a relative depletion. Some Flores lavas also have negative Ti anomalies. Overall, the most primitive lavas from Flores appear to be somewhat more enriched in

incompatible trace elements compared with Corvo lavas with similar MgO concentrations. A slightly stronger depletion in the heavy rare earth elements (HREE) over light rare earth elements (LREE) is characteristic of Corvo.

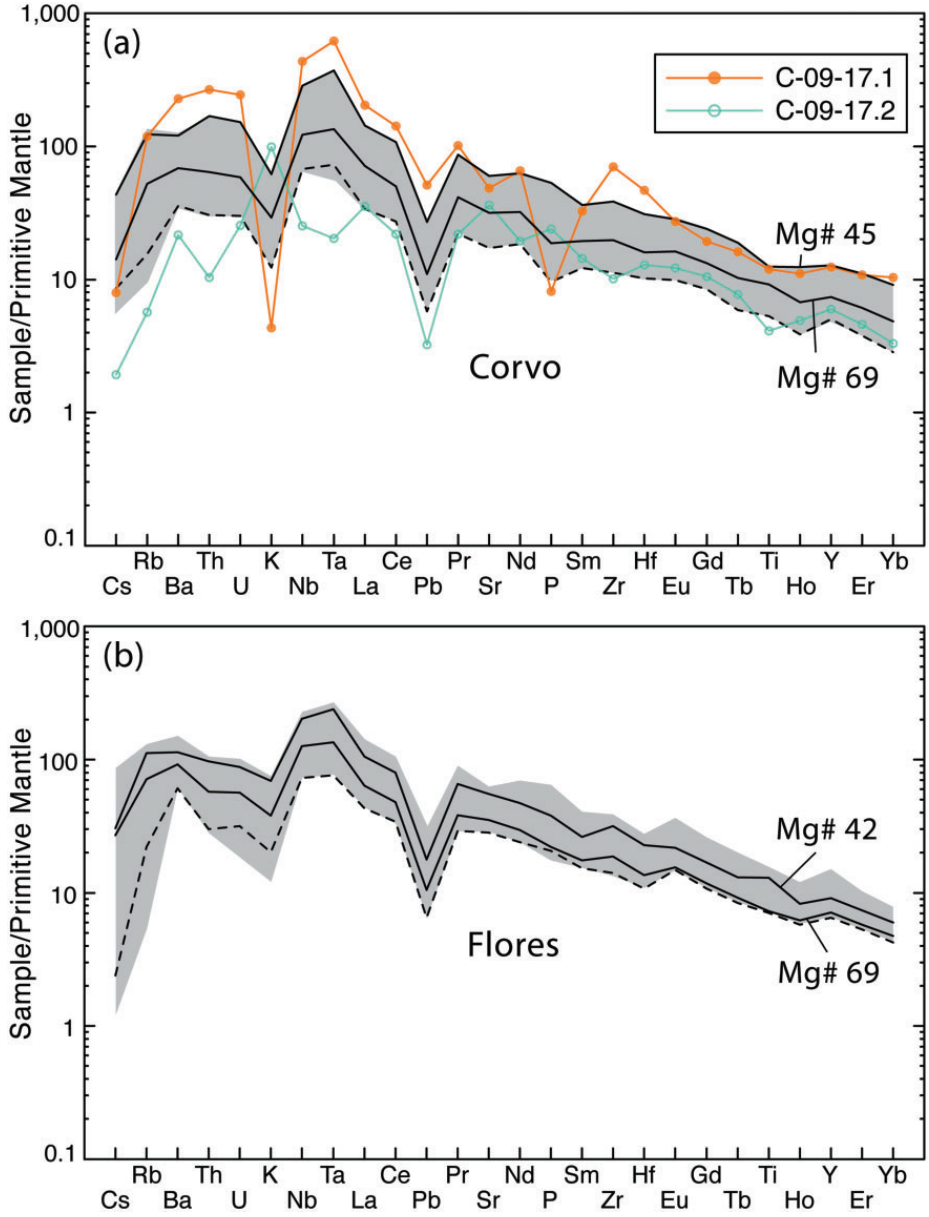

Fig. 13. Primitive mantle normalized (Sun & McDonough, 1989) multi-element plots showing (a) Corvo and (b) Flores lavas (grey fields). Each plot shows the evolution from a primitive sample (Mg# 69) towards an evolved composition (Mg# 45 and 42, respectively). Panel (a) also highlights the Vila do Corvo flank eruption showing the host lava (C-09-17.1) and the gabbroic cumulate (C-09-17.2). The dashed lines reflect accumulative rocks (ankaramites), which are more abundant in the Corvo suite. Both islands have comparable trace-element character- istics with negative K and Pb anomalies; however, slightly positive Eu and Y anomalies are more prominent in the Flores lava suite. Also, the more mobile large ion lithophile elements (Sr, Rb, Ba, K) reveal a different trace-element signature in the Flores rocks when compared with Corvo.

The variation of Dy/Yb and Nd/Sr versus Dy and Nd is sensitive to the depth of partial melting and fractionation, respectively (Fig. 14). Corvo lavas have a relatively restricted range in both diagrams, whereas the data from Flores scatter significantly. However, the trends, especially for Corvo, do not back-project towards the ankaramites as clearly as in Figs 11 and 12, but still fall within the observed overall range of compositions. The Dy/Yb plot suggests that there may be two compositional groups within the Flores samples, possibly reflecting differences in the presence of residual garnet during source melting (Fig. 14a).

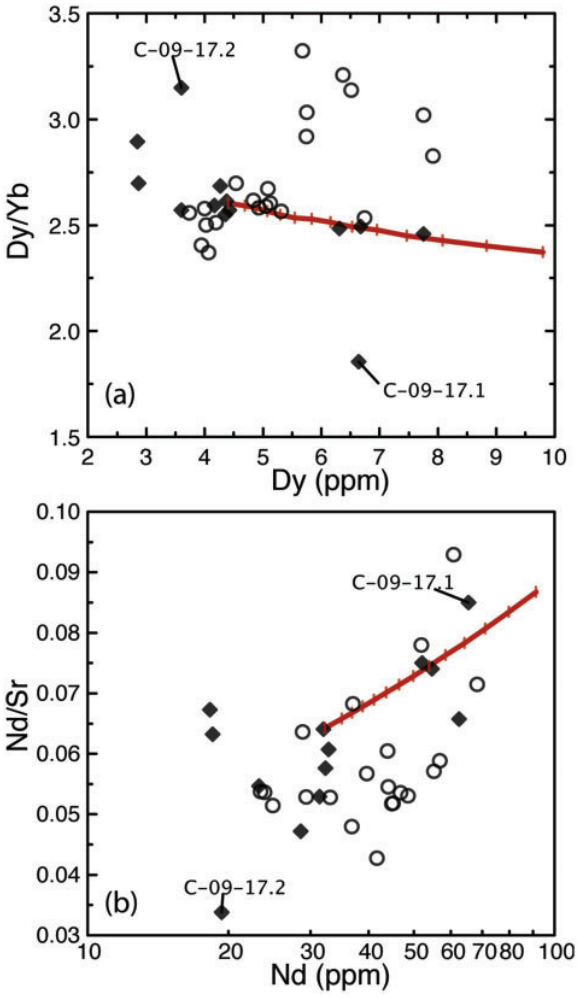

Fig. 14. Element-ratio plots for fractionation-sensitive elements in the Flores and Corvo magmatic systems. (a) Dy/Yb versus Dy indicates a similar differentiation path for both islands; however, a cluster of samples with higher Dy/Yb ratios from Flores may indicate a contri- bution from a different source or assimilation processes within the deep lithosphere. (b) Nd/Sr versus Nd also illustrates similar differentiation processes for both magmatic systems. The ankaramitic cumulates from Corvo have Dy ~3ppm and Nd ~20ppm. The Rayleigh-fractionation model shown by the continuous line uses the same parameters as that in Fig. 12. The tick marks represent 5% increments of fractional crystallization and the model trend stops at 70% total fractionation.

2.4.3.2 Sr-Nd isotope systematics

The lavas from Corvo and Flores are very similar in their Sr and Nd isotopic compositions. Lavas from Corvo appear to be relatively invariant in their $^{143}Nd/^{144}Nd$ ratios (~0·51293), whereas the Flores lavas form a broad negative trend of $^{87}Sr/^{86}Sr$ versus $^{143}Nd/^{144}Nd$, which is comparable with data from the eastern Azores islands of Pico and São Miguel (Fig. 15).

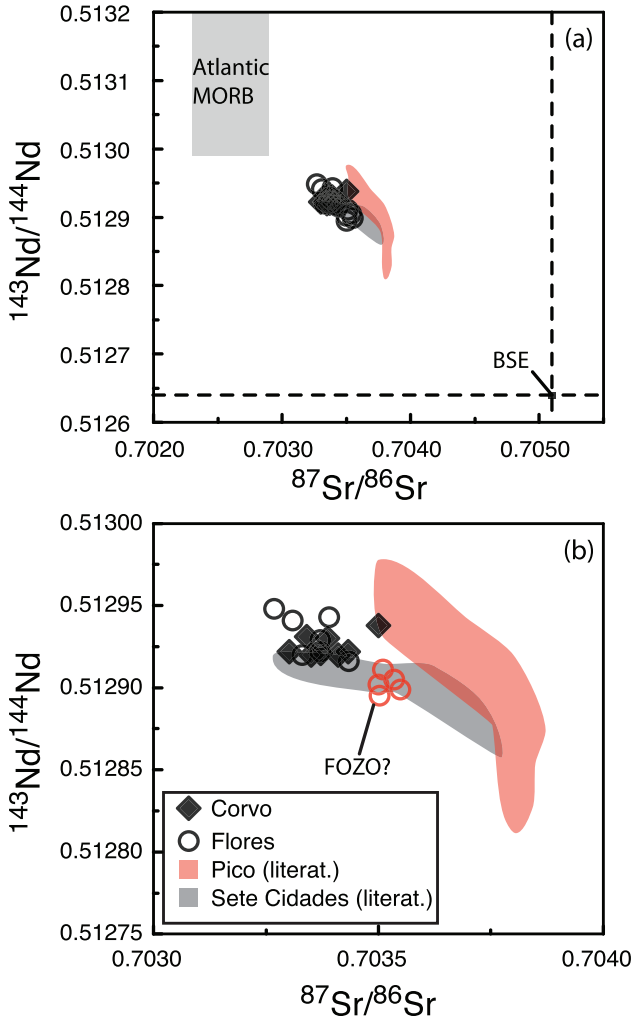

Fig. 15. Nd-Sr isotopic variations in the Flores and Corvo lavas. Literature data from Pico (red field) and Sete Cidades (Sao Miguel, grey field) are plotted for comparison (data from Turner et al., 1997; Beier et al., 2006, 2007). The samples plot within the mantle array (a) between Bulk Silicate Earth (BSE) and Atlantic MORB (data from Chauvel & Blichert-Toft, 2001). (b) Close-up of the Flores and Corvo data highlighting the differences between the two systems, with Flores trending towards more radiogenic $^{87}Sr/^{86}Sr$. A distinct group of Flores lavas is characterized as FOZO-like (red circles).

However, the Flores and Corvo data show a more restricted range in Sr and Nd isotope compositions and are more MORB-like when compared with the eastern Azores data.

The most radiogenic sample in Sr from Corvo (C-09-13, $^{87}Sr/^{86}Sr$ ~ 0·70350) is interpreted to be an ankaramitic cumulate; however, sea- water alteration could be the reason for this more radiogenic composition (e.g. Whipkey et al., 2000). Figure 15b reveals a distinct group of lavas from Flores (red symbols) that were predominantly sampled from a section of the stratigraphic unit UVC1 around the east and north coast of the island. It should be noted that these samples are characterized by higher TiO2 contents (refer to Table 1) and by differences in their trace-element ratios (see below). These characteristics are not restricted to samples from a discrete stratigraphic unit or location, but are found in lavas throughout the island.

2.5 QUANTIFICATION OF INTENSIVE PARAMETERS

Differentiation and crystallization of OIB is generally considered to take place near isobarically at shallow crustal depths (e.g. Widom et al., 1992; Ablay et al., 1998; Beier et al., 2006). However, we find that there is evidence for deeper, and arguably polybaric, processes occurring beneath Corvo and Flores. We have attempted to calculate intensive parameters for this magmatic system to provide constraints for subsequent major- and trace-element models for magmatic differentiation in the western portion of the Azores archipelago.

2.5.1 Geothermobarometry

The iron-magnesium silicates, as well as the feldspars, from the Corvo and Flores lavas were used to estimate intensive parameters such as the pressure (P) and temperature (T) of the ascending magmas below the islands. For the calculation of these parameters only crystals in chemical equilibrium (e.g. Fig. 5) with their host-rocks were utilized. One sample from each island (C-09-08, FL-09-44) containing kaersutite phenocrysts was also used in an attempt to calculate the stability conditions of the amphibole in the shallower part of the magmatic system. A K-feldspar geothermometer was also applied to the highly evolved samples from Flores (MgO<1wt %) to estimate the (shallowest) temperature conditions of the crystallizing magmas.

Table 4: Geothermobarometric estimates on lavas from Flores and Corvo.

Sample	MgO (wt %)	Putirka (2003) cpx–liquid				Putirka (2008) cpx (anhydr)			
		T (°C)	1SD	*P* (GPa)	1SD	*T* (°C)	1SD	*P* (GPa)	1SD
C-09-01	9·3	1238	9	0·94	0·90	1192	22	0·55	2·13
C-09-05	6·0	1166	4	0·71	0·43	1141	11	0·44	1·09
C-09-06	8·8	1222	9	0·82	0·94	1187	14	0·51	1·51
C-09-07	11·5	1302	6	1·19	0·62	1193	9	1·04	1·10
C-09-08	3·3	1074	13	0·59	1·49	1145	5	0·29	1·81
C-09-15b	11·3	1283	9	1·18	0·87	1213	23	0·89	1·84
C-09-17.2	10·7	1341	63	1·70	3·99	1205	15	1·36	9·30
C-09-18	8·1	1211	11	0·85	0·90	1159	17	0·58	1·54
FL-09-01	6·7	1186	8	0·79	0·76	1171	19	0·61	1·44
FL-09-11	4·4	1122	8	0·56	0·95	1121	23	0·35	1·42
FL-09-23	8·8	1239	10	1·04	1·02	1183	20	0·72	1·90
FL-09-41	10·5	1256	9	1·05	0·99	1211	17	0·68	1·59
FL-09-59	6·5	1179	11	0·85	1·30	1147	6	0·49	1·56
FL-09-69	5·7	1153	9	0·66	0·98	1157	18	0·49	1·25

Sample	MgO (wt %)	Fo content	Putirka (2008) ol–liquid			Beattie (1993) melt (ol)		
			1SD	*T* (°C)	1SD	*n* =	*T* (°C)	Diff. from Putirka
C-09-01	9·3	84·6	0·7	1308	3	14	1311	3
C-09-03	12·3	89·7	0·9	1375	8	2	1374	−2
C-09-05	6·0	75·2	0·1	1230	1	2	1235	5
C-09-06	8·8	83·0	1·7	1299	5	4	1302	3
C-09-07	11·5	88·2	0·2	1349	1	5	1353	3
C-09-15b	11·3	87·6	0·8	1356	5	4	1362	6
C-09-18	8·1	81·8	1·0	1284	3	4	1286	2
C-09-20	10·7	87·0	0·5	1332	2	6	1334	3
FL-09-01	6·7	80·7	0·8	1253	7	4	1257	5
FL-09-20	5·5	76·1	0·5	1208	2	4	1210	2
FL-09-23	8·8	85·2	0·6	1287	0	2	1293	5
FL-09-26	7·8	82·2	1·5	1257	4	3	1256	−1
FL-09-32	7·9	80·5	0·8	1292	3	19	1299	7
FL-09-41	10·5	86·6	1·0	1336	3	7	1344	8
FL-09-58	6·4	76·7	0·2	1244	1	3	1236	−8
FL-09-59	6·5	78·7	1·0	1238	3	4	1242	4
FL-09-69	5·7	77·4	1·0	1228	3	7	1230	2

Sample	MgO (wt %)	Putirka (2008) K-fsp–liquid			Ridolfi *et al.* (2010) amph				
		T (°C)	1SD	*n* =	*T* (°C)	1SD	*P* (GPa)	1SD	*n* =
C-09-08	3·3				960	22	0·30	0·33	1
FL-09-07	0·5	920	1	8					
FL-09-44	0·9				1003	14	0·31	0·21	25
FL-09-60	0·4	926	3	17					

2.5.1.1 Ti-augite geothermobarometry

Geothermobarometric calculations were performed on clinopyroxene phenocryst cores using the models of Putirka (2003, 2008). Table 4 summarizes the P-T estimates from the different methods; the most consistent and statistically robust results are provided by the

cpx-liquid model (Putirka, 2003). The whole-rock compositions of single lavas were used to represent the nominal liquid com- positions; corresponding mineral core analyses were tested for equilibrium with that liquid before proceeding to calculate pressures and temperatures. This was achieved by comparing the stoichiometrically calculated clinopyroxene components from the lava compositions with those of the measured mineral components (Putirka, 1999). Samples whose measured and predicted components deviated strongly were not used for P-T estimates. Furthermore, mineral data that revealed Fe-Mg exchange [$K_D(Fe\text{-}Mg)^{cpx\text{-}liq}$] values outside the range of 0·27 ± 0·03 were also inferred to be out of equilibrium with the liquid and therefore not used for P-T estimates.

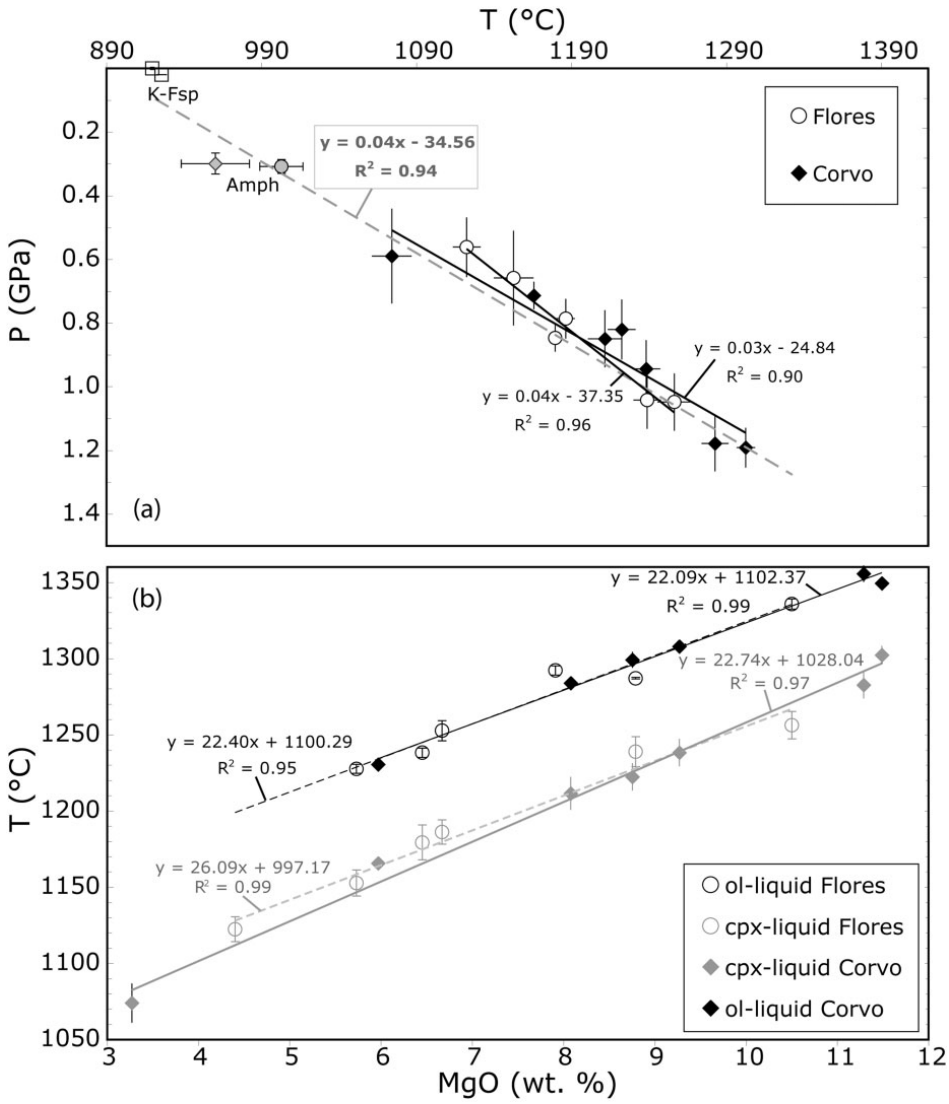

Fig. 16. Temperature and pressure estimates from equilibrium minerals (summarized inTable 4). (a) Approximate P-T path for the lavas from Corvo and Flores during clinopyroxene-dominated differentiation. Clinopyroxene, amphibole and K-feldspar were used for these calculations. The grey dashed P^T path is a

summary of Flores and Corvo clinopyroxenes (linear regression, R2 ~ 0·9), as they are the most abundant phase and therefore the calculated values are statistically more robust. Amphibole and K-feldspar intensive parameters are plotted for informa- tion only, but appear to confirm the trend (linear regression through all clinopyroxene P^T estimates). (b) Temperature vs MgO content (wt %) of the lavas highlighting the consistency between olivine- and clinopyroxene-derived temperature paths. Regression lines here correspond to Flores (dashed lines) and Corvo (continuous lines), each with R2 values >0·9, which may imply continuous P-T evolution of the magmas.

Figure 16a summarizes the P-T estimates from equilibrated clinopyroxenes from Corvo and Flores. Each data point reflects a single lava, where the P-T values are based on the average compositions of corresponding equilibrated clinopyroxenes. The highest temperatures and pressures calculated for Corvo were 1302 (±6) °C and 1·19 (±0·06) GPa, respectively. Maximum values for Flores are 1256 (±9) °C and 1·05 (±0·10) GPa. Strikingly, there is a continuum towards lower P and T and thus a discrete magma chamber seems unlikely at lithospheric depths. In detail, a linear fit through the data array from each island (R^2=0·9) suggests that the P-T gradient of the ascending magmas differs slightly between the two islands and that the magmas from Corvo appear to have a slightly deeper (c. + 5 km) onset of crystallization than those from Flores. These observations contrast with inferences from some of the eastern islands [e.g. see Beier et al. (2006) for São Miguel], where two distinct and shallow magma chambers have been suggested. It should be noted that the gabbroic cumulate from the Vila do Corvo flank eruption does not allow for reliable P-T calculations owing to the heterogeneity in its mineral compositions and small size that makes it unrepresentative in terms of a whole-rock analysis.

The Ti-augites were also plotted in the pyroxene quadrilateral for a first-order approximation of the temperature conditions (Fig. 6). Because the Lindsley (1983) geothermometer is isobaric, a 1·5 GPa projection (not shown) best approximates the most primitive compositions, whereas the 0·5 GPa projection (Fig. 6) displays the best correspondence to temperatures calculated using Putirka (2008) for the more evolved (trachytic) samples. The 0·5 GPa projection is illustrated in Fig. 6, because this best reflects the crystallization depths reported for comparable ocean island setting (e.g. São Miguel, the Canary Islands, Madeira; Hansteen et al., 1998; Klügel et al., 2000; Schwarz et al., 2004; Beier et al., 2006).

2.5.1.2 Olivine thermometry

Because olivine represents one of the earliest crystallizing phases it was used to estimate the liquidus temperatures of both systems. The Putirka (2008) approach was chosen as the resulting liquidus temperatures are consistent with the observed whole-rock MgO-temperature dependence in the clinopyroxene (Fig. 16b). The Beattie (1993) model, which uses the melt composition to calculate olivine equilibrium temperatures, is consistent (±10K) with the Putirka (2008) model. Accordingly, the liquidus temperature of the most primitive lava from Corvo (C-09-03, 12·3 MgO wt %) is estimated to be ~1375°C (Table 4).

2.5.1.3 Amphibole and feldspar thermobarometry

To estimate the lower end of the intensive parameter range (i.e. the shallowest conditions), feldspar and amphibole thermometry was applied. Amphibole thermobarometry (Ridolfi et al., 2010) provides estimates consistent with the dP/dT path determined from the ferromagnesian silicates (Table 4); the amphibole P-T parameters lie on the extrapolated path illustrated in Fig. 16a.

Feldspar thermometry was conducted using the approaches described by Fuhrman & Lindsley (1988), Benisek et al. (2004, 2010) and Putirka (2005). The ternary projection of the feldspar compositions onto experimentally determined temperature curves is shown in Fig. 7, where panels (a) and (b) (Corvo and Flores respectively) provide temperatures for a 0·1GPa projection, whereas in panel (c) both islands are plotted onto a 1·0 GPa projection. Even though the 900°C isotherm does not change be- tween the two depth projections, the process of continuous cooling with decreasing pressure, and hence continuous fractionation, becomes apparent in both projections be- cause both island suites cross multiple isotherms with evolving composition (900-700°C). The intersection of the observed lava trend with the temperature contours of Benisek et al. (2010) is generally consistent with the cooling of the magmas during ascent, although the anorthoclase temperatures of ~700°C are substantially lower than those inferred from the approach of Fuhrman & Lindsley (1988). It almost appears as if the observed trend of the plagioclases follows an inverse temperature path (i.e. 650 - 750°C) when applying the models of Fuhrman & Lindsley (1988). Therefore, we also attempted to use the equations described by Putirka (2005) to obtain additional feldspar temperature estimates (Table 4). These estimates result in a good fit to the projected P-T gradient from the clinopyroxene

calculations, potentially placing the alkali feldspar crystallization near the surface at Flores (Fig. 16a).

In summary, estimates of the pressure and temperature conditions of crystallization of the lavas from Flores and Corvo have been made using a number of independent methods; the resulting P-T paths, based on the three major phenocryst phases, are internally consistent. A poly- baric evolution model is suggested and we infer that fractional crystallization took place during magma ascent in volcanic conduits rather than in a single magma chamber at any specific depth. This conclusion, however, does not negate the existence of magma chambers per se, as the more evolved samples show petrographic (e.g. kaersutite, K-feldspar, large apatite) and morphological (e.g. large caldera on Corvo) features that are readily explained by the existence of a shallow (crustal) magma chamber.

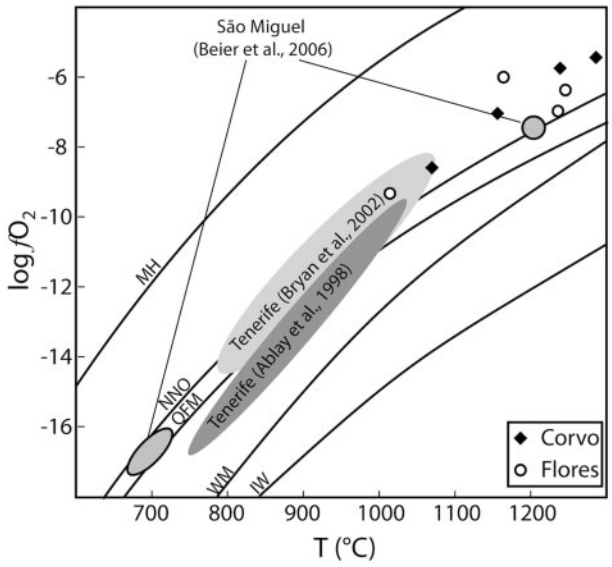

Fig. 17. Log fO_2 vs temperature estimates for lavas from Flores and Corvo. Ulvöspinel-magnetite solid solution experiments from Buddington & Lindsley (1964) were graphically applied to Ti-magnetites for the oxygen fugacity estimates for different lavas. The data are compared with the evolution of pre-caldera lavas from Sete Cidades from Sao Miguel (Beier et al., 2006), and with lavas from Tenerife (Ablay et al., 1998; Bryan et al., 2002). The Ti-magnetites appear to plot consistently above the NNO buffer, which reflects similar oxidation states for all magmas. MH, magnetite-hematite; NNO, nickel-nickel oxide; QFM, quartz-fayalite-magnetite; WM, wüstite-magnetite; IW, iron-wüstite.

2.5.2 Oxygen fugacity

Lavas containing abundant iron-titanium oxides were used to estimate the oxygen fugacity at the different differentiation stages, and hence at different inferred depths and

temperatures. The titanomagnetite mineral chemistry (Table 3) was stoichiometrically evaluated for the various ulvöspinel proportions for comparison with the solid-solution experiments of Buddington & Lindsley (1964). The data are illustrated in Fig. 17 in comparison with studies from Tenerife (Ablay et al., 1998; Bryan et al., 2002) and São Miguel (Beier et al., 2006), which highlight the similarity between these OIB systems. The lavas from Corvo and Flores appear to lie somewhat above the nickel-nickel oxide buffer (NNO). The lavas from Flores may indicate open-system behaviour, as they do not define a buffer-parallel trend. However, the clearer trend of the Corvo samples is consistent with a closed-system fractional crystallization process.

2.6 LIQUID LINE OF DESCENT

2.6.1 Primary magma compositions of Flores and Corvo

The major-element trends from Flores and Corvo suggest a similar liquid line of descent for each island coupled with crystallization over a comparable range of depths (Figs 9, 16 and 18). The most primitive samples from each island have MgO contents >11wt %. However, especially in the case of Corvo, the most MgO-rich lavas show clear petrographic evidence for olivine and clinopyroxene accumulation (refer to Figs 4 and 5, respectively). Mineral analyses from these samples (C-09-10 and C-09-13) reveal that olivine and clinopyroxene are not in equilibrium with the host magma (Table 3). These minerals are most probably accumulated crystals derived from gravitational settling during fractional crystallization. Therefore, these rocks must be ruled out as potential parental or primary magmas.

The most primitive lavas (e.g. whole-rock Mg# = 71, Fig. 5) containing olivine (Fo~88, Ni ~ 1750 ppm) and clinopyroxene in equilibrium with their whole-rock compositions are characterized by 10-11wt % MgO and Ni contents of 200-300 ppm (Tables 1 and 3). Hence, samples C-09-20 and FL-09-41 are considered to resemble near-primary magma compositions for Corvo and Flores, respectively. Although their nickel content may be slightly too low for these to be true primary magmas according to the criteria of Hess (1992), the model of Hart & Davis (1978) suggests that these samples could reflect near primary magmas formed by ~3% melting of peridotite. The relatively low nickel contents of the olivines and the primitive lavas, however, are consistent with eruption on young and thin lithosphere, as has been described in detail by Niu et al. (2011). In the following

discussion, these two samples will be used for further investigation of melting and crystallization processes beneath both islands.

Table 5: Primary magma compositions and their P&T conditions of the Flores and Corvo suites using different model calculations.

	Herzberg & Asimow (2008)		Lee *et al.* (2009)		Putirka (2005)	
	FL-09-41	C-09-20	FL-09-41	C-09-20	FL-09-41	C-09-20
SiO_2	46·3	45·5	46·3	45·4		
TiO_2	1·7	2·0	1·6	2·0		
Al_2O_3	12·4	11·3	12·3	11·2		
Cr_2O_3	0·1	0·1	0·0	0·0		
Fe_2O_3	1·0	1·0	1·0	1·0		
FeO	9·0	9·4	9·0	9·5		
MnO	0·2	0·2	0·2	0·2		
MgO	14·2	15·0	14·8	15·7		
CaO	10·7	11·8	10·5	11·7		
Na_2O	2·9	2·1	2·9	2·0		
K_2O	1·0	0·8	1·0	0·8		
NiO	0·0	0·1				
P_2O_5	0·0	0·3				
H_2O	0·5	0·4	0·5	0·4		
Fo	0·90	0·90	0·90	0·90		
T (°C)	1439	1458	1432	1468	1438	1467
P (GPa)			2·5	2·7		

Primary magma compositions for the parental magma samples C-09-20 and FL-09-41 were calculated following the approach of Lee et al. (2009). The corresponding estimated temperature and pressure conditions for basaltic magma generation in the mantle beneath Flores and Corvo are summarized in Fig. 19b and Table 5. The Lee et al. (2009) method places constraints for the calculations of MgO>9 wt %, Fe^{3+}/Fe^{T} = 0·1 in the basalts and Fo90 in the mantle source; hence P-T conditions of equilibration for the parental magmas of five lavas are plotted in Fig. 19a, including the ankaramitic cumulates. A consequence of this analysis is an independent estimate of the amount of H2O present in the source. The two primary, non-ankaramitic lavas (Fig. 19b) suggest between 0·5 and 1·0% H2O. Accordingly, our best estimates for the conditions of primary magma generation are just above the spinel-garnet transition of Robinson & Wood (1998) at depths of ~84km and at a maximum temperature of ~1450°C.

2.6.2 Fractional crystallization

The mineralogy, textures and bulk-rock compositions of the lavas are consistent with fractional crystallization being the dominant differentiation process for both the Corvo and Flores magmatic systems. The decrease in size of the olivine and clinopyroxene phenocrysts (from 20 to 0·5 mm) and the accompanying increase in the size of plagioclase phenocrysts (from 0·5 to 10 mm) with decreasing inferred pressure support this notion. Moreover, the major-element trends show clear evidence of clinopyroxene-dominated fractionation towards more evolved magma compositions. The first minerals to crystallize from the melt were forsteritic olivine (decrease of MgO accompanied by subtle increase of iron) in minor modal abundance followed by clinopyroxene, which is inferred from the decrease of CaO with decreasing MgO. The latter relationship, together with the flattening trend of increase of aluminium with differentiation (Fig. 9d), also suggests that the amount of plagioclase fractionation increases as the liquid evolves. The most evolved lava compositions (MgO<3·5 wt %) show petrographic evidence for crystallization of Fe-Ti oxides and apatite and fractionation of these phases as evidenced by decreasing titanium, iron and phosphorus contents (Fig. 9a and f).

Table 6: Mineral modes extracted from the MELTS models.

P (GPa)	*T* (°C)	1 – *F* (%)	cpx	ol	plag	spin + mag	apt	Total
12–5·6	1370–1040	70·0	39·4	2·9	3·7	2·6	0·3	49·0
0·1	1210–1010	72·8	29·4	9·3	11·8	2·2	0·2	52·9
0·5	1270–1040	72·6	36·6	6·6	7·0	2·2	0·3	52·7
1·0	1340–1090	69·1	44·8	0·0	0·0	2·7	0·4	47·8
1·5	1410–1150	69·6	46·0	0·0	0·0	1·9	0·4	48·3

The MgO range of the liquid evolution is ~9 wt % in all models. Sample C-09-20 is the starting composition used for all calculations.

The major-element compositions of the lavas from Corvo indicate that the samples lie on a single liquid line of descent. This is not the case for the lavas from Flores. The two sub-parallel trends seen in the Flores major-element data, especially TiO2 and P2O5 versus MgO, suggest similar fractional crystallization histories to the Corvo suite, but different liquid lines of descent. This suggests that not all the samples are of cogenetic origin and that other processes, such as source mixing or (deep) combined fractional crystallization-assimilation (AFC), may be needed to explain the different lava groups on Flores. The occasional appearance of reversely zoned clinopyroxene in some of these lavas may be attributed to such processes.

The major-element data trends do not require that plagioclase is a dominant fractionating phase in the most mafic magmas (Fig. 9); however, it appears to have been crystallizing throughout the range of compositions and apparently accumulated in some magmas from the Flores suite. In the first instance we model the Flores and Corvo suites with a single fractional crystallization model using the MELTS algorithm (Ghiorso & Sack, 1995; Asimow & Ghiorso, 1998).

Table 7: Partition coefficients used during the Rayleigh-fractionation calculations

	ol	cpx	plag	mag
Cr	0·64	8·49	0·04	150
Ni	32	8·5		29
P	0·038	0·02		
Ti	0·011	0·49	0·1	8
Rb	0·0004	0·00008	0·1	
Sr	0·001	0·113	2·1*	
Y	0	0·34	0·009	
Zr	0·001	0·06	0·003	
Nb	0·00007	0·0012	0·01	
Ba	0·0001	0·0003	0·15*	
La	0·0001	0·03	0·07	
Ce	0·0001	0·057	0·05	
Pr			0·13	
Nd	0·0005	0·14	0·1	
Sm	0·001	0·22	0·06	
Eu			0·73	
Gd		0·3	0·07	
Tb	0·001	0·33	0·06	
Dy	0·0017	0·33	0·06	
Ho	0·0031	0·35	0·05	
Er		0·3	0·05	
Yb	0·05	0·25	0·04	
Lu	0·024	0·31	0·03	
Hf	0·0008	0·12	0·03	
Ta	0·0002	0·0022	0·04	
Pb	0·001	0·008	0·6*	
Th	0·0002	0·007	0·17	
U	0·0003	0·006	0·11	

Olivine (ol) and clinopyroxene (cpx) data from Adam & Green (2006). Plagioclase (plag) data from Aigner-Torres *et al*. (2007). Magnetite (mag) values are estimates based on Esperana *et al*. (1997).
*Data calculated based on Blundy & Wood (1991, 2003).

2.6.2.1 MELTS modeling

MELTS modelling used 10°C steps and assumed the major-element composition of the inferred parental lava from Corvo (C-09-20) as the starting composition. Intensive parameter inputs of 1375°C at 1·2GPa were chosen on the basis of the thermobarometric

estimates described above. Isobaric models were then calculated at 0·1, 0·5, 1·0 and 1·5 GPa with corresponding liquidus temperatures and compared with a polybaric model con- strained by the dP/dT gradient suggested by the Fe-Mg silicates (e.g. Fig. 16). The polybaric model uses the same starting composition as the isobaric models, but starts at an equilibrium pressure of 1·2 GPa and evolves down to 0·56 GPa, along a dP/dT gradient based on the estimates obtained from the geothermobarometric models. The fractionating solids in all models were based on petrographic observations. From the geochemical data and the observed petrology, the following phases are inferred to have crystallized from both the Flores and Corvo magmatic systems: clinopyroxene, olivine, magnetite, ilmenite, plagioclase, apatite (± alkali feldspar, ± amphibole). This is broadly consistent with the fractionating phases deter- mined by MELTS (Table 6).

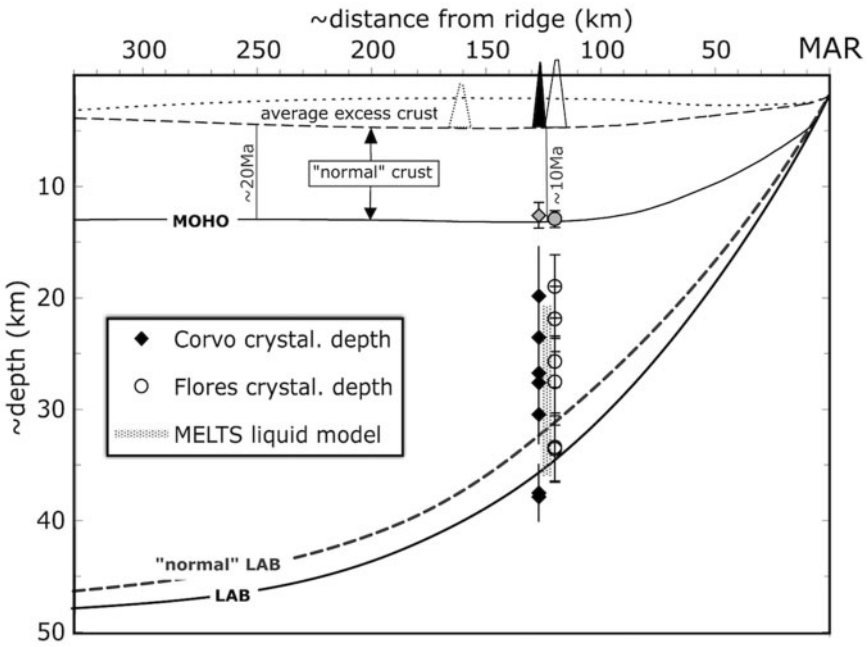

Fig. 18. Schematic cross-section beneath the western Azores plateau (excess crust) indicating the ascent of the crystallizing magmas beneath Flores and Corvo. P-T estimates as well as the MELTS liquid model coincide and both imply the onset of crystallization near the litho-sphere-asthenosphere boundary (LAB). Stalling of the magmas at the mantle-crust boundary (MOHO) may be inferred from amphibole pres- sure estimates; however, clinopyroxene-dominated fractionation occurred at greater depths (>0·5 GPa). The volcanic edifices of Flores and Corvo, as well as the submarine seamount ~50 km to the west, are shown at their present-day distance from the MAR.

As illustrated in Fig. 9, the polybaric MELTS model seems to provide the best fit to the observed whole-rock major-element data. This is particularly apparent for the Corvo lavas in Fig. 9a-d. The closest isobaric model for these lavas occurs at 1·0 GPa, which

roughly coincides with the depth of the lithosphere-asthenosphere boundary (LAB) beneath the islands (Fig. 18). Nevertheless, this cannot reproduce the low-MgO, low-TiO2 end of the arrays in Fig. 9a, and storing and fractionating all of the magmas at or near the LAB is unlikely to produce the chemical evolution of the olivine, clinopyroxene and plagioclase phenocrysts observed in the lavas. Conversely, the existence of transitory shallow magma chambers (<0·1 GPa) is indicated by the presence of calderas on both islands and is consistent with the presence of low-temperature K-feldspars in the most evolved rocks (<0·8 MgO wt %) on Flores. In summary, we prefer the polybaric differentiation model for Corvo. We note that the Flores data are significantly more scattered. However, there is no reason from the point of view of the mineralogical and major-element data that this model does not equally apply to this island as well.

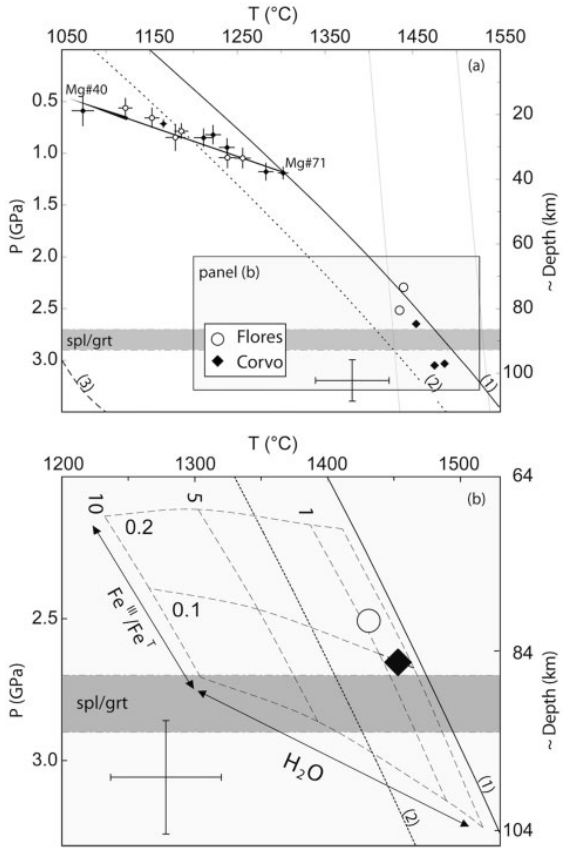

Fig. 19. Temperature and pressure estimates for the generation of the primary melts using the model from Lee et al. (2009). The P-T path of clinopyroxene crystallization in the lavas is taken from Fig. 16a. The spinel-garnet (Spl/Grt) transition is from Robinson & Wood (1998). Only near-primary magmas (Mg#~70) were used for P-T estimates of the primary melts (a). (b) The effect of changing input parameters (e.g. water content and oxidation state) on the estimated P-Tconditions. The preferred conditions are shown for representative primary magmas from Flores (Fl-09-42) and Corvo (C-09-07). Solidus lines are referenced from (1) Green & Falloon (1998), (2) Katz et al. (2003) and (3) Green et al. (2010).

2.6.2.2 Trace-element behaviour

The fractional crystallization model calculated using MELTS, and supported by the geothermobarometric estimates, was then further appraised using the trace-element data. Because the observed mineralogy of the basalts is fairly simple in terms of crystallization order, a Rayleigh-fractionation model was used (Fig. 12). Mineral modes for the fractionating assemblage were extracted from the MELTS outputs and cross-checked with the petrography and mineral chemistry. Because the evolution of the magmas is dominated by clinopyroxene fractionation (see caption of Fig. 12), it is not expected that the Rayleigh-fractionation models will discriminate between isobaric and polybaric processes. Clinopyroxene and olivine distribution coefficients were taken from Adam & Green (2006) to best match the highest P-T conditions inferred here for the near-primary magmas. However, these have only limited applicability for shallower and cooler conditions and must be treated with caution when calculating the trace-element evolution during fractional crystallization. Appropriate K_D values for Sr, Ba and Pb for plagioclase were calculated following the model of Blundy & Wood (1991) to best represent the anorthite contents of the plagioclase in the more evolved compositions. The work of Aigner-Torres et al. (2007) was used for partition coefficients for the remaining trace elements in plagioclase. Magnetite KD values were estimated based on data provided by Esperança et al. (1997). Clinopyroxene and olivine fractionation, however, dominates most strongly at the highest pressures, whereas plagioclase and Fe-Ti oxides are increasingly fractionated towards shallower depths (<< 0·5 GPa).

Unfortunately, because the trace-element trends exhibit significant scatter in the Flores lava suite, this exercise does not provide an especially robust test of the MELTS models. Nevertheless, the Rayleigh fractional crystallization model satisfactorily reproduces the trace- element trends with reasonable adherence to the better-defined Corvo data. Because this single-step model (i.e. fixed mineral assemblage) predicts the behaviour of the trace elements over a large range of MgO ($\Delta \sim 9$ wt %), it may be argued that some of the discrepancies between the calculated and observed trend (Fig. 12) are mainly due to continuous modal changes during the ascent of the crystallizing magma. Alternatively, the discrepancies between the modelled trends and the observed concentrations may be due to the KD values used and mineral-mode dependence of the crystallization pressures. In the case of Sr, which is compatible in plagioclase and apatite, we observed a linear negative correlation with the pressures extracted from the MELTS model (not shown),

and also with the pressures obtained from the clinopyroxene barometry. This relationship may reflect two processes. First, the plagioclase component in the residual liquid gradually increases with decreasing pressure and, second, strontium partitions more strongly into more albite-rich plagioclase as demonstrated by Blundy & Wood (1991). This latter relationship could not be tested sufficiently, as plagioclase becomes efficiently fractionated from the magmas only at shallower levels (<<0·5 GPa), and even then only in minor amounts (~ 5%).

Figure 12 shows the predicted fractional crystallization trends based on a starting composition assumed to be that of sample C-09-20. The trends of the compatible elements (Ni, Cr) against Nb clearly support clinopyroxene-dominated fractional crystallization as the major process controlling the evolution of both basaltic suites. Again, the scatter in the Flores lavas is probably indicative of other ascent-related processes, such as assimilation. This is even more prominent in the variation of Sr, Y and Zr versus Nb. The low-Nb samples are ankaramitic cumulates. The Corvo sample C-09-17.2 with the lowest Nb concentration indicates clinopyroxene crystallization at depths close to the lithosphere asthenosphere boundary (Table 4).

In Fig. 14 we compare the MELTS model-based Rayleigh-fractionation model with the variation of Nd/Sr vs Nd and Dy/Yb vs Dy in the lavas. These element pairs were chosen to investigate the relative roles of garnet and plagioclase in the system. The samples with Nd concentrations ~20 ppm and Dy ~3 ppm are petrologically classified as ankaramitic cumulate rocks. The crystallization model confirms this interpretation because these samples lie on the Corvo fractionation trend at 15·5 and 18·2 wt % MgO. The parental starting composition has a Sr content of ~500 ppm and a Nd content of ~30 ppm (Table 1). As the magmas fractionate to shallower levels the Nd concentration increases as well as the Nd/Sr ratio. Furthermore, two sub-parallel trends for Flores are apparent when com- pared with Corvo, reflected in variable Nd/Sr at a given Nd concentration (Fig. 14b).

The trends of Dy/Yb versus Dy in Fig. 14a are different between the two islands, but the Dy and Yb concentrations of the most primitive magmas are comparable. The Dy/Yb ratio remains relatively consistent for Corvo, but appears to define two distinct groups for Flores. This may reflect subtle differences in the mantle source beneath Flores and/or some deep fractional crystallization-assimilation process. The differences in the

behaviour of these trace elements during magmatic differentiation between the two islands may be explained by temporal variations (e.g. different ascent rates and thus different amounts of assimilated material in some magmas), but also by a difference in the source composition between the two islands.

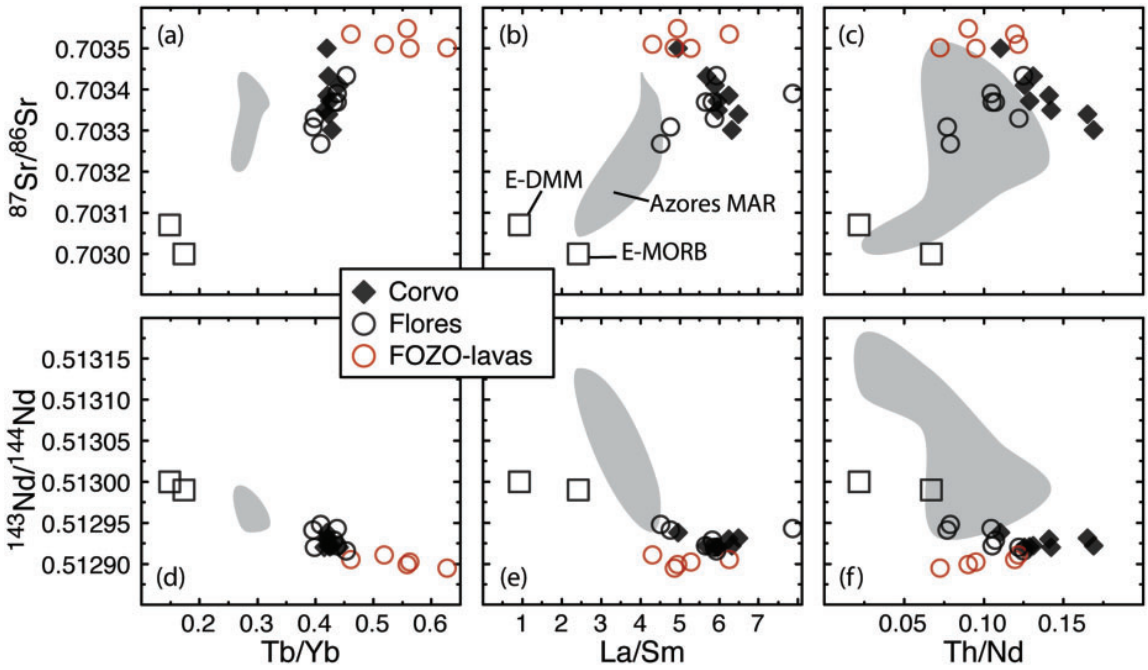

Fig. 20. Strontium and neodymium isotopic compositions for lavas from Flores and Corvo. Panels (a)-(c) highlight the Sr isotopic composition and (d)-(f) the Nd isotopic composition versus garnet signature (Tb/Yb), degree of melting (La/Sm) and source composition (Th/Nd). The field of the Azores MAR is based on data from Bourdon et al. (1996) and Dosso et al. (1999), and references therein. The red circled Flores samples may represent a common mantle end-member similar to the FOZO mantle reservoir (e.g. Stracke et al., 2005).

The polybaric, fractional crystallization model from MELTS is broadly consistent with Rayleigh-fractionation of the trace elements. A total fraction of ~70% of the parental magma is crystallized in the preferred model to explain the most evolved compositions (Table 6). Arguably, crystallization commenced close to the lithosphere asthenosphere boundary, the depth of which was calculated using the equations of Parsons & Sclater (1977) and Stein & Stein (1992), illustrated in a geological cross-section in Fig. 18. The onset of crystallization was slightly deeper beneath Corvo (~38km), although the range of crystallization pressures beneath both islands is inferred to be similar. The occasional appearance of reversely zoned clinopyroxene in some of the Flores lavas may also suggest mixing of more mafic liquid with the crystallizing ascending magmas (e.g. Neumann et al., 1999). Convection in the magma conduits can readily explain some of

the observed disequilibrium features, with small-scale stagnation perhaps occurring in magma pockets in sidewalls. Such a model has been invoked for basaltic magma systems previously, especially where there is clear evidence in the evolution of the fractionated mineral assemblages (e.g. Cox & Jamieson, 1974; Cox, 1980; Fram & Lesher, 1997; Nekvasil et al., 2004).

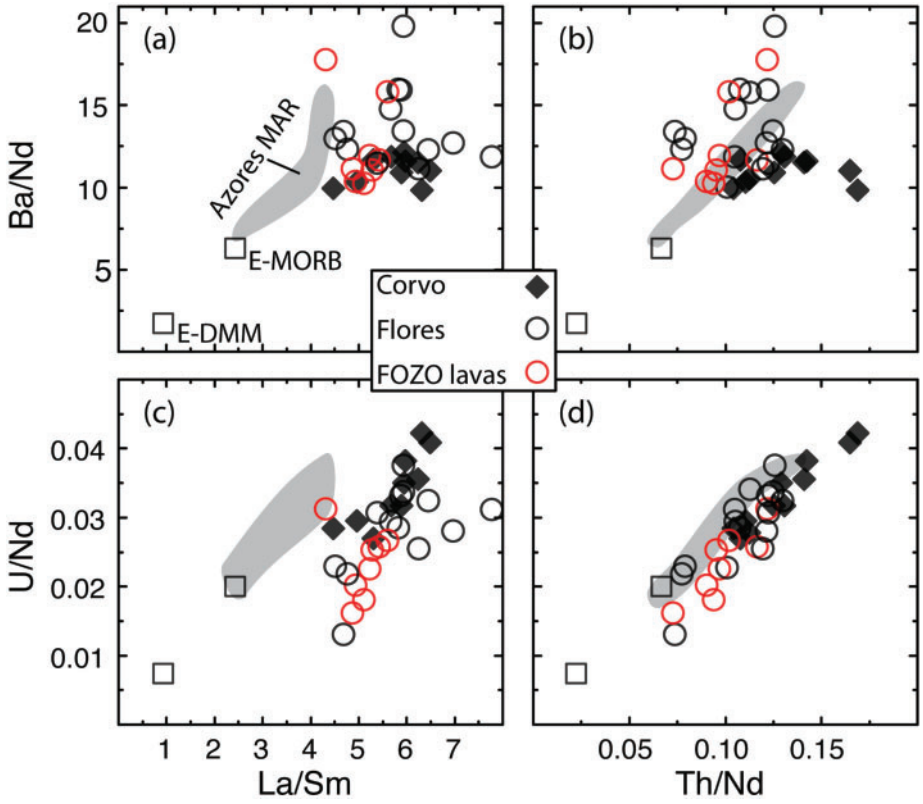

Fig. 21. Variation of Ba/Nd (a, b) and U/Nd (c, d) versus La/Sm and Th/Nd. Red Flores data points reflect the same enriched source as high- lighted in Figs 15 and 20. Mantle sources are as follows: E-DMM from Workman & Hart (2005), E-MORB from Sun & McDonough (1989). Panels (a) and (b) illustrate the differences between the Flores and Corvo lava suites. U/Nd (c and d) variations, in contrast, appear to confirm a general mixing trend towards a common enriched mantle source for the two islands.

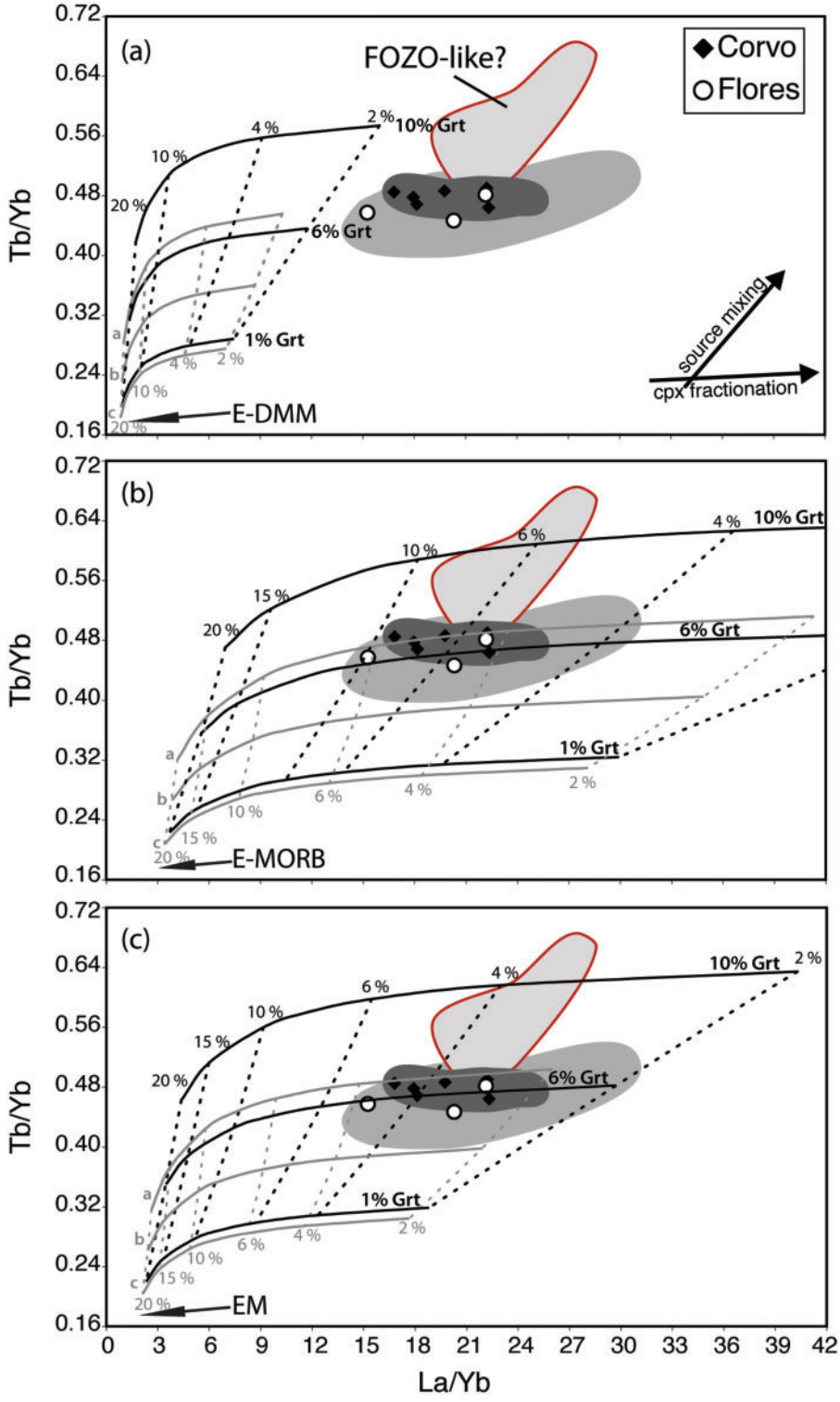

Fig. 22. Tb/Yb versus La/Yb diagrams after Pearce & Parkinson (1993) highlighting the role of garnet and spinel in the melting region. Only primitive samples (Mg#>65) are plotted for sensitivity purposes; however, the grey fields reflect the general fractionation trends of both islands (dark grey, Corvo; medium and light grey, Flores). Both islands require 3-5% melting of a peridotitic enriched mantle source to produce the primary magmas. The melting models are based on the following parameters: (a) E-DMM from Workman & Hart (2005), (b) E-MORB from Sun & McDonough (1989), (c) EM source from Donnelly et al. (2004); batch melting of a peridotite mantle mineralogy with 55% Ol, 25% Opx, 10-19%

Cpx, 10-1% Grt, respectively. Garnet was evenly mixed with spinel to further constrain the depth of melting; that is, curve a represents 5% Grt + 5% Spl, b is 3% Grt + 3% Spl and c is 0·5% Grt + 0·5% Spl. The red highlighted Flores field may indicate mixing towards a FOZO-type reservoir (e.g. Stracke et al., 2005). Alternatively, these samples could reflect deeper storage and fractionation at the LAB with associated assimilation.

2.7 SOURCE COMPOSITION

The P-T conditions in the source region of the melts were constrained through application of the model of Lee et al. (2009) and confirmed by calculations based on the work of Herzberg & Asimow (2008); this indicates temperatures and pressures of ~1470°C, 2·7 GPa for Corvoand ~1430°C, 2·5 GPa for Flores (Table 5). These depths are comparable with those inferred for Sao Miguel, but considerably greater (~15 km deeper) than those for Graciosa, Terceira and Joao de Castro [compare fig. 11 of Beier et al. (2008)].

The mantle source composition beneath Flores and Corvo was evaluated using the radiogenic isotope systematics in combination with key trace-element ratios. Sr and Nd isotope variations are plotted versus key trace-element ratios in Fig. 20 along with data for the MAR basalts in the vicinity of the Azores plateau (Bourdon et al., 1996; Dosso et al., 1999). Most lavas from the two islands overlap on the various plots, but, as described above, there is a group of lavas from Flores with a consistently different composition. These lavas are characterized by Sr-Nd isotope compositions similar to the so-called 'FOZO' mantle reservoir (e.g. Workman et al., 2004; Stracke et al., 2005) and have elevated Tb/Yb ratios (Fig. 20a and d). When combined with plots of Sr and Nd isotopes versus Th/Nd and $(La/Sm)_N$, respectively, it becomes apparent that the bulk of the lavas from the two islands plot between the MAR basalts and the distinct FOZO-like group from Flores (Fig. 20). We note that it is primarily their elevated Sr isotope ratio that distinguishes these latter rocks. This might be attributed to contamination by earlier basalts that evolved to higher $^{87}Sr/^{86}Sr$ during ageing in the lower crust. However, this is precluded by the low Rb/Sr ratios of all of the lavas, coupled with the likely 10 Ma maximum age of the islands. Therefore we conclude that a distinct radiogenic source component ($^{87}Sr/^{86}Sr$ ~ 0·70355), only observed locally on Flores, was involved during magma generation. The melts from this reservoir are also characterized by relatively high Tb/Yb (>0·55).

On a plot of U/Nd versus Th/Nd (Fig. 21d) the lavas from Flores and Corvo define a mixing trend, in which the data from Corvo extend the trend towards more enriched compositions. The enriched MORB samples from the adjacent MAR (Bourdon et al., 1996; Dosso et al., 1999) are similar to the majority of the Flores lavas in Th/Nd and U/Nd. In contrast, divergent trace-element trends for the two islands are evident on a plot of Ba/Nd versus Th/Nd (Fig. 21b), with the MAR basalts plotting somewhat between the two islands. The relationships in Fig. 21 in general suggest that the MORB-source mantle beneath the MAR (also shown in Fig. 20) is a common end-member from which the lavas from Flores and Corvo extend towards distinct compositions. Thus, three mantle source components, two of which are enriched and one is MORB-source like, appear to be required to explain the compositions of the Flores and Corvo lavas.

Finally, we attempt to constrain the extent of partial melting and the possible role of residual garnet in the source of the Flores and Corvo lavas using a plot of Tb/ Yb, largely sensitive to residual garnet, versus La/Yb, which is largely sensitive to the extent of melting (Fig. 22). The three panels in Fig. 22 are contoured for melt fraction using different mantle source compositions from which we infer that around 3-5% melting of an enriched mantle source containing around 5-6% residual garnet (but see below) could explain the primitive lavas from both islands. However, as suggested above, there is a group of Flores lavas that seems to require a different source composition, which is also apparent in the Tb/Yb and La/Yb systematics (see also Figs 20 and 21). These magmas appear to require amounts of garnet that exceed 10% and might be attributed to either deeper melting or mixing with melts from a distinct mantle source.

Despite the above discussion, the implication of Fig. 19 is that melting may not, in fact, reach into the garnet stability zone. To reconcile these apparently conflicting observations, we suggest that the garnet trace-element signature may be inherited. Indeed, because the $^{143}Nd/^{144}Nd$ ratios of all the lavas are consistently higher than CHUR, with epsilon Nd values around +5·5, they must have been derived from mantle source regions that had evolved with time-integrated LREE depletion. However, the degree of LREE enrichment observed in the lavas could not plausibly have been produced by reasonable degrees of melting of a depleted source. Therefore, it seems likely that the LREE enrichment of the lavas reflects recent metasomatism of their source region (e.g. Hawkesworth et al., 1979; Lustrino et al., 2007). The corollary is that the preceding

arguments for the presence and amounts of residual garnet are subject to this caveat and we suggest that melting may not have commenced this deep.

2.8 CONCLUSIONS

Lavas from Flores and Corvo provide new constraints on the evolution of the Azores archipelago. New major-element data from these westernmost islands provide evidence for continuous, polybaric, fractional crystallization from the lithosphere asthenosphere boundary (~38 km depth) to the crust-mantle boundary (~12 km depth). Corvo lavas are, on average, slightly more primitive than those from Flores and constrain initial fractionation assemblages from the presence of ankaramitic cumulate rocks. Corvo lavas require deeper melting conditions at higher temperatures than lavas from Flores. Modelling of the major elements supports the polybaric fractionation model and we propose that no long-lived magma chamber is required to explain the most differentiated lavas, which have <3wt % MgO. Only more evolved lavas (>3 wt % MgO) may have formed through stagnation at shallow crustal levels (1-3 km), consistent with the caldera system observed on Corvo.

The Nd-Sr isotope ratios of the Corvo and Flores lavas are similar to those observed amongst the eastern islands of Terceira, Graciosa and western São Miguel, but display a more restricted range. Trace-element ratios (e.g. Nb/Zr, Ta/Hf, La/Sm) suggest the involvement of an enriched source composition that is not observed in the eastern Azores islands or along the Mid-Atlantic Ridge. A discrete mantle component [e.g. high Tb/Yb and lower $(La/Sm)_N$] is seen in a particular lava suite on Flores but is not observed on Corvo, suggesting a limited geographical distribution. We conclude that 3-5% melting of an enriched mantle formed the primary melts underneath Flores and Corvo at depths around 80 km and temperatures around 1450°C. The resultant primary melts commenced to fractionate upon entering the lithosphere, potentially undergoing short-term storage at the lithosphere asthenosphere boundary. Only small, short-lived magma chambers are interpreted to have existed immediately below the current volcanic edifices.

ACKNOWLEDGMENTS

V. H. Forjaz and the Observatório Geotérmico dos Açores are gratefully acknowledged for their assistance with the sample logistics. B. W. Chappell is thanked for help with the XRF analyses, and P. Wieland for help with the ICP-MS trace-element and TIMS isotope

analyses. We thank K. Grant for assisting with the EMP analyses. The paper benefited from constructive reviews by E.-R. Neumann, V. Salters and an anonymous reviewer, which led to great improvement. M. Wilson is thanked for extremely patient editorial handling and helpful com- ments. This is contribution 169 from the ARC Centre of Excellence for Core to Crust Fluid Systems (http://www.ccfs.mq.edu.au) and 819 in the GEMOC Key Centre (http://www.gemoc.mq.edu.au).

FUNDING

The analytical data were obtained using instrumentation funded by DEST Systemic Infrastructure Grants, ARC LIEF, NCRIS, industry partners and Macquarie University. C. B. was supported by a Feodor-Lynen fellowship from the Alexander von Humboldt-Foundation. S.P.T. was supported by an Australian Research Council Professorial Fellowship (DP0988658).

SUPPLEMENTARY DATA

Supplementary data for this paper are available at Journal of Petrology online.

REFERENCES

Abdel-Monem, A. A., Fernandez, L. A. & Boone, G. M. (1975). K-Ar ages from the eastern Azores group (Santa Maria, Sa‹ o Miguel and the Formigas Islands). Lithos 8, 247-254.

Ablay, G. J., Carroll, M. R., Palmer, M. R., Mart|¤, J. & Sparks, R. S. J. (1998). Basanite-phonolite lineages of the Teide-Pico Viejo volcanic complex, Tenerife, Canary Islands. Journal of Petrology 39, 905-936.

Adam, J. & Green, T. (2006). Trace element partitioning between mica- and amphibole-bearing garnet lherzolite and hydrous basa- nitic melt: 1. Experimental results and the investigation of controls on partitioning behaviour. Contributions to Mineralogy and Petrology 152, 1-17.

Aigner-Torres, M., Blundy, J. D., Ulmer, P. & Pettke, T. (2007). Laser ablation ICPMS study of trace element partitioning between plagioclase and basaltic melts: an experimental approach. Contributions to Mineralogy and Petrology 153, 647-667.

Asimow, P. D. & Ghiorso, M. S. (1998). Algorithmic modifications extending MELTS to calculate subsolidus phase relations. American Mineralogist 83, 1127-1132.

Azevedo, J. M. M. & Ferreira, M. R. P. (1999). Volcanic gaps and subaerial records of palaeo-sea-levels on Flores Island (Azores): tectonic and morphological implications. Journal of Geodynamics 28, 117-129.

Azevedo, J. M. M. & Ferreira, M. R. P. (2006). The volcanotectonic evolution of Flores Island, Azores (Portugal). Journal of Volcanology and Geothermal Research 156, 90-102.

Baptista, P., Osório, J., Bastos, L., Fernandes, R. & Borges, F. S. (1999). Aplicação de técnicas geodésicas ao estudo do comportamento geodinâmico actual da Junção Tripla dos Açores. GEOlogos 5, 1-12.

Beattie, P. (1993). Olivine-melt and orthopyroxene-melt equilibria. Contributions to Mineralogy and Petrology 115, 103-111.

Beier, C., Haase, K. M. & Hansteen, T. H. (2006). Magma Evolution of the Sete Cidades

Volcano, São Miguel, Azores. Journal of Petrology 47, 1375-1411.

Beier, C., Stracke, A. & Haase, K. M. (2007). The peculiar geochemical signatures of São Miguel (Azores) lavas: Metasomatised or recycled mantle sources? Earth and Planetary Science Letters 259, 186-199.

Beier, C., Haase, K. M., Abouchami, W., Krienitz, M.-S. & Hauff, F. (2008). Magma genesis by rifting of oceanic lithosphere above anomalous mantle: Terceira Rift, Azores. Geochemistry, Geophysics, Geosystems 9, Q12013.

Beier, C., Turner, S., Plank, T. & White, W. (2010). A preliminary assessment of the symmetry of source composition and melting dynamics across the Azores plume. Geochemistry, Geophysics, Geosystems 11, Q02004.

Benisek, A., Kroll, H. & Cemic, L. (2004). New developments in two-feldspar thermometry. American Mineralogist 89, 1496-1504.

Benisek, A., Dachs, E. & Kroll, H. (2010). A ternary feldspar-mixing model based on calorimetric data: development and application. Contributions to Mineralogy and Petrology 160, 327-337.

Blundy, J. D. & Wood, B. J. (1991). Crystal-chemical controls on the partitioning of Sr and Ba between plagioclase feldspar, silicate melts, and hydrothermal solutions. Geochimica et Cosmochimica Acta 55, 193-209.

Blundy, J. & Wood, B. (2003). Partitioning of trace elements between crystals and melts. Earth and Planetary Science Letters 210, 383-397.

Bourdon, B., Langmuir, C. H. & Zindler, A. (1996). Ridge-hotspot nteraction along the Mid-Atlantic Ridge between 37°30’ and 40°30’N: the U-Th disequilibrium evidence. Earth and Planetary Science Letters 142, 175-189.

Bryan, S. E., Martí, J. & Leosson, M. (2002). Petrology and geochemistry of the Bandas del Sur Formation, Las Cañadas Edifice, Tenerife (Canary Islands) Journal of Petrology 43, 1815-1856.

Buddington, A. F. & Lindsley, D. H. (1964). Iron-titanium oxide minerals and synthetic equivalents. Journal of Petrology 5, 310-357.

Cannat, M., Briais, A., Deplus, C., Escartín, J., Georgen, J., Lin, J., Mercouriev, S., Meyzen, C., Muller, M., Pouliquen, G., Rabain, A. & da Silva, P. (1999). Mid-Atlantic Ridge-Azores hotspot interactions: along-axis migration of a hotspot-derived event of enhanced magmatism 10 to 4 Ma ago. Earth and Planetary Science Letters 173, 257-269.

Charlou, J. L., Donval, J. P., Douville, E., Jean-Baptiste, P., Radford- Knoery, J., Fouquet, Y., Dapoigny, A. & Stievenard, M. (2000). Compared geochemical signatures and the evolution of Menez Gwen (37°50'N) and Lucky Strike (37°17'N) hydrothermal fluids, south of the Azores Triple Junction on the Mid-Atlantic Ridge. Chemical Geology 171, 49-75.

Chauvel, C. & Blichert-Toft, J. (2001). A hafnium isotope and trace element perspective on melting of the depleted mantle. Earth and Planetary Science Letters 190, 137-151.

Chen, C.-Y. & Frey, F. A. (1983). Origin of Hawaiian tholeiite and alkalic basalt. Nature 302, 785-789.

Clague, D. A. (1987). Hawaiian alkaline volcanism. In: Fitton, J. G. & Upton, B. G. J. (eds) Alkaline Igneous Rocks. Geological Society, London, Special Publications 30, 227-252.

Claude-Ivanaj, C., Joron, J.-L. & Allègre, C. J. (2001). 238U-230Th-226Ra fractionation in historical lavas from the Azores: long-lived source heterogeneity vs. metasomatism fingerprints. Chemical Geology 176, 295-310.

Cox, K. G. (1980). A model for flood basalt vulcanism. Journal of Petrology 21, 629-650.

Cox, K. G. & Jamieson, B. G. (1974). The olivine-rich lavas of Nuanetsi: a study of polybaric magmatic evolution. Journal of Petrology 15, 269-301.

Deer, W. A., Howie, R. A. & Zussman, J. (1992). An Introduction to the Rock-forming Minerals. Harlow: Pearson.

Donnelly, K. E., Goldstein, S. L., Langmuir, C. H. & Spiegelman, M. (2004). Origin of enriched ocean ridge basalts and implications for mantle dynamics. Earth and Planetary Science Letters 226, 347-366.

Dosso, L., Bougault, H., Langmuir, C. H., Bollinger, C., Bonnier, O. & Etoubleau, J. (1999). The age and distribution of mantle heterogeneity along the Mid-Atlantic Ridge (31-41°N). Earth and Planetary Science Letters 170, 269-286.

Droop, G. T. R. (1987). A general equation for estimating Fe3+ concentrations in ferromagnesian silicates and oxides from microprobe analyses, using stoichiometric criteria. Mineralogical Magazine 51, 431-435.

Dupré, B., Lambret, B. & Allègre, C. J. (1982). Isotopic variations within a single oceanic island: the Terceira case. Nature 299, 620-622.

Eggins, S. M., Woodhead, J. D., Kinsley, L. P. J., Mortimer, G. E., Sylvester, P., McCulloch, M. T., Hergt, J. M. & Handler, M. R. (1997). A simple method for the precise determination of □40 trace elements in geological samples by ICPMS using enriched iso- tope internal standardisation. Chemical Geology 134, 311-326.

Esperança, S., Carlson, R. W., Shirey, S. B. & Smith, D. (1997). Dating crust-mantle separation: Re-Os isotopic study of mafic xenoliths from central Arizona. Geology 25, 651-654.

Fernandes, R. M. S., Bastos, L., Miranda, J. M., Lourenço, N., Ambrosius, B. A. C., Noomen, R. & Simons, W. (2006). Defining the plate boundaries in the Azores region. Journal of Volcanology and Geothermal Research 156, 1-9.

Flower, M. F. J., Schmincke, H. U. & Bowman, H. (1976). Rare earth and other trace elements in historic azorean lavas. Journal of Volcanology and Geothermal Research 1, 127-147.

Fram, M. S. & Lesher, C. E. (1997). Generation and polybaric differ- entiation of East Greenland Early Tertiary flood basalts. Journal of Petrology 38, 231-275.

França, Z., Lago, M., Nunes, J. C., Gale, C., Forjaz, V. H., Pueyo, O. & Arranz, E. (2006a). Geochemistry of alkaline basalts of Corvo Island (Azores, Portugal): preliminary data. Geogaceta 40, 87-90.

França, Z. T. M., Tassinari, C. C. G., Cruz, J. V., Aparicio, A. Y., Aran‹ a, V. & Rodrigues, B. N. (2006b). Petrology, geochemistry and Sr-Nd-Pb isotopes of the volcanic rocks from Pico Island- Azores (Portugal). Journal of Volcanology and

Geothermal Research 156, 71-89.

França, Z., Lago, M., Gale, C., Ubide, T., Widom, E., Arranz, E. & Forjaz, V. H. (2008). Composition of gabbroic xenoliths in Flores Island (Azores, Portugal). Revista de la Sociedad Espanola de Mineralogica 9, 103-104.

Fuhrman, M. L. & Lindsley, D. H. (1988). Ternary-feldspar modeling and thermometry. American Mineralogist 73, 201-215.

Gente, P., Dyment, J. R. M., Maia, M. & Goslin, J. (2003). Interaction between the Mid-Atlantic Ridge and the Azores hot spot during the last 85 Myr: Emplacement and rifting of the hot spot-derived plateaus. Geochemistry, Geophysics, Geosystems 4, Q8514.

Georgen, J. E. (2008). Mantle flow and melting beneath oceanic ridge-ridge-ridge triple junctions. Earth and Planetary Science Letters 270, 231-240.

Georgen, J. E. & Sankar, R. D. (2010). Effects of ridge geometry on mantle dynamics in an oceanic triple junction region: Implications for the Azores Plateau. Earth and Planetary Science Letters 298, 23-34.

Ghiorso, M. S. & Sack, R. O. (1995). Chemical mass transfer in magmatic processes IV. A revised and internally consistent thermodynamic model for the interpolation and extrapolation of liquid-solid equilibria in magmatic systems at elevated temperatures and pressures. Contributions to Mineralogy and Petrology 119, 197-212.

Green, D. H. & Falloon, T. J. (1998). Pyrolite: A Ringwood concept and its current expression. In: Jackson, I. N. S. (ed.) The Earth's Mantle; Composition, Structure, and Evolution. Cambridge: Cambridge University Press, pp. 311-378.

Green, D. H., Hibberson, W. O., Kovacs, I. & Rosenthal, A. (2010). Water and its influence on the lithosphere-asthenosphere boundary. Nature 467, 448-451.

Gudmundsson, A. (2000). Dynamics of volcanic systems in Iceland: example of tectonism and volcanism at juxtaposed hot spot and mid-ocean ridge systems. Annual Review of Earth and Planetary Sciences 28, 107-140.

Haase, K. M. & Beier, C. (2003). Tectonic control of ocean island basalt sources on Sa‹ o

Miguel, Azores? Geophysical Research Letters 30, doi:10.1029/2003GL017500.

Hansteen, T. H., Klugel, A. & Schmincke, H.-U. (1998). Multi-stage magma ascent beneath the Canary Islands: evidence from fluid in- clusions. Contributions to Mineralogy and Petrology 132, 48-64.

Hart, S. R. & Davis, K. E. (1978). Nickel partitioning between olivine and silicate melt. Earth and Planetary Science Letters 40, 203-219.

Hawkesworth, C. J., Norry, M. J., Roddick, J. C. & Vollmer, R. (1979). 143Nd/144Nd and 87Sr/86Sr ratios from the Azores and their significance in LIL-element enriched mantle. Nature 280, 28-31.

Herzberg, C. & Asimow, P. D. (2008). Petrology of some oceanic island basalts: PRIMELT2.XLS software for primary magma calculation. Geochemistry, Geophysics, Geosystems 9, Q09001.

Hess, P. (1992). Phase equilibria constraints on the origin of ocean floor basalts. In: Phipps Morgan, J., Blackman, D. K. & Sinton, J. M. (eds) Mantle Flow and Melt Generation at Mid-Ocean Ridges. Geophysical Monographs, American Geophysical Union 71, 67-102.

Jochum, K. P. & Nohl, U. (2008). Reference materials in geochemistry and environmental research and the GeoReM database. Chemical Geology 253, 50-53.

Katz, R. F., Spiegelman, M. & Langmuir, C. H. (2003). A new par- ameterization of hydrous mantle melting. Geochemistry, Geophysics, Geosystems 4, 1073.

Kingsley, R. H. & Schilling, J.-G. (1995). Carbon in Mid-Atlantic Ridge basalt glasses from 28°N to 63°N: Evidence for a carbon-enriched Azores mantle plume. Earth and Planetary Science Letters 129, 31-53.

Klügel, A., Hoernle, K. A., Schmincke, H.-U. & White, J. D. L. (2000). The chemically zoned 1949 eruption on La Palma (Canary Islands): Petrologic evolution and magma supply dynamics of a rift zone eruption. Journal of Geophysical Research 105, 5997-6016.

Kokfelt, T. F., Hoernle, K., Lundstrom, C., Hauff, F. & van den Bogaard, C. (2009).

Time-scales for magmatic differentiation at the Snaefellsjökull centralvolcano, western Iceland: Constraints from U-Th-Pa-Ra disequilibria in post-glacial lavas. Geochimica et Cosmochimica Acta 73, 1120-1144.

Krause, D. C. & Watkins, N. D. (1970). North Atlantic crustal genesis in the vicinity of the Azores. Geophysical Journal of the Royal Astronomical Society 19, 261-283.

Lee, C.-T. A., Luffi, P., Plank, T., Dalton, H. & Leeman, W. P. (2009). Constraints on the depths and temperatures of basaltic magma generation on Earth and other terrestrial planets using new thermobarometers for mafic magmas. Earth and Planetary Science Letters 279, 20-33.

Le Maitre, R. W., Bateman, P., Dudek, A., Keller, J., LeBas, M. J., Sabine, P. A., Schmid, R., Sorensen, H., Streckeiesn, A., Woolley, A. R. & Zanettin, B. (1989). A Classification of Igneous Rocks and Glossary of Terms. Oxford: Blackwell.

Lindsley, D. H. (1983). Pyroxene thermometry. American Mineralogist 68, 477-493.

Luis, J. F., Miranda, J. M., Galdeano, A. & Patriat, P. (1998). Constraints on the structure of the Azores spreading center from gravity data. Marine Geophysical Researches 20, 157-170.

Lustrino, M., Melluso, L. & Morra, V. (2007). The geochemical peculiarity of 'Plio-Quaternary' volcanic rocks of Sardinia in the circum-Mediterranean area. In: Beccaluva, L., Bianchini, G. & Wilson, M. (eds) Cenozoic Volcanism in the Mediterranean Area: Geological Society of America Special Papers 418, 277-301.

Macdonald, G. A. (1968). Composition of Hawaiian lavas. In: Coats, R. R., Hay, R. L. & Anderson, C. A. (eds) Studies in Volcanology: A Memoir in Honor of Howel Williams. Boulder, CO: Geological Society of America, pp. 477-522.

Madeira, J. & Ribeiro, A. (1990). Geodynamic models for the Azores triple junction: A contribution from tectonics. Tectonophysics 184, 405-415.

Madureira, P., Moreira, M., Mata, J. & Allègre, C. J. (2005). Primitive neon isotopes in Terceira Island (Azores archipelago). Earth and Planetary Science Letters 233, 429-440.

Millet, M.-A., Doucelance, R., Baker, J. A. & Schiano, P. (2009). Reconsidering the origins of isotopic variations in Ocean Island Basalts: Insights from fine-scale study of São Jorge Island, Azores archipelago. Chemical Geology 265, 289-302.

Montelli, R., Nolet, G., Dahlen, F. A., Masters, G., Engdahl, E. R. & Hung, S.-H. (2004). Finite-frequency tomography reveals a variety of plumes in the mantle. Science 303, 338-343.

Moreira, M., Doucelance, R., Kurz, M. D., Dupré, B. & Allègre, C. J. (1999). Helium and lead isotope geochemistry of the Azores Archipelago. Earth and Planetary Science Letters 169, 189-205.

Nekvasil, H., Dondolini, A., Horn, J., Filiberto, J., Long, H. & Lindsley, D. H. (2004). The origin and evolution of silica- saturated alkalic suites: an experimental study. Journal of Petrology 45, 693-721.

Neumann, E.-R., Wulff-Pedersen, E., Simonsen, S. L., Pearson, N. J., Marti, J. & Mitjavila, J. (1999). Evidence for fractional crystallization of periodically refilled magma chambers in Tenerife, Canary Islands. Journal of Petrology 40, 1089-1123.

Niu, Y., Wilson, M., Humphreys, E. R. & O'Hara, M. J. (2011). The origin of intra-plate ocean island basalts (OIB): the lid effect and its geodynamic implications. Journal of Petrology 52, 1443-1468.

Nunes, J. C., Camacho, A., França, Z., Montesinos, F. G., Alves, M., Vieira, R., Velez, E. & Ortiz, E. (2006). Gravity anomalies and crustal signature of volcano-tectonic structures of Pico Island (Azores). Journal of Volcanology and Geothermal Research 156, 55-70.

Parsons, B. & Sclater, J. G. (1977). An analysis of the variation of ocean floor bathymetry and heat flow with age. Journal of Geophysical Research 82, 803-827.

Pearce, J. A. & Parkinson, I. J. (1993). Trace element models for mantle melting: application to volcanic arc petrogenesis. In: Prichard, H. M., Alabaster, T., Harris, N. B. W. & Neary, C. R. (eds) Magmatic Processes and Plate Tectonics. Geological Society, London, Special Publications 76, 373-403.

Pin, C. & Zalduegui, J. S. (1997). Sequential separation of light rare-earth elements,

thorium and uranium by miniaturized extrac- tion chromatography: Application to isotopic analyses of silicate rocks. Analytica Chimica Acta 339, 79-89.

Potts, P. J., Webb, P. C. & Watson, J. S. (1984). Energy-dispersive X-ray fluorescence analysis of silicate rocks for major and trace elements. X-Ray Spectrometry 13, 2-15.

Presnall, D. C., Dixon, S. A., Dixon, J. R., O'Donnell, T. H., Brenner, N. L., Schrock, R. L. & Dycus, D. W. (1978). Liquidus phase relations on the join diopside-forsterite-anorthite from 1 atm to 20 kbar: Their bearing on the generation and crystallization of basaltic magma. Contributions to Mineralogy and Petrology 66, 203-220.

Prytulak, J. & Elliott, T. (2009). Determining melt productivity of mantle sources from 238U-230Th and 235U-231Pa disequilibria; an example from Pico Island, Azores. Geochimica et Cosmochimica Acta 73, 2103-2122.

Putirka, K. D. (1999). Clinopyroxene + liquid equilibria to 100 kbar and 2450 K. Contributions to Mineralogy and Petrology 135, 151-163.

Putirka, K. D., Ryerson, F. J. & Mikaelian, H. (2003). New igneous thermobarometers for mafic and evolved lava compositions, based on clinopyroxene + liquid equilibria. American Mineralogist 88, 1542-1554.

Putirka, K. D. (2005). Igneous thermometers and barometers based on plagioclase + liquid equilibria: Tests of some existing models and new calibrations. American Mineralogist 90, 336-346.

Putirka, K. D. (2008). Thermometers and barometers for volcanic systems. In: Putirka, K. D. & Tepley, F. J., III (eds) Minerals, Inclusions and Volcanic Processes. Mineralogical Society of America and Geochemical Society, Reviews in Mineralogy and Geochemistry 69, 61-120.

Rhodes, J. M., Dungan, M. A., Blanchard, D. P. & Long, P. E. (1979). Magma mixing at mid-ocean ridges: Evidence from basalts drilled near 228N on the Mid-Atlantic Ridge. Tectonophysics 55, 35-61.

Ridolfi, F., Renzulli, A. & Puerini, M. (2010). Stability and chemical equilibrium of amphibole in calc-alkaline magmas: an overview, new thermobarometric formulations and application to subduction- related volcanoes. Contributions to

Mineralogy and Petrology 160, 45-66.

Robinson, J. A. C. & Wood, B. J. (1998). The depth of the spinel to garnet transition at the peridotite solidus. Earth and Planetary Science Letters 164, 277-284.

Ryall, P., Blanchard, M. C. & Medioli, F. (1983). A subsided island west of Flores. Canadian Journal of Earth Sciences 20, 764-775.

Schaefer, B. F., Turner, S., Parkinson, I., Rogers, N. & Hawkesworth, C. (2002). Evidence for recycled Archaean oceanic mantle lithosphere in the Azores plume. Nature 420, 304-307.

Schwarz, S., Klügel, A. & Wohlgemuth-Ueberwasser, C. (2004). Melt extraction pathways and stagnation depths beneath the Madeira and Desertas rift zones (NE Atlantic) inferred from barometric stu- dies. Contributions to Mineralogy and Petrology 147, 228-240.

Searle, R. (1980). Tectonic pattern of the Azores spreading centre and triple junction. Earth and Planetary Science Letters 51, 415-434.

Shorttle, O., Maclennan, J. & Jones, S. M. (2010). Control of the symmetry of plume-ridge interaction by spreading ridge geometry. Geochemistry, Geophysics, Geosystems 11, Q0AC05.

Skovgaard, A. C., Storey, M., Baker, J., Blusztajn, J. & Hart, S. R. (2001). Osmium-oxygen isotopic evidence for a recycled and strongly depleted component in the Iceland mantle plume. Earth and Planetary Science Letters 194, 259-275.

Sleep, N. H. (1990). Hotspots and mantle plumes: some phenomenology. Journal of Geophysical Research 95, 6715-6736.

Sleep, N. H. (2006). Mantle plumes from top to bottom. Earth-Science Reviews 77, 231-271.

Sobolev, A. V., Hofmann, A. W., Sobolev, S. V. & Nikogosian, I. K. (2005). An olivine-free mantle source of Hawaiian shield basalts. Nature 434, 590-597.

Stein, C. A. & Stein, S. (1992). A model for the global variation in oceanic depth and heat flow with lithospheric age. Nature 359, 123-129.

Stolper, E. (1980). A phase diagram for mid-ocean ridge basalts: Preliminary results and implications for petrogenesis. Contributions to Mineralogy and Petrology 74, 13-27.

Stracke, A., Hofmann, A. W. & Hart, S. R. (2005). FOZO, HIMU, and the rest of the mantle zoo. Geochemistry, Geophysics, Geosystems 6, Q05007.

Sun, S. s. & McDonough, W. F. (1989). Chemical and isotopic system- atics of oceanic basalts: implications for mantle composition and processes. In: Saunders, A. D. & Norry, M. J. (eds) Magmatism in the Ocean Basins. Geological Society, London, Special Publications 42, 313-345.

Turner, S., Hawkesworth, C., Rogers, N. & King, P. (1997). U-Th isotope disequilibria and ocean island basalt generation in the Azores. Chemical Geology 139, 145-164.

Turner, S., Tonarini, S., Bindeman, I., Leeman, W. P. & Schaefer, B. F. (2007). Boron and oxygen isotope evidence for recycling of subducted components over the past 2·5 Gyr. Nature 447, 702-705.

Vernon, R. H. (2004). A Practical Guide to Rock Microstructure. Cambridge: Cambridge University Press.

Vogt, P. R. & Jung, W. Y. (2004). The Terceira Rift as hyper-slow, hotspot-dominated oblique spreading axis: A comparison with other slow-spreading plate boundaries. Earth and Planetary Science Letters 218, 77-90.

Watson, S. & McKenzie, D. (1991). Melt generation by plumes: a study of Hawaiian volcanism. Journal of Petrology 32, 501-537.

Wessel, P. & Smith, W. H. F. (1991). Free software helps map and display data. EOS Transactions, American Geophysical Union 72, 441.

Wessel, P. & Smith, W. H. F. (1995). New version of the Generic Mapping Tools released. EOS Transactions, American Geophysical Union79, 579.

Whipkey, C. E., Capo, R. C., Chadwick, O. A. & Stewart, B. W. (2000). The importance of sea spray to the cation budget of a coastal Hawaiian soil: a strontium isotope approach. Chemical Geology 168, 37-48.

White, W. M., Tapia, M. D. M. & Schilling, J. G. (1979). The petrology and

geochemistry of the Azores Islands. Contributions to Mineralogy and Petrology 69, 201-213.

Widom, E., Schmincke, H. U. & Gill, J. B. (1992). Processes and time- scales in the evolution of a chemically zoned trachyte: Fogo A, Sao Miguel, Azores. Contributions to Mineralogy and Petrology 111, 311-328.

Woodhead, J. D. (1992). Temporal geochemical evolution in oceanic intra-plate volcanics: a case study from the Marquesas (French Polynesia) and comparison with other hotspots. Contributions to Mineralogy and Petrology 111, 458-467.

Workman, R. K. & Hart, S. R. (2005). Major and trace element com- position of the depleted MORB mantle (DMM). Earth and Planetary Science Letters 231, 53-72.

Workman, R. K., Hart, S. R., Jackson, M., Regelous, M., Farley, K. A., Blusztajn, J., Kurz, M. & Staudigel, H. (2004). Recycled metasomatized lithosphere as the origin of the Enriched Mantle II (EM2) end-member: Evidence from the Samoan Volcanic Chain. Geochemistry, Geophysics, Geosystems 5, Q04008.

Yu, D., Fontignie, D. & Schilling, J.-G. (1997). Mantle plume-ridge interactions in the Central North Atlantic: A Nd isotope study of Mid-Atlantic Ridge basalts from 30°N to 50°N. Earth and Planetary Science Letters 146, 259-272.

Zhao, D. (2007). Seismic images under 60 hotspots: Search for mantle plumes. Gondwana Research 12, 335-355.

CHAPTER 3: OXYGEN ISOTOPES IN THE AZORES ISLANDS: CRUSTAL ASSIMILATION RECORDED IN OLIVINE

Felix S. Genske[1,2], Christoph Beier[1,2], Karsten M. Haase[1], Simon P. Turner[2], Stefan Krumm[1] and Philipp A. Brandl[1]

[1]GeoZentrum Nordbayern, Friedrich-Alexander-Universität Erlangen-Nürnberg, Schlossgarten 5, D-91054 Erlangen, Germany, felix.genske@gzn.uni-erlangen.de

[2]Australian Research Council Centre of Excellence for Core to Crust Fluid Systems/GEMOC, Macquarie University, Sydney, NSW 2109, Australia

ABSTRACT

Oxygen isotope ratios of olivine have become a widely used tool for the study of magmatic systems, especially in the interpreta- tion of source heterogeneities in mantle plume–derived ocean island basalts. The underlying assumption is that fresh minerals provide a better guide to magma $\delta^{18}O$ than bulk rock analyses and that olivine is also likely to be a major phenocryst phase in primitive magmas. However, distinctions between source compositions and the effects of subsequent magma evolution have not always been thoroughly scrutinized. For the Azores samples investigated here, we can dem- onstrate that the $\delta^{18}O$ variation (+4.84‰ to +5.25‰ Vienna standard mean ocean water) observed in the olivine phenocryst population is closely linked to evolution in the host magmas during ascent to the surface. We observe a linear, positive correlation between forsterite (Fo) content and $\delta^{18}O$ in all of the individual island lava suites. This forces us to conclude that the low oxygen isotope ratios result from combined assimilation and fractional crystallization processes, the assimilant being hydrothermally

(temperature > 250 °C) altered, lower oceanic crust. Linear regression of the measured $\delta^{18}O$ olivine values to Fo89 suggests a homogeneous mantle source with $\delta^{18}O$ = +5.2‰ ± 0.1‰.

KEYWORDS: Oxygen isotopes, OIB, olivine, lower crust assimilation, Laser fluorination

3.1 INTRODUCTION

Oxygen isotopes have been widely used as a petrogenetic tool to decipher the source of igneous rocks (e.g., Magaritz et al., 1978; Harris et al., 2000; Garcia et al., 2007; Day et al., 2009; Gurenko et al., 2011). Early studies used the oxygen isotopic fractionation between coexisting minerals to develop thermometers for igneous systems (e.g., Anderson Jr et al., 1971; Kyser et al., 1981), whereas more recent studies focus on the isotopic composition of melts and their sources. Experimentally and thermodynamically derived fractionation factors between coexisting minerals, and between minerals and host magma, provide a means of estimating the bulk oxygen isotopic composition of melts and their derivatives (e.g., Eiler, 2001; Zhao and Zheng, 2002).

Over the last two decades, advances in analytical techniques from conventional to laser fluorination and more recently ion microprobe analysis have increased the amount of data from natural and synthetic samples (Eiler, 2001; Bindeman, 2008; Eiler et al., 2011). This has afforded precise determination of oxygen isotopic variability in basaltic rocks, which in turn may provide tighter constraints on the nature of their mantle source regions (e.g., Magaritz et al., 1978; Thirlwall et al., 2006). Equilibrium fractionation between coexisting phases at mantle temperatures is an underlying assumption. In the case of olivine, it is widely established that this mineral represents an early-liquidus phase in the crystallization of basaltic melts and therefore may provide the best proxy for the oxygen isotopic composition of the primary mantle melt and its source region. The fact that forsteritic olivines are rarely zoned in $d^{18}O$ is taken as support for this notion (Eiler et al., 2011). However, as with any crystallizing system, there are additional complexities that need to be considered. For example, wall-rock assimilation processes can significantly change the composition of a rising magma, such that earlier crystallized minerals, that formed deeper and when magmas were hottest and most able to promote fusion of their host rocks, may be out of chemical equilibrium with their host magma.

Our objective here was to constrain the primary oxygen isotope composition of Azores lavas, including, for the first time, the islands west of the Mid-Atlantic Ridge (MAR). We show that, despite the fact that most olivines have forsterite and $d^{18}O$ compositions very close to mantle values, reaction with hydrothermally altered crust was nearly ubiquitous. We conclude that the range in mantle oxygen isotope composition beneath the Azores region is significantly smaller than previously inferred and that, in order to better constrain the oxygen isotope composition of the mantle, the effects of assimilation need to be appraised more closely.

3.2 APPROACH AND GEOLOGICAL BACKGROUND

3.2.1 Lavas from the Azores islands

The samples investigated in this study are lavas originating from five Azores islands, encompassing Corvo, Faial, Pico, São Jorge and São Miguel. These islands are thought to reflect the surface expressions of a mantle plume and hence have been studied intensively for their chemical and isotopic composition (e.g., White et al., 1976; Turner et al., 1997; Beier et al., 2008). Briefly, incompatible trace element ratios and Sr-Nd-Pb isotope ratios of the Azores lavas are consistent with a mantle source that is heterogeneous on a small-scale (Fig. 1), with significant trace element and isotope variability occurring even within a single island (Turner et al., 1997; Elliott et al., 2007; Beier et al., 2007). Oxygen isotope values however are relatively scarce for these islands and most studies so far focused on the islands located to the east of the mid-Atlantic ridge (MAR) (Widom and Farquhar, 2003; Turner et al., 2007).

3.2.2 Methods

Olivines from selected lavas (MgO >5 wt.%) that are known to have distinct and variable radiogenic isotopic compositions (Fig. 1; Corvo, Pico, Faial, São Jorge and São Miguel) were handpicked to avoid contamination, alteration and, where visible, inclusions. Single grains were coarsely crushed in a steel mortar to obtain splits. These were treated separately to obtain mineral chemical compositions via electron microprobe (EMP) analysis and the oxygen isotope composition via laser fluorination from the same crystal. All analyses were performed at the GeoZentrum Nordbayern, University of Erlangen-Nürnberg. The full method description is given in supplementary file DR1.

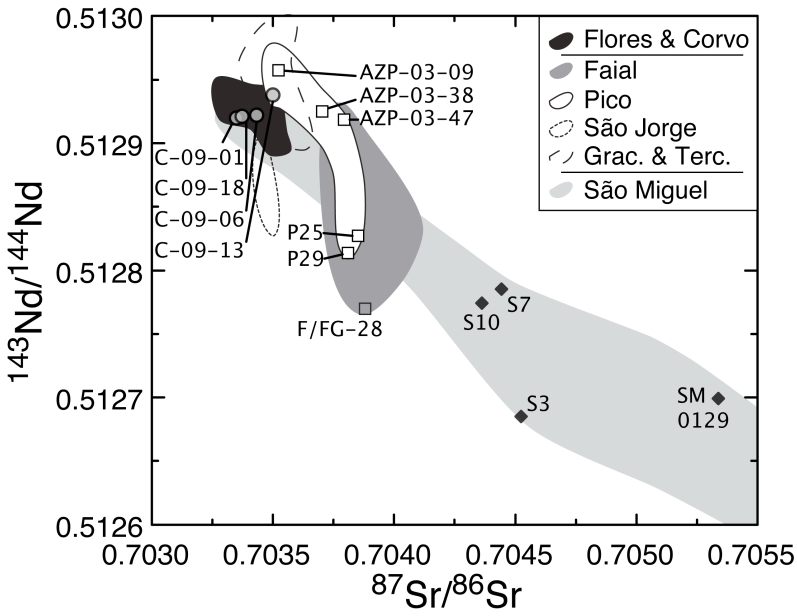

Figure 1. Strontium versus neodymium isotope ratios of lavas from the Azores islands highlighting the extreme small-scale heterogeneity of the Azores mantle plume, which is expressed even within single islands (e.g. São Miguel). The fields summarize published data of individual islands (Turner et al., 1997; Beier et al., 2008; Genske et al., 2012). Samples with Nd and Sr isotope data are labeled, as olivines from these lavas are analyzed herein for oxygen isotope composition.

3.3 RESULTS

3.3.1 $\delta^{18}O$ values of Azores olivines

The observed values of oxygen isotope ratios from single olivines are presented in Table 1 of the supplementary file DR1. The islands in the center of the Azores archipelago, and therefore closest to the plume center (Terceira, (Bourdon et al., 2005)), have low $d^{18}O$ values, extending to lower values than normally considered to be representative of pristine mantle olivine with $d^{18}O = +5.2 \pm 0.2‰$ (Mattey et al., 1994). However, low $d^{18}O$ olivines are also observed on the islands furthest from the plume center at the margin of the plateau (e.g., São Miguel and Corvo). The overall range for the olivines is $d^{18}O = +4.84–5.25$ ‰ V-SMOW, thus the olivine population of the Azores lavas exceeds the range in $d^{18}O$ of the pristine mantle.

3.3.2 Mineral Chemistry

The phenocryst nature of the olivines investigated in this study is evident from the major and minor element oxides versus forsterite (Fo) contents (Fig. 2A), which vary from Fo_{77} to Fo_{90}. Calcium and Ni reveal similar behavior during magmatic differentiation as their

concentrations decrease continuously (CaO, 0.41–0.17 wt. %; NiO, 0.31–0.08 wt. %) with decreasing Fo. However, the NiO concentrations (not shown, Table DR1) at a given Fo content are slightly, but systematically, lower in olivines from Corvo relative to the olivines from islands to the east of the MAR.

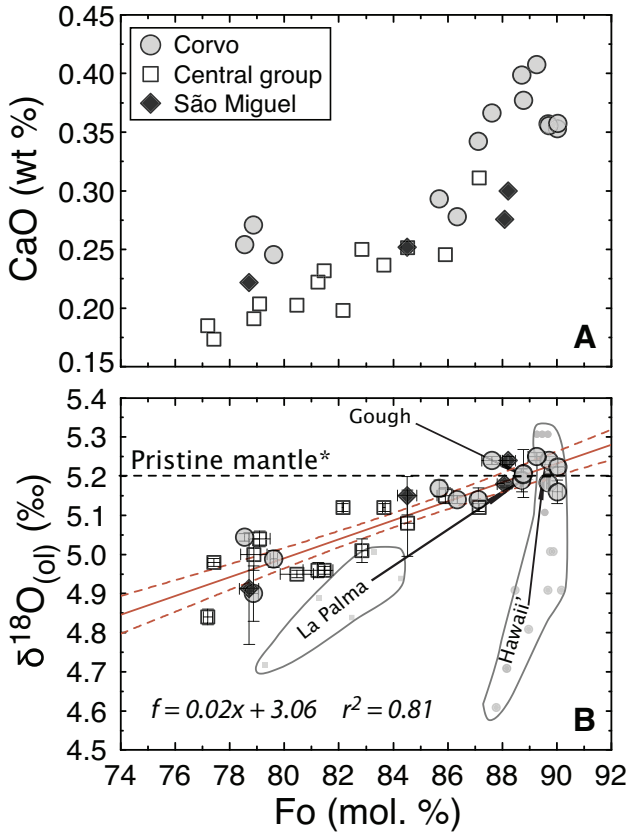

Figure 2. Mineral composition of single olivines from selected Azores lavas. Calcium (A) content indicate these phenocrysts follow fractional crystallization trends (i.e. decreasing concentrations with decreasing Fo contents). Note that the olivine population from Corvo is somewhat different at a given Fo content. B: $\delta^{18}O$ versus forsterite contents of olivines measured during this study emphasize a clear correlation below pristine mantle compositions (Mattey et al., 1994). Fields of other hotspot localities (Wang and Eiler, 2008; Day et al., 2009; Harris et al., 2000) are shown to highlight homogeneous $\delta^{18}O$ ~5.2 ‰ for Fo~89-90, indistinguishable from upper mantle olivine.

3.3 DISCUSSION

The oxygen isotope fractionation factor between olivine and basaltic melt at mantle temperatures is well constrained (Eiler, 2001). Yet there is increasing evidence, from detailed studies of individual lava flows (Wang and Eiler, 2008) and of individual volcanoes (Harris et al., 2000), that oxygen isotopes can provide clues to assimilation processes and there is enhanced utility in studies that combine phenocryst compositions

with oxygen isotope determinations from the same crystal. Assuming that the partition coefficient K_D of Fe-Mg between olivine and melt ~0.3 (Roeder and Emslie, 1970), the oxygen isotope composition of primary basalts will be most closely approximated by olivines with Fo ~89 (host magma Mg# ~71). For the Azores, magma differentiation histories are comparable between the islands (cf. Beier et al., 2008; Genske et al., 2012) and are dominated by olivine and clinopyroxene crystallization. These minerals typically have $\delta^{18}O$ values lower than the melt, thus their removal would increase the $\delta^{18}O$ value of the differentiated melt (e.g., Muehlenbachs and Byerly, 1982). This is in contrast with what we observe here. The range of forsterite content in our data set is very large, but correlates positively with $\delta^{18}O$. This strong correlation (r^2 ~0.81; Fig. 2B) allows us to extrapolate $\delta^{18}O$ values for putative mantle olivines ($Fo_{89–93}$; results are given in Table DR1). The relationship observed in this study implies assimilation fractional crystallization (AFC) processes, which we will discuss in detail further below. In the following section we will constrain the primary oxygen isotope composition of Azores mantle sources.

3.3.1 Primary oxygen isotopic compositions of the Azores mantle

The main observation of this work is the tight correlation of $\delta^{18}O$ with Fo, and thus we aim to constrain the primary oxygen isotope signals of the individual volcanic suites, i.e., the $\delta^{18}O$ of $Fo_{(>89)}$. Yet there is no resolvable difference in the $\delta^{18}O$-Fo arrays between the islands (Fig. 2B), although each of the sampled volcanic systems has a distinct mantle source in terms of Sr-Nd-(Pb-Hf) isotopes (cf. Figure 1, Table DR1). Thus, when applying linear regression to the measured $\delta^{18}O_{(ol)}$ data, it becomes evident that the mantle sources beneath the Azores islands are extremely homogeneous in terms of the oxygen isotopic composition, at least given the currently available analytical resolution. This also implies that the variability observed in radiogenic isotopes must be high temperature and thus reflects mostly intra-mantle processes, which only permits limited contribution from recycled components.

The calculated $\delta^{18}O_{(Fo89)}$ values here average at +5.2 ± 0.1 ‰ (2SD; Table DR1), which is in excellent agreement with estimates for pristine upper mantle olivine (Mattey et al., 1994). If the source were characterized by Fe-depletion (e.g., Schaefer et al., 2002; Turner et al., 2007), and thus Fo ~93, it would have slightly higher oxygen isotope values ($d^{18}O_{(ol)}$ ~ +5.29 ‰). From this we conclude that the oxygen isotope ratios of Azores

mantle olivine (i.e., $Fo_{(>89)}$) are very homogeneous. Whether or not our observation in terms of homogeneous oxygen isotope compositions in the mantle apply globally remains a matter to be tested in other geodynamic settings. Yet, olivine from off-ridge and ridge centered OIB has very similar $d^{18}O$ compositions: Hawaii, Mauna Loa, $d^{18}O_{(Fo90)}$ = +5.24 ± 0.09 ‰; Canary islands, La Palma, $d^{18}O_{(Fo89)}$ = +5.20 ± 0.12 ‰; Tristan da Cunha, Gough island $d^{18}O_{(Fo>85)}$ = +5.19 ± 0.14 ‰; Azores islands $d^{18}O_{(Fo89)}$ = +5.20 ± 0.10 ‰ ((Wang and Eiler, 2008; Day et al., 2009; Harris et al., 2000), Azores this study, Fig. 2B). Thus there is striking evidence that olivine phenocrysts from ridge centered and off-ridge hotspot settings, and by implication from the deeper mantle, are indistinguishable in the primary $d^{18}O$ composition from upper mantle olivine, unless one assumes higher Fo contents.

In order to further evaluate the deviation from mantle values, we will now discuss models involving AFC, similarly to what has been described for Hawaii' (Wang and Eiler, 2008) and Tristan da Cunha and Gough island (Harris et al., 2000).

3.3.2 Assimilation fractional crystallization

Since our measured data set is limited to five islands, we applied the equation derived in Figure 2B to a larger sample set. This sample set includes primitive lavas (MgO = 5–12 wt. %) from the western Azores (Flores and Corvo), the central Azores (Faial, Pico, Graciosa, Terceira and São Jorge) and the eastern Azores island of São Miguel (Turner et al., 1997; Beier et al., 2007; Beier et al., 2008; Genske et al., 2012). In detail, we first estimated Fo-values in equilibrium with lava compositions (Roeder and Emslie, 1970) and subsequently calculated their $d^{18}O$ based on the equation of the correlation. To account for olivine-melt $d^{18}O$ fractionation, we added 0.4 ‰ to the $d^{18}O_{(Fo)}$ to estimate $d^{18}O_{(melt)}$ values (Eiler, 2001). We also applied olivine-liquid thermometers following the models by Putirka (2008), where we used equilibrium-liquid compositions from the larger Azores data set. The temperature results are given in Table DR1 and are in good agreement with previously published temperatures of Azores lavas (Beier et al., 2012; Genske et al., 2012). These estimates are useful since they show that the magmas were much hotter than the overlying oceanic crust and thus promote significant fusion (cf. DePaolo (1981)).

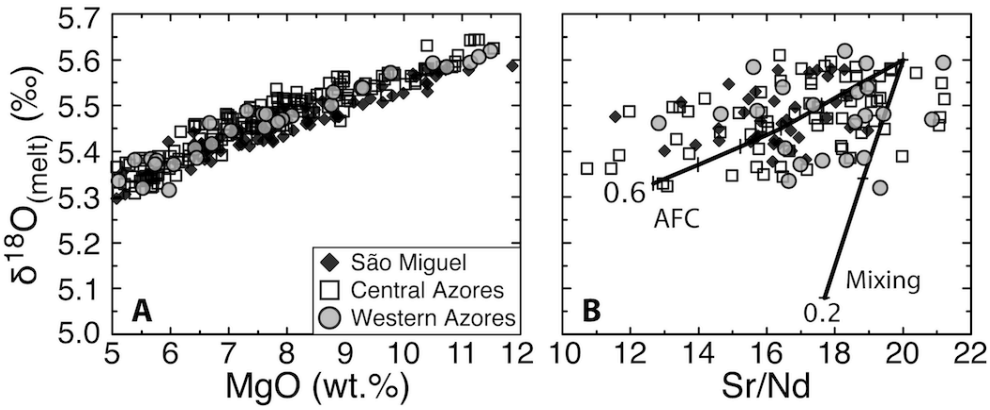

Figure 3. Calculated $d^{18}O_{(melt)}$ versus MgO (A) and Sr/Nd (B) compositions of Azores lavas. Details of the calculation of melt $d^{18}O$ from olivine data and of AFC models are given in the text. The AFC and mixing model end members are: $d^{18}O$ = +5.6 ‰ and +4.0 ‰, Sr/Nd = 20 and 10, for melt and assimilant, respectively. The extent of magmatic differentiation (~60 %) is consistent with previous estimates for the basalts (Genske et al., 2012). The assimilant was constrained to be hydrothermally altered gabbro of the underlying oceanic crust with $d^{18}O$ <4 ‰. In contrast, ~10 % mixing with AOC would explain the $d^{18}O$ range, but not Sr/Nd observed in the lavas.

The oxygen isotopic composition of the hydrothermally altered oceanic crust (AOC) is significantly different from that of pristine mantle. Analyses of AOC confirm that high-temperature, altered gabbro layers may extend down to $d^{18}O$ values of +2.5 ‰ (e.g., Alt and Honnorez, 1984; Gao et al., 2006), but globally do not average significantly below +4 ‰ (Thirlwall et al., 2006). We performed AFC modeling, using the equations by DePaolo (1981), as illustrated on Figure 3B, with a broad correlation of Sr/Nd with $d^{18}O$. The MgO content of the lavas was used to monitor the degree of magmatic differentiation. Since the range in $d^{18}O_{(melt)}$ at a given trace element concentration (e.g., Sr and Nd, not shown) is relatively limited and similar across the islands, it is ambiguous to further discriminate AFC parameters that may have resulted in the slight differences of $d^{18}O$ behavior during magma differentiation. However, changing the proportion of assimilation relative to fractionation has large effects on the modeled $d^{18}O$, but relatively minor effects on Sr/Nd or $^{87}Sr/^{86}Sr$. The proportion of the assimilant with $d^{18}O$ ~ +4 ‰ chosen to fit the data in Figure 3B is r ~0.25. Indeed, the range of $^{87}Sr/^{86}Sr$ observed in the Azores lavas, even within the homogeneous suites of Flores and Corvo, exceeds that of calculated values with different proportions of the assimilant (i.e. r = 0.1-0.5). Furthermore, the correlation coefficient for the Azores olivine population (Figure 2B) suggests that $d^{18}O$ evolution of olivine is due to very similar assimilation processes even between the islands. We suggest that the assimilant in each island has to be

compositionally similar. Also, if significant amounts of volcanic conduit material, altered by precipitation water, had been assimilated on the different islands, the slopes in $d^{18}O$ versus forsterite would be more diverse than observed here (Fig. 2B). Different trends would then most likely represent different localities (i.e., volcanoes) or stratigraphic units (i.e., post-shield versus shield stages), as has been observed in the Hawaiian volcanic chain (Wang and Eiler, 2008). Thus, we constrain the $d^{18}O$ of the assimilant (hydrothermally altered gabbroic layers of the oceanic crust) to be characterized by values below +4.5 ‰. This has been suggested for AOC in OIB settings previously (e.g., Eiler, 2001; Wang and Eiler, 2008). We further conclude that assimilation of hydrothermally altered oceanic crust occurs in magmas across the whole Azores archipelago. Whereas MORB generally show constant or higher $d^{18}O$ with increasing magma evolution (e.g., Wanless et al., 2011) OIB magmas show lower oxygen isotopes, which result from assimilation of ocean crust that underwent variable degrees of hydrothermal alteration.

In the following section we discuss the significance of our findings for the interpretation of mantle sources in OIB settings, with a focus on the origin of the Azores mantle plume source.

3.3.3 Implications for the Azores mantle plume

Deviations of the olivine oxygen isotopic signal from the accepted mantle range of Mattey et al. (1994), led numerous authors to speculate whether this can be used to constrain possible contributing source components within mantle plumes. The fact, that oxygen isotopes are only efficiently fractionated in near surface environments and thus at temperatures much lower than initial mantle and magmatic temperatures, has been taken as evidence that anomalously high or low olivine oxygen isotope ratios (i.e., < +5.0 ‰ or > +5.4 ‰) reflect subducted and recycled oceanic crust (±sediment) (e.g., Turner et al., 2007). This may indeed be the case in some settings; however, the assimilation of AOC may not always be evident from the major and trace element ratios in the host lavas. For example, if only small volumes are assimilated then even the more sensitive $^{87}Sr/^{86}Sr$ isotope ratios may not reflect assimilation as a result of the much greater variability of Sr isotope composition in the mantle (e.g., White et al., 1976; Hart et al., 1992).

The homogeneous $d^{18}O$ of +5.2 ± 0.1 ‰ in Azores olivines indicates that the oxygen in the mantle of this volcanic region was not affected significantly by recycled components that are seen in other isotopic tracers (e.g., Beier et al., 2007; Turner et al., 2007).

3.4 CONCLUSION

Selected olivines from the Azores islands display a strong (r^2 ~0.81), near linear covariation of mineral major element chemistry and $d^{18}O$. Decreasing $d^{18}O$ with decreasing Fo contents lead us to conclude that AFC-style processes involving the gabbroic layers of the underlying hydrothermally AOC as the dominant assimilant ($d^{18}O$ ~ +4.0 ‰), had greatest effect on the change in $d^{18}O$ of the magmatic systems beneath the individual volcanic islands. Additionally, the forsterite contents of most olivines are too low (Fo <<89) to be of primary (peridotite mantle) origin. The homogeneity of oxygen isotopes observed in the Azores mantle is in strong contrast with the highly variable Sr-Nd-(Hf-Pb) isotope systems. Our results shown here reveal no sign of recycled material in the oxygen isotopes. Instead, these support abundant high-temperature altered material beneath the entire Azores plateau that ultimately affects the ascending magmas. This is in contrast to what had been proposed previously.

ACKNOWLEDGMENTS

This project was funded by projects BE4459/1-1 and BE4459/4-1 of the Deutsche Forschungsgemeinschaft. We acknowledge the help of Victor Hugo For- jaz and the Observatório Vulcanológico e Geotérmico dos Açores during various stays in the Azores. We thank M. Joachimski and D. Lutz for providing the mass spectrometers for oxygen measurements in Erlangen. Reviews by C. Harris and M. Thirlwall considerably improved the manuscript. This is contribution 241 from the ARC Centre of Excellence for Core to Crust Fluid Systems (http://www.ccfs. mq.edu.au) and 866 in the GEMOC Key Centre (http://www.gemoc.mq.edu.au).

REFERENCES

Anderson Jr, A.T., Clayton, R.N., and Mayeda, T.K., 1971, Oxygen isotope thermometry of mafic igneous rocks: The Journal of Geology, v. 79, no. 6, p. 715–729, doi:10.1086/627700.

Alt, J.C., and Honnorez, J., 1984, Alteration of the upper oceanic crust, DSDP site 417: Mineralogy and chemistry: Contributions to Mineralogy and Petrology, v. 87, no. 2, p. 149–169, doi:10.1007/BF00376221.

Beier, C., Stracke, A., and Haase, K.M., 2007, The peculiar geochemical signatures of São Miguel (Azores) lavas: Metasomatised or recycled mantle sources?: Earth and Planetary Science Letters, v. 259, no. 1–2, p. 186–199, doi:10.1016/j.epsl.2007.04.038.

Beier, C., Haase, K.M., Abouchami, W., Krienitz, M.S., and Hauff, F., 2008, Magma genesis by rifting of oceanic lithosphere above anomalous mantle: Terceira Rift, Azores: Geochemistry Geophysics Geosystems, v. 9, Q12013, doi:10.1029/2008GC002112.

Beier, C., Haase, K.M., and Turner, S.P., 2012, Conditions of melting beneath the Azores: Lithos, v. 144–145, no. 0, p. 1–11, doi:10.1016/j.lithos.2012.02.019.

Bindeman, I.N., 2008, Oxygen isotopes in mantle and crustal magmas as revealed by single crystal analysis: Reviews in Mineralogy and Geochemistry, v. 69, no. 1, p. 445–478, doi:10.2138/rmg.2008.69.12.

Bourdon, B., Turner, S.P., and Ribe, N.M., 2005, Partial melting and upwelling rates beneath the Azores from a U-series isotope perspective: Earth and Planetary Science Letters, v. 239, no. 1–2, p. 42–56, doi:10.1016/j.epsl.2005.08.008.

Day, J.M.D., Pearson, G.D., Macpherson, C.G., Lowry, D., and Carracedo, J.-C., 2009, Pyroxenite-rich mantle formed by recycled oceanic lithosphere: Oxygen-osmium isotope evidence from Canary Island lavas: Geology, v. 37, no. 6, p. 555–558, doi:10.1130/G25613A.1.

DePaolo, D.J., 1981, Trace element and isotopic effects of combined wallrock assimilation and fractional crystallization: Earth and Planetary Science Letters, v. 53,

no. 2, p. 189–202, doi:10.1016/0012-821X(81)90153-9.

Eiler, J.M., 2001, Oxygen isotope variations of basaltic lavas and upper mantle rocks: Reviews in Mineralogy and Geochemistry, v. 43, no. 1, p. 319–364, doi:10.2138/gsrmg.43.1.319.

Eiler, J.M., Stolper, E.M., and McCanta, M.C., 2011, Intra- and intercrystalline oxygen isotope variations in minerals from basalts and peridotites: Journal of Petrology, v. 52, no. 7–8, p. 1393–1413, doi:10.1093/petrology/egr006.

Elliott, T., Blichert-Toft, J., Heumann, A., Koetsier, G., and Forjaz, V.H., 2007, The origin of enriched mantle beneath São Miguel, Azores: Geochimica et Cosmochimica Acta, v. 71, no. 1, p. 219–240, doi:10.1016/j.gca.2006.07.043.

Gao, Y., Hoefs, J., Przybilla, R., and Snow, J.E., 2006, A complete oxygen isotope profile through the lower oceanic crust, ODP Hole 735B: Chemical Geology, v. 233, no. 3–4, p. 217–234, doi:10.1016/j.chemgeo.2006.03.005.

Garcia, M.O., Ito, E., and Eiler, J.M., 2007, Oxygen isotope evidence for chemical interaction of Kilauea historical magmas with basement rocks: Journal of Petrology, v. 49, no. 4, p. 757–769, doi:10.1093/petrology/egm034.

Genske, F.S., Turner, S.P., Beier, C., and Schaefer, B.F., 2012, The petrology and geochemistry of lavas from the western Azores Islands of Flores and Corvo: Journal of Petrology, v. 53, no. 8, p. 1673–1708, doi:10.1093/petrology/egs029.

Gurenko, A.A., Bindeman, I.N., and Chaussidon, M., 2011, Oxygen isotope heterogeneity of the mantle beneath the Canary Islands: insights from olivine phenocrysts: Contributions to Mineralogy and Petrology, v. 162, no. 2, p. 349–363, doi:10.1007/s00410-010-0600-5.

Harris, C., Smith, H.S., and Le Roex, A.P., 2000, Oxygen isotope composition of phenocrysts from Tristan da Cunha and Gough Island lavas: variation with fractional crystallization and evidence for assimilation: Contributions to Mineralogy and Petrology, v. 138, no. 2, p. 164–175, doi:10.1007/s004100050015.

Hart, S.R., Hauri, E.H., Oschmann, L.A., and Whitehead, J.A., 1992, Mantle plumes and entrainment: Isotopic evidence: Science, v. 256, no. 5056, p. 517–520,

doi:10.1126/science.256.5056.517.

Kyser, T.K., O'Neil, J.R., and Carmichael, I.S.E., 1981, Oxygen isotope thermometry of basic lavas and mantle nodules: Contributions to Mineralogy and Petrology, v. 77, no. 1, p. 11–23, doi:10.1007/BF01161498.

Magaritz, M., Whitford, D.J., and James, D.E., 1978, Oxygen isotopes and the origin of high-87Sr/86Sr andesites: Earth and Planetary Science Letters, v. 40, no. 2, p. 220–230, doi:10.1016/0012-821X(78)90092-4.

Mattey, D., Lowry, D., and Macpherson, C., 1994, Oxygen isotope composition of mantle peridotite: Earth and Planetary Science Letters, v. 128, no. 3–4, p. 231–241, doi:10.1016/0012-821X(94)90147-3.

Muehlenbachs, K., and Byerly, G., 1982, 18O-Enrichment of silicic magmas caused by crystal fractionation at the Galapagos Spreading Center: Contributions to Mineralogy and Petrology, v. 79, no. 1, p. 76–79, doi:10.1007/BF00376963.

Putirka, K.D., 2008, Thermometers and barometers for volcanic systems: Reviews in Mineralogy and Geochemistry, v. 69, no. 1, p. 61–120, doi:10.2138/rmg.2008.69.3.

Roeder, P.L., and Emslie, R.F., 1970, Olivine-liquid equilibrium: Contributions to Mineralogy and Petrology, v. 29, no. 4, p. 275–289, doi:10.1007/BF00371276.

Schaefer, B.F., Turner, S.P., Parkinson, I.J., Rogers, N., and Hawkesworth, C.J., 2002, Evidence for recycled Archaean oceanic mantle lithosphere in the Azores plume: Nature, v. 420, no. 6913, p. 304–307, doi:10.1038/nature01172.

Thirlwall, M.F., Jenkins, C., Vroon, P.Z., and Mattey, D.P., 1997, Crustal interaction during construction of ocean islands: Pb-Sr-Nd-O isotope geochemistry of the shield basalts of Gran Canaria, Canary Islands: Chemical Geology, v. 135, no. 3-4, p. 233-262, doi:10.1016/S0009-2541(96)00118-0.

Thirlwall, M.F., Gee, M.A.M., Lowry, D., Mattey, D., Murton, B.J., and Taylor, R.N., 2006, Low d18O in the Icelandic mantle and its origins: Evidence from Reykjanes Ridge and Icelandic lavas: Geochimica et Cosmochimica Acta, v. 70, no. 4, p. 993–1019, doi:10.1016/j.gca.2005.09.008.

Turner, S.P., Hawkesworth, C.J., Rogers, N., and King, P., 1997, U-Th isotope disequilibria and ocean island basalt generation in the Azores: Chemical Geology, v. 139, no. 1–4, p. 145–164, doi:10.1016/S0009-2541(97)00031-4.

Turner, S.P., Tonarini, S., Bindeman, I.N., Leeman, W.P., and Schaefer, B.F., 2007, Boron and oxygen isotope evidence for recycling of subducted components over the past 2.5 Gyr: Nature, v. 447, no. 7145, p. 702–705, doi:10.1038/nature05898.

Wang, Z., and Eiler, J.M., 2008, Insights into the origin of low-[delta]18O basaltic magmas in Hawaii revealed from in situ measurements of oxygen isotope compositions of olivines: Earth and Planetary Science Letters, v. 269, no. 3–4, p. 377–387, doi:10.1016/j.epsl.2008.02.018.

Wanless, V.D., Perfit, M.R., Ridley, W.I., Wallace, P.J., Grimes, C.B., and Klein, E.M., 2011, Volatile abundances and oxygen isotopes in basaltic to dacitic lavas on mid-ocean ridges: The role of assimilation at spreading centers: Chemical Geology, v. 287, no. 1–2, p. 54–65, doi:10.1016/j.chemgeo.2011.05.017.

White, W.M., Schilling, J.-G., and Hart, S.R., 1976, Evidence for the Azores mantle plume from strontium isotope geochemistry of the Central North Atlantic: Nature, v. 263, no. 5579, p. 659–663, doi:10.1038/263659a0.

Widom, E., and Farquhar, J., 2003, Oxygen isotope signatures in olivines from São Miguel (Azores) basalts: Implications for crustal and mantle processes: Chemical Geology, v. 193, no. 3–4, p. 237–255, doi: doi: 10.1016/S0009-2541(02)00264-4.

Zhao, Z.-F., and Zheng, Y.-F., 2002, Calculation of oxygen isotope fractionation in magmatic rocks: Chemical Geology, v. 193, no. 1–2, p. 59–80.Alfred, T.A.J., Clayton, R.N., and Mayeda, T.K., 1971, Oxygen Isotope Thermometry of Mafic Igneous Rocks: The Journal of Geology, v. 79, no. 6, p. 715–729.

CHAPTER 4: LITHIUM AND BORON ISOTOPIC CONSTRAINTS ON THE SOURCE OF MAGMAS IN THE AZORES ISLANDS

Felix S. Genske[a,b,*], Simon P. Turner[a], Christoph Beier[a,b], Mei-Fei Chu[a,c], Sonia Tonarini[d], Norman J. Pearson[a], Karsten M. Haase[b]

[a]ARC Centre of Excellence for Core to Crust Fluid Systems/GEMOC, Dept. of Earth and Planetary Sciences, Macquarie University, Sydney NSW 2109, Australia

[b]GeoZentrum Nordbayern, Friedrich-Alexander-Universität Erlangen-Nürnberg, Schlossgarten 5, 91054 Erlangen, Germany

[c]Department of Geosciences, National Taiwan University, Taipei 10617, Taiwan

[d]Istituto di Geoscienze e Georisorse-CNR, Via Moruzzi 1, Pisa, Italy

*corresponding author: felix.genske@uni-muenster.de, now at: Institut für Mineralogie, Westfälische Wilhelms-Universität Münster, Corrensstraße 24, 48149 Münster

ABSTRACT

New lithium and boron data are presented for well-characterised lavas from the Azores islands. These ocean islands reflect the surface expression of a low-buoyancy mantle plume. From traditional radiogenic isotope studies of these islands it has been suggested that the plume source is heterogeneous on a small scale. However, little information is available from stable isotopes even though these should be particularly useful in fingerprinting low-temperature, recycled components such as sediments or crustal rocks. Also, until recently there has been a lack of data from the islands to the west of the Mid-Atlantic ridge (Flores and Corvo). Building on a recent detailed study of these two islands, we document here the variability of lithium and boron concentrations and their

isotopic compositions across the full archipelago on well-defined samples. We show that both systems yield some values that are typical for ocean island basalts. However, the variability of both δ^7Li and $\delta^{11}B$ observed in primitive lavas is most extreme on the western islands of Flores and Corvo (δ^7Li ~ 3.5-8.2 ‰ and $\delta^{11}B$ ~ -3.5-+11.8 ‰). Overall, these are most likely due to contamination of the magmas during ascent through hydrothermally altered oceanic crust. Models of assimilation fractional crystallisation best explain the variability observed on each island and allow for robust estimates of the mantle source. The implication of these observations is that the interpretation of the radiogenic isotopes and trace elements may have to be treated with care if the stable isotopes display a contamination of magmas by assimilation of hydrothermally altered material and that the use of Li and B as mantle source tracers may be obscured by shallow level processes.

Keywords: Lithium-Boron isotopes, Ocean Island Basalts, Azores mantle plume, recycling, assimilation

4.1. INTRODUCTION

Ocean Island Basalts (OIB) have the potential to provide important information on mantle convection and recycling of crustal material (Gast et al., 1964; Hofmann, 1997). The presence of OIB has generally been associated with the presence of thermally induced melting ("hotspots", (Montelli et al., 2004; Ritsema and Allen, 2003)), but also heterogeneity, in the form of enriched, volatile-rich mantle (e.g. "wetspots" (Bonatti, 1990)). Fluid dynamic models suggest that most mantle plumes should be radially symmetric (Campbell, 1990; Shorttle et al., 2010; White et al., 1979). For example, radiogenic isotopes from the Galápagos OIB exhibit a horseshoe shaped pattern thought to reflect a cross-section through a toroidal plume head that is enfolding shallow mantle material (White et al., 1993). However, other plumes erupted close to Mid-Ocean Ridges (MOR) appear even more complex (e.g. the Easter Hotspot (Haase, 2002)).

If plumes are situated close to spreading axes, plume material is likely to preferentially flow into the spreading axis creating a geochemical and geophysical anomaly along the spreading axis (e.g. (Vogt and Jung, 2004) and (Schilling, 1991; 1975)). In the Azores, seven of the volcanic islands are situated on east-west alignments on the eastern part of the plateau, which provides an ideal opportunity to study the flow and distribution of the enriched material in the upper mantle towards the Mid-Atlantic Ridge (MAR) (e.g. (Beier

et al., 2008)). Combined with new data from the western Azores islands (Genske et al., 2012), it is now possible to more fully appraise the across-plateau volcanism.

The eastern islands have been the subject of many geochemical studies (Beier et al., 2008; 2012; 2010; Elliott et al., 2007; Prytulak and Elliott, 2009; Turner et al., 1997; White et al., 1979; Widom et al., 1997; Widom and Shirey, 1996) and typically erupt alkaline basaltic to trachytic lavas that are enriched in incompatible elements. Mid-Ocean Ridge Basalts (MORB) from the adjacent MAR are also enriched in incompatible elements and have relatively high $^{87}Sr/^{86}Sr$, $^{206}Pb/^{204}Pb$ and relatively low $^{143}Nd/^{144}Nd$ and $^{4}He/^{3}He$ isotope ratios compared to normal depleted MORB (Dosso et al., 1999; Moreira and Allègre, 2002; Moreira et al., 2012). Seismic results suggest the plateau has a crustal thickness of 14 km (Escartín et al., 2001) consistent with increased partial melting due the impact of a mantle plume head some 10 million years ago (Cannat et al., 1999).

The formation of melts beneath the eastern islands has generally been associated with melting as a result of a mantle plume beneath the island of Terceira (Bourdon et al., 2005). Nevertheless, the causes of melting and volcanism in the western Azores remain poorly understood. From Sr-Nd isotope data, it appears that the source region beneath these two western islands is relatively homogeneous and characterised by a FOZO-like composition (Genske et al., 2012). To further assess and better refine the source heterogeneity across the Azores we have analysed well-characterised samples for the stable isotopes of lithium (Li) and boron (B). Studies of these two light elements and their isotopic composition may allow us to further decipher the nature of individual recycled components because they provide a powerful tracer of crustal material that has undergone low temperature alteration near the Earth's surface (e.g. (Chan et al., 2009; Elliott et al., 2006b; Kobayashi et al., 2004; Tomascak et al., 2002; Turner et al., 2007)).

The normal (i.e. MORB) mantle range in $\delta^{7}Li$ is relatively well defined to lie between 3-4 ‰ (e.g. (Elliott et al., 2006b; Jeffcoate et al., 2007; Magna et al., 2008; Seitz et al., 2004) and recent studies have shown that most OIB lavas exhibit a range of $\delta^{7}Li$ (~ 2-8 ‰, including analytical uncertainty) larger than that of MORB (Krienitz et al., 2012; Magna et al., 2011; Ryan and Kyle, 2004; Tomascak et al., 2008). However, few studies have attempted to assign more concise Li isotope signatures to enriched mantle end members (i.e. elevated, heavy Li signatures for HIMU type lavas (Chan et al., 2009; Vlastélic et al.,

2009). The Li isotopic composition of other enriched mantle types is much less well constrained (e.g. (Magna et al., 2011; Tomascak, 2004)). The other reservoir that may be crucial when assessing the δ^7Li composition of OIB lavas is altered oceanic crust, since assimilation during magma ascent will affect their primary signature. Assimilation fractional crystallization (AFC) processes have recently been demonstrated to be important for the Azores lavas using oxygen isotope data (Genske et al., 2013) and thus may be of importance for the assessment of the Li and B isotope data. The assimilant was constrained to be the lower layers of hydrothermally altered crust (i.e. gabbro layers). The composition of hydrothermally altered gabbros that equilibrated with seawater shows Li depletion with high δ^7Li (up to ~+14 ‰, e.g. (Chan et al., 2002)) relative to unaltered seafloor basalt, whereas overlying altered basalts are only slightly heavier in Li isotopic composition (~+7 ‰, e.g. (Nishio et al., 2005)) than fresh MORB. A study of oceanic crustal rocks from the East Pacific Rise (EPR) revealed that young alteration is commonly characterised by Li depletion (Brant et al., 2012). However, depending on the particular style of fluid-rock interaction (i.e. plagioclase leaching vs. dissolution of igneous minerals and subsequent formation of hydrothermal phases), basaltic products of hydrothermal alteration are characterised by a variable δ^7Li at low Li concentrations (Brant et al., 2012).

Like Li, boron is a strongly fluid-mobile element, but unlike Li it cannot substitute into iron-magnesium silicates. However, B and its isotopic composition are potentially sensitive tools to distinguish between processes of assimilation, surface alteration including seawater and subducting materials, since all of these can arguably account for the low-T geochemical signature in OIB (e.g. (Tanaka and Nakamura, 2005)). This arises because B is highly incompatible in solids in equilibrium with fluids and/or melts; ^{11}B is strongly fractionated from ^{10}B during water-rock interaction under low-T conditions (Ryan et al., 1996; Spivack and Edmond, 1987; Tanaka and Nakamura, 2005) and seawater is much heavier (+39.5 ‰, (Smith et al., 1995)) than typical upper mantle compositions (~ -3 to -12 ‰, (Chaussidon and Jambon, 1994; Chaussidon and Marty, 1995; Spivack and Edmond, 1987)). Nevertheless, only few studies have yet determined the B isotopic composition of OIB sources (e.g. (Brounce et al., 2012; Chaussidon and Jambon, 1994; Kobayashi et al., 2004)). This is partly due to the unique behaviour of B during water-rock and rock-melt interaction, which is still not well understood. Depending of the nature of such interaction and the isotopic composition of the

participating end members during such processes the final product can be characterised by higher or lower than mantle-like B isotope ratios. For example, a recent study by Brounce et al. (2012) on Icelandic melt inclusions revealed that resolvable differences in B isotopes are caused by contamination during magma ascent through hydrothermally altered oceanic crust. The style of alteration here was driven by the influence of meteoric water, such that the altered crust carries light, rather than heavy, B. This contrasts with a similar study of melt inclusions from Hawaiian lavas (Kobayashi et al., 2004), where a positive correlation was observed between B and Li isotopes, providing evidence for an isotopically light, recycled end member. Nevertheless, these authors also concluded that higher than mantle-like values resulted either from recent alteration and/or assimilation of altered crustal materials.

In the Azores Turner et al. (2007) presented preliminary B isotope data on lavas from selected eastern islands, but to date no Li isotope data has been reported from any of the islands. Here, we present the first comprehensive Li-B isotope dataset for the western two islands of Corvo and Flores. In addition, well-characterised samples from the eastern Azores islands have been selected for Li isotope analyses to allow for an across-plume comparison. We infer that the source signature is relatively homogeneous underneath the entire oceanic plateau. Unusually high boron isotope ratios, which are observed primarily on Flores and Corvo, are consistent with AFC processes that were constrained by oxygen isotope data for olivines from primitive Azores lavas (Genske et al., 2013), however they differ slightly from those occurring underneath the eastern volcanic centres. We interpret the difference in the boron isotopes to be due assimilation of different proportions of high and low temperature altered oceanic crust beneath Flores and Corvo. Assimilation of the gabbroic sections during magma ascent may potentially explain the boron isotope signature in the western islands, whereas assimilation of altered basalts could explain the limited B isotope variability observed in the eastern islands. In addition, the North American crust underneath Flores and Corvo may have altered at lower temperatures than the European crust above the plume centre. The assimilation of crustal material into the magmas as indicated by the stable isotopes may also have implications for the interpretation of the incompatible trace elements and radiogenic isotopes.

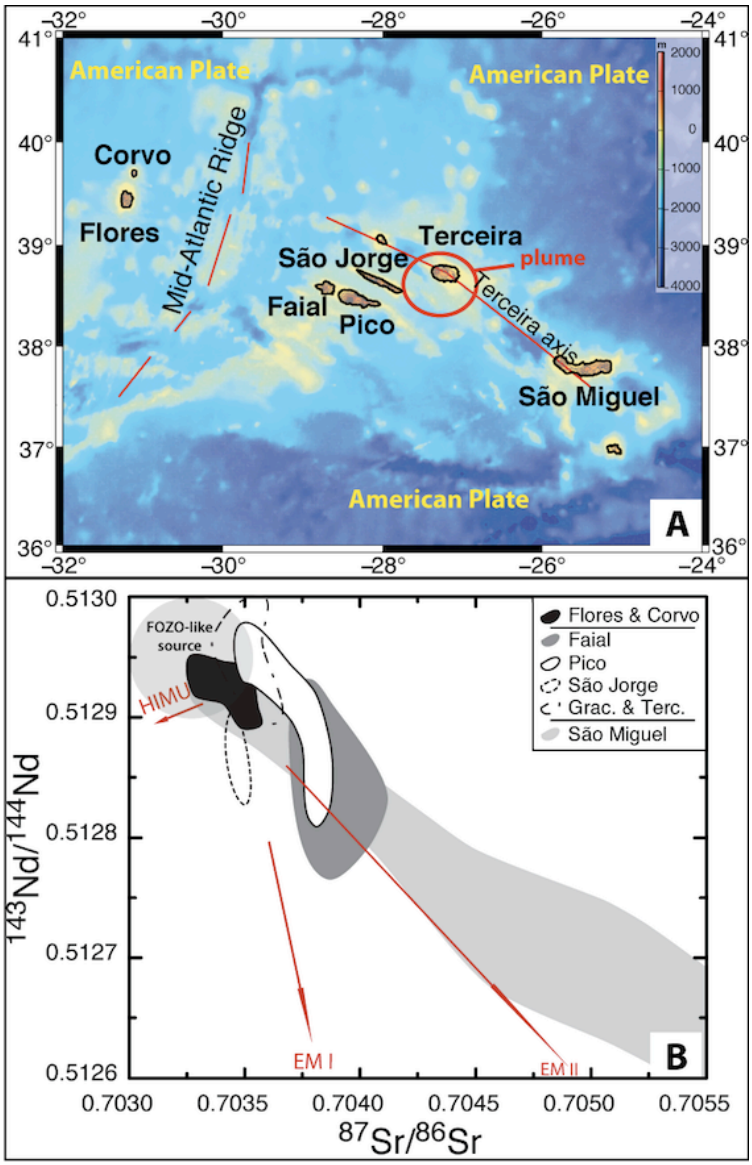

Fig. 1: A Bathymetric map of the Azores region highlighting the emerging islands that are separated by the Mid-Atlantic ridge (MAR). B Strontium versus neodymium isotope ratios of lavas from the Azores islands highlighting the small-scale heterogeneity of the Azores mantle plume, which is expressed even within single islands (e.g. São Miguel). The fields summarize published data of individual islands (Beier et al., 2008; Genske et al., 2012; Turner et al., 1997).

4.2. GEOCHEMICAL BACKGROUND AND SAMPLE SELECTION

4.2.1 Geochemical background

The eastern Azores islands display variability in trace element and radiogenic Sr-Nd-Hf-Pb isotope compositions at both the regional and with-in island length scales. Several authors have attributed this heterogeneity to unique sources within the Azores mantle plume such as ancient recycled oceanic lithosphere (e.g. (Beier et al., 2008; 2007;

Prytulak and Elliott, 2007; Schaefer et al., 2002; Turner et al., 2007; Widom and Shirey, 1996)). The central islands of Faial, Pico, Graciosa and Terceira provide evidence for a highly radiogenic Pb isotope component (Beier et al., 2008; França et al., 2006; Millet et al., 2009) and the observation of subchondritic Os isotope ratios in lavas from Pico and Faial suggest that some of this recycled material may even be of Archaean age (Schaefer et al., 2002). Evidence for the involvement of recycled oceanic crust in Azores magma genesis forms part of a wider debate on the involvement of mafic lithologies, such as pyroxenite and eclogite, in the formation of melts beneath ocean islands (e.g. (Niu and O'Hara, 2003; Niu et al., 2011; Pilet and Baker, 2008; Sobolev et al., 2005)). In the Azores, a recent study by Prytulak and Elliott (2009) has shown that a peridotite mantle lithology recently metasomatised by small volumes of dispersed eclogitic melts can explain both the enriched chemical signatures and the low melt productivity observed on Pico island.

The origin of a highly enriched component on the eastern end of the island of São Miguel, is still a subject of debate (e.g. (Beier et al., 2007; Elliott et al., 2007; Widom and Farquhar, 2003). However, the less enriched signature present in the western Sete Cidades volcano is generally attributed to a common Azores plume component that is also found on most of the other islands (Beier et al., 2012; 2008; 2006). The composition of this common component has been frequently documented in other OIB (see Hart et al. (1992) and Stracke et al. (2005)). A final constituent, present in some Azores lavas, is a depleted mantle component (e.g. (Beier et al., 2008; Moreira et al., 1999; Turner et al., 1997)), which may be irregularly entrained by the rising plume material and causes additional complexity when assessing the distribution of individual mantle sources underneath the Azores.

4.2.2 Sample selection

The samples investigated in this study are well-characterized basalts spanning the end members described above (*cf.* Fig. 1B). They are all primitive basalts (i.e. MgO > 5 wt. %, thus the effects of fractional crystallisation should be minimised. We group these as follows: western group islands (Flores and Corvo), central group islands (Faial, Pico, São Jorge, Terceira) and finally São Miguel, reflecting the eastern end member. In order to avoid surficial alteration, only cores of petrographically fresh looking samples were chosen for this study. No visual signs of seawater alteration were obvious during the

petrographic inspection of the samples. Furthermore, most of these samples have previously been analysed for major elements, trace elements and Sr-Nd-Pb isotopes (Beier et al., 2008; 2006; Turner et al., 1997) and none of these data indicate seawater alteration for the samples investigated here.

4.3. ANALYTICAL METHODS

4.3.1 Lithium isotope analysis

Standard digestion procedures (HF–HNO_3–HCl) were performed and followed by single-column chromatographic separation to obtain purified Li cuts of each sample for isotopic analysis. The method generally follows that described by Seitz et al. (2004) and references therein. Briefly, AG 50W-X8 (200-400 mesh) resin was used for elution of Li using a nitric acid–methanol mixture as an eluent. The recovery yield of Li was checked by analysing solutions collected before and after the Li cuts on an Agilent 7500c/s quadrupole (Q-) ICP-MS at GEMOC, Macquarie University, Sydney. More than 99.9 % of Li recovery was typical in the course of our separation procedure. Impurities in the eluted samples are capable of shifting Li isotopic ratios during MC-ICP-MS analysis, and these were assessed before isotope analysis (e.g. Na/Li ratios << 4 in this study) by Q-ICP-MS analyses. The isotopic analysis of each unknown sample was bracketed by two L-SVEC standard solutions to correct for mass fractionation on the Nu034 Plasma MC-ICP-MS at GEMOC, Macquarie University, Sydney. Additionally, one ACR Li single-element standard solution was measured multiple times as a secondary check on instrument performance (δ^7Li=14.2 ± 0.4 ‰ (2sd, n=19)). Replicates of several samples were undertaken to further evaluate reproducibility. The analytical data including reproducibility are listed in Table 1.

Table 1: Major element and radiogenic isotope composition of lavas analysed herein for Li and B isotopes. B values in italic are from Turner et al. (2007).

	Island	Long [°W]	Lat [°N]	MgO [wt.%]	K2O [wt.%]	87Sr/86Sr	143Nd/144Nd	d11B	2sd	n	B (ppm)	1/B (ppm)	d7Li	2sd	n	Li (ppm)	1/Li (ppm)
C-09-01	Corvo	31.10	39.68	9.27	1.17	0.703350	0.512920	4.88			5.19	0.19	3.54	1.26	3	5.53	0.18
C-09-02	Corvo	31.10	39.68	4.23	1.97	0.703386	0.512930						5.62	0.82	3	6.15	0.16
C-09-06	Corvo	31.10	39.68	8.76	1.12	0.703432	0.512922	8.12			5.46	0.18				4.58	0.22
C-09-18	Corvo	31.11	39.67	8.08	1.18	0.703372	0.512921	2.99	0.76	2	6.50	0.15	4.83	1.82	4	4.32	0.23
C-09-20	Corvo	31.11	39.67	10.74	0.88	0.703410	0.512920	2.02	0.39	2	3.35	0.30	5.25	1.94	5	3.78	0.26
F/CA-6	Faial	28.73	38.55	9.73	1.01	0.703770	0.512927	*-3.30*			*2.60*	0.38	6.04	0.32	2	4.92	0.20
F/CP-18	Faial	28.73	38.55	7.83	1.55	0.704012	0.512797	*-7.60*			*4.40*	0.23	8.75	0.38	4	6.48	0.15
F/FG-28	Faial	28.73	38.55	8.13	1.55	0.703875	0.512768						5.78	1.30	2	6.34	0.16
FL-09-23	Flores	31.23	39.51	8.79	0.61	0.703268	0.512948	11.80			4.03	0.25				3.73	0.27
FL-09-26	Flores	31.23	39.51	7.57	0.62	0.703309	0.512941	0.38			3.16	0.32	5.90	0.48	2	4.03	0.25
FL-09-38	Flores	31.25	39.43	5.76	1.45	0.703370	0.512922						5.02	1.24	3	4.94	0.20
FL-09-41	Flores	31.24	39.42	10.50	1.14	0.703330	0.512920	-3.52			4.78	0.21	5.05	0.78	3	3.71	0.27
FL-09-42	Flores	31.24	39.42	9.30	1.09	0.703370	0.512929	6.50	1.03	2	4.64	0.22	8.13	1.72	5	3.44	0.29
P25	Pico	28.40	38.45	8.24	1.18	0.703840	0.512827	*-3.50*			*3.80*	0.26	4.94	0.66	3	5.76	0.17
P29	Pico	28.40	38.51	8.16	1.59	0.703800	0.512813	*-4.10*			*3.70*	0.27	4.95	0.48	2	7.84	0.13
P4	Pico	28.40	38.50	10.36	0.96	0.703788	0.512818	-3.28	0.61	2	4.34	0.23	5.34	1.04	2	5.50	0.18
P5	Pico	28.40	38.50	9.63	1.01	0.703756	0.512887	*-3.60*			*2.40*	0.42	5.69	0.70	2	5.21	0.19
SJ31b	Sao Jorge	28.10	38.60	8.91	1.01	0.703481	0.512835						6.02	0.72	2	5.21	0.19
SJ26	Sao Jorge	28.10	38.60	4.71	1.82	0.703460	0.512903	*-3.30*			*5.40*	0.19	4.96	0.44	2	8.69	0.12
SJ30	Sao Jorge	28.10	38.60	9.70	1.06	0.703502	0.512831	*-4.70*			*3.10*	0.32	4.62	0.58	3	4.99	0.20
S1	Sao Miguel	25.67	37.44	7.76	1.70	0.704255	0.512739	*-6.00*			*5.40*	0.19	5.56	0.92	2	5.59	0.18
S10	Sao Miguel	25.67	37.44	8.33	1.75	0.704362	0.512774	*5.00*					4.76	1.10	2	5.81	0.17
S19	Sao Miguel	25.67	37.44	6.38	4.26	0.704990	0.512620	*-7.40*			*5.90*	0.17	4.36	0.20	1	7.32	0.14
S3	Sao Miguel	25.67	37.44	8.34	1.87	0.704524	0.512685	*-6.80*			*6.20*	0.16	4.63	0.52	4	6.18	0.16
SP2	Sao Miguel	25.67	37.44	7.93	1.69	0.704220	0.512729	-4.85			4.79	0.21	5.13	1.84	2	5.58	0.18
SP8	Sao Miguel	25.67	37.44	9.10	2.49	0.704785	0.512650	-3.30			4.20	0.24	4.63	0.40	4	7.14	0.14
T18	Terceira	27.32	38.55	7.94	1.10	0.703551	0.512900	*-6.00*			*3.40*	0.29	5.46	1.52	3	5.80	0.17
T2	Terceira	27.32	38.80	5.54	1.48	0.703565	0.512960	-6.82	0.92	2	10.40	0.10				6.48	0.15
T6	Terceira	27.32	38.80	8.70	0.96	0.703483	0.512915	*-7.27*			*4.74*	0.21	5.42	0.44	2	4.26	0.23
Standards																	
JB-2								7.25	0.64	33			4.65	0.60	3		
BHVO-2													4.36	0.78	11		
BCR-2													3.14	0.88	9		

4.3.2 Boron isotope analyses

The concentrations of B were determined by isotope dilution (using the NBS SRM 952 spike) after alkaline fusion (K_2CO_3) and B separation and purification by ion exchange procedures (the full method description is given by Tonarini et al. (1997)). Boron contents and isotope compositions were determined using a VG Isomass 54E at the IGG, C.N.R. Pisa. The accuracy of the procedure was evaluated by repeated analyses of the NBS SRM 951 standard, which was run through the full chemistry and through replicate analyses of samples. Precision and accuracy of isotopically homogeneous samples treated with alkaline fusion chemistry is approximately ± 0.5 ‰ (Tonarini et al., 1997; 2003) and replicate analyses of all samples agree within this limit. The international rock standard JB-2, which was processed during the course of this study, gave the following data: $\delta^{11}B$ = 7.25 ± 0.64 ‰ (2sd), (n = 33 analyses with independent chemistry). All sample data, including statistical evaluation of accuracy and precision are reported in Table 1.

4.4. RESULTS

4.4.1 Lithium

Trace element concentrations of Li in the primitive Azores lavas typically vary from 3.5-8.5 ppm, and the overall isotopic range is δ^7Li = 3.5-8.2 ‰. The Li isotopes do not show significant co-variation with the extent of magmatic fractionation, as recorded by MgO contents (Fig. 2C), though there may be a subtle correlation between δ^7Li and Li concentration (Fig. 2D), as observed in basalts from NE Japan (Moriguti et al., 2004). However, most of the data fall within a range smaller than the typical analytical error of the isotopic measurements. Two unusually isotopically heavy outliers were found in lavas from the islands of Flores (Fl-09-41) and Faial (F/CP-18). The Li isotopic composition of all samples was determined via duplicate analysis and, to confirm the extreme compositions, triplicate analyses were performed (Table 1). Samples from the western islands have comparable δ^7Li to the islands east of the MAR, such that all lavas (except the two outliers) overlap within analytical error for lithium isotopic composition and yield an average δ^7Li of +5.14±1.16 ‰ (2sd, n = 24).

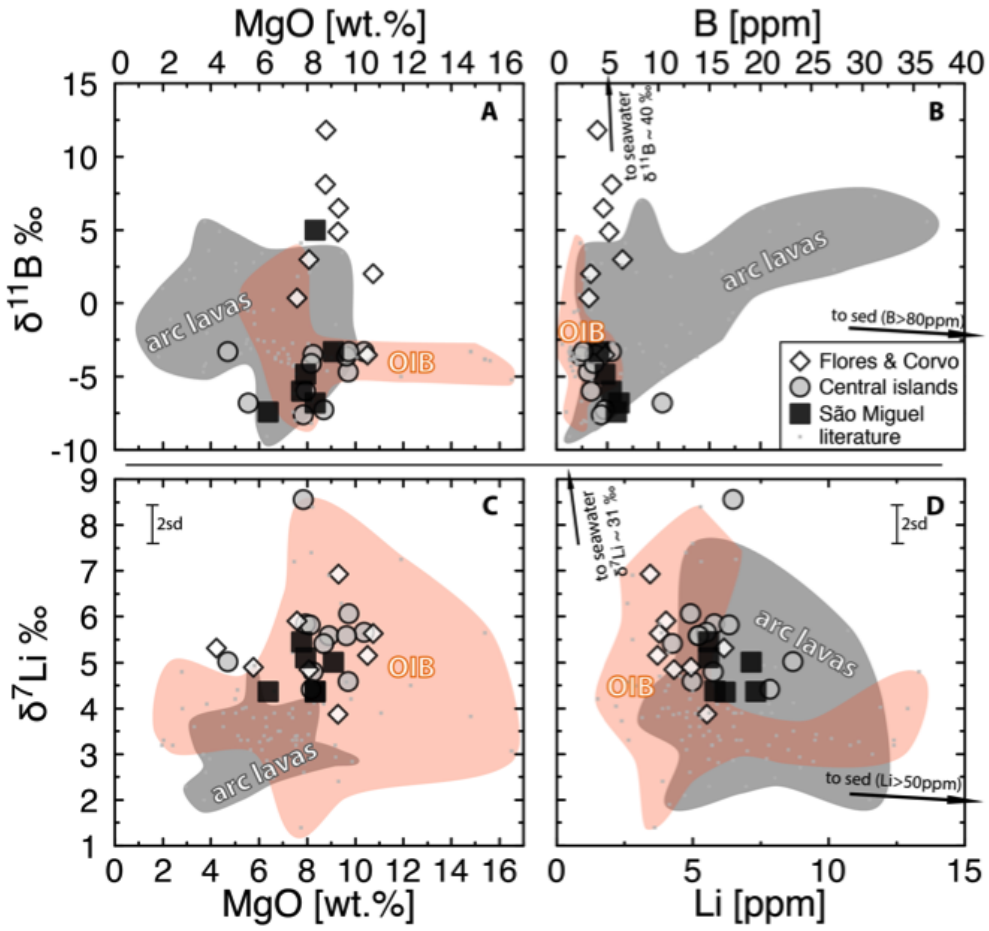

Fig. 2: Lithium and boron isotopic composition of primitive lavas across the Azores islands, versus MgO content (A & C) and Li and B trace element concentration (B & D). Also shown are fields for typical OIB (Chaussidon and Jambon, 1994; Kobayashi et al., 2004; Krienitz et al., 2012; Magna et al., 2011; Tanaka and Nakamura, 2005) and island arc lavas (Ishikawa et al., 2001; Leeman et al., 2004; Moriguti et al., 2004; Moriguti and Nakamura, 1998). The arrow towards sediments is based on data from (Leeman et al., 2004). The Li isotope data from the Azores fall within the field typical for OIB, however the higher B isotope ratios observed mainly in the Flores and Corvo lavas are atypical for OIB, thus a seawater component is invoked for these rocks.

4.4.2 B content and isotopic composition

Whereas the B content of all the lavas varies similarly across all of the islands (~2.2-10.5 ppm), again with no correlation with MgO contents (Fig. 2A), the western islands posses isotopic values of $\delta^{11}B$ extending to much heavier B compositions than seen in any other OIB so far (Fig. 2B). However, heavy B (up to +7.3 ‰) was reported for lavas from the Izu-Arc (Moriguti and Nakamura, 1998). The overall range of $\delta^{11}B$ in the Azores lavas is -7.5 to +11.8 ‰. There was no correlation observed between the B content and its isotopic composition (Fig. 2B). We also have not observed other correlation with indices

of weathering (K/Rb), magmatic differentiation (MgO, SiO_2) or source enrichment (La/Sm).

On Figure 3 it can be seen that lavas from the central islands overlap in $\delta^{11}B$ versus $\delta^{7}Li$ composition with those from MORB (Tomascak et al., 2008) and other OIB (Iceland (Magna et al., 2011) and Hawaii (Chan and Frey, 2003; Tanaka and Nakamura, 2005)). In contrast, most island arc lavas are characterized by lighter Li isotopic compositions, as are sediments (e.g. (Leeman et al., 2004), Fig. 2-4).

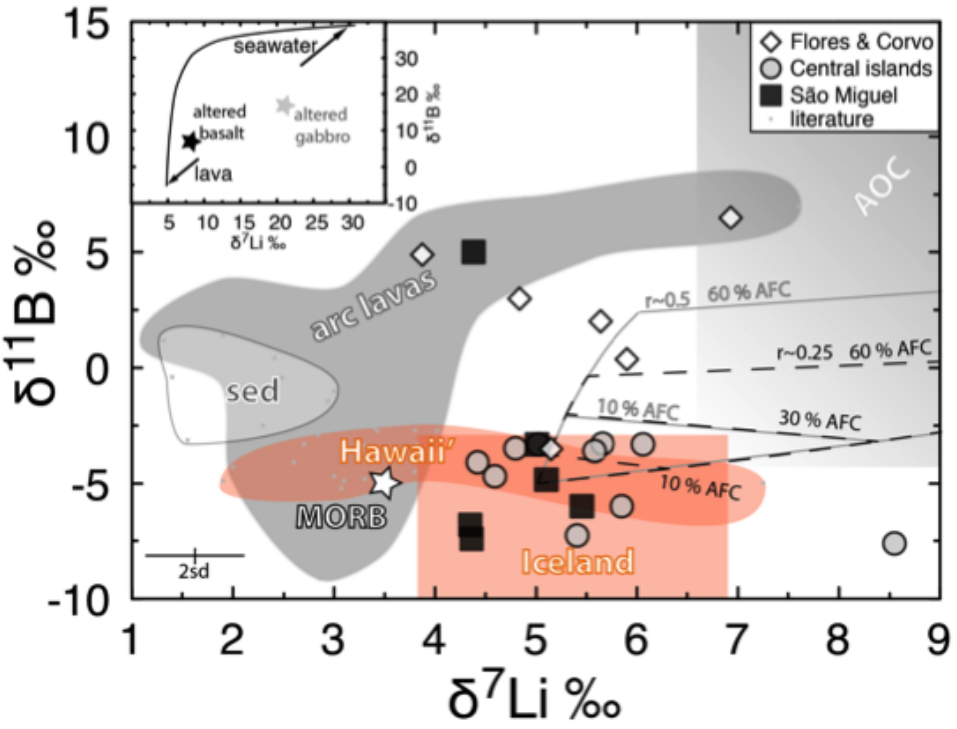

Fig. 3: Boron versus Li isotopic composition of the Azores lavas. Same fields as in Fig 2 are illustrated, however due to the scarcity of combined B-Li isotope studies only Hawaiian data (Kobayashi et al., 2004) are plotted as representative OIBs. The Iceland field is referenced from Gurenko and Chaussidon (1997) for B and Magna et al. (2011) for Li. Altered oceanic crust (AOC) is taken from Chan et al. (2002) for Li and Smith et al. (1995) for B. The average MORB composition (white star) is taken from Tomascak et al. (2008) for Li and Chaussidon et al. (1994) for B. Assimilation fractional crystallisation models with different end members spanning lower and upper sections of the altered crust, as well as different ratios of assimilation to fractional crystallisation (*r*), are also plotted. For full details of the modelling and end member compositions refer to the text and Table 2. Briefly, the upper grey lines reflect AFC with a gabbroic assimilant representing the lower crustal layers, whereas the lower black lines refer to a less altered basaltic assimilant. The inset shows a mixing curve between a typical (eastern) lava composition and seawater. The strong curvature is due to the large compositional difference between these end members, and reflects that post-eruptive seawater-rock interaction cannot solely explain the observed spectrum of the Li-B isotope data.

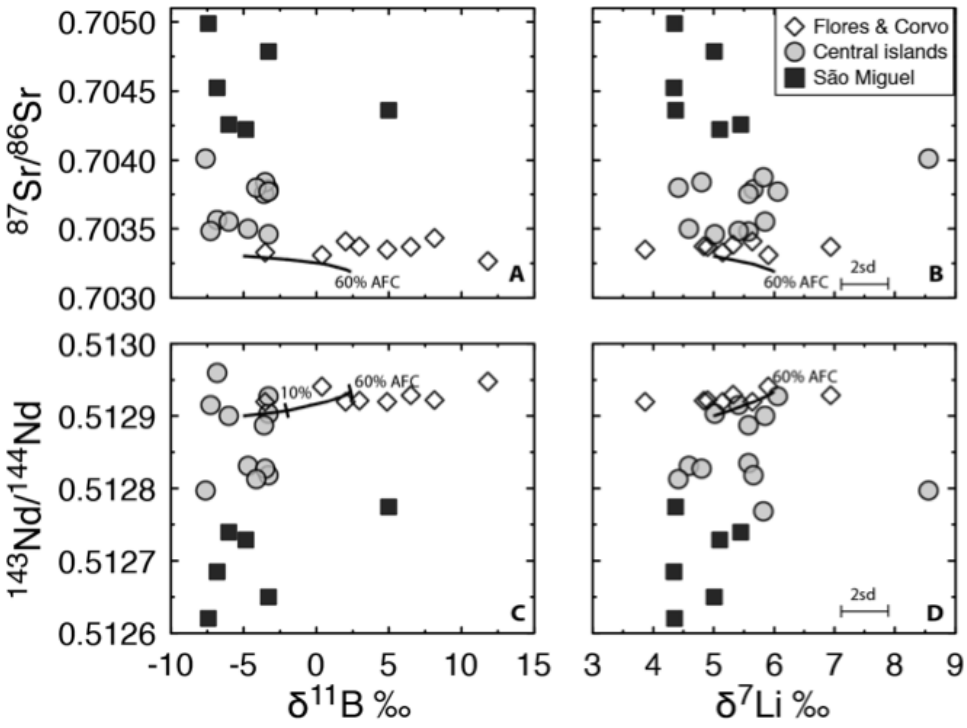

Fig. 4: Strontium (A & B) and Nd (C & D) isotopic composition versus $\delta^{11}B$ and $\delta^{7}Li$ of Azores lavas. The composition of AOC chosen for the AFC model calculations here is given in Table 2. Note that the AFC model (black solid line) represents a total of 60% fractional crystallisation and may explain the variability in $\delta^{7}Li$, but this model cannot account for the large variations observed in the radiogenic isotopes. Thus, the latter must originate intra mantle. Furthermore, the Li and B isotope data seem to rule out significant contribution from recycled sediments to the source of the Azores lavas, as these have lower Li and B ratios than observed in the lavas. Yet there are insufficient data on subducting sediments concerning these two isotopic systems to completely dismiss their contributions to the source of OIBs.

4.5. DISCUSSION

The variation in Li and B isotopes across the Azores islands mostly lies within the range observed for OIB and MORB (Figs 2&3). However, some lavas are displaced towards higher B and/or higher Li isotope ratios that are more commonly found in island arc rocks or altered oceanic crust. In the following discussion we aim to constrain the nature of this variability by exploring the role of surficial reservoirs such as young and hydrothermally altered oceanic crust and seawater that need to be constrained before inferring on the Li and B mantle source composition.

4.5.1 Seawater influence

The (subaerial) lavas from the islands of Corvo and Flores have been exposed to seawater spray for up to 2 Ma (Azevedo and Ferreira, 2006; Genske et al., 2012) and so it could be

suggested that the heavy boron isotopic signature in some of these lavas reflects the adsorption and incorporation of seawater. However, we consider this unlikely because any surface contamination was carefully removed during the initial stages of sample preparation. Furthermore, a study of Hawaiian *submarine* lavas by Tanaka and Nakamura (2005) showed that samples that were exposed much stronger to seawater-rock interaction only had $\delta^{11}B \sim +2.6$ ‰. This is significantly lower than our data that come from *subaerial* lavas and extend up to $\delta^{11}B \sim +11.8$ ‰. Thus, we conclude that seawater alone cannot be responsible for the boron signature observed. Also, if seaspray were the source of the unusually heavy boron signal in the western island group lavas it would be expected to have similarly affected the eastern Azores lavas, which is clearly not the case.

Simple mixing calculations between seawater ($\delta^{11}B \sim +39.5$ ‰, (Spivack and Edmond, 1987)) and a hypothetical pristine lava composition ($\delta^{11}B \sim -5.0$ ‰) indicate that up to 40 % of seawater-boron would have to be exchanged with that of the lavas. Such inferred high water-rock ratios appear unlikely for subaerial lavas that are also exposed to meteoric water. Despite a large variability and the absence of freshwater data from the Azores, meteoric waters are commonly characterised by lighter B isotopic compositions than seawater (e.g. (Aggarwal et al., 2000)).

Due to its much lower abundance in seawater (Table 2), Li is not thought to be as sensitive as B with respect to seaspray. However, the lack of extremely variable and elevated Li isotope ratios in the lavas further implies that direct seawater contamination is unlikely.

4.5.2 Assimilation of hydrothermally altered oceanic crust

A single sample from Terceira (sample T2, Table 1) has a B concentration of 10.4 ppm which is much higher than found in any other sample from the Azores, while OIBs are generally characterized by uniformly low B contents (<<5 ppm, e.g (Chaussidon and Jambon, 1994; Gurenko and Chaussidon, 1997; Ryan et al., 1996; Ryan and Langmuir, 1993). In contrast, lavas from island arcs are relatively enriched in B (>10 ppm) (Ryan and Langmuir, 1993). The elevated B concentrations in oceanic basalts have previously been linked to hydrothermal alteration (Ishikawa and Nakamura, 1992), where altered basalts typically have concentrations >20 ppm, mainly resulting from the formation of secondary phases, such as alumo- and/or phyllosilicates (Simon et al., 2006). We note here again, that the lavas analysed here do not contain any zeolite, serpentine or chlorite

minerals that could explain the higher B isotope ratios. Thus, this signature is derived from assimilation of altered material. The behaviour of Li during alteration processes differs compared to that of B, as it tends to be leached from the rock (Brant et al., 2012).

Nonetheless, studies of oxygen isotopes of OIB have documented the involvement of AFC processes in the generation of ocean island lavas, where the assimilant is often considered to be the underlying altered oceanic crust (e.g. (Harris et al., 2000; Wang and Eiler, 2008)). A detailed oxygen isotope study of olivine phenocrysts from the Azores appears to confirm this view suggesting that such assimilation may be ubiquitous across the Azores islands (Genske et al., 2013). Thus we aim here at using and refining these published AFC models to constrain the least contaminated compositions of Li and B isotopes of the Azores lavas.

Since the Azores B concentrations do not deviate strongly from what is considered "typical" for OIB, we conclude that the amount of assimilation during magma ascent may not be large in general. The rate of assimilation versus crystallisation (r) during AFC processes should not change dramatically within one magmatic system, but may be different between volcanoes that are a few hundred kilometres apart, as these may possess different heat capacities in their feeder systems (Bohrson and Spera, 2007). Accurate estimates of absolute amounts of potential assimilants require better elemental and isotopic constraints on the composition of the end members involved. That is, only a few studies provide such data on the different zones/layers from the altered oceanic crust. For example, Ishikawa and Nakamura (1992) already noted that oceanic crust has considerable variation of both the B content and its isotopic composition, which are primarily controlled by the nature of alteration processes within the crust. The latter strongly depends on factors such as temperature and duration of cold seawater circulation (e.g. Gillis and Robinson (1988)), such that the width of the altered zones within the crust varies between different localities/ocean islands.

However, from the variability and trend towards much heavier isotopic compositions of Li and particularly B in the western Azores islands we propose that the extent of assimilation underneath these volcanic centres may have been more pronounced ($r > 0.4$) than for the volcanoes east of the MAR ($r << 0.4$). The model end members used in these calculations are summarised in Table 2. Equations given by DePaolo (1981) provided the

basis for the modelling and the initial *r* value was taken from the model presented by Genske et al. (2013).

From the modelling it appears that contributions from different sections of the AOC must be invoked beneath the volcanic centres (*cf.* Table 2). To test the role of different assimilants we modelled AFC with a constant rate of assimilation versus fractionation ($r \sim 0.5$), and only changed the B and Li content and isotopic composition of assimilants according to values reported for the different layers of the oceanic crust (i.e. layer 3 gabbros representing high T alteration vs. lower T altered upper sections; e.g. (Brant et al., 2012; Chan et al., 2002; Seyfried et al., 1984; Yamaoka et al., 2012)). The results of this AFC modelling are illustrated on figure 3. It should be noted here that the analytical uncertainty of the Li isotope measurements encompasses most of the data range observed in the lavas; hence the AFC models can explain these illustrated deviations from the model curves.

The conclusions from the oxygen isotope data, that lower gabbro layers are the dominant assimilant, may still hold true but more variable isotopic compositions observed in the lavas, especially in the B isotopes, may additionally require shallower contributions from the more strongly altered basalt layers (i.e. with higher B contents (Chaussidon and Jambon, 1994; Smith et al., 1995)). Another observation on figure 3 is that some lavas exhibit negative $\delta^{11}B$ values, that plot below the field referenced for Hawaii' but are encompassed by the field of Icelandic lavas. A recent study of the latter revealed that alteration in the form of adsorption of meteoric water-derived boron could explain such negative $\delta^{11}B$ values and may then be incorporated into ascending lavas by assimilation (Brounce et al., 2012). Perhaps such components are also present in the Azorean crust. Since our data set here is only representative for more primitive compositions with higher MgO contents, a more detailed comparison with bulk oxygen isotope data remains elusive. Either different assimilants or different AFC processes could explain the variations between the islands east and west of the MAR in terms of their B isotopic composition. We propose that the assimilation of the gabbroic sections is slightly more pronounced in the western Azores islands of Flores and Corvo, which is consistent with the greater distance of these islands from the plume centre beneath the island of Terceira (*cf.* Fig. 1).

Table 2: End member components used in modeling

Model component	sea water	altered gabbros	altered basalts	pristine Azores
Sr [ppm]	8[a]	300[d]	300[d]	400
$^{87}Sr/^{86}Sr$	0.70907[a]	0.703[d]	0.704[d]	0.7033
Nd [ppm]		30[e]	30[e]	35
$^{143}Nd/^{144}Nd$		0.5129[e]	0.5129[e]	0.5129
Li [ppm]	0.19[b]	5[f]	5[g]	5
d7Li (per mill)	30.77[b]	14[f]	7[g]	5
B [ppm]	4.5[c]	2.7[c]	7[c]	3
d11B (per mill)	39.5[c]	5.7[c]	13[c]	-5

references
a Burke et al. (1982)
b Jeffcoate et al. (2004)
c Smith et al. (1995)
d Alt et al. (2000)
e Eiler et al. (1997)
f Chan et al. (2002)
g Nishio et a. (2005)

4.5.3 Mantle source constraints from Li-B systematics

The AFC models apply most specifically to those samples with heavy Li and B isotopic compositions. The composition of unmodified plume material may be estimated by back-projection along the AFC trends, that is, a common Azores source composition for Li and B isotopes is inferred. However, due to the limitation of the data set, which only represents more primitive compositions, an assessment of unmodified Li-B isotope values using indices of magmatic differentiation is problematic. Also, the use of (reciprocal) element vs. isotope ratio plots is not applicable here due to the limited range of the concentrations in the lavas and in the case of Li, the isotopic range is too narrow across the bulk of the samples analysed here to investigate such relationships. Radiogenic isotope data, which are not changed during magmatic differentiation, may help to further explore the source composition of the stable isotopes. On the panels of figure 4, radiogenic isotope compositions of Sr and Nd are plotted versus δ^7Li and $\delta^{11}B$, respectively. From these plots it is striking that most of the variability in δ^7Li and $\delta^{11}B$ in the Azores is contained in lavas from Flores and Corvo. The Sr and Nd isotope composition used in the AFC models were chosen from an average of Flores and Corvo lavas, but may equally be estimated for the individual islands and their respective mantle source. This figure also shows that neither the Sr nor the Nd isotopic compositions can be explained by assimilation of appropriate crustal components, as hydrothermal alteration

of the lower sections (i.e. gabbros, > 2km depth) of oceanic crust would not result in shifts of Sr and Nd isotopes large enough (e.g. (Kempton and Hawkesworth, 1991; Staudigel et al., 1981; Teagle et al., 1998)) to be recorded during assimilation. This is manly due to the low abundance of these elements in seawater compared to their concentration in fresh rocks of the oceanic crust. Furthermore, the combination of low water-rock ratios and the fact that low T hydrothermal fluids with seawater derived Sr (and Nd) isotopic composition do not penetrate efficiently into the deeper gabbro layers of the ocean crust limits their influence on Sr and Nd isotopes during alteration (Alt and Teagle, 2000) and subsequent contamination of ascending magma. In summary our least affected samples seem to record similar $\delta^{11}B$ and $\delta^{7}Li$ values that are relatively indistinguishable across the islands. We thus propose a source value of $\delta^{7}Li \sim 5$ ‰ for the islands, with São Miguel possibly extending towards slightly lighter compositions (~ 4.5 ‰). However, due to the analytical resolution of the Li isotope measurements, this latter value is indicative only.

For boron, this evaluation is somewhat more difficult due to its greater sensitivity to AFC and other contamination processes. Whereas the lowest $\delta^{11}B$ compositions (average ~ -5 ‰) are again characteristic for São Miguel, equally low compositions are also found on Terceira. The western islands of Flores and Corvo in contrast are supposedly characterised by least uncontaminated $\delta^{11}B$ values in agreement with normal MORB (~ -3 ‰).

In summary, we conclude that if the uncontaminated lavas have low $\delta^{11}B$ and $\delta^{7}Li$ then the plots from Figure 4 show that there must be a big range in Sr and Nd isotopes with little or no correlated variation in Li and B isotopes. Thus, it seems unlikely that the range in Sr and Nd isotopes can reflect variable contributions from recycled low-T materials such as sediment or altered MORB. This favors models presented by Schaefer et al. (2002) and Elliott et al. (2006a) over models proposed by Shirey et al. (1987), Hawkesworth et al. (1979) and Turner et al. (1997). Subduction modified ancient MORB crust may provide the enriched end member to the mantle (Elliott et al., 2006a), as suggested previously for the source of the Azores mantle plume (Prytulak and Elliott, 2007).

4.6. CONCLUSION

New data from the Li and B stable isotope systems across lavas from the Azores islands indicate a relatively narrow source signature underneath the entire archipelago, which appears to be decoupled from the radiogenic isotope systems. Unusually high boron isotope ratios, as observed in Flores and Corvo lavas having values up to +11.8 ‰, are consistent with assimilation fractional crystallization processes that differ slightly from those occurring underneath the eastern volcanic centres as a result of different contaminants. We conclude that Li, rather than B, should be used for the study of mantle heterogeneities, since its isotopic composition is less sensitive to recent alteration and/or assimilation processes.

Further Li and especially B isotope data of altered crustal materials, both locally and globally, and also of more evolved lava suites, are required to better constrain shallow-level contamination processes in OIB settings, since these may potentially also have an impact on the trace elements and radiogenic isotopes. The stable isotopes reveal that crustal assimilation played an important role in the evolution of the Azores lavas. However, it is also important that these processes cannot explain the entire variability that is observed in the traditional radiogenic isotope systems, thus the latter reflect intra mantle processes. The role of recycling in generating OIB has commonly been accepted, but the nature of the enriched components within the Azores mantle plume remains a matter of debate.

ACKNOWLEDGEMENTS

V. H. Forjaz and the Observatório Vulcanológico e Geotérmico dos Açores are gratefully acknowledged for their assistance with the logistics of Flores and Corvo samples. The Li isotope data were obtained using instrumentation funded by DEST Systemic Infrastructure Grants, ARC LIEF, NCRIS, industry partners and Macquarie University. Sincere thanks go to P. Wieland for assistance during the analytical procedures at Macquarie University. This is contribution XXX from the ARC Centre of Excellence for Core to Crust Fluid Systems (http://www.ccfs.mq.edu.au) and XXX in the GEMOC Key Centre (http://www.gemoc.mq.edu.au).

REFERENCES

Aggarwal, J.K., Palmer, M.R., Bullen, T.D., Arnórsson, S., Ragnarsdóttir, K.V., 2000. The boron isotope systematics of Icelandic geothermal waters: 1. Meteoric water charged systems. Geochimica et Cosmochimica Acta 64, 579–585.

Alt, J.C., Teagle, D.A.H., 2000. Hydrothermal alteration and fluid fluxes in ophiolites and oceanic crust. SPECIAL PAPERS-GEOLOGICAL SOCIETY OF AMERICA 273–282.

Azevedo, J.M.M., Ferreira, M.R.P., 2006. The volcanotectonic evolution of Flores Island, Azores (Portugal). Journal of Volcanology and Geothermal Research 156, 90–102.

Beier, C., Haase, K.M., Abouchami, W., Krienitz, M.S., Hauff, F., 2008. Magma genesis by rifting of oceanic lithosphere above anomalous mantle: Terceira Rift, Azores. Geochem. Geophys. Geosyst. 9.

Beier, C., Haase, K.M., Hansteen, T.H., 2006. Magma Evolution of the Sete Cidades Volcano, São Miguel, Azores. J Petrology 47, 1375–1411.

Beier, C., Haase, K.M., Turner, S.P., 2012. Conditions of melting beneath the Azores. Lithos 144–145, 1–11.

Beier, C., Stracke, A., Haase, K.M., 2007. The peculiar geochemical signatures of São Miguel (Azores) lavas: Metasomatised or recycled mantle sources? Earth and Planetary Science Letters 259, 186–199.

Beier, C., Turner, S.P., Plank, T., White, W.M., 2010. A preliminary assessment of the symmetry of source composition and melting dynamics across the Azores plume. Geochem. Geophys. Geosyst. 11, Q02004.

Bohrson, W.A., Spera, F.J., 2007. Energy-Constrained Recharge, Assimilation, and Fractional Crystallization (EC-RAχFC): A Visual Basic computer code for calculating trace element and isotope variations of open-system magmatic systems. Geochem. Geophys. Geosyst. 8, Q11003–n/a.

Bonatti, E., 1990. Not So Hot "Hot Spots" in the Oceanic Mantle. Science 250, 107–111.

Bourdon, B., Turner, S.P., Ribe, N.M., 2005. Partial melting and upwelling rates beneath

the Azores from a U-series isotope perspective. Earth and Planetary Science Letters 239, 42–56.

Brant, C., Coogan, L.A., Gillis, K.M., Seyfried, W.E., Pester, N.J., Spence, J., 2012. Lithium and Li-isotopes in young altered upper oceanic crust from the East Pacific Rise. Geochimica et Cosmochimica Acta 96, 272–293.

Brounce, M., Feineman, M., LaFemina, P., Gurenko, A., 2012. Insights into crustal assimilation by Icelandic basalts from boron isotopes in melt inclusions from the 1783–1784 Lakagígar eruption. Geochimica et Cosmochimica Acta 94, 164–180.

Campbell, I.H., 1990. Implications of mantle plume structure for the evolution of flood basalts 10.1016/0012-821X(90)90072-6 : Earth and Planetary Science Letters | ScienceDirect.com. Earth and Planetary Science Letters.

Cannat, M., Briais, A., Deplus, C., Escartín, J., Georgen, J.E., Lin, J., Mercouriev, S., Meyzen, C., Muller, M., Pouliquen, G., Rabain, A., da Silva, P., 1999. Mid-Atlantic Ridge-Azores hotspot interactions: along-axis migration of a hotspot-derived event of enhanced magmatism 10 to 4 Ma ago. Earth and Planetary Science Letters 173, 257–269.

Chan, L.-H., Alt, J.C., Teagle, D.A.H., 2002. Lithium and lithium isotope profiles through the upper oceanic crust: a study of seawater–basalt exchange at ODP Sites 504B and 896A. Earth and Planetary Science Letters 201, 187–201.

Chan, L.-H., Frey, F.A., 2003. Lithium isotope geochemistry of the Hawaiian plume: Results from the Hawaii Scientific Drilling Project and Koolau Volcano. Geochem. Geophys. Geosyst. 4, 8707–.

Chan, L.-H., Lassiter, J.C., Hauri, E.H., Hart, S.R., Blusztajn, J., 2009. Lithium isotope systematics of lavas from the Cook–Austral Islands: Constraints on the origin of HIMU mantle. Earth and Planetary Science Letters 277, 433–442.

Chaussidon, M., Jambon, A., 1994. Boron content and isotopic composition of oceanic basalts: Geochemical and cosmochemical implications. Earth and Planetary Science Letters 121, 277–291.

Chaussidon, M., Marty, B., 1995. Primitive Boron Isotope Composition of the Mantle.

Science 269, 383–386.

DePaolo, D.J., 1981. Trace element and isotopic effects of combined wallrock assimilation and fractional crystallization. Earth and Planetary Science Letters 53, 189–202.

Dosso, L., Bougault, H., Langmuir, C.H., Bollinger, C., Bonnier, O., Etoubleau, J., 1999. The age and distribution of mantle heterogeneity along the Mid-Atlantic Ridge (31-41∞N). Earth and Planetary Science Letters 170, 269–286.

Elliott, T., Blichert-Toft, J., Heumann, A., Koetsier, G., Forjaz, V.H., 2007. The origin of enriched mantle beneath São Miguel, Azores. Geochimica et Cosmochimica Acta 71, 219–240.

Elliott, T., Jeffcoate, A.B., Kasemann, S.A., 2006a. Li isotopic evidence for subduction induced mantle heterogeneity. Geochimica et Cosmochimica Acta 70, A159–A159.

Elliott, T., Thomas, A., Jeffcoate, A.B., Niu, Y., 2006b. Lithium isotope evidence for subduction-enriched mantle in the source of mid-ocean-ridge basalts. Nature 443, 565–568.

Escartín, J., Cannat, M., Pouliquen, G., Rabain, A., Lin, J., 2001. Crustal thickness of V-shaped ridges south of the Azores: Interaction of the Mid-Atlantic Ridge (36¬∞,Äì39¬∞N) and the Azores hot spot. J. Geophys. Res. 106.

França, Z.T.M., Tassinari, C.C.G., Cruz, J.V., Aparicio, A.Y., Araña, V., Rodrigues, B.N., 2006. Petrology, geochemistry and Sr-Nd-Pb isotopes of the volcanic rocks from Pico Island--Azores (Portugal). Journal of Volcanology and Geothermal Research 156, 71–89.

Gast, P.W., Tilton, G.R., Hedge, C., 1964. Isotopic Composition of Lead and Strontium from Ascension and Gough Islands. Science 145, 1181–1185.

Genske, F.S., Beier, C., Haase, K.M., Turner, S.P., Krumm, S., Brandl, P.A., 2013. Oxygen isotopes in the Azores islands: Crustal assimilation recorded in olivine. Geol.

Genske, F.S., Turner, S.P., Beier, C., Schaefer, B.F., 2012. The Petrology and Geochemistry of Lavas from the Western Azores Islands of Flores and Corvo. J

Petrology 53, 1673–1708.

Gillis, K.M., Robinson, P.T., 1988. Distribution of alteration zones in the upper oceanic crust. Geol 16, 262.

Gurenko, A.A., Chaussidon, M., 1997. Boron concentrations and isotopic composition of the Icelandic mantle: evidence from glass inclusions in olivine. Chemical Geology 135, 21–34.

Haase, K.M., 2002. Geochemical constraints on magma sources and mixing processes in Easter Microplate MORB (SE Pacific): a case study of plume–ridge interaction. Chemical Geology 182, 335–355.

Harris, C., Smith, H.S., Le Roex, A.P., 2000. Oxygen isotope composition of phenocrysts from Tristan da Cunha and Gough Island lavas: variation with fractional crystallization and evidence for assimilation. Contributions to Mineralogy and Petrology 138, 164–175.

Hart, S.R., Hauri, E.H., Oschmann, L.A., Whitehead, J.A., 1992. Mantle Plumes and Entrainment: Isotopic Evidence. Science 256, 517–520.

Hawkesworth, C.J., Norry, M.J., Roddick, J.C., Vollmer, R., 1979. 143Nd/144Nd and 87Sr/86Sr ratios from the Azores and their significance in LIL-element enriched mantle. Nature 280, 28–31.

Hofmann, A.W., 1997. Mantle geochemistry: the message from oceanic volcanism. Nature 385, 219–229.

Ishikawa, T., Nakamura, E., 1992. Boron isotope geochemistry of the oceanic crust from DSDP/ODP Hole 504B. Geochimica et Cosmochimica Acta 56, 1633–1639.

Ishikawa, T., Tera, F., Nakazawa, T., 2001. Boron isotope and trace element systematics of the three volcanic zones in the Kamchatka arc. Geochimica et Cosmochimica Acta 65, 4523–4537.

Jeffcoate, A.B., Elliott, T., Kasemann, S.A., Ionov, D.A., Cooper, K.M., Brooker, R., 2007. Li isotope fractionation in peridotites and mafic melts. Geochimica et Cosmochimica Acta 71, 202–218.

Kempton, P.D., Hawkesworth, C.J., 1991. Geochemistry and isotopic composition of gabbros from layer 3 of the Indian Ocean crust, Hole 735B. … Ocean Drill Program Sci ….

Kobayashi, K., Tanaka, R., Moriguti, T., Shimizu, K., 2004. Lithium, boron, and lead isotope systematics of glass inclusions in olivines from Hawaiian lavas: evidence for recycled components in the Hawaiian plume. Chemical Geology.

Krienitz, M.S., Garbe-Schönberg, C.D., Romer, R.L., Meixner, A., Haase, K.M., Stroncik, N.A., 2012. Lithium Isotope Variations in Ocean Island Basalts—Implications for the Development of Mantle Heterogeneity. J Petrology.

Leeman, W.P., Tonarini, S., Chan, L.H., Borg, L.E., 2004. Boron and lithium isotopic variations in a hot subduction zone—the southern Washington Cascades. Chemical Geology 212, 101–124.

Magna, T., Ionov, D.A., Oberli, F., Wiechert, U., 2008. Links between mantle metasomatism and lithium isotopes: Evidence from glass-bearing and cryptically metasomatized xenoliths from Mongolia. Earth and Planetary Science Letters 276, 214–222.

Magna, T., Wiechert, U., Stuart, F.M., Halliday, A.N., Harrison, D., 2011. Combined Li-He isotopes in Iceland and Jan Mayen basalts and constraints on the nature of the North Atlantic mantle. Geochimica et Cosmochimica Acta 75, 922–936.

Millet, M.-A., Doucelance, R., Baker, J.A., Schiano, P., 2009. Reconsidering the origins of isotopic variations in Ocean Island Basalts: Insights from fine-scale study of São Jorge Island, Azores archipelago. Chemical Geology 265, 289–302.

Montelli, R., Nolet, G., Dahlen, F.A., Masters, G., Engdahl, E.R., Hung, S.-H., 2004. Finite-Frequency Tomography Reveals a Variety of Plumes in the Mantle. Science 303, 338–343.

Moreira, M., Allègre, C.J., 2002. Rare gas systematics on Mid Atlantic Ridge (37-40° N). Earth and Planetary Science Letters 198, 401–416.

Moreira, M., Doucelance, R., Kurz, M.D., Dupré, B., Allègre, C.J., 1999. Helium and lead isotope geochemistry of the Azores Archipelago. Earth and Planetary Science

Letters 169, 189–205.

Moreira, M., Kanzari, A., Madureira, P., 2012. Helium and neon isotopes in São Miguel island basalts, Azores Archipelago: New constraints on the “low 3He” hotspot origin. Chemical Geology 322–323, 91–98.

Moriguti, T., Nakamura, E., 1998. Across-arc variation of Li isotopes in lavas and implications for crust/mantle recycling at subduction zones. Earth and Planetary Science Letters 163, 167–174.

Moriguti, T., Shibata, T., Nakamura, E., 2004. Lithium, boron and lead isotope and trace element systematics of Quaternary basaltic volcanic rocks in northeastern Japan: mineralogical controls on slab-derived fluid composition. Chemical Geology 212, 81–100.

Nishio, Y., Nakai, S., Kogiso, T., Barsczus, H.G., 2005. Lithium, strontium, and neodymium isotopic compositions of oceanic island basalts in the Polynesian region: constraints on a Polynesian HIMU origin. Geochem. J. 39, 91–103.

Niu, Y., O'Hara, M.J., 2003. Origin of ocean island basalts: A new perspective from petrology, geochemistry, and mineral physics considerations. J. Geophys. Res. 108, 2209.

Niu, Y., Wilson, M., Humphreys, E.R., O'Hara, M.J., 2011. The Origin of Intra-plate Ocean Island Basalts (OIB): the Lid Effect and its Geodynamic Implications. J Petrology 52, 1443–1468.

Pilet, S., Baker, M.B., 2008. Metasomatized lithosphere and the origin of alkaline lavas. Science.

Prytulak, J., Elliott, T., 2007. TiO2 enrichment in ocean island basalts. Earth and Planetary Science Letters 263, 388–403.

Prytulak, J., Elliott, T., 2009. Determining melt productivity of mantle sources from 238U-230Th and 235U-231Pa disequilibria; an example from Pico Island, Azores. Geochimica et Cosmochimica Acta 73, 2103–2122.

Ritsema, J., Allen, R.M., 2003. The elusive mantle plume. Earth and Planetary Science

Letters 207, 1–12.

Ryan, J.G., Kyle, P.R., 2004. Lithium abundance and lithium isotope variations in mantle sources: insights from intraplate volcanic rocks from Ross Island and Marie Byrd Land (Antarctica) and other oceanic islands. Chemical Geology 212, 125–142.

Ryan, J.G., Langmuir, C.H., 1993. The systematics of boron abundances in young volcanic rocks. Geochimica et Cosmochimica Acta 57, 1489–1498.

Ryan, J.G., Leeman, W.P., Morris, J., Langmuir, C.H., 1996. The boron systematics of intraplate lavas: Implications for crust and mantle evolution. Geochimica et Cosmochimica Acta 60, 415–422.

Schaefer, B.F., Turner, S.P., Parkinson, I.J., Rogers, N., Hawkesworth, C.J., 2002. Evidence for recycled Archaean oceanic mantle lithosphere in the Azores plume. Nature 420, 304–307.

Schilling, J.-G., 1975. Azores mantle blob: Rare-earth evidence. Earth and Planetary Science Letters 25, 103–115.

Schilling, J.-G., 1991. Fluxes and excess temperatures of mantle plumes inferred from their interaction with migrating mid-ocean ridges. Nature 352, 397–403.

Seitz, H.-M., Brey, G.P., Lahaye, Y., Durali, S., Weyer, S., 2004. Lithium isotopic signatures of peridotite xenoliths and isotopic fractionation at high temperature between olivine and pyroxenes. Chemical Geology 212, 163–177.

Seyfried, W.E., Jr, Janecky, D.R., Mottl, M.J., 1984. Alteration of the oceanic crust: Implications for geochemical cycles of lithium and boron. Geochimica et Cosmochimica Acta 48, 557–569.

Shirey, S.B., Bender, J.F., Langmuir, C.H., 1987. Three-component isotopic heterogeneity near the Oceanographer transform, Mid-Atlantic Ridge. Nature.

Shorttle, O., Maclennan, J., Jones, S.M., 2010. Control of the symmetry of plume-ridge interaction by spreading ridge geometry. Geochem. Geophys. Geosyst. 11, Q0AC05.

Simon, L., Lecuyer, C., MarÈchal, C., Coltice, N., 2006. Modelling the geochemical cycle of boron: Implications for the long-term [delta]11B evolution of seawater and

oceanic crust. Chemical Geology 225, 61–76.

Smith, H.J., Spivack, A.J., Staudigel, H., Hart, S.R., 1995. The boron isotopic composition of altered oceanic crust. Chemical Geology 126, 119–135.

Sobolev, A.V., Hofmann, A.W., Sobolev, S.V., Nikogosian, I.K., 2005. An olivine-free mantle source of Hawaiian shield basalts. Nature 434, 590–597.

Spivack, A.J., Edmond, J.M., 1987. Boron isotope exchange between seawater and the oceanic crust. Geochimica et Cosmochimica Acta 51, 1033–1043.

Staudigel, H., Hart, S.R., Richardson, S.H., 1981. Alteration of the oceanic crust: Processes and timing. Earth and Planetary Science Letters 52, 311–327.

Stracke, A., Hofmann, A.W., Hart, S.R., 2005. FOZO, HIMU, and the rest of the mantle zoo. Geochem. Geophys. Geosyst. 6.

Tanaka, R., Nakamura, E., 2005. Boron isotopic constraints on the source of Hawaiian shield lavas. Geochimica et Cosmochimica Acta 69, 3385–3399.

Teagle, D.A.H., Alt, J.C., Halliday, A.N., 1998. Tracing the evolution of hydrothermal fluids in the upper oceanic crust: Sr-isotopic constraints from DSDP/ODP Holes 504B and 896A. Geological Society, London, Special Publications 148, 81–97.

Tomascak, P.B., 2004. Developments in the Understanding and Application of Lithium Isotopes in the Earth and Planetary Sciences. Reviews in Mineralogy and Geochemistry 55, 153–195.

Tomascak, P.B., Langmuir, C.H., le Roux, P.J., Shirey, S.B., 2008. Lithium isotopes in global mid-ocean ridge basalts. Geochimica et Cosmochimica Acta 72, 1626–1637.

Tomascak, P.B., Widom, E., Benton, L.D., Goldstein, S.L., Ryan, J.G., 2002. The control of lithium budgets in island arcs. Earth and Planetary Science Letters 196, 227–238.

Tonarini, S., Pennisi, M., Alessandra, A.-B., Dini, A., Giorgio, F., Roberto, G., Wiedenbeck, M., Gröning, M., 2003. Intercomparison of Boron Isotope and Concentration Measurements. Part I: Selection, Preparation and Homogeneity Tests of the Intercomparison Materials. Geostandards and Geoanalytical Research 27, 21–39.

Tonarini, S., Pennisi, M., Leeman, W.P., 1997. Precise boron isotopic analysis of complex silicate (rock) samples using alkali carbonate fusion and ion-exchange separation. Chemical Geology 142, 129–137.

Turner, S.P., Hawkesworth, C.J., Rogers, N., King, P., 1997. U---Th isotope disequilibria and ocean island basalt generation in the Azores. Chemical Geology 139, 145–164.

Turner, S.P., Tonarini, S., Bindeman, I.N., Leeman, W.P., Schaefer, B.F., 2007. Boron and oxygen isotope evidence for recycling of subducted components over the past 2.5 Gyr. Nature 447, 702–705.

Vlastélic, I., Koga, K., Chauvel, C., Jacques, G., Télouk, P., 2009. Survival of lithium isotopic heterogeneities in the mantle supported by HIMU-lavas from Rurutu Island, Austral Chain. Earth and Planetary Science Letters 286, 456–466.

Vogt, P.R., Jung, W.Y., 2004. The Terceira Rift as hyper-slow, hotspot-dominated oblique spreading axis: A comparison with other slow-spreading plate boundaries. Earth and Planetary Science Letters 218, 77–90.

Wang, Z., Eiler, J.M., 2008. Insights into the origin of low-[delta]18O basaltic magmas in Hawaii revealed from in situ measurements of oxygen isotope compositions of olivines. Earth and Planetary Science Letters 269, 377–387.

White, W.M., McBirney, A.R., DUNCAN, R.A., 1993. Petrology and Geochemistry of the Galápagos Islands: Portrait of a Pathological Mantle Plume. J. Geophys. Res. 98, 19533–19563.

White, W.M., Tapia, M.D.M., Schilling, J.-G., 1979. The petrology and geochemistry of the Azores Islands. Contributions to Mineralogy and Petrology 69, 201–213.

Widom, E., Carlson, R.W., Gill, J.B., Schmincke, H.-U., 1997. Th-Sr-Nd-Pb isotope and trace element evidence for the origin of the Sao Miguel, Azores, enriched mantle source. Chemical Geology 140, 49–68.

Widom, E., Farquhar, J., 2003. Oxygen isotope signatures in olivines from São Miguel (Azores) basalts: implications for crustal and mantle processes. Chemical Geology 193, 237–255.

Widom, E., Shirey, S.B., 1996. Os isotope systematics in the Azores: implications for mantle plume sources. Earth and Planetary Science Letters 142, 451–465.

Yamaoka, K., Ishikawa, T., Matsubaya, O., Ishiyama, D., Nagaishi, K., Hiroyasu, Y., Chiba, H., Kawahata, H., 2012. Boron and oxygen isotope systematics for a complete section of oceanic crustal rocks in the Oman ophiolite. Geochimica et Cosmochimica Acta 84, 543–559.

CHAPTER 5: CONSTRAINING THE NATURE OF THE WESTERN AZORES MANTLE SOURCE USING PB-HF-OS ISOTOPE SYSTEMATICS AND HIGH FIELD STRENGTH ELEMENTS

Felix S. Genske[a,b,*], Simon P. Turner[a], Christoph Beier[a,b], Bruce F. Schaefer[a], Norman J. Pearson[a], Folkmar Hauff[c], Karsten M. Haase[b]

[a]ARC Centre of Excellence for Core to Crust Fluid Systems/GEMOC, Dept. of Earth and Planetary Sciences, Macquarie University, Sydney NSW 2109, Australia

[b]GeoZentrum Nordbayern, Universität Erlangen-Nürnberg, Schlossgarten 5, 91054 Erlangen, Germany

[c]GEOMAR, Helmholtz-Zentrum für Ozeanforschung Kiel, Wischhofstrasse 1-3, 24148 Kiel

*corresponding author: felix.genske@mq.edu.au

ABSTRACT

The Azores islands in the central North-Atlantic provide an ideal opportunity to study the recycled components that are entrained and delivered to the surface in a mantle plume. Here, we present Hf, Pb and Os isotopes in otherwise well-characterised primitive lavas across the islands to infer the nature and distribution of enriched mantle materials. This includes new data from the islands Flores and Corvo that are situated west of the Mid-Atlantic ridge (MAR), as well as a few submarine samples from the far west of the Azores plateau. The geodynamic positioning of the two islands west of the ridge axis and furthest from the inferred plume centre in the east is not well understood. The radiogenic isotopes provide an opportunity to better constrain the source composition for the Flores and Corvo lavas and to compare and contrast this to that inferred for the islands to the east

of the MAR. The $^{176}Hf/^{177}Hf$ isotope ratios range from 0.282957 to 0.283069 and the $^{206}Pb/^{204}Pb$ isotope ratios range from 19.5166 to 19.7799 whilst some of the $^{187}Os/^{188}Os$ isotope ratios are subchrondritic, ranging from 0.12485 to 0.13698. We demonstrate the presence of a plume component to the west of the MAR, which has the same origin as that underneath the eastern islands. Osmium isotope data from the western islands confirm the existence of an ancient component within this plume, however the highly enriched, EMII-type component found on São Miguel is absent in the western lavas. Further, differences observed in Nb/Zr and Ta/Hf between islands east and west of the MAR indicate the presence of a third component beneath Flores and Corvo. This component is characterised by stronger fractionation of Zr, Hf (and Ti) from Nb and Ta, respectively.

Keywords: Azores mantle plume, Hf-Pb-Os isotopes, high-field-strength elements, lithosphere recycling, plume-ridge interaction

5.1. INTRODUCTION

Ocean Island Basalts (OIB) provide important information on mantle convection and the recycling of crustal material (Gast et al., 1964; Hofmann, 1997). The preservation of the enriched sources as a result of lower degrees of partial melting and a thicker lithosphere compared to the Mid-Ocean Ridges (MOR) provide constraints on the composition and origin of these sources (e.g. (Stracke et al., 2003)).

The Azores Plateau is a bathymetric swell with a diameter of about 450 km divided by the Mid-Atlantic Ridge (MAR) into eastern and western parts (Fig. 1a). Seven volcanic islands are situated to the eastern of the MAR while two are situated west (Flores and Corvo). The eastern islands have been the subject of numerous geochemical studies (Beier et al., 2008; 2012; 2010; Elliott et al., 2007; Prytulak and Elliott, 2009; Turner et al., 1997; White et al., 1979; Widom et al., 1997; Widom and Shirey, 1996) and typically erupt alkaline basaltic to trachytic lavas that are enriched in incompatible elements and display enriched Sr-Nd-Pb and Hf isotope ratios. Melting underneath the eastern islands has generally been ascribed to the presence of a volatile-rich mantle plume and slightly higher excess temperatures compared to the surrounding mantle (Asimow, 2004; Beier et al., 2012; Bourdon et al., 2005). The quantification of uniquely enriched sources on the eastern island of São Miguel implies the presence of variably enriched recycled oceanic crust component (Beier et al., 2007; Elliott et al., 2007). In addition, lavas from the easternmost island of Santa Maria display isotopic source compositions that are

commonly found in the Azores but the melting dynamics indicate the presence of a volatile-rich carbonatite component (Beier et al., 2013). In contrast, the causes of melting and volcanism beneath the western Azores Plateau remain poorly understood. Genske et al. (2012) presented Sr-Nd isotope data that imply a source composition comparable to that underneath most of the eastern islands. However, the São Miguel lavas in the east are uniquely enriched in Pb isotope space, displaying unusually radiogenic $^{87}Sr/^{86}Sr$ and $^{208}Pb/^{204}Pb$ isotope ratios at a given $^{206}Pb/^{204}Pb$, which is unique amongst the global array of ocean islands. The positioning of São Miguel and Santa Maria and Corvo and Flores at the eastern and western edges of the Azores affords quantification and comparison of the sources and origin of melting at the edge of the Azores mantle plume. To date, no Pb, Hf and Os isotope data (with the exception of data from two Flores lavas (Schaefer et al., 2002)) have been published from the western islands of Corvo and Flores.

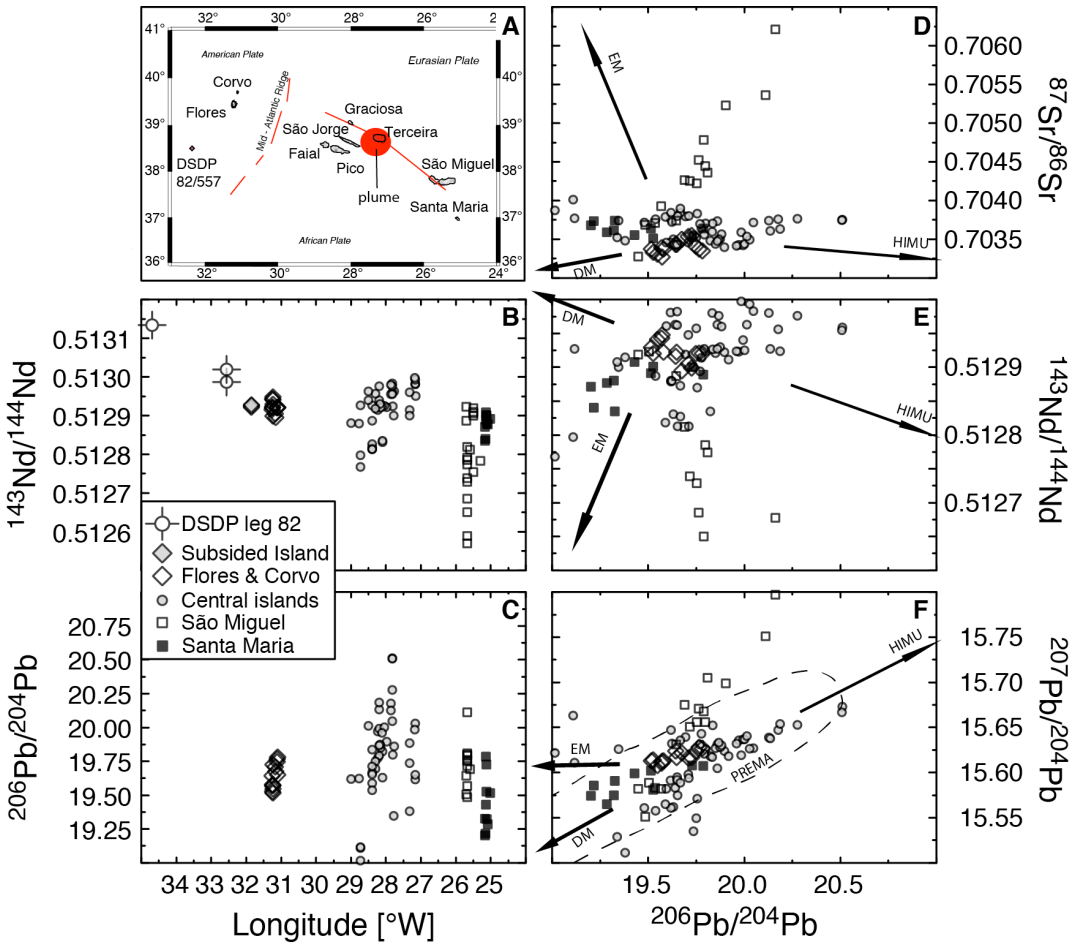

Fig. 1: a) Map of the Azores Plateau using GMT (Wessel and Smith, 1995; 1991). Red lines highlight the two spreading axes of the MAR and the Terceira rift. Submarine localities are Deep Sea Drilling Project Leg 82 Holes 556 and 557, where the former hole is not plotted on the map (refer to Table 1 for grid

coordinates). Note that the extreme variability observed on São Miguel is not seen on any of the other islands. d) $^{87}Sr/^{86}Sr$, e) $^{143}Nd/^{144}Nd$, and f) $^{207}Pb/^{204}Pb$ versus $^{206}Pb/^{204}Pb$ isotope ratios of the Azores lavas. Sample west of Flores are from a subsided submarine seamount described in more detail in Ryall et al. (1983), b) isotopic data of $^{87}Sr/^{86}Sr$ and c) $^{206}Pb/^{204}Pb$ versus longitude for lavas across the Azores plateau. Published data are from Beier et al. (2006, 2007, 2008, 2012, 2013) for Terceira, São Miguel, Faial, Pico, São Jorge and Santa Maria, Turner et al. (1997) for Pico, São Miguel, São Jorge, Faial, Terceira and Genske et al. (2012) for Flores and Corvo.

Here, we present the first comprehensive Pb-Hf-Os isotope dataset along with published major element, trace element and Sr-Nd isotope data for the western two islands of Corvo and Flores and few submarine samples from the western Plateau and compare these with available data from the neighbouring MAR and the eastern islands to better constrain the spatial variability of the Azores mantle plume. We show that most isotope systems underneath the western islands reflect the presence of an ancient (>> 500 Ma inferred from Os isotopes (Schaefer et al., 2002)), enriched (Sr-Nd-Pb-Hf) mantle source that is also common underneath the eastern Azores islands. Further, we can show that the high-field-strength elements, Nb and Ta, are more enriched than Zr and Hf, respectively, when compared to the eastern islands (Genske et al., 2012). We present a model involving 10 % recycled mafic crust that can explain the radiogenic isotopes found on Flores and Corvo. Further, we can show that 2-4% melting of this mafic component and subsequent mixing with melts from depleted (normal mid-ocean ridge basalt (N-MORB)) mantle can explain the elevated Nb/Zr and Ta/Hf ratios.

5.2. PUBLISHED GEOCHEMICAL CONSTRAINTS

The eastern Azores islands display variability in trace element and radiogenic Sr-Nd-Hf-Pb isotope compositions at both the regional and within-island scales, though the latter is mostly restricted to the island of São Miguel. Nevertheless, the available data sets from São Miguel require across-plateau heterogeneity even when excluding the peculiar signature characteristic for the eastern part of the island (i.e. essentially only leaving samples from the Sete Cidades volcano (*cf.* Beier et al. (2007) and discussion further below). Several authors have attributed this heterogeneity to unique sources within the plume such as an ancient recycled oceanic lithosphere (e.g. (Beier et al., 2008; 2007; Prytulak and Elliott, 2007; Schaefer et al., 2002; Turner et al., 2007; Widom and Shirey, 1996)). The central islands of Faial, Pico, Graciosa and Terceira provide evidence for a highly radiogenic Pb isotope component, comparable to a HIMU source composition

(Beier et al., 2008; França et al., 2006; Millet et al., 2009). The observation of subchondritic Os isotope ratios in lavas from Pico and Faial suggests that some of this recycled material may even be of Archaean age (Schaefer et al., 2002). Evidence for the involvement of recycled oceanic crust in Azores magma genesis contributes to the active debate on the involvement of mafic lithologies, such as pyroxenite and eclogite, in the formation of melts beneath ocean islands (e.g. (Niu and O'Hara, 2003; Niu et al., 2011; Pilet and Baker, 2008; Sobolev et al., 2005)). A recent study by Prytulak and Elliott (2009) has shown that a peridotite mantle lithology with small volumes of dispersed eclogitic melts can explain both the enriched chemical signatures and the low melt productivity observed on Pico island.

The less enriched signature present in the western Sete Cidades volcano (São Miguel) is generally attributed to a common Azores plume source present on the other islands, such as the neighbouring island of Santa Maria but also on Faial and Pico (Beier et al., 2012; 2008; 2006). This common component is frequently found on other ocean islands (e.g. Hart et al. (1992) and Stracke et al. (2005)) and could possibly be the least enriched end-member component in the Azores mantle plume. Another component present in some Azores lavas is a depleted mantle component (e.g., (Beier et al., 2008; Moreira et al., 1999; Turner et al., 1997)), which is irregularly entrained by the rising plume material and causes additional complexity when assessing the distribution and flow of the mantle underneath the Azores.

Although the islands are unevenly spread across the plateau and only provide local snap-shots of the underlying mantle composition, detailed geochemical studies along the Azores MAR have shown that the plume influence extends far to the south of the islands and stops abruptly just to the north of the bathymetric high of the plateau (e.g. (Bourdon et al., 1996; Dosso et al., 1999; Gale et al., 2011; Laubier et al., 2012)). This may indicate a southward flow of the enriched mantle plume material. A study investigating the nature of recycled components in terms of dehydrated lithosphere by Dixon et al. (2002) has lead Asimow et al. (2004) to observe correlations between H_2O contents and trace element enrichment indices and thus they developed a hydrous melting and fractionation model for the MAR lavas. Their model accounts for the enriched character of the MAR basalts at significantly lower mantle potential temperatures than might be inferred for a water free source (Herzberg and Asimow, 2008; Putirka, 2008). Although there are no volatile data available from the islands or the submarine eastern Azores plateau, there is

increasing evidence that the Azores plume may indeed contain significant amounts of water (Asimow, 2004; Beier et al., 2012).

5.3. ANALYTICAL METHODS

Major element, trace element and Sr-Nd-Pb(-Hf)-Os data for the eastern islands are from Schaefer et al. (2002) Beier et al. (2008; 2007; 2006) and Turner et al. (1997) unless stated otherwise in the figure caption. Three samples from São Jorge and Pico, previously presented in Turner et al. (1997), have been analysed for Hf isotope ratios. Sample localities, a detailed petrological description and major and trace element data for samples from Flores and Corvo along with Sr and Nd isotope data are given in Genske et al. (2012). Sample localities as well as the petrography of the basalts from a subsided island to the west of Flores are described in Ryall et al. (1983). Therein the authors pointed out that the nature of these samples is subalkaline based on mineral chemical analyses. Three samples are from Deep Sea Drilling Project Holes 556 and 557 (Leg 82). Whereas the former hole was drilled into normal oceanic crust, the latter was attempted to recover westernmost enriched samples from the Azores platform (Bougault and Cande, 1985). The major and trace elements, Sr-Nd-Hf isotopes of these new samples were analysed following the methods described in Genske et al. (2012). All samples used here are presented in the appendix of this thesis.

5.3.1 Radiogenic isotopes

New radiogenic Hf, Pb and Os isotope data were obtained for selected lavas from Flores and Corvo and the submarine samples (see Table 1 for a comprehensive dataset). The double-spiked Pb isotope analysis was carried out on 2N HCl-leached 1 - 2 mm sized chips at the Leibniz Institute of Marine Geosciences (GEOMAR, Kiel), following procedures described in Hoernle et al. ((2011) and references therein). Selected chips were dissolved in a hot HF-HNO_3 mixture and Pb was separated using standard ion exchange procedures (Hoernle et al., 2008). The isotopic ratios were measured on a Finnigan MAT262 RPQ^{2+} system operating in static multi-collection mode. Multiple analyses of NBS 981 (n = 99) resulted in $^{206}Pb/^{204}Pb = 16.942 \pm 0.003$, $^{207}Pb/^{204}Pb = 15.500 \pm 0.003$, $^{208}Pb/^{204}Pb = 36.726 \pm 0.007$. The total chemistry blank was < 20 pg, and is thus negligible.

Selected powdered samples were analysed for their Hf isotopic composition using standard anionic and cationic column separation procedures (e.g. (Blichert-Toft, 2001)). Hafnium isotope data were obtained using a Nu Instruments 34 multi collector inductively coupled plasma mass spectrometer (MC-ICP-MS) at the Geochemical Analysis Unit (GAU), at Macquarie University. Reference materials BHVO-2 and JMC-475 gave $^{176}Hf/^{177}Hf$ values, which were close to published values. Ratios were normalized to $^{176}Hf/^{177}Hf = 0.7325$ to correct for mass fractionation. Repeated measurements of JMC-475 standard (n = 25) yielded $^{176}Hf/^{177}Hf$ of 0.282154 ± 0.000032 (2 sd). BHVO-2 was also processed with the samples and repeated measurements (n = 8) gave values of $^{176}Hf/^{177}Hf = 0.283101 \pm 0.000016$ (2 sd). All sample data including duplicate analyses are listed in Table 1.

For Osmium concentration and isotopic composition of the Flores and Corvo lavas, 4-5 g of powder was spiked with 0.01642 ppm Os (internal spike used at Macquarie University), according to the anticipated Os contents in the lavas. The samples were then digested in inverse aqua regia by Carius tube dissolution followed by solvent extraction and micro distillation techniques, as described in detail elsewhere (Birck et al., 1997; Cohen and Waters, 1996). All samples were run on a Thermo Finnigan Triton thermal ionisation mass spectrometer in negative-ion mode (N-TIMS) at the GAU at Macquarie University. Due to the low Os abundance in the samples, total procedural blank (TPB) levels of typically 3 pg or better were achieved so that blank contributions were typically less than 1.1 % on 5 g sample dissolutions. The WPR-1 standard was processed along with unknown samples to monitor chemical separation reproducibility and gave $^{187}Os/^{188}Os = 0.14462 \pm 0.00018$ (2 sd, n = 2) and Os (ppb) = 17.97 ± 0.15 (2sd). These values are in good agreement with published values (e.g. (Correia et al., 2007)). 5ng solutions of the JMC-2 standard run to monitor instrument performance during the course of the study resulted in $^{187}Os/^{188}Os = 0.183447 \pm 0.00004$ (2sd). Analytical results are given in Table 1.

5.4. RESULTS

We have grouped the samples discussed here according to their sample locality and geochemical composition for clarity. We distinguish the following groups: a) lavas from Santa Maria (Beier et al., 2013), b) São Miguel including the enriched eastern Nordeste volcano (Beier et al., 2007; 2006; Turner et al., 1997) separated from the other Azores

lavas as a result of their unique, enriched geochemical character, c) lavas including the central islands Terceira, Faial, Pico and São Jorge (Beier et al., 2012; 2008; Turner et al., 1997) and d) lavas from the western islands of Corvo and Flores (Genske et al., 2012), e) submarine samples from the entire plateau and beyond (Fig. 1).

All Azores lavas discussed here are alkali basalts *sensu lato* (*cf.* Table 1). The major elements of samples from Flores and Corvo have been discussed in detail in Genske et al. (2012). The data set used here was restricted to lavas with 5-12 wt.% MgO in order to limit fractional crystallisation. This will also minimize the effects of assimilation fractional crystallisation (AFC)-derived chemical signature imprints onto the lavas. We use exclusively fresh samples with a loss on ignition < 2% and without petrographic signs of alteration with the exception of the submarine samples.

5.4.1. Trace elements

The trace elements of lavas from Corvo and Flores are comparable to those of the other Azores islands with respect to their incompatible elements and Rare Earth Element (REE) concentrations and have been published elsewhere (Genske et al., 2012). However, it has to be noted that lavas from Corvo and Flores and the samples from the nearby subsided island (samples 54B core, 58 core, 68 core) have distinctively higher, and more variable Nb/Zr, Nb/Y and Ta/Hf ratios that are the result of elevated Nb and Ta concentrations and slightly lower Zr and Hf concentrations, respectively (Fig. 2). Ratios of Nb/Zr are, on average, almost twice as high as the common Azores value observed across the islands and the ridge and a ratio of ~ 0.19, which is typical for OIB (*cf.* (Willbold and Stracke, 2006)). The TiO_2 contents of the western islands are subtly lower than those of the eastern islands and we will discuss the significance of the more variable and more elevated High Field Strength Element (HFSE) ratios in more detail below. Note that the Nb/Zr, Nb/Y and Ta/Hf ratios of the lavas do not give any evidence for fractionation during crystallisation, as they do not show co-variation with MgO or SiO_2 contents of the lavas.

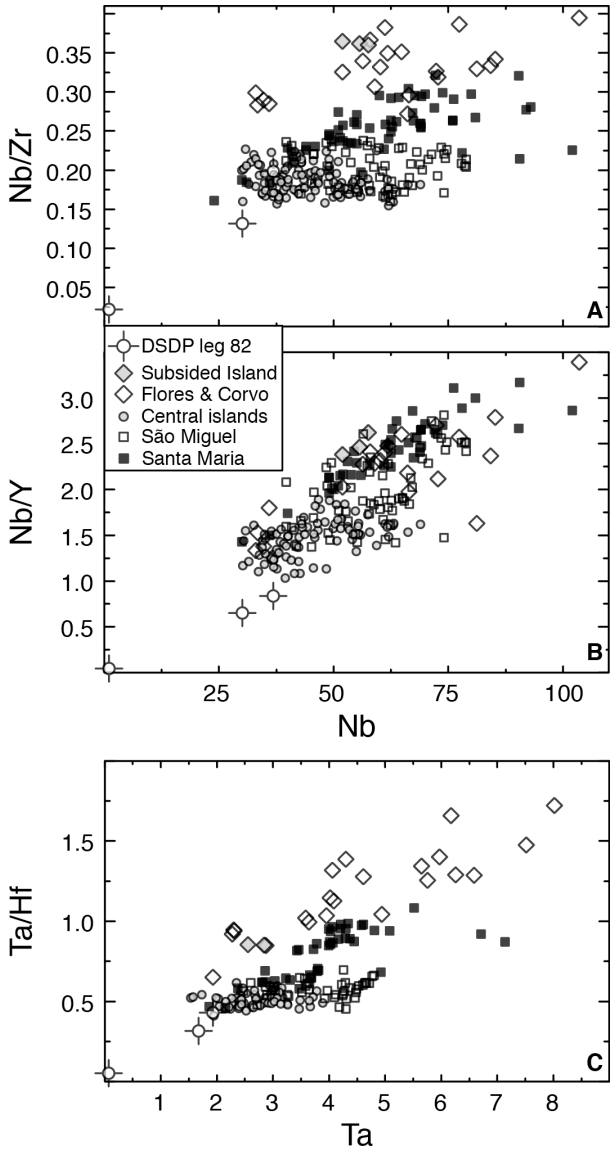

Fig. 2: a) Nb/Zr, b) Nb/Y versus Nb concentration and c) Ta/Hf versus Ta concentration for lavas with 5-12 wt.% MgO. Data sources as in Figure 1.

5.4.2. (Sr-Nd)-Pb-Hf-Os isotopes

In Pb-Pb isotope space (Figs. 1 and 3) it is apparent that lavas from Corvo and Flores cluster within a tight field at $^{206}Pb/^{204}Pb$ ratios of ±19.50 to 19.90, which is also common to lavas from the central island group and western São Miguel (Beier et al., 2012; 2008), but slightly higher than the basalts from the MAR. With fewer data available for Hf isotopes, samples from Corvo and Flores display a smaller Hf isotope range than lavas from São Miguel (Fig. 3). Three samples from the central islands (i.e. two from Pico and one from São Jorge, Table 1) were also analysed for Hf isotope ratios during the course of this study. Even though this small number of samples may not represent the full range

of the eastern islands, it is striking that they display a very restricted range in $^{176}Hf/^{177}Hf$ (~ 0.283), comparable to the average Hf isotopic composition of Flores and Corvo. Overall, the radiogenic isotope variability of the eastern island lavas is slightly larger than that of Corvo and Flores but mostly as a result of the radiogenic isotopes variability on São Miguel. The compositional field defined by the western lavas in Sr-Nd and Pb-Pb isotope spaces, but also in Hf isotope ratios, is consistent with a FOZO-type signature, which is common to most OIBs (e.g. (Hart et al., 1992; Stracke et al., 2005; Workman et al., 2004)).

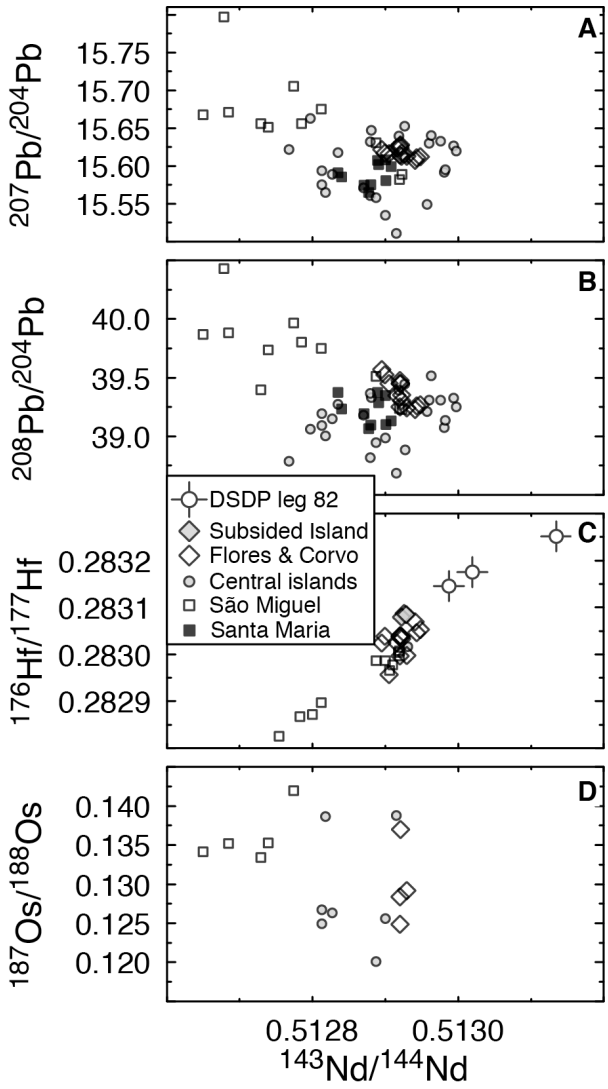

Fig. 3: a) Radiogenic compositions of $^{176}Hf/^{177}Hf$ versus $^{143}Nd/^{144}Nd$. b), c) and d) showing radiogenic Pb and Os compositions ($^{207}Pb/^{204}Pb$, $^{208}Pb/^{204}Pb$ and $^{187}Os/^{188}Os$, respectively) versus $^{143}Nd/^{144}Nd$. Same sample set as previously shown (*cf* Fig. 1).

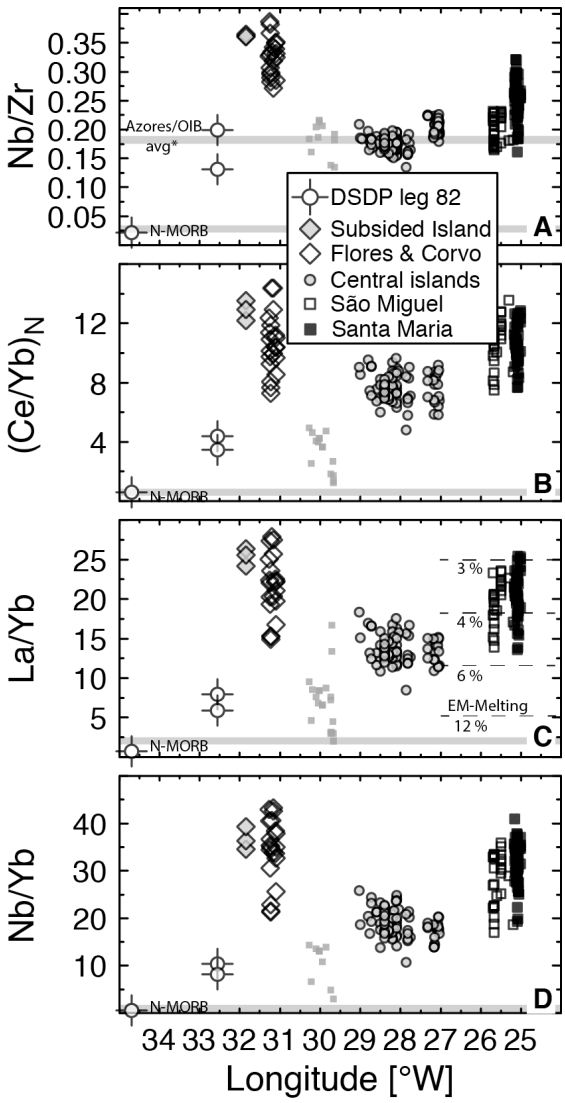

Fig. 4: a) Nb/Zr b) primitive mantle normalised $(Ce/Yb)_N$, c) La/Yb, d) Nb/Yb ratios versus longitude [°W] across the Azores archipelago. The ratios of Nb/Zr (and Ta/Hf, not shown) reveal an asymmetry with highest values and largest variation ascribed to Flores and Corvo lavas. Different melting degrees using an EM-melting similar to that described in detail in Genske et al. (2012) are illustrated in panel c). Compositional ranges for typical N-MORB and normal OIB are shown for comparison ((Arevalo and McDonough, 2010) and (Willbold and Stracke, 2006), respectively).

The new Os isotope data for Corvo and Flores lavas are supra- to slightly subchondritic and range in $^{187}Os/^{188}Os$ from 0.1249 to 0.1370. This is in agreement with Os isotope ratios published by Schaefer et al. (2002) and Widom and Shirey (1996) on other Azores lavas (Fig. 3). We did not observe any correlation with $^{87}Sr/^{86}Sr$ but a broad correlation with $^{208}Pb/^{204}Pb$ and $^{207}Pb/^{204}Pb$ is apparent (not shown).

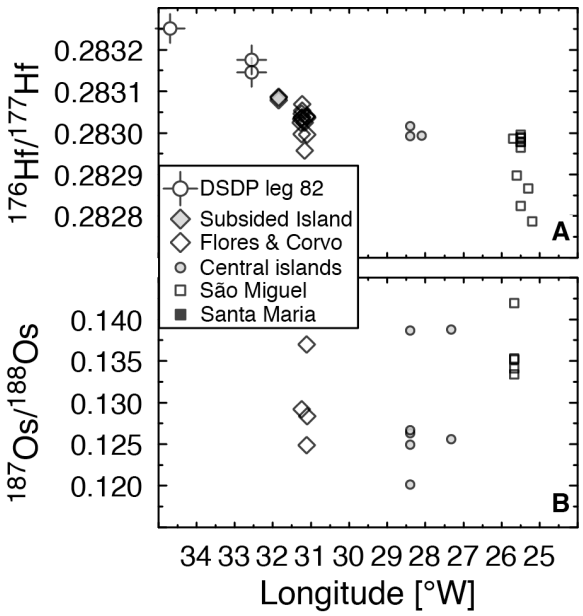

Fig. 5: Radiogenic isotope ratios of Hf and Os of selected Azores lavas versus longitudinal distance across the plateau.

The Os contents of the new samples (see appendix) are systematically higher than those reported for the central island group by Schaefer et al. (2002), but comparable to those of São Miguel presented by Widom and Shirey (1996). In contrast, samples from the MAR with highly radiogenic $^{187}Os/^{188}Os$ are characterised by Os contents commonly observed in the central islands (Table 1). We did not observe correlations of the elevated HFSE trace element ratios of Flores and Corvo with any of the radiogenic isotopes, which indicates a decoupling of the trace elements and isotopes.

5.5. DISCUSSION

5.5.1. Across-plateau variability

The Azores mantle plume is thought to be situated underneath the central island group (Cannat et al., 1999; Gente et al., 2003; Moreira et al., 1999; Shorttle et al., 2010) with the central part of the plume either being situated underneath the island of Terceira (Bourdon et al., 2005) or São Jorge (Beier et al., 2012; Millet et al., 2009). If the plume material were to flow radially outward from the plume centre and mix with ambient mantle then any chemical signature associated with the plume source should in principle vary systematically with distance from that centre (Shorttle et al., 2010). Such a simple pattern is not observed in the Azores (Figs. 4 and 5, and e.g. (Beier et al., 2010)). Rather,

the Azores mantle plume, as expressed in the eastern islands, appears to be asymmetrically heterogeneous on a variety of scales, both inter- and intra-island.

Source heterogeneity has long been discussed in the Azores, but most authors conclude that the mantle plume itself carries distinct chemical compositions that most probably reflect recycled lithosphere derived components (Beier et al., 2008; 2007; Elliott et al., 2007; França et al., 2006; Prytulak and Elliott, 2009; Schaefer et al., 2002; Turner et al., 2007; Widom et al., 1993). Additionally, detailed studies on São Miguel lavas and other islands have shown that that the role of assimilation during magma ascent needs to be considered when assessing source composition (e.g. (Snyder et al., 2004; Widom et al., 1993). As the data set investigated here has been filtered for samples > 5 wt. % MgO, these contamination effects should be limited and not strongly influence the elements and isotope ratios discussed. The incompatible trace elements and radiogenic isotopes afford a means to better define the composition and origin of the mantle source underneath the western Azores islands and to further our understanding of the origin of melting underneath these islands.

On ratio-longitude plots (Figs 4 and 5) it is shown that commonly used source indicators such as Nb/Zr are relatively homogenous in the central islands, whereas the outermost islands with respect to the plume centre display much more variability and, on average, higher values. However, the Nb/Zr (and Ta/Hf) values indicate a common source component, which is present underneath the entire plateau (Fig. 4), with the possible exception of the Flores and Corvo region (but see discussion below). The stronger HFSE fractionation appears to be a local feature of the Flores-Corvo region, where Nb/Zr and Ta/Hf ratios yield average values of 0.33, and ~1, respectively. The far west on-plateau drill hole DSDP 82-557 yields common Azores/normal OIB values. Thus, we will initially discuss the role and distribution of the recycled component in the Azores plume, using first order observations. The off-plateau drill hole sample from DSDP 82-556 displays an N-MORB composition (Arevalo and McDonough, 2010; Sun and McDonough, 1989) and will be used in the modelling below. Following this we will investigate the origin of this HFSE fractionation in more detail.

Table 2: End member compositions used for modeling the DMM-MORB and DMM-SED mixing.

	$^{87}Sr/^{86}Sr$	$^{143}Nd/^{144}Nd$	ε Nd	$^{206}Pb/^{204}Pb$	$^{207}Pb/^{204}Pb$	$^{176}Hf/^{177}Hf$	ε Hf
GERM DMM Data	0.7025	0.51321	11.16	18.50	15.50	0.2833	14.14
GLOSS	0.7173	0.51220	-8.93	18.91	15.67	0.2828	-0.35
N-MORB	0.7025	0.51316	10.18	17.50	15.40		
PUM	0.7033	0.51300	7.06	18.35			
2.5 Ga MORB	0.7025	0.51290	5.11	18.90	15.67	0.2828	-1.45

The DMM data is a compilation from the GERM database. The GLOSS composition is from Plank and Langmuir (1998). The N-MORB is taken from Sun and McDonough (1989). Primitive upper mantle (PUM) after Sun (1982) and McDonough et al. (1992). Refer to text for details on the composition of 2.5 Ga MORB.

5.5.2. Quantitative constraints on source composition

The Sr-Nd-Hf-Pb-Os isotope ratios from the western islands are broadly uniform when compared with São Miguel and the central group islands (Figs. 1 and 3). A common suggestion to explain unusually enriched Sr-Pb isotope arrays, as indicated on São Miguel (Hawkesworth et al., 1979; Shirey et al., 1987), has been the role of sediment (*cf.* EM1 and EM2 reservoirs, e.g. (Jackson and Dasgupta, 2008) and references therein). However, as discussed in Elliott et al. (2007) and Beier et al. (2007), a sedimentary origin of the radiogenic Pb sources on São Miguel seems unlikely. Instead the highly radiogenic Pb isotopes may best be explained by the presence of small-degree melts from recycled oceanic crust with variably enriched components with a common Azores mantle source. This common enriched end-member was defined by Beier et al. (2008) as an average "Azores plume component" with a FOZO-like character, based on lavas from the island of Graciosa. Modelling this common source using available constraints from isotopes and trace elements suggests up to 10 % contribution of recycled mafic crust to the plume. Prytulak and Elliott (2007) pointed out previously, that this is also consistent with Ti enrichments observed in OIB in general. However, for consistency with published Os isotope constraints (i.e. Schaefer et al. (2000)) we here calculated a model of ~2.5 Ga recycled MORB, whose composition was derived from taking a 2.5 Ga primitive mantle (PUM, Table 2), which was evolved to an N-MORB composition with an appropriate $^{187}Re/^{188}Os$ ratio of ~ 2000.

Figure 6 shows that, assuming a common (i.e. average) Azores source, its radiogenic isotope composition may best be explained by the addition of around 10 % ancient mafic crust to a depleted MORB mantle (DMM). In contrast, taking a young (i.e. 15 Ma)

MORB composition to represent the recycled component in such a model cannot reproduce the observed isotopic compositions. The possibility of the HIMU reservoir to purely account for the Azores plume signature appears unlikely from both isotopic and trace element observations, even though the HIMU reservoir is commonly identified as recycled MORB crust (Stracke et al., 2005). While most incompatible trace element ratios can be explained with this model, the distinct enrichment of the HFSE in the Corvo and Flores region requires a different explanation.

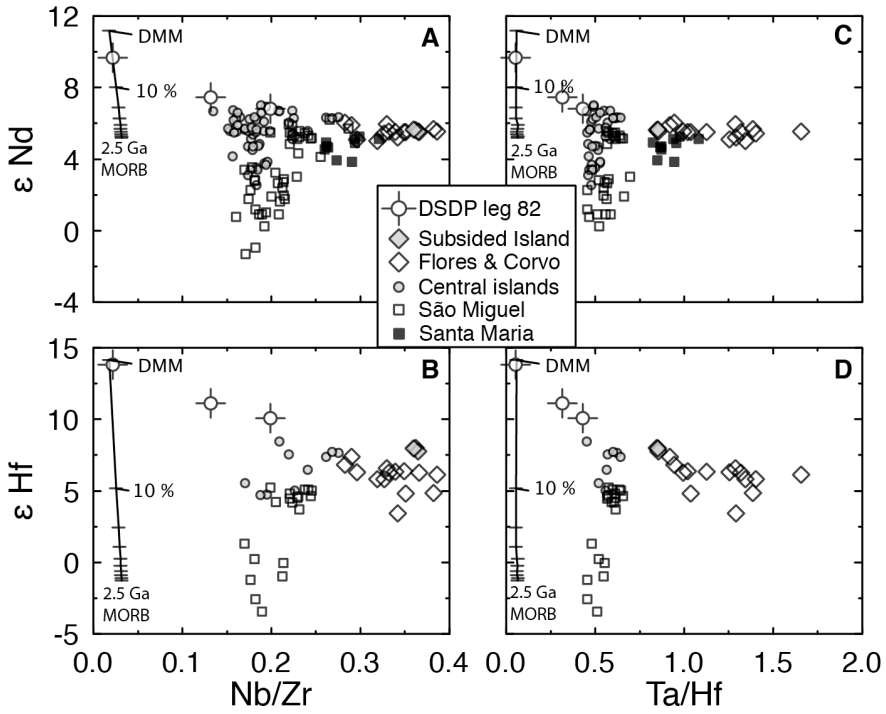

Fig. 6: Mixing model of depleted MORB mantle (DMM) and 2.5 Ga old recycled MORB (black line) on plots of epsilon Nd (panels a and c) and epsilon Hf (panels b and d) vs Nb/Zr and Ta/Hf, respectively. Epsilon values represent normalization of the radiogenic ratios to CHUR (Bouvier et al., 2008). The full model parameters are summarized in Table 2 and described in the text. Tick marks on the DMM-2.5 Ga MORB model are 10% intervals. The average range in Hf isotopic composition (i.e. epsilon Hf = 5-7) may be explained by different amounts of recycled mafic crust, however a third component may be required in the models to explain the high ratios of Nb/Zr (see discussion in the main text). As previously suggested by Prytulak and Elliott (2007), the data do not support a contribution from sediments to the plume source, as this would have unobserved impacts in Hf-Nd isotope space (not shown). Instead the mixing model of ~10% recycled mafic crust (i.e. ancient MORB) is consistent with the radiogenic isotope data.

5.5.3. HFSE systematics in the Azores

The distinct fractionation of $HFSE^{4+}$ from the $HFSE^{5+}$ in Corvo and Flores and the subsided island lavas may be the result of fractional crystallisation, assimilation-fractional crystallisation, melting processes or a distinct source component exclusively present in the western Azores mantle. We will discuss the origin of these signatures in more detail below.

5.5.3.1 AFC and fractional crystallization

Fractional crystallization, with or without accompanying assimilation, appears unlikely to account for the HFSE systematics in the western lavas for a number of reasons. Firstly, the Nb/Zr and Ta/Hf ratios do not vary with common fractionation indices such as Mg#, MgO or SiO_2 contents, even though there is some scatter in the HFSE data. Thus, the elevated ratios from the Flores-Corvo area do not back project to a common primitive (i.e. Mg# ~72) composition, as was been suggested previously by Beier et al. (2010), but instead reflect parental melts that were characterized by higher ratios of Nb/Zr and Ta/Hf. The petrography and order of crystallisation is broadly similar across the islands, such that clinopyroxene fractionation dominates the crystallizing assemblage on all islands (*cf.* (Beier et al., 2006; Genske et al., 2012)). Thus, minerals such as Fe-Ti oxides and/or amphibole that might potentially fractionate the HFSE have not been observed in significant quantitites.

Assimilation of crustal material is also unlikely to account for the higher Nb/Zr values, since the localized HFSE "anomaly" is in contrast to the ubiquitous assimilation as discussed by Genske et al. (2013). Therefore we will now consider the effects of melting dynamics and/or source features in more detail to investigate the origin of the higher HFSE ratios.

5.5.3.2 Melting dynamics

The parental melts in the Azores are inferred to have been generated under conditions of ~1450°C and 2.5-3.0 GPa (Beier et al. 2012). HFSE-fractionating minerals such as pargasite and kaersutite are only stable up to a maximum of 1075 °C and 3 GPa under water under-saturated conditions (Niida and Green, 1999). These are therefore unlikely to be primary constituents of the plume, but they might be present in the shallow mantle Where they could be assimilated by upwardly rising plume melts.

The extent of melting beneath each island can be estimated using La/Yb or $(Ce/Yb)_N$ values and an assumed source composition (e.g. (Pearce and Parkinson, 1993)). Figure 4 compares the systematics of these ratios across the Azores plateau, where higher degree melts from the Azores MAR (filtered for latitudes between 38.50-40.00°N to reflect the latitudes oft the islands) and the DSDP-82/556 drill core are also plotted. The relationships suggest that the melts at the margin of the plateau are characterized by slightly lower extents of melting and also highlights that the islands are somewhat more enriched than the submarine lavas, including the on-plateau drill samples from DSDP-82/557. The latter are characterized by melting degrees of 10-12 % melting, using the same model parameters for an enriched mantle as in Beier et al. (2013) and Genske et al. (2012). The ratios of Nb/Zr, Nb/Yb (and Ta/Hf, not shown) may also be affected by melt extraction and are not necessarily indicative of source enrichment. The importance of this effect has been discussed in much detail by Stracke and Bourdon (2009). We therefore suggest that the Flores and Corvo lavas represent low degree melts that originate in an overall more efficiently MORB-plume mixed source, based on their Sr-Nd-Hf-Pb ratios. The submarine lavas from DSDP-82/557 further to the west also support the view of substantial (increasing) contribution from the local depleted MORB source in the western Azores lavas when compared to lavas from the east (Figs. 4 and 5).

5.5.3.3 Source effects on HFSE

The question remains whether or not the Flores-Corvo lavas contain contributions from a component in the plume source that is not seen in any of the other islands. For example, the elevated Nb/Zr and Ta/Hf ratios that characterise the western islands, cannot be explained by mixing of a common Azores source with Flores-Corvo compositions, since the isotope mixing lines for Nd and Hf with Nb/Zr or Ta/Hf do not simulate the data well, i.e. the observed epsilon Nd values are too low even though epsilon Hf values can be explained by such mixing (Fig. 6c and d). It must be noted that the constraints on the trace element composition of HIMU mantle to potentially account for this local source feature remain elusive (Willbold and Stracke, 2006) and do not allow for robust modelling. Furthermore, the lower Hf isotope ratios of HIMU are not expressed in the data and in Pb-Os isotope space the data trend back towards DMM, not HIMU. As mentioned above, the striking difference in HFSE ratios observed between eastern and western Azores lavas is clearly decoupled from the isotopic ratios. Recycled mafic crust may experience different degrees of alteration, first at the mid-ocean ridge and

subsequently during dehydration and subduction; hence different degrees of dehydration may change the bulk mineralogy of that crust both in terms of modal abundance and composition. Rutile and amphibole are two phases that are capable of fractionating HFSE ratios (Foley et al., 2000; Tiepolo et al., 2001), and that are associated with subduction processes. However, the latter is not stable at great mantle depths and is thus unlikely to reflect the fractionation of Nb/Zr observed in mantle plumes/OIBs. In contrast, recycled MORB crust may carry compositionally different (and different amounts of) residual rutile, which may then further fractionate the bulk HFSE plume budget during OIB melt generation, though the latter is not necessarily required. However, rutile is not stable in normal peridotite, but in titanium enriched eclogites (i.e. subducting slabs). The stability of rutile further depends on oxygen fugacity and H_2O content (e.g. (Foley et al., 2000; John et al., 2010; Rudnick, 2000)). To account for the differences of the HFSE observed in the Azores, however we regard the role of residual rutile as minor, since there are no differences of Nb/Ta or Zr/Hf observed in the data set, even though small amounts of this phase would dominate the Nb-Ta budget and thus drive these ratios to superchondritic values (Rudnick, 2000). This again is not observed in the Azores lavas.

The model proposed by Beier et al. (2013) to invoke melting of carbonated peridotite to explain the chemical composition of lavas from the far eastern island of Santa Maria is not applicable to the western islands of Flores and Corvo, even though their Nb/Zr and Ta/Hf systematics are similar. However, ratios of K/La and Ti/Sm, but also the SiO_2 contents of the western islands cannot be explained by this model.

5.5.3.1 Geodynamic implications

In agreement with their location in the periphery of the Azores plume (i.e. greatest distance to the plume centre) spatial differences in residual plume mineralogy may directly reflect different lithological contributions and/or degrees of alteration of recycled mafic crust in the source of the Flores and Corvo and also the Santa Maria lavas. However, since the radiogenic isotopes and also the trace elements imply a common component to be present in the entire Azores mantle the same recycled MORB source is invoked across the Azores plume. Based on Re-depletion model ages as presented in Schaefer et al. (2002), the Os isotope signature determined for Flores and Corvo lavas implies a minimum age of ~500 Ma and thus may have a similar age to the plume component underneath Faial and Pico islands on the eastern plateau. Hence the

commonly enriched radiogenic isotope nature of Corvo and Flores, and possibly also its age, appear comparable to those of the central island group.

5.6. CONCLUSIONS

We conclude here that lavas from the islands of Corvo and Flores require a similar contribution from the enriched source that is also inferred to be present underneath the central island group. Neither the trace element ratios of the HFSE nor the full spectrum of distinct radiogenic isotope ratios can be explained by sediments contribution into the source of neither the western nor the eastern lavas. Instead, we can show that a recycled mafic (MORB) crust is required. Additionally, we can show that the recycled crust underneath the Azores plateau must be at least 500 Ma old based on Re depletion ages from Os isotope analyses. The local feature of elevated and more variable Nb/Zr and Ta/Hf ratios in the Flores and Corvo lavas and also in the Santa Maria lavas is clearly decoupled from the radiogenic isotopes of Sr, Nd, Pb, Hf and Os. Whereas it was demonstrated previously that Santa Maria contains evidence for carbonated peridotite in its source, we can show that this is unlikely for the Flores and Corvo system. Instead we suggest that melting dynamics invoking a two-stage melting model of a low-*F* Azores plume melt to metasomatise the depleted MORB mantle to then generate the Flores-Corvo magmas can account for the unique HFSE feature and is consistent with other melting sensitive tracers such as La/Yb or La/Sm, but due to its small difference is not seen in major elements such as Na.

ACKNOWLEDGEMENTS

V. H. Forjaz and the Observatório Vulcanológico e Geotérmico dos Açores are gratefully acknowledged for their assistance with the logistics of Flores and Corvo samples. We particularly thank P. Wieland and M. Locmelis for help during the Hf and Os isotope analytical work at CCFS/GEMOC. The Hf and Os isotope data were obtained using instrumentation funded by DEST Systemic Infrastructure Grants, ARC LIEF, NCRIS, industry partners and Macquarie University. This is contribution XXX from the ARC Centre of Excellence for Core to Crust Fluid Systems (http://www.ccfs.mq.edu.au) and XXX in the GEMOC Key Centre (http://www.gemoc.mq.edu.au). FSG acknowledges support from an ECORD research grant to analyse a sample subset from DSDP leg 82.

REFERENCES

Arevalo, R., Jr, McDonough, W.F., 2010. Chemical variations and regional diversity observed in MORB. Chemical Geology 271, 70–85.

Asimow, P.D., 2004. A hydrous melting and fractionation model for mid-ocean ridge basalts: Application to the Mid-Atlantic Ridge near the Azores. Geochem. Geophys. Geosyst. 5.

Beier, C., Haase, K.M., Abouchami, W., Krienitz, M.S., Hauff, F., 2008. Magma genesis by rifting of oceanic lithosphere above anomalous mantle: Terceira Rift, Azores. Geochem. Geophys. Geosyst. 9.

Beier, C., Haase, K.M., Hansteen, T.H., 2006. Magma Evolution of the Sete Cidades Volcano, São Miguel, Azores. J Petrology 47, 1375–1411.

Beier, C., Haase, K.M., Turner, S.P., 2012. Conditions of melting beneath the Azores. Lithos 144–145, 1–11.

Beier, C., Mata, J., Stöckhert, F., Mattielli, N., Brandl, P.A., Madureira, P., Genske, F.S., Martins, S., Madeira, J., Haase, K.M., 2013. Geochemical evidence for melting of carbonated peridotite on Santa Maria Island, Azores. Contributions to Mineralogy and Petrology 1–19.

Beier, C., Stracke, A., Haase, K.M., 2007. The peculiar geochemical signatures of São Miguel (Azores) lavas: Metasomatised or recycled mantle sources? Earth and Planetary Science Letters 259, 186–199.

Beier, C., Turner, S.P., Plank, T., White, W.M., 2010. A preliminary assessment of the symmetry of source composition and melting dynamics across the Azores plume. Geochem. Geophys. Geosyst. 11, Q02004.

Birck, J.L., Barman, M.R., Capmas, F., 1997. Re-Os Isotopic Measurements at the Femtomole Level in Natural Samples. Geostandards and Geoanalytical Research 21, 19–27.

Blichert-Toft, J., 2001. On the Lu-Hf Isotope Geochemistry of Silicate Rocks. Geostandards and Geoanalytical Research 25, 41–56.

Bougault, H., Cande, S.C., 1985. Background, Objectives, and Summary of Principal Results: Deep Sea Drilling Project Sites 556-564, in: Initial Reports of the Deep Sea Drilling Project, Initial Reports of the Deep Sea Drilling Project. U.S. Government Printing Office.

Bourdon, B., Langmuir, C.H., Zindler, A., 1996. Ridge-hotspot interaction along the Mid-Atlantic Ridge between 37°30“ and 40°30” N: the U-Th disequilibrium evidence. Earth and Planetary Science Letters 142, 175–189.

Bourdon, B., Turner, S.P., Ribe, N.M., 2005. Partial melting and upwelling rates beneath the Azores from a U-series isotope perspective. Earth and Planetary Science Letters 239, 42–56.

Bouvier, A., Vervoort, J.D., Patchett, P.J., 2008. The Lu–Hf and Sm–Nd isotopic composition of CHUR: Constraints from unequilibrated chondrites and implications for the bulk composition of terrestrial planets. Earth and Planetary Science Letters 273, 48–57.

Cannat, M., Briais, A., Deplus, C., Escartín, J., Georgen, J.E., Lin, J., Mercouriev, S., Meyzen, C., Muller, M., Pouliquen, G., Rabain, A., da Silva, P., 1999. Mid-Atlantic Ridge-Azores hotspot interactions: along-axis migration of a hotspot-derived event of enhanced magmatism 10 to 4 Ma ago. Earth and Planetary Science Letters 173, 257–269.

Cohen, A., 1996. Separation of osmium from geological materials by solvent extraction for analysis by thermal ionisation mass spectrometry. Analytica Chimica Acta 332, 269–275.

Correia, C.T., Kirk, J.D., Frick, L.R., Petronilho, L.A., Tassinari, C.C.G., Sato, K., 2007. The Re-Os isotopic system: geochemistry and methodology at the Geochronological Research Center (CPGeo) of the University of S„o Paulo, Brazil. Geologia USP. SÈrie CientÌfica 7, 45–56.

Dixon, J.E., Leist, L., Langmuir, C.H., Schilling, J.-G., 2002. Recycled dehydrated lithosphere observed in plume-influenced mid-ocean-ridge basalt. Nature.

Donnelly, K.E., Goldstein, S.L., Langmuir, C.H., Spiegelman, M., 2004. Origin of

enriched ocean ridge basalts and implications for mantle dynamics. Earth and Planetary Science Letters 226, 347–366.

Dosso, L., Bougault, H., Langmuir, C.H., Bollinger, C., Bonnier, O., Etoubleau, J., 1999. The age and distribution of mantle heterogeneity along the Mid-Atlantic Ridge (31-41∞N). Earth and Planetary Science Letters 170, 269–286.

Elliott, T., Blichert-Toft, J., Heumann, A., Koetsier, G., Forjaz, V.H., 2007. The origin of enriched mantle beneath São Miguel, Azores. Geochimica et Cosmochimica Acta 71, 219–240.

Foley, S.F., Barth, M.G., Jenner, G.A., 2000. Rutile/melt partition coefficients for trace elements and an assessment of the influence of rutile on the trace element characteristics of subduction zone magmas. Geochimica et Cosmochimica Acta 64, 933–938.

França, Z.T.M., Tassinari, C.C.G., Cruz, J.V., Aparicio, A.Y., Araña, V., Rodrigues, B.N., 2006. Petrology, geochemistry and Sr-Nd-Pb isotopes of the volcanic rocks from Pico Island--Azores (Portugal). Journal of Volcanology and Geothermal Research 156, 71–89.

Gale, A., Escrig, S., Gier, E.J., Langmuir, C.H., Goldstein, S.L., 2011. Enriched basalts at segment centers: The Lucky Strike (37°17′N) and Menez Gwen (37°50′N) segments of the Mid-Atlantic Ridge. Geochem. Geophys. Geosyst. 12.

Gast, P.W., Tilton, G.R., Hedge, C., 1964. Isotopic Composition of Lead and Strontium from Ascension and Gough Islands. Science 145, 1181–1185.

Genske, F.S., Beier, C., Haase, K.M., Turner, S.P., Krumm, S., Brandl, P.A., 2013. Oxygen isotopes in the Azores islands: Crustal assimilation recorded in olivine. Geol.

Genske, F.S., Turner, S.P., Beier, C., Schaefer, B.F., 2012. The Petrology and Geochemistry of Lavas from the Western Azores Islands of Flores and Corvo. J Petrology 53, 1673–1708.

Gente, P., Dyment, J., Maia, M., Goslin, J., 2003. Interaction between the Mid-Atlantic Ridge and the Azores hot spot during the last 85 Myr: Emplacement and rifting of the hot spot-derived plateaus. Geochem. Geophys. Geosyst. 4.

Hart, S.R., Hauri, E.H., Oschmann, L.A., Whitehead, J.A., 1992. Mantle Plumes and Entrainment: Isotopic Evidence. Science 256, 517–520.

Hawkesworth, C.J., Norry, M.J., Roddick, J.C., Vollmer, R., 1979. 143Nd/144Nd and 87Sr/86Sr ratios from the Azores and their significance in LIL-element enriched mantle. Nature 280, 28–31.

Herzberg, C., Asimow, P.D., 2008. Petrology of some oceanic island basalts: PRIMELT2.XLS software for primary magma calculation. Geochem. Geophys. Geosyst. 9, Q09001.

Hoernle, K.A., Abt, D.L., Fischer, K.M., Nichols, H., Hauff, F., Abers, G.A., van den Bogaard, P., Heydolph, K., Alvarado, G., Protti, M., Strauch, W., 2008. Arc-parallel flow in the mantle wedge beneath Costa Rica and Nicaragua. Nature 451, 1094–1097.

Hoernle, K.A., Hauff, F., Kokfelt, T.F., Haase, K.M., Garbe-Schönberg, D., Werner, R., 2011. On- and off-axis chemical heterogeneities along the South Atlantic Mid-Ocean-Ridge (5–11°S): Shallow or deep recycling of ocean crust and/or intraplate volcanism? Earth and Planetary Science Letters 306, 86–97.

Hofmann, A.W., 1997. Mantle geochemistry: the message from oceanic volcanism. Nature 385, 219–229.

Jackson, M.G., Dasgupta, R., 2008. Compositions of HIMU, EM1, and EM2 from global trends between radiogenic isotopes and major elements in ocean island basalts. Earth and Planetary Science Letters 276, 175–186.

John, T., Klemd, R., Klemme, S., Pfänder, J.A., Elis Hoffmann, J., Gao, J., 2010. Nb–Ta fractionation by partial melting at the titanite–rutile transition. Contributions to Mineralogy and Petrology 1–11.

Laubier, M., Gale, A., Langmuir, C.H., 2012. Melting and Crustal Processes at the FAMOUS Segment (Mid-Atlantic Ridge): New Insights from Olivine-hosted Melt Inclusions from Multiple Samples. J Petrology.

McDonough, W.F., Sun, S.-S., Ringwood, A.E., Jagoutz, E., Hofmann, A.W., 1992. Potassium, rubidium, and cesium in the Earth and Moon and the evolution of the

mantle of the Earth. Geochimica et Cosmochimica Acta 56, 1001–1012.

Millet, M.-A., Doucelance, R., Baker, J.A., Schiano, P., 2009. Reconsidering the origins of isotopic variations in Ocean Island Basalts: Insights from fine-scale study of São Jorge Island, Azores archipelago. Chemical Geology 265, 289–302.

Moreira, M., Doucelance, R., Kurz, M.D., Dupré, B., Allègre, C.J., 1999. Helium and lead isotope geochemistry of the Azores Archipelago. Earth and Planetary Science Letters 169, 189–205.

Niida, K., Green, D.H., 1999. Stability and chemical composition of pargasitic amphibole in MORB pyrolite under upper mantle conditions. Contributions to Mineralogy and Petrology 135, 18–40.

Niu, Y., O'Hara, M.J., 2003. Origin of ocean island basalts: A new perspective from petrology, geochemistry, and mineral physics considerations. J. Geophys. Res. 108, 2209.

Niu, Y., Wilson, M., Humphreys, E.R., O'Hara, M.J., 2011. The Origin of Intra-plate Ocean Island Basalts (OIB): the Lid Effect and its Geodynamic Implications. J Petrology 52, 1443–1468.

Pearce, J.A., Parkinson, I.J., 1993. Trace element models for mantle melting: application to volcanic arc petrogenesis. Geological Society, London, Special Publications 76, 373–403.

Pilet, S., Baker, M.B., 2008. Metasomatized lithosphere and the origin of alkaline lavas. Science.

Prytulak, J., Elliott, T., 2007. TiO2 enrichment in ocean island basalts. Earth and Planetary Science Letters 263, 388–403.

Prytulak, J., Elliott, T., 2009. Determining melt productivity of mantle sources from 238U-230Th and 235U-231Pa disequilibria; an example from Pico Island, Azores. Geochimica et Cosmochimica Acta 73, 2103–2122.

Putirka, K.D., 2008. Excess temperatures at ocean islands: Implications for mantle layering and convection. Geol 36, 283.

Rudnick, R.L., 2000. Rutile-Bearing Refractory Eclogites: Missing Link Between Continents and Depleted Mantle. Science 287, 278–281.

Ryall, P.J.C., Blanchard, M.-C., Medioli, F., 1983. A subsided island west of Flores, Azores. Canadian Journal of Earth Sciences 20, 764–775.

Schaefer, B.F., Turner, S.P., Parkinson, I.J., Rogers, N., Hawkesworth, C.J., 2002. Evidence for recycled Archaean oceanic mantle lithosphere in the Azores plume. Nature 420, 304–307.

Shirey, S.B., Bender, J.F., Langmuir, C.H., 1987. Three-component isotopic heterogeneity near the Oceanographer transform, Mid-Atlantic Ridge. Nature.

Shorttle, O., Maclennan, J., Jones, S.M., 2010. Control of the symmetry of plume-ridge interaction by spreading ridge geometry. Geochem. Geophys. Geosyst. 11, Q0AC05.

Snyder, D.C., Widom, E., Pietruszka, A.J., Carlson, R.W., 2004. The Role of Open-System Processes in the Development of Silicic Magma Chambers: a Chemical and Isotopic Investigation of the Fogo A Trachyte Deposit, São Miguel, Azores. J Petrology 45, 723–738.

Sobolev, A.V., Hofmann, A.W., Sobolev, S.V., Nikogosian, I.K., 2005. An olivine-free mantle source of Hawaiian shield basalts. Nature 434, 590–597.

Stracke, A., Bizimis, M., Salters, V.J.M., 2003. Recycling oceanic crust: Quantitative constraints. Geochem. Geophys. Geosyst. 4.

Stracke, A., Bourdon, B., 2009. The importance of melt extraction for tracing mantle heterogeneity. Geochimica et Cosmochimica Acta 73, 218–238.

Stracke, A., Hofmann, A.W., Hart, S.R., 2005. FOZO, HIMU, and the rest of the mantle zoo. Geochem. Geophys. Geosyst. 6.

Sun, S.-S., 1982. Chemical composition and origin of the earth's primitive mantle. Geochimica et Cosmochimica Acta 46, 179–192.

Sun, S.-S., McDonough, W.F., 1989. Chemical and isotopic systematics of oceanic basalts: implications for mantle composition and processes. Geological Society, London, Special Publications 42, 313–345.

Tiepolo, M., Bottazzi, P., Foley, S.F., Oberti, R., Vannucci, R., Zanetti, A., 2001. Fractionation of Nb and Ta from Zr and Hf at Mantle Depths: the Role of Titanian Pargasite and Kaersutite. J Petrology 42, 221–232.

Turner, S.P., Hawkesworth, C.J., Rogers, N., King, P., 1997. U---Th isotope disequilibria and ocean island basalt generation in the Azores. Chemical Geology 139, 145–164.

Turner, S.P., Tonarini, S., Bindeman, I.N., Leeman, W.P., Schaefer, B.F., 2007. Boron and oxygen isotope evidence for recycling of subducted components over the past 2.5 Gyr. Nature 447, 702–705.

Wessel, P., Smith, W.H.F., 1991. Free software helps map and display data. Eos Trans. AGU 72.

Wessel, P., Smith, W.H.F., 1995. New version of the Generic Mapping Tools released. Eos Trans. AGU.

White, W.M., Tapia, M.D.M., Schilling, J.-G., 1979. The petrology and geochemistry of the Azores Islands. Contributions to Mineralogy and Petrology 69, 201–213.

Widom, E., Carlson, R.W., Gill, J.B., Schmincke, H.-U., 1997. Th-Sr-Nd-Pb isotope and trace element evidence for the origin of the Sao Miguel, Azores, enriched mantle source. Chemical Geology 140, 49–68.

Widom, E., Gill, J.B., Schmincke, H.-U., 1993. Syenite Nodules as a Long-Term Record of Magmatic Activity in Agua de Pao Volcano, Sao Miguel, Azores. J Petrology 34, 929–953.

Widom, E., Shirey, S.B., 1996. Os isotope systematics in the Azores: implications for mantle plume sources. Earth and Planetary Science Letters 142, 451–465.

Willbold, M., Stracke, A., 2006. Trace element composition of mantle end-members: Implications for recycling of oceanic and upper and lower continental crust. Geochem. Geophys. Geosyst. 7, Q04004.

Workman, R.K., Hart, S.R., Jackson, M.G., Regelous, M., Farley, K.A., Blusztajn, J., Kurz, M.D., Staudigel, H., 2004. Recycled metasomatized lithosphere as the origin of the Enriched Mantle II (EM2) end-member: Evidence from the Samoan Volcanic

Chain. Geochem. Geophys. Geosyst. 5.

CHAPTER 6: GEOCHEMICAL EVIDENCE FOR MELTING OF CARBONATED PERIDOTITE ON SANTA MARIA ISLAND, AZORES

Christoph Beier[a*], João Mata[b], Ferdinand Stöckhert[a], Nadine Mattielli[c], Philipp A. Brandl[a], Pedro Madureira[d], Felix S. Genske[a], Sofia Martins[b], José Madeira[e], Karsten M. Haase[a]

[a]GeoZentrum Nordbayern, Universität Erlangen-Nürnberg, Schloßgarten 5, D-91054 Erlangen, Germany

[b]Departamento de Geologia da Universidade de Lisboa; Centro de Geologia da Universidade de Lisboa, Faculdade de Ciências, Campo Grande C6, 1749-016 Lisboa, Portugal

[c]Université Libre de Bruxelles., Laboratoire G-Time CP160/02, Avenue F.D. Roosevelt 50, 1050 Brussels, Belgium

[d]Centro de Geofísica de Évora/Dep. Geociências da Universidade de Évora, R. Romão Ramalho, 59, 7000 Évora, Portugal and Estrutura de Missão para a Extensão da Plataforma Continental, R. Costa Pinto, 165, 2770-047 Paço de Arcos, Portugal

[e]Departamento de Geologia da Universidade de Lisboa; Instituto D. Luiz, Faculdade de Ciências, Campo Grande C6, 1749-016 Lisboa, Portugal

[*]corresponding author, present address: GeoZentrum Nordbayern, Universität Erlangen-Nürnberg, Schloßgarten 5, D-91054 Erlangen, Germany, Tel.: +49/9131/85-26064, Fax.: +49/9131/85-29295, Email: Christoph.Beier@gzn.uni-erlangen.de

ABSTRACT

The islands of the Azores archipelago emerge from an oceanic plateau built on lithosphere increasing in age with distance from the Mid-Atlantic Ridge from 10 to 45 Ma. Here, we present the first comprehensive major and trace element and Sr-Nd-Pb isotope data from Santa Maria, the easternmost island of the archipelago, along with

published data from the other Azores islands situated much closer to the Mid-Atlantic ridge axis. We can show that the distinctively more variable and more enriched trace element ratios at Santa Maria combined with a relatively small range in Sr-Nd-Pb isotope ratios may best be explained by low degrees of partial melting of a common Azores mantle plume source underneath thicker lithosphere. This implies that melt extraction processes and melting dynamics may be able to better preserve the geochemical mantle source variability underneath thicker lithosphere. These conclusions may apply widely for oceanic melts erupted on relatively thick lithosphere. In addition lower Ti/Sm and K/La ratios and SiO_2 contents of Santa Maria lavas imply melting of a carbonated peridotite source. Mixing of variable portions of deep small degree carbonated peridotite melts and shallow volatile-free garnet-peridotite may best explain the geochemical variability underneath Santa Maria in agreement with the volatile-rich nature of the Azores mantle source. However, Santa Maria is the island where the CO_2 – rich nature of the mantle source is more evident compared to the other Azores islands, reflecting a combination of a smaller extent of partial melting and the off-axis positioning relatively to the tilted Azores mantle plume.

Key words: Ocean Island Basalts, Azores, lithosphere thickness, melting dynamics, carbonated peridotite

6. 1 INTRODUCTION

Basalts erupted at Ocean Islands (OIB) display a larger trace element and isotopic variability compared to those erupted along mid-ocean ridges (MOR) (e.g., Dupré and Allègre 1983; Hofmann 1997; Hofmann 2003; McKenzie and O'Nions 1995; Salters and White 1998; Stracke, et al. 2003). The geochemical composition of melts erupted at ocean islands may be influenced by a number of parameters that involve the composition of the mantle source (enriched vs. depleted), the mantle lithology (pyroxenite vs. peridotite or volatile-rich peridotite), extent of partial melting and melt extraction processes (Dasgupta, et al. 2009; Dasgupta, et al. 2006; Sobolev, et al. 2005; Stracke and Bourdon 2009). Additionally, the along-chain (temporal) variations in lava compositions described for long-lived seamount chains in the Pacific imply that changes in the melting process may be induced by changes in thickness of the oceanic lithosphere these seamounts are situated on (e.g., Beier, et al. 2011; Haase 1996; Humphreys and Niu 2009; Ito and Mahoney 2005; Regelous, et al. 2003).

It still remains a matter of active debate whether the Azores archipelago is related to the upwelling of a deep mantle plume (Montelli, et al. 2004) or whether the melting anomaly is restricted to the upper mantle (Courtillot, et al. 2003; Ritsema and Allen 2003). The Azores Plateau in the Central Northern Atlantic has been associated with the presence of melting anomaly which was first recognized by the Sr enriched isotope compositions of the islands and along the Mid-Atlantic Ridge (MAR) in the vicinity of the Azores (Schilling 1975; White, et al. 1975; White and Hofmann 1982). Several of the Azores islands have been the subject of geochemical and petrological studies (Beier, et al. 2008; Beier, et al. 2010; Bourdon, et al. 2005; Cannat, et al. 1999; Madureira, et al. 2005; Millet, et al. 2009; Moreira, et al. 1999; Nowell, et al. 1998; Prytulak and Elliott 2009; Schaefer, et al. 2002; Schmincke 1973; Turner, et al. 1997; Widom, et al. 1997) that have shown that this archipelago has isotopic and trace element compositions comparable to those found in other hotspots associated with mantle plumes. This is supported by finite-frequency seismic tomography imaging a plume-like column extending down to at least 400 km depth (Yang, et al. 2006), by a reduction of the transition zone thickness beneath the Azores (Courtier, et al. 2007) and by unradiogenic $^{3}He/^{4}He$ ratios (up to 13.5 times of the atmospheric value) and air-corrected $^{21}Ne/^{22}Ne = 0.052$ obtained for magmatic fluids and olivine phenocrysts which points to the contribution of a deep mantle source component (Jean-Baptiste, et al. 2009; Madureira, et al. 2005; Moreira, et al. 1999). However, the mantle potential temperatures in the Azores imply that the mantle sources may contain a significant amount of volatiles which lowers its solidus temperatures and thus, magmatism in the Azores may best be explained by the combined effect of volatile induced melting ('wetspot') and a thermal anomaly ('hotspot') (Asimow, et al. 2004; Beier, et al. 2012).

The Azores archipelago is geochemically variable on a regional scale (Beier, et al. 2010; Millet, et al. 2009; Moreira, et al. 1999; White, et al. 1979), preserving small-scale intra-island heterogeneities (Beier, et al. 2007; Elliott, et al. 2007; Turner, et al. 1997; Widom, et al. 1997) even for coeval lavas erupted less than 10 km from each other (Haase and Beier 2003; Madureira, et al. 2011). For Santa Maria most published works have focused on the occurrence of fossiliferous sediments and carbonates (Madeira, et al. 2007) and, along with selected petrographical/geochemical data, few K-Ar age data are available (Abdel Monem, et al. 1975; Anderson and Flower 1982; Esenwein 1929; Féraud, et al. 1980; Féraud, et al. 1981). The higher alkalinity of lavas from Santa Maria compared to

the other Azores islands was first observed by White et al. (1979). The position of Santa Maria at the eastern edge of the submarine Azores Plateau (Fig.1) allows to address several questions on the conditions of melting at the edge of the Azores melting anomaly some 5-8 Ma ago (Abdel Monem, et al. 1975; Féraud, et al. 1981). In addition, by comparing Santa Maria with the much younger neighboring islands, we can constrain the evolution of the Azores islands mantle sources from their earliest formation stages 5-8 Ma ago to the younger stages observed today.

Here, we present the first comprehensive major element, trace element and Sr-Nd-Pb radiogenic isotope data for basalts of Santa Maria, the easternmost island in the Azores. We can show that the Sr-Nd-Pb isotope ratios of Santa Maria lavas are comparable to those of islands closer to the MAR and the magmas thus originate from isotopically similar mantle. However, the trace element ratios of Santa Maria lavas are both more enriched and more variable than those observed in islands erupted closer to the MAR. We explain this discrepancy by smaller degrees of partial melting beneath Santa Maria compared to the other Azores islands, in agreement with the higher alkalinity (White, et al. 1979). However, we find that K_2O, TiO_2, and Rb concentrations are lower at Santa Maria compared to the other islands which is inconsistent with lower degrees of partial melting. We can show that these geochemical signatures underneath Santa Maria give evidence for melting of a CO_2-rich peridotite lithology. While this carbonatite signal is weakened underneath the other islands due to larger degrees of partial melting and mixing between melts of carbonated peridotite and volatile-free garnet-peridotite, the thicker lithosphere and smaller degrees of partial melting preserve this signature underneath Santa Maria. At larger degrees of partial melting or a longer melting column this carbonatite source fingerprint may be obscured.

6. 2 GEOLOGIC BACKGROUND

The Azores islands are built on an oceanic plateau which has generally been accepted to be the result of a melting anomaly, but the origin of this anomaly is still a matter of debate, i.e. whether the Azores are a deep mantle plume or whether the anomaly is solely restricted to the upper mantle (see 1. Introduction). Tectonic structures in the Azores area are mainly controlled by the Ridge-Ridge-Ridge-type triple junction between the North American, African and Eurasian lithospheric plates formed by the two active spreading centers: a) the Mid-Atlantic Ridge (MAR), splitting the Azores Plateau into a larger

eastern and a smaller western part and b) the 550 km long WNW-ESE trending ultraslow spreading Terceira Rift (2-4 mm/a) at the northern boundary of the plateau, (Fig. 1; Vogt and Jung 2004). Spreading rates of the MAR in this region are on the order of 23 mm/a (Fernandes, et al. 2006), which classifies it as slow spreading ridge amongst the global ridge system. The East Azores Fracture Zone marks the previous, nowadays seismically inactive, boundary between the African and Eurasian plates.

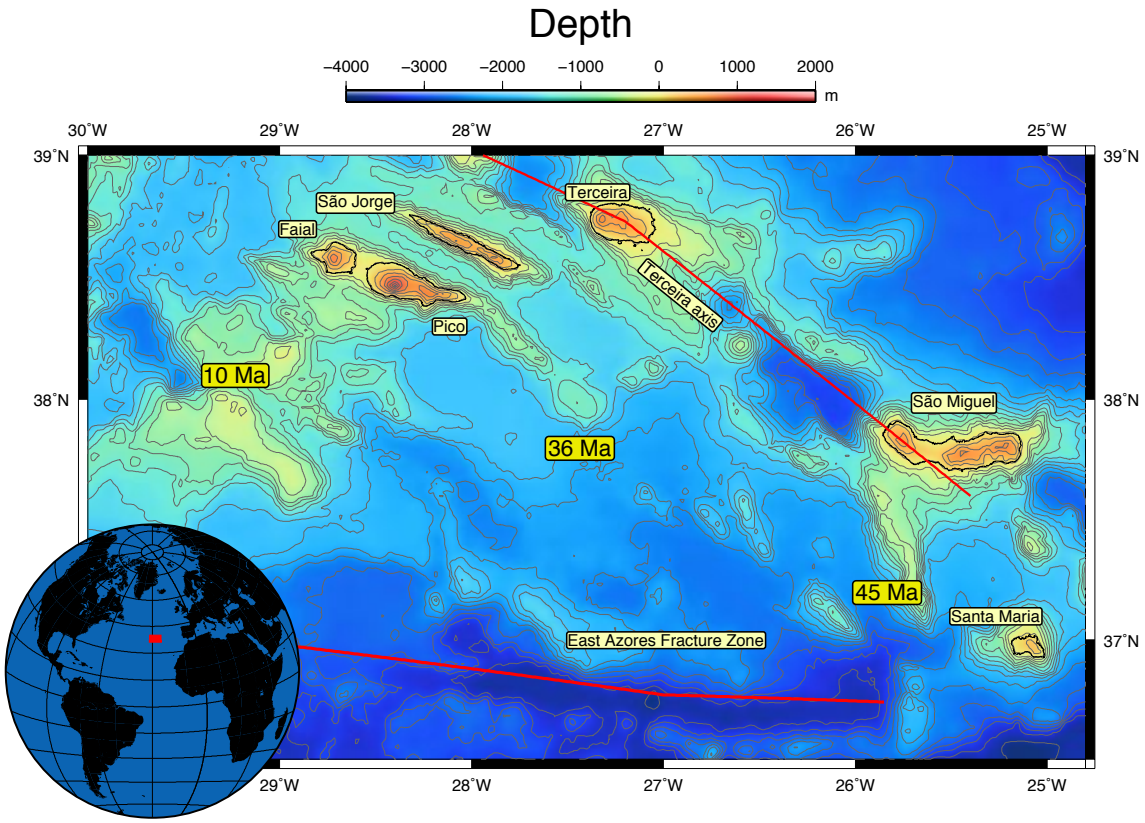

Figure 1. Map of the eastern Azores Plateau using Generic Mapping Tools (GMT (Wessel and Smith 1991; Wessel and Smith 1998)). Lithosphere ages from Searle (1980), Cannat, et al. (1999) and Luis and Miranda (2008). Main tectonic features are the ultraslow spreading Terceira axis and the seismically inactive East Azores fracture zone.

The ultraslow spreading Terceira Rift comprises, from west to east, the islands of Graciosa, Terceira, the seamount Dom João de Castro and the island of São Miguel, providing trace element and isotopic evidence for short length-scale heterogeneity in the mantle (Beier, et al. 2008; Beier, et al. 2010). The age range given for the Azores islands and geophysical constraints imply a build up of the plateau from around 10 Ma (Abdel Monem, et al. 1975; Cannat, et al. 1999; Féraud, et al. 1980; Gente, et al. 2003). Crustal thickness in the Azores has been considered to be around 12-14 km (Escartín, et al. 2001) and thus significantly thicker than normal oceanic crust (Grose 2012; White, et al. 1992).

Most of the islands are volcanically active today, with the notable exception of the easternmost island of Santa Maria. Indeed, K-Ar and Ar-Ar ages from the islands imply that most of the central and eastern Azores islands were formed <2 Ma (Johnson, et al. 1998) with selected lavas from Santa Maria reaching up to 8 Ma (Abdel Monem, et al. 1975; Féraud, et al. 1980). Crustal ages on the Azores Plateau range from 10 Ma at Princesa Alice bank (south of Pico and Faial) (Cannat, et al. 1999) to ~45 Ma south of Santa Maria (Luis and Miranda 2008). Thus, by implication, the range in lithosphere thickness in the Azores is relatively large ranging from ~35 km at 10 Ma to about 76 km at 45 Ma (using the 1300°C isotherm; see Stein and Stein 1992). The relatively large range in lithosphere ages with increasing distance from the Mid-Atlantic ridge (MAR) compared to the age range covered by the islands allows to estimate the influence of lithosphere thickness on the melting regime in low-buoyancy upwelling plumes like the Azores (Davies 1988; Sleep 1990).

6. 3 METHODS

Altered rinds were removed by sawing. Samples were then coarsely crushed and the freshest fragments selected, avoiding secondary alteration. The grains were washed in an ultrasonic bath with deionized water, and powdered in an agate ball mill. For the majority of samples presented in supplemental Table 1 major element concentrations of whole rock sample powders were measured on fused glass beads on a Philips PW 2400 XRF spectrometer at the GeoZentrum Nordbayern in Erlangen. The major elements SiO_2, TiO_2, Al_2O_3, Fe_2O_3, MnO, MgO, Na_2O, K_2O, CaO, P_2O_5 along with a subset of trace elements (V, Cr, Co, Ni, Cu, Zn, Rb, Sr, Y, Zr, Nb, Ba) were analysed. Loss on ignition (LOI) was determined by weighing 1 g of sample before and after heating the samples for 12 hours at 1300°C. Precision and accuracy were generally better than 0.8% and 1% (2σ) for most elements and <0.5% for SiO_2. Major elements of glasses were measured on a JEOL JXA-8200 Superprobe at the GeoZentrum Nordbayern along with samples presented by Brandl et al. (2012) using methods and standards described therein. Trace element analyses were carried out using an Agilent 7500cs inductively coupled plasma mass spectrometer at the Institut für Geowissenschaften, Universität Kiel using the methods described in Garbe-Schönberg (1993). Accuracy was checked using international rock standards (BHVO-2, AGV-2, JA-2) and the external precision for duplicate analyses was better than 3% for all elements. For a subset of samples marked in italics in supplemental Table 1, the major and trace elements were analyzed at Activation

Laboratories (Canada). Major elements of this set were analyzed using inductively coupled plasma-optical emission spectrometry (ICP-OES) on a Thermo Jarrell-Ash ENVIRO II ICP and/or Spectro Cirros ICP. Trace element concentrations were obtained using inductively coupled plasma-mass spectrometry (ICP-MS) on a Perkin Elmer SCIEX ELAN 6000, 6100 or 9000 ICP/MS, with the exception of Sc, V, Ba and Sr, which were obtained by ICP-OES. Alkaline dissolution with lithium metaborate/tetraborate followed by nitric acid dissolution was performed for all analyses, except for the analyses of Cd, Cu, Ni and Zn, for which a multi-acid digestion (hydrofluoric followed by a mixture of nitric and perchloric acids) was carried out. Calibration was performed using USGS and CANMET certified reference materials. The instrumental drift was monitored by analyzing one of the standards for every group of ten samples. Duplicate measurements of samples shows that reproducibility is better than 3 % for major element analyses, 7 % for rare earth elements, 5 % for highly incompatible elements (i.e., Rb, Ba, U and Th). The accuracy of analyses can be assessed by comparing measured and certified values for the USGS standard reference W-2a (see supplementary Table 2). More information on the analytical procedures can be found at http://www.actlabs.com.

The chemical preparation of 18 samples analyzed for Sr-Nd-Pb isotope ratios was performed at the Laboratoire G-Time at the Department of Earth and Environmental Sciences of the “Université Libre de Bruxelles” (Belgium). To remove alteration and any potential contamination, a leaching procedure was applied to powdered whole rock samples (250 mg), with repeated additions of 6N sub-boiled HCl (5-6 times) followed by 30-minutes ultrasonic baths until the solution was clear. Samples were then rinsed twice with milli-Q water and were then ultrasonicated for 30 minutes (Weis and Frey 1996). Samples were then dissolved for 48 hours on a hotplate at about 130°C with a mixture of sub-boiled HF (48%) and HNO_3 (14 N) acids in closed Savillex® beakers. After evaporation, the samples were re-dissolved in 6N sub-boiled HCl for 24 hours at 130ºC. The Sr, Nd and Pb fractions were all extracted from the same initial sample solution. All samples were first processed on Pb micro-columns loaded with AG1-X8 100-200 mesh Biorad resin (Weis, et al. 2006). Strontium and the Rare Earth Elements (REE) were further separated using a column loaded with Dowex AG50W-X8 100-200 mesh cation exchange resin. Nd was recovered by loading the REE fraction onto a column filled with

HDEHP-coated Teflon. Measurements of the total procedural Nd, Sr and Pb blanks gave 8 pg, 8 pg, and 10 pg, respectively.

The isotopic compositions of Nd and Pb were determined on a Nu Instruments Plasma MC-ICP-MS at the Laboratoire G-Time of the "Université Libre de Bruxelles". Each session of analyses started with a "batch run" of 10 analyses of the standard solutions in order to monitor the optimization (stability and sensitivity) of the machine. In addition, during this batch run, the reproducibility and accuracy of the values were checked. Standards were systematically run between every two samples to monitor the instrumental mass bias during the analysis session. Nd and Pb isotopes are measured in static multicollection mode in wet mode. When Nd isotopes were analyzed, masses 147 (Sm) and 140 (Ce) were simultaneously monitored for interference corrections on masses 144, 148, 150 and 142. With the exception of Ce (with a sensitivity always less than 1/30 of the Nd ion beam), all interference corrections on masses were entirely negligible. The Nd isotopic measurements were internally normalized to $^{146}Nd/^{144}Nd=0.7219$. During data collection, the average $^{143}Nd/^{144}Nd$ value for the Rennes Nd standard was 0.511978± 22(2σ, n=44). For Pb isotopic analyses Tl was added, to both sample and standard, to control instrumental mass fractionation. Solutions were prepared to obtain a [Pb]/[Tl] ratio of 4. Except for two samples where the amount of sample material was insufficient (but the signal for (^{204}Pb) was > 100 mV in the axial collector), all samples were run with a total Pb ion beam between 12 to 40V. During the Pb sessions, 20 analyses of the SRM981 Pb standard solution were performed and gave $^{208}Pb/^{204}Pb = 36.7174 \pm 47$ (2σ), $^{207}Pb/^{204}Pb = 15.4978 \pm 13$ (2σ), and $^{206}Pb/^{204}Pb = 16.9408 \pm 20$ (2σ). Pb measurements were automatically corrected according with the Tl mass fractionation and using the sample-standard bracketing method (using the triple-spike values of Abouchami, et al. 2000 and; Galer and Abouchami 1998).

The Sr isotopic ratios were obtained on the Finnigan Triton Thermo-Ionization Mass Spectrometer (TIMS) at the Pacific Centre for Isotopic and Geochemical Research at the University of British Columbia (Canada). Sr isotopic compositions were measured in a static mode on a single T filament, and corrections for mass fractionation by normalization to $^{86}Sr/^{88}Sr=0.1194$ were systematically applied. For every ten samples, the NBS 987 Sr standard was run and gave a mean value of $^{87}Sr/^{86}Sr=0.710248\pm12$ (2σ, n=9).

The reproducibility of isotopic measurements, can be assessed by sample replicate and duplicate analyses. The replicate analyses are better than 3-4 ppm and 13 ppm for $^{143}Nd/^{144}Nd$ and $^{87}Sr/^{86}Sr$, respectively. For $^{206}Pb/^{204}Pb$, $^{207}Pb/^{204}Pb$, and $^{208}Pb/^{204}Pb$ the external reproducibility obtained on duplicate samples is ~ 20, 28 and 30 ppm, respectively. Additional information on the analytical procedures used at the Université Libre de Bruxelles and the University of British Columbia, can be found in Weis, et al. (2006).

6. 4 RESULTS

In this paper we discuss major element, trace element and Sr-Nd-Pb isotope data from five Azores islands, grouped into samples from: 1) Faial and Pico, 2) Terceira, 3) São Miguel (Beier, et al. 2008; Beier, et al. 2006; Beier, et al. 2012; Beier, et al. 2007; Beier, et al. 2010) and 4) the new samples from Santa Maria (supplemental Table 1). The lavas of Faial and Pico islands were erupted on 10 Ma-old lithosphere, while the island of Terceira is situated on lithosphere that has an age of 20 Ma. The island of São Miguel lies north of Santa Maria and thus on lithosphere with a comparable age (~45 Ma).

6. 4.1 Major elements

The studied lavas and dikes from Santa Maria are alkaline and cover a range in MgO contents from 1.95 wt.% to 15.94 wt.% (Fig. 2), with the majority of the samples ranging from 3.3 to 13.8 wt.%. Their Al_2O_3 and CaO contents are comparable to those observed for the other Azores islands. Potassium ranges from those contents observed in Pico and Faial to slightly lower values. For most elements, samples from Santa Maria form liquid lines of descent similar to those from the other Azores islands, but display lower SiO_2 and TiO_2 contents. For those samples that have loss on ignition <3 wt.% lavas from Santa Maria display slightly higher Na_2O contents than the other Azores islands, as previously noted by White et al. (1979). Here, we focus on those samples with MgO >7 wt.% in order to avoid a potential bias by fractional crystallization processes.

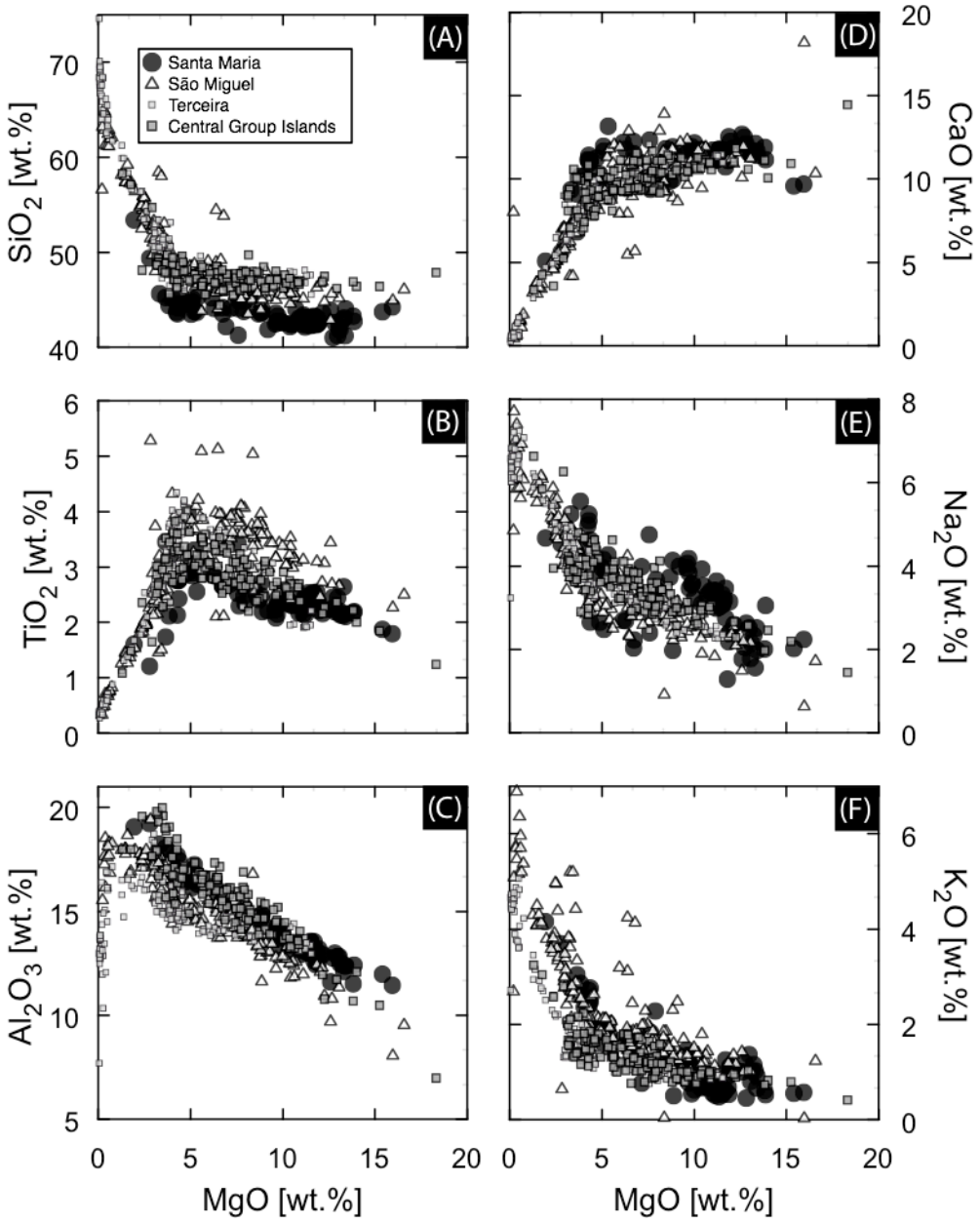

Figure 2. a) SiO_2, b) TiO_2, c) Al_2O_3, d) CaO, e) Na_2O and f) K_2O contents of the Azores lavas. Literature data are from Beier, et al. (2008; 2006; 2010) for Terceira and São Miguel and Beier, et al. (2012) for Pico and Faial.

6. 4.2 Trace elements

Samples with MgO >7 wt.% display multi-element trace element patterns normalized to primitive mantle that are convex upward with negative anomalies for K, Th and Pb (not shown) being comparable to those of the other Azores islands (Beier, et al. 2008) The composition of primitive lavas from Santa Maria are similar to those from the other Azores islands for some trace element ratios (e.g. Ba/Th; see supplemental Table 1). However, they are characterized by significantly higher and more variable Nb/Zr (and

Ba/Nb) and lower Rb/Th, K/La and Ti/Sm ratios compared to rocks with similar MgO contents from the other Azores islands (Fig. 3). trace element ratios like La/Yb, La/Sm, primitive mantle normalized $(Ce/Yb)_N$, and, to a lesser extent, $(Dy/Yb)_N$ are comparable to those found in São Miguel (Fig 3) but are more variable and higher than those from Pico, Faial and Terceira islands.

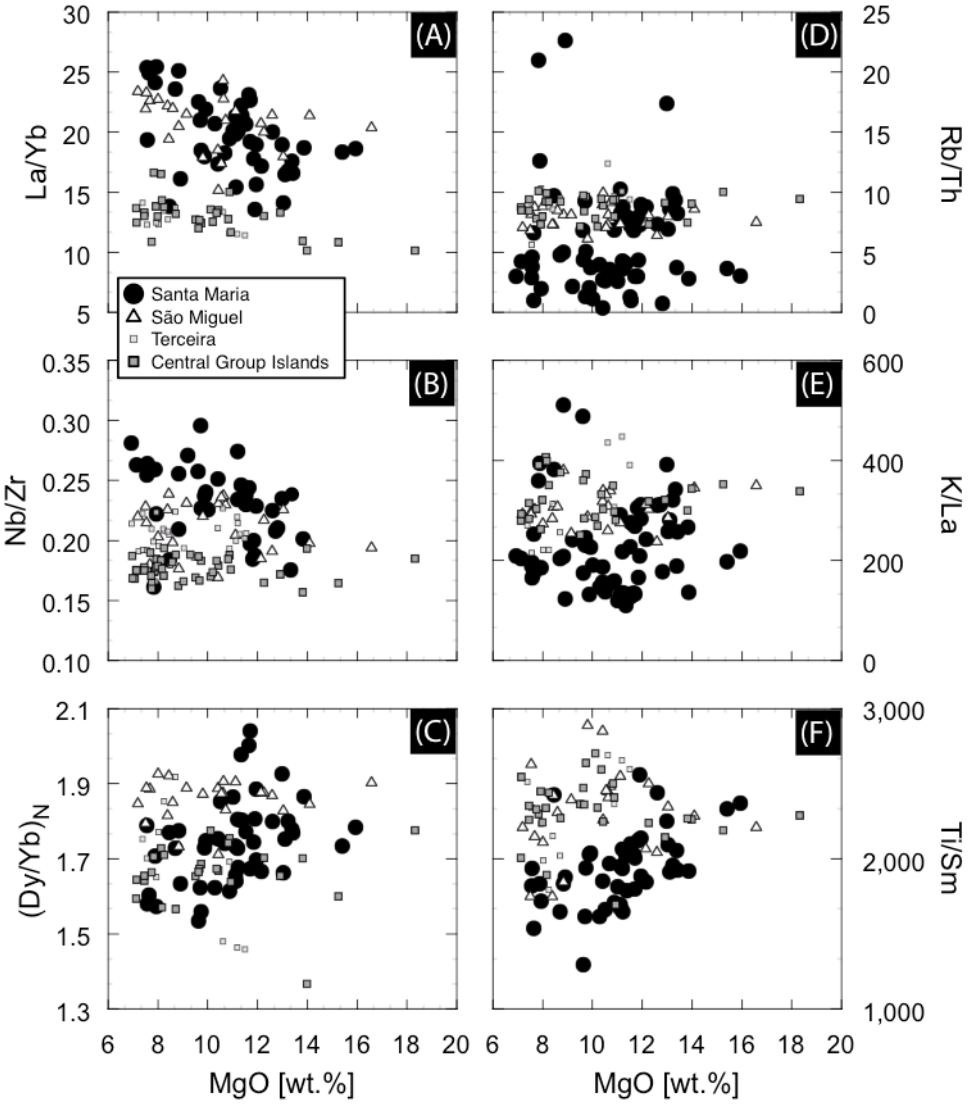

Figure 3. a) La/Yb, b) Nb/Zr, c) primitive mantle normalized $(Dy/Yb)_N$, d) Rb/Th, e) K/La and f) Ti/Sm ratios of the Azores lavas. Data sources as in Figure 2. Primitive mantle from Lyubetskaya and Korenaga (2007). Note that Santa Maria lavas have higher La/Yb and Nb/Zr but lower Rb/Th, K/La and Ti/Sm ratios than the Central Group Islands.

6. 4.3 Sr-Nd-Pb isotopes

The primitive lavas from Santa Maria display a small variability of $^{87}Sr/^{86}Sr$ and $^{143}Nd/^{144}Nd$ isotope compositions (Fig. 4). They range from $^{87}Sr/^{86}Sr$ = 0.70351 and

$^{143}Nd/^{144}Nd$ = 0.51290 to 0.70376 and 0.51285, respectively. They cover a much smaller range than that observed in Faial, Pico, Terceira and in particular São Miguel (Fig. 4).

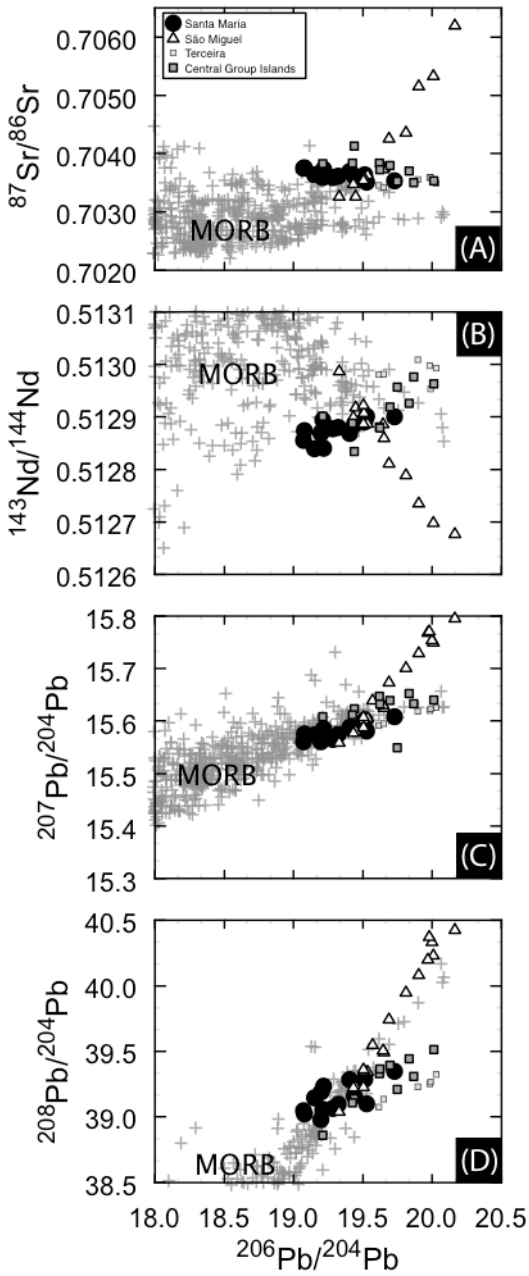

Figure 4. a) $^{87}Sr/^{86}Sr$, b) $^{143}Nd/^{144}Nd$ c) $^{207}Pb/^{204}Pb$ and d) $^{208}Pb/^{204}Pb$ versus $^{206}Pb/^{204}Pb$ isotope ratios of the Azores lavas. Data sources as in Figure 2 and MORB data are from the GEOROC database. Santa Maria isotope compositions merge at isotope ratios commonly associated with the Azores mantle plume (Beier, et al. 2008; Beier, et al. 2012).

In the Pb isotope space (Fig. 4) Santa Maria lavas ($^{206}Pb/^{204}Pb$ = 19.0705 to 19.7863; $^{207}Pb/^{204}Pb$ = 15.506 to 15.6080; $^{208}Pb/^{204}Pb$ = 39.0233 to 39.3742) are within the range commonly found in the Azores at the intersection of compositions from São Miguel (Sete

Cidades volcano, (Beier, et al. 2007), Terceira (and Graciosa), (Beier, et al. 2008), and Pico and Faial islands (Beier, et al. 2012). These compositions are similar to the FOZO mantle component that frequently occurs in intraplate settings (Hart, et al. 1992; Hofmann 1997; Stracke, et al. 2005; Zindler and Hart 1986). We did not find any evidence for an enriched mantle component that might be related to the highly Sr- and Pb- radiogenic sources of eastern São Miguel (Beier, et al. 2007; Elliott, et al. 2007; Turner, et al. 1997; Widom, et al. 1997).

6. 5 DISCUSSION

6. 5.1. Mantle source compositions

The Azores islands are well known for small-scale variability of the mantle sources (Beier, et al. 2008; Madureira, et al. 2011; Millet, et al. 2009), and for the unique trace element and isotope signature reported for the eastern São Miguel lavas, not observed in any other ocean island (Beier, et al. 2007; Elliott, et al. 2007; Turner, et al. 1997; Widom, et al. 1997). Although Santa Maria lavas display relatively low Sr and Pb isotope ratios compared to the other Azores islands they are still significantly more radiogenic and more enriched in incompatible elements than lavas from the MAR (Fig. 4). For example, for rocks with MgO > 7 wt.%, Santa Maria lavas have Nb/Zr ratios ($x = 0.23 \pm 0.02$; 1σ) significantly higher than primitive mantle (0.064; Lyubetskaya and Korenaga 2007) or MORB in the vicinity of Azores ($x = 0.19 \pm 0.08$; 1σ; Bourdon, et al. 1996). The Sr-Nd-Pb radiogenic isotopes of Santa Maria differ from the extreme compositions of the eastern São Miguel lavas and rather form a relatively homogeneous cluster comparable to rocks from Faial and Pico. This is particularly interesting given that Santa Maria is only some 80 km distant from the eastern Nordeste volcano on São Miguel. Moreover, at Santa Maria we do not find evidence for significant small-scale heterogeneity in radiogenic isotopes. A correlation of the Pb isotope and Nb/Zr elemental ratios on São Miguel implies that the variability of trace element ratios in São Miguel mainly reflects a distinct mantle source composition (Beier, et al. 2007). However, this might not be applicable to the particular case of Santa Maria because we do not see a correlation between La/Yb (and Nb/Zr; not shown) ratios and any of the radiogenic isotopic ratios of the Santa Maria lavas (Fig. 5). In addition, the parent/daughter ratios of Rb/Sr and Sm/Nd are not correlated with the Sr and Nd isotope ratios indicating that the trace element enrichment on Santa Maria is not the result of a long-term enriched mantle source

composition (Fig. 5), but suggests that the trace element are fractionated during partial melting.

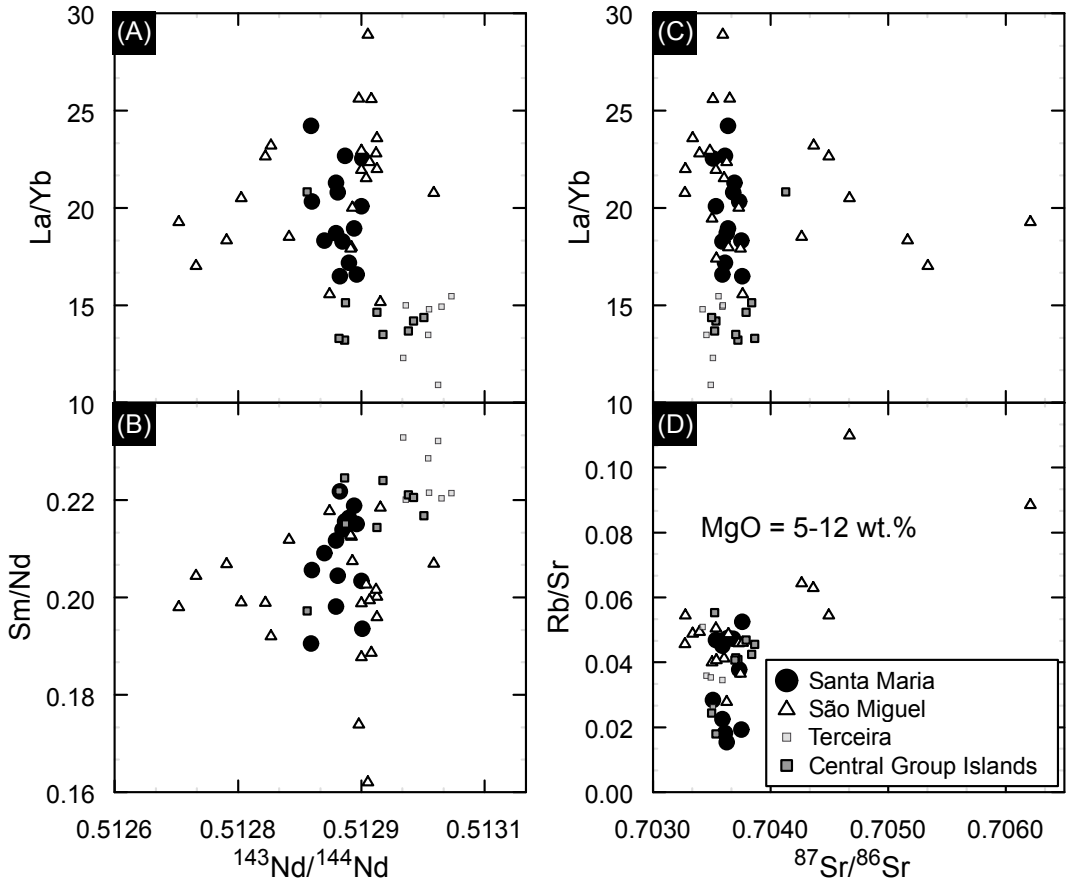

Figure 5. a) La/Yb, b) Sm/Nd versus $^{143}Nd/^{144}Nd$ and c) La/Yb, d) Rb/Sr versus $^{87}Sr/^{86}Sr$ isotope ratios of the Azores lavas. Note that for Figure 5d only lavas with 5-12 wt.% MgO were selected. Data sources as in Figure 2.

The Azores islands formed from a relatively enriched mantle plume source that has frequently been associated with the presence of recycled material (Beier, et al. 2008; Beier, et al. 2007; Elliott, et al. 2007; Turner, et al. 1997; Widom, et al. 1997). However, Santa Maria is the oldest island of the Azores and is the most distant from the center of the melting anomaly proposed to be underneath Terceira (Bourdon, et al. 2005; Moreira, et al. 1999). The published ages (up to 8 Ma; Abdel Monem, et al. 1975) indicate that Santa Maria lavas represent the oldest emerged Azores mantle plume activity, thus reflecting the early stage melting dynamics at the edge of the mantle plume head some 8 Ma ago. Considering the absolute motion of the lithospheric plate to the east, it is not expectable that lava geochemistry may reflect the transition from plume head melts to melts from the plume tail. The age of oldest lavas from Santa Maria is 8 Ma and, at a half

spreading rate of 11.5 mm/a at the MAR (Fernandes, et al. 2006), Santa Maria likely moved on the order of 90 km in an eastward direction. Thus, at its formation Santa Maria was situated approximately at the present-day longitude of the Sete Cidades volcano on the western end of the island of São Miguel or slightly further west (Fig. 1).

6. 5.2 Melting constraints

Magma composition in oceanic intraplate settings may be influenced by a variety of parameters: a) depth and temperature of melting, b) geochemical source composition, c) interaction with lithosphere during ascent (Ito and Mahoney 2005) and, finally, d) mantle lithology, i.e. the presence of pyroxenite and/or peridotite sources (Dasgupta, et al. 2009; Dasgupta, et al. 2006; Hirschmann and Stolper 1996; Pertermann and Hirschmann 2003; Sobolev, et al. 2007; Stracke and Bourdon 2009; Stracke, et al. 1999). In order to determine the dynamics of melting during the early stages of the formation of the Azores we will discuss the significance of these parameters below.

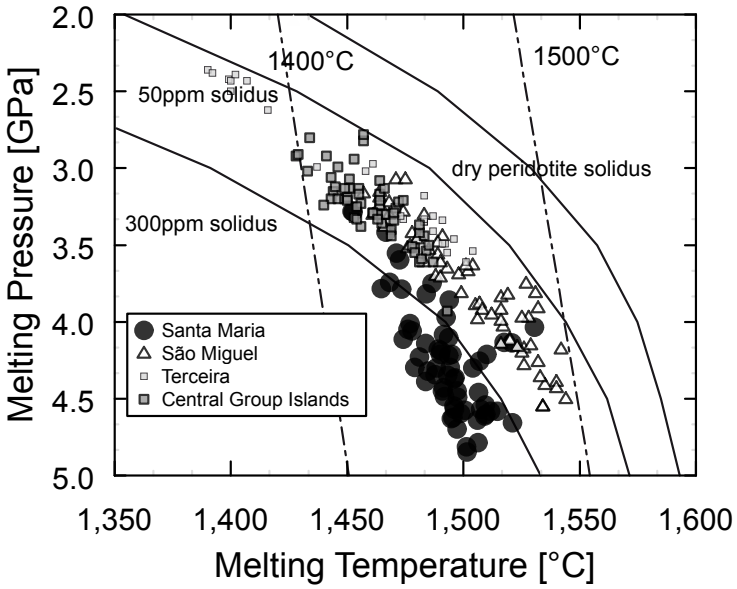

Figure 6. Pressures and temperatures of the Azores lavas calculated using Putirka (2008). Mantle potential temperatures are from Lee, et al. (2009). Solidus for dry peridotite and 50 ppm and 300 ppm H_2O are from Asimow, et al. (2004). Data source as in Figure 2.

Melting dynamics in a mantle plume may be controlled by a gradient in temperature which decreases with increasing distance from the center of upwelling. In the Azores, the U-Th-Pa disequilibria indicate that at present the strongest upwelling rate occurs underneath Terceira Island (Bourdon, et al. 2005) but, for the islands studied by Beier, et

al. (2012), temperatures and pressures of melting are highest underneath the island of São Jorge. Santa Maria formed some 8 Ma ago on the edge of the plateau suggesting that it was situated at the edge of the plume head, possibly at lower temperatures. Its temperatures and pressures were calculated following the approach described in more detail in Beier, et al. (2012). On a P-T space (Fig. 6) Santa Maria samples clearly describe a trend characterized by a lower temperature for a given pressure, compared with the other islands considered in this study, including the neighboring island of São Miguel located at almost the same longitude (Fig. 1). Interestingly, compared to the other Azores islands, Santa Maria magmas form at much lower temperatures than the dry peridotite solidus suggesting partial melting in the presence of volatiles (but see also discussion below) (Asimow, et al. 2004; Beier, et al. 2012).

If we assume similar peridotite mantle sources beneath Santa Maria and the other islands of the archipelago, then the degrees of partial melting underneath Santa Maria are lower than those observed in Pico and Faial and similar to those determined for São Miguel; degrees of partial melting underneath most Azores islands have been estimated to be on the order of 4-6% but range between 2-4% for Santa Maria (Fig. 7). At these low degrees of partial melting (<3% degree of partial melting) Nb will be fractionated from Zr leading to a pronounced enrichment of Nb/Zr ratios (Pfänder, et al. 2007) (Fig. 7). Considering the similarity of the radiogenic isotopes of Santa Maria compared to those of Faial and Pico and combined with their higher Nb/Zr and La/Yb ratios, the lack of correlation of La/Yb (and Nb/Zr; not shown) and the radiogenic isotope ratios (Fig. 5) indicates that the elevated trace element ratios underneath Santa Maria cannot be a source feature but instead are reflecting a melting signal (Fig. 7). In the following, we will discuss the lithospheric lid effect that may influence the final depth of melting.

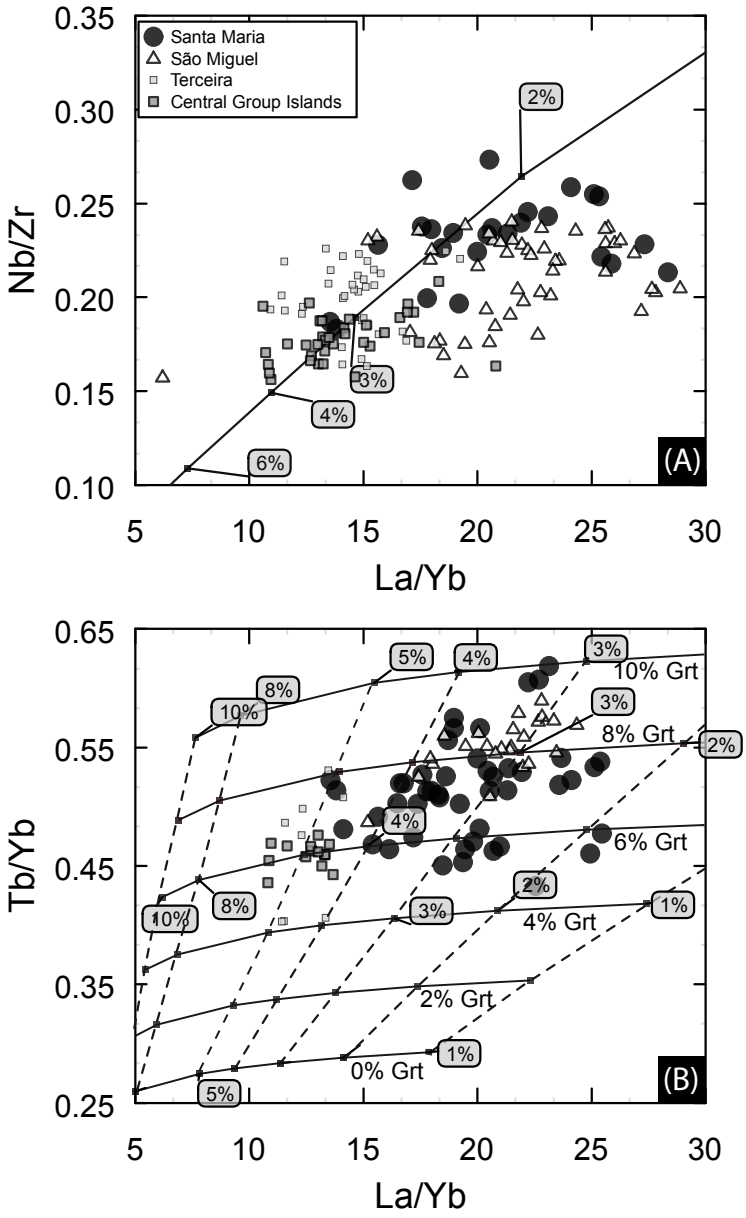

Figure 7. La/Yb versus Nb/Zr and Tb/Yb ratios of the Azores lavas using fractional melting model used in Bourdon, et al. (2005) and Beier, et al. (2010). Partition coefficients for Nb and Zr are those used in Pfänder, et al. (2007) for all other elements we used those compiled in Halliday, et al. (1995) and Blundy, et al. (1998). Mantle source compositions are those used in Beier, et al. (2007) for Sete Cidades volcano. Grey labelled markers are degrees of partial melting in a) and b). Amount of garnet in the mantle lithology varies from 0-12 %.

6. 5.3 Influence of lithosphere thickness

As a result of the progressive cooling the total thickness of the oceanic lithosphere will increase with age, an effect theoretically significant at the Azores given that the strongest increase in thickness is observed at lithosphere ages less than 60 Ma (Stein and Stein 1992). Thus, comparing the Faial and Pico islands erupted on 10 Ma-old lithosphere

(Cannat, et al. 1999) with Terceira at ~20 Ma and Santa Maria erupted on lithosphere of ~45 Ma (Luis and Miranda 2008) will allow to determine the effects of increasing lithosphere thickness on the degrees of partial melting. If the final depth of melting underneath the Azores islands and thus also the overall degree of partial melting is controlled by a lithospheric lid effect then melting dynamics across the Azores Plateau should be correlated with increasing lithosphere thickness.

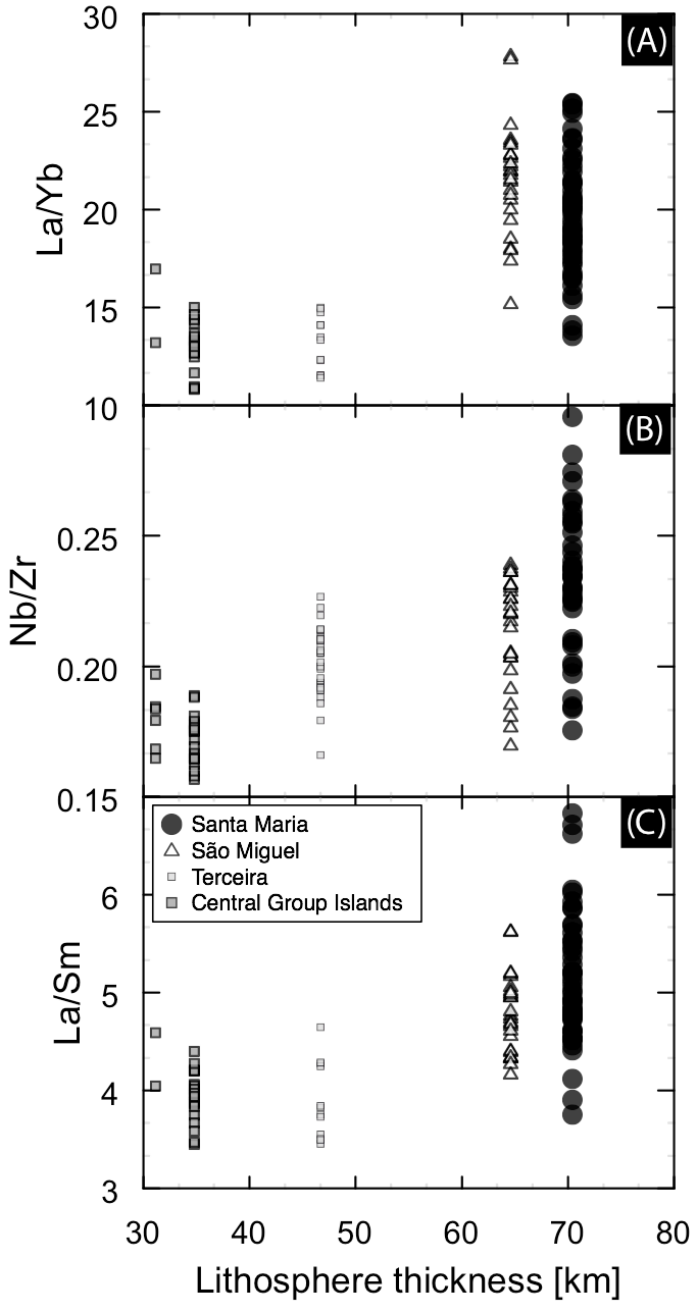

Figure 8. Trace elements of the Azores islands versus lithosphere thickness of the Azores islands. Lithosphere thickness is calculated from lithosphere ages (Cannat, et al. 1999; Luis and Miranda 2008; Searle 1980) using the 1300° isotherm of Stein and Stein (1992).

Figure 8 shows selected trace element ratios against lithosphere thickness. Elemental ratios of La/Yb, Nb/Zr, La/Sm, all increase in absolute value and variability with increasing lithosphere thickness implying that likely depth and degree of partial melting may largely be controlled by lithosphere thickness. A similar correlation has been observed in other mantle plume settings (Beier, et al. 2011). Geodynamic models predict that the increase in lithosphere thickness will limit the extent of partial melting (Ito and Mahoney 2005) and thus magmas will be more enriched in incompatible elements when the overall length of the melting column is shorter (McKenzie and Bickle 1988; Stracke and Bourdon 2009). Underneath old and thick lithosphere (i.e. underneath Santa Maria), the overall extent of melting will be small and compositions will be more enriched than underneath thinner and younger lithosphere (e.g., underneath Faial and Pico) in agreement with Figure 8.

At higher potential temperatures most melting models suggest that the variability and enrichment of melts decreases (Brandl, et al. 2012; Ito and Mahoney 2005; Stracke and Bourdon 2009). However, in the Azores we did not observe a systematic variability of potential temperatures across lithosphere thickness and thus potential temperatures (Fig. 6). Thus, the potential temperatures and source compositions in the Azores imply that melting overall starts at similar depths but that the mean melting pressures calculated indicate that an increasing lithosphere thickness will actually control the total length of the melting column. Finally, this will lead to generally lower degrees of partial melting and a stronger enrichment in trace element signatures observed at Santa Maria and, to a certain extent, at São Miguel (e.g., in Ce/Yb). These effects may be of global significance in most intraplate localities that are situated on old lithosphere.

Summarizing, from isotope signatures we conclude that the mantle sources underneath Santa Maria are similar compared to those erupting today at Faial and Pico islands. Temperatures of melting are comparable to Faial and Pico but at higher pressures and indicate lower extents of partial melting (<3%), explaining why the incompatible elements underneath Santa Maria are more enriched compared to the other islands. However, we find that Rb, TiO_2, K_2O, and SiO_2 are lower underneath Santa Maria (Figs. 2 and 3) which is contradictory with the observations made above. One major source of variability that may influence the conditions of melting and the geochemical signatures is the lithology of the mantle source, which will be discussed below.

6. 5.4 Source lithology and implications for carbonated peridotite melting

A consequence of the oceanic crust being recycled to the mantle is the introduction of mafic eclogitic components into the mantle (Allègre and Turcotte 1986), which may lead to pyroxenite, either by solid-state reaction with the dominant peridotite (Herzberg 2011) or, after melting, through melt reaction with ambient peridotite mantle (Sobolev, et al. 2007). Melting of volatile-free MORB-eclogites or pyroxenites is not able to generate alkali basalts, particularly with respect to their MgO, Mg# and SiO_2 contents (Mallik and Dasgupta 2012). However, recent experiments have shown that such lithologies may indirectly be involved in alkali basalt genesis (Herzberg 2011; Mallik and Dasgupta 2012).

The presence of pyroxenites and/or eclogites in the mantle sources will significantly change the melting dynamics (Ito and Mahoney 2005) and the overall degree of partial melting. Indeed, the melt productivity in pyroxenite and eclogite is higher than that of peridotite (Hirschmann and Stolper 1996; Pertermann and Hirschmann 2003) and this will also affect the trace element compositions and short-lived isotope signatures (Stracke and Bourdon 2009; Stracke, et al. 1999). The presence of a HIMU-type mantle source component in the Azores from ancient recycling of oceanic crust has repeatedly been proposed (Madureira, et al. 2011; Millet, et al. 2009; Moreira, et al. 1999), strongly suggesting the occurrence of mafic lithologies involved during mantle melting. However, uranium series disequilibria for the Azores samples are better explained by melting of an enriched garnet peridotite rather than from eclogites or pyroxenites (Elkins, et al. 2008; Prytulak and Elliott 2009).

An additional test for the presence of pyroxenite/eclogite sources has been proposed using transition elements (Le Roux, et al. 2011; Le Roux, et al. 2010; Lee, et al. 2005). Le Roux, et al. (2010) propose the use of Zn/Fe ratios for discriminating lithologies that diverge from normal peridotite dominated by an olivine/orthopyroxene assemblage. Due to the distinct geochemical behavior of Zn/Fe ratios in the presence of residual olivine/orthopyroxene ($K_{(olv/melt)}^{Zn/Fe} \approx K_{(opx/melt)}^{Zn/Fe} \approx 1$) compared to clinopyroxene/garnet parageneses ($K_{(cpx/melt)}^{Zn/Fe}$ and $K_{(grt/melt)}^{Zn/Fe} < 1$), Zn/Fe ratios of primitive magmas are expected to be identical to the peridotite sources, but are proposed to be significantly higher in those cases where clinopyroxene dominates as residual mineral phase. After applying the correction for the effects of crystal fractionation proposed by Le Roux, et al. (2010) to

those lavas with MgO higher than 8.5 wt.%, Santa Maria lavas have $(Zn/Fe)*10^4$ ratios of 8.8, very close to the average peridotite value of 8.5, but significantly lower than those expected for magmas in equilibrium with pyroxenite/eclogite sources ($(Zn/Fe)*10^4$ >12; (Le Roux, et al. 2011)).

As discussed above, Santa Maria lavas are depleted in SiO_2, TiO_2, Rb and K_2O compared to the other Azores islands. A potential source of depletion of these oxides and elements could be the presence of residual amphibole and/or phlogopite in the mantle (LaTourrette, et al. 1995). Mantle metasomatism involving amphibole has been proposed for a variety of settings to best explain the origin and/or the chemical peculiarities of some alkaline melts in the oceanic environment (Pilet, et al. 2008). However, one particular caveat with this model is the stability fields of those minerals (Class and Goldstein 1997) which is at temperatures <1200°C and pressures of <3.3 GPa clearly below the range of the melting pressures and temperatures observed underneath Santa Maria (see above). Additionally, there is no petrological evidence from mantle xenoliths from any of the Azores islands for amphibole and/or phlogopite (unpublished data), however, there are no detailed published studies of the Azores mantle xenoliths yet available. One additional explanation could be the equilibration with and assimilation of lithospheric lithologies during the ascent of the melt which has also been proposed to be the case at Grande Comore (Class, et al. 1998). In the presence of residual amphibole and/or phlogopite, K becomes less incompatible during melting, given the relatively high K partition coefficients between these minerals and silicate melts (LaTourrette, et al. 1995; Späth, et al. 2001). This leads to a fractionation of the Light Rare Earth Elements (LREE) and K, which is not expected during melting of anhydrous mantle lithologies. Considering the low melting temperatures of amphiboles and phlogopites (Class and Goldstein 1997), they are preferentially consumed during the initial steps of melting. Consequently the K/La or K/Ce ratios will be correlated with elemental signatures sensitive to extent of melting like La/Yb (Mata, et al. 1998; Späth, et al. 2001). For Santa Maria this is clearly not the case (Fig. 9a) thus strongly arguing against the presence of K-bearing minerals as residues of melting.

Recently, an alternative explanation for enriched alkaline melts in ocean islands has been melting of a carbonated peridotite at ≈3 GPa (Dasgupta, et al. 2007; Dasgupta, et al. 2006; Gudfinnsson 2005). The presence of carbonated lithologies in intraplate oceanic environments has been invoked as a source for carbonatite melts (Hoernle, et al.

2002; Mata, et al. 2010; Mourão, et al. 2012) and for CO_2-rich metasomatic agents affecting the lithospheric (Hauri and Hart 1993; Kogarko, et al. 2001; Martins, et al. 2010; Mattielli, et al. 1999) or sub-lithospheric mantle (Dasgupta and Hirschmann 2006). Melts generated from a carbonated peridotite lithology will form at greater depth than volatile-free garnet-peridotite (Dasgupta, et al. 2006) which would explain the deeper melting signatures observed underneath Santa Maria, and is also consistent with the volatile rich nature of the Azores (Asimow, et al. 2004; Beier, et al. 2012). Dasgupta, et al. (2007) performed partial melting experiments on carbonate-bearing natural lherzolite. The compositions of the near-solidus partial melts and associated crystal phases allowed these authors to conclude that the amount of dissolved CO_2 is a very significant factor resulting in increased CaO and diminished SiO_2 in peridotite partial melts, probably due to the suppression of near-liquidus crystallisation of olivine and clinopyroxene with respect to orthopyroxene stabilization (Brey and Green 1977). The Santa Maria lavas (MgO >7 wt.%) have a range of 9.4 to 12.0 wt.% of CaO associated with less than 45 wt.% SiO_2 close to carbonated peridotite experimental partial melts and distinct from partial melts derived from volatile-free peridotite that are characterized by higher SiO_2 and lower CaO contents (Fig. 10).

As mentioned above, previous studies have shown that the Azores lavas are characterized by a large range of isotope ratios, demonstrating that the mantle beneath the archipelago is heterogeneous at various length-scales which may possibly reflect the mantle plume heterogeneity. The depth at which the ascending plume will start to melt will be controlled by its composition and potential temperature. Hypothetical CO_2-rich lithologies dispersed in a volatile-free peridotitic matrix will start melting deep in the upper mantle or even the transition zone producing carbonatite melts, at depths strongly depending on the lithology (Dasgupta, et al. 2007) and oxygen fugacity (Rohrbach and Schmidt 2011; Stagno and Frost 2010). As a result of their high wetting capacity (Hunter and McKenzie 1989), carbonatite melts will be extracted from the source even when the fraction of melting is significantly below 1% (Dasgupta, et al. 2007); i.e. they have a strong capability to percolate in mantle rocks (Hammouda and Laporte 2000), migrating upwards in channels or through porous flow. The migration of these deep carbonatite melts to shallower mantle levels can trigger the generation of alkaline basalts with characteristics similar to those observed at Santa Maria by either mixing with melts from volatile-free (shallower) lithologies, or by reaction with these mantle rocks, lowering

their solidii and imprinting their chemical fingerprint (Dasgupta, et al. 2007). Our model shows that mixing of carbonatites, generated at greater depths and resulting from circa 1% melting of a carbonated mantle, with melts from volatile-free garnet-peridotite lithologies may best explain the geochemical variability in the Santa Maria lavas. Indeed Figure 9 shows that melting of a volatile-free garnet-peridotite cannot solely explain the observed range in terms of K/La and Ti/Sm ratios given that it will hardly fractionate these element pairs. In contrast, the genesis of carbonatite melts from a carbonated peridotite will fractionate K from La and Ti from Sm respectively, producing highly variable K/La and Ti/Sm ratios. The partition coefficients determined/compiled by Dasgupta et al. (2009) for carbonated peridotite/carbonatite pairs show that partition coefficients for Rb/Th are $D_{Rb/Th} \approx 1$ contrasting those reported for lherzolite/basalt ($D_{Rb/Th} << 1$) which explains why Santa Maria magmas have Rb/Th ratios lower than the other Azores islands considered in this study (Fig. 3). In addition, oceanic carbonatites that are associated with mantle melts from the Canary and Cape Verde islands (Hoernle et al., 2002) display a marked negative anomaly of Rb to the same extent than K or Ti which could indicate that Rb is clearly more compatible than Th during the genesis of carbonatites.

Our model proposed here, requires that carbonatites contributed more than 20% of the mixture, reasonably accounting for the geochemical variability of the Santa Maria lavas. If less than 20% carbonatite are present in the final melt, or if degrees of partial melting for the volatile-free peridotite are higher than 4% (in particular for K/La), the carbonate signature will be obscured, being less obvious (Fig. 9). This model can also explain the lower SiO_2 in addition to the lower K_2O and TiO_2 contents of Santa Maria (Figs. 2 and 10). We suggest that the geochemical signatures underneath Santa Maria are the result of melt mixing as opposed to fluid metasomatism. If the geochemical signatures of the carbonated peridotite was added to the volatile-free garnet peridotite by fluid metasomatism prior to melting of the garnet peridotite, the K/La and Ti/Sm ratios will not be fractionated during melting of this metasomatized lithology, i.e. the melting curves will be parallel to those calculated for Figure 9. The Santa Maria melts however, are clearly situated on mixing trajectories between low-degree melts from carbonated and volatile-free peridotite (Fig. 9).

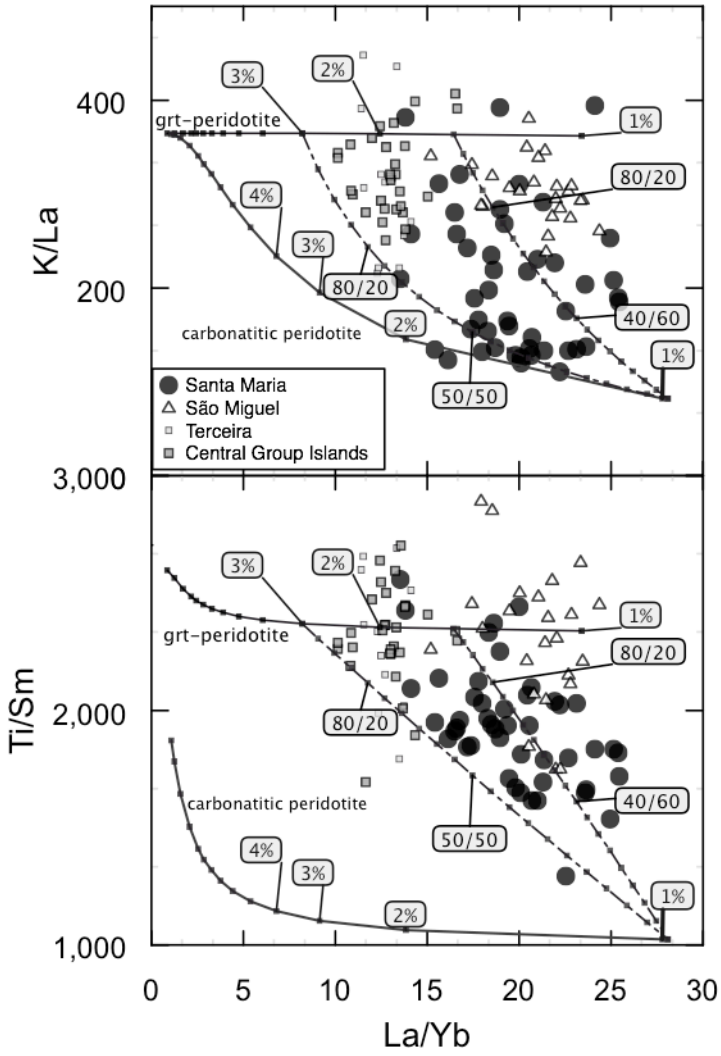

Figure 9. a) K/La and b) Ti/Sm ratios versus La/Yb ratios of the Azores lavas. Melting models are calculated for fractional melting of volatile-free garnet peridotite (55% Ol, 25% Opx, 12% Cpx and 8% Grt, melting modes 5% Ol, 5% Opx, 45% Cpx and 45% Grt) and carbonated peridotite (Dasgupta, et al. 2006)(61% Ol, 9% Opx, 18% Cpx and 12% Grt with melting modes of 5% Ol, 5% Opx, 45% Cpx and 45% Grt). Partition coefficients for garnet peridotite melting are those used in Figure 7 by Halliday, et al. (1995) and Blundy, et al. (1998) in addition to those by Philpotts and Schnetzler (1970) for K in olivine, Kelemen and Dunn (1992) for K in Opx and Grt and from Hart and Dunn (1993) for K in Cpx. Partition coefficients for carbonated peridotite are from Dasgupta, et al. (2009). K partition coefficents in carbonated peridotite are from Sweeney, et al. (1992) for Grt, from Blundy and Dalton (2000) for Cpx. In the absence of K-partition coefficients for Ol and Opx we assume K to behave entirely incompatibly with a partition coefficient of 0. Mixing curves are mixing of 3% and 1.5% grt-peridotite melt with 1% carbonated peridotite, respectively. Most lavas from Santa Maria require more than 20% of a 1% melt from carbonated peridotite in their source.

Summarizing we can show that mixing of variable portions of deep small degree carbonatitic melts and shallower melts from volatile-free garnet-peridotite may best explain the geochemical variability underneath Santa Maria.. This can best explain the

enrichment and variability in incompatible element ratios (e.g. La/Yb and Nb/Zr) by melt extraction of small degree melts but also accounts for the lower K/La and Ti/Sm ratios as well as lower SiO_2 contents of the Santa Maria lavas.

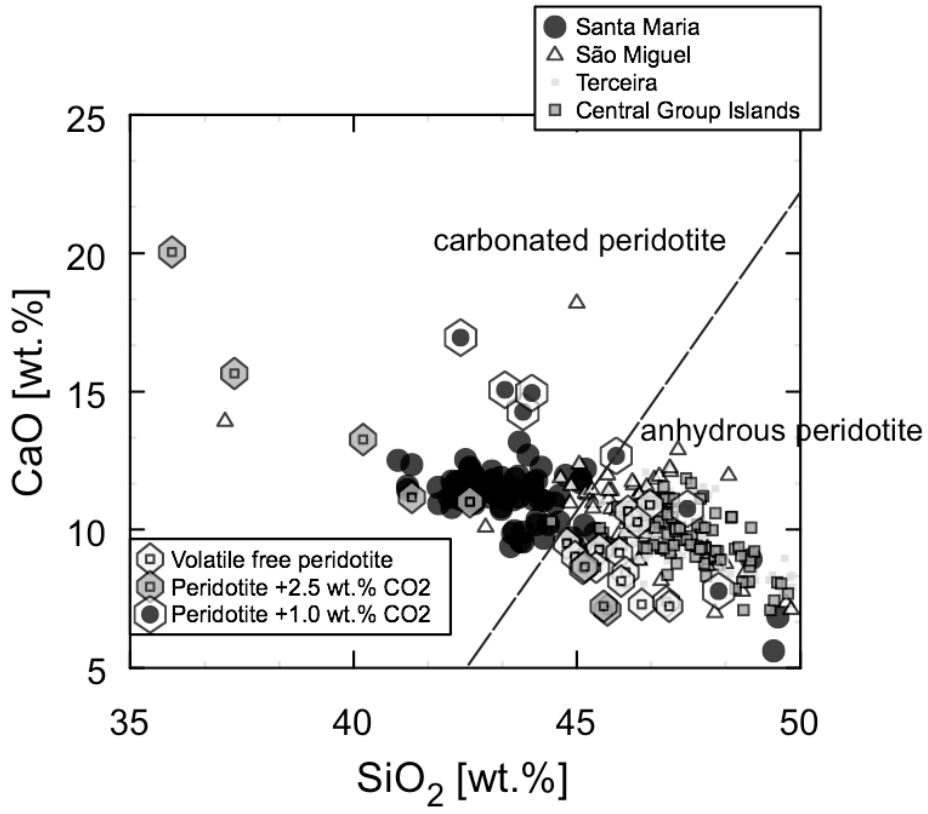

Figure 10. SiO_2 vs. CaO contents of the Santa Maria lavas, along with carbonate-bearing silicate partial melts from carbonated peridotite partial melting experiments at 3 GPa (Dasgupta, et al. 2007) and experimental partial melts from volatile free peridotite from 3 to 7 GPa (Walter 1998). The black line represents an approximate limit that separates CO_2-enriched and CO_2-deficient melts (Herzberg and Asimow 2008).

Hofmann, et al. (2011) suggested that, due to its low viscosity and density, carbonatite melts tend to move upwards vertically, being displaced from the plume center particularly in the case of a tilted plume. P-wave velocity modeling of the Azores region suggest that the plume conduit is deflected to the southwest in the shallow mantle by asthenospheric flow (Yang, et al. 2006). This could provide an explanation for the fact that in the Azores, the geochemical evidence for a contribution of melts from carbonated peridotite is restricted to Santa Maria which is located at the edge of the Azores Plateau and thus presumably formed at the most distant position relatively to the mantle plume. For the Azores, Silveira, et al. (2010) described a significant reduction of the S-wave velocity at depths between 460 and 500 km, which can be interpreted as resulting from

ponding of the upwelling plume at the transition zone or, alternatively, from deep mantle redox melting of carbon-rich heterogeneities (Dasgupta and Hirschmann 2006; Dasgupta, et al. 2006; Rohrbach and Schmidt 2011). Interestingly, as also noted by Silveira, et al. (2010), such low velocities zones at the transition zone have also been described beneath other oceanic hotspots. If carbonatite melts are responsible for such seismic anomalies, this implies that the association of such magmas with oceanic hotspots is more common than can be inferred from the rare occurrence of carbonatites that are actually erupted. Our data on Santa Maria reinforce this idea, in agreement with evidences for carbonate metasomatism gathered from xenoliths carried to the surface by oceanic magmas (Kogarko, et al. 2001; Martins, et al. 2010; Mattielli, et al. 1999).

6. 6. CONCLUSIONS

The Azores archipelago provides a type example of a low buoyancy flux plume where the overall age range of the islands is small compared to the age range of the lithosphere these seamounts were erupted on. Lithosphere ages increase from west to east from ~10 Ma to ~45 Ma with increasing distance from the MAR and thus with an increase of lithosphere thickness. The source compositions inferred from Sr-Nd-Pb isotope ratios imply that the mantle source of the easternmost island Santa Maria is almost similar to that of islands erupted closer to the MAR and does not display evidence for similarities to the peculiar source composition of the neighboring island São Miguel. The greater enrichment and variability of incompatible trace element ratios may best be explained by melt extraction at small degrees of partial melting preserving the heterogeneous nature of the mantle below Santa Maria. In addition, a larger (> 20%) contribution of small degree melts (carbonatites) of carbonated mantle may explain the lower K2O, TiO2, Rb and SiO2 contents of Santa Maria magmas. The preservation of these unique signatures from the CO2 bearing mantle lithologies during magma genesis probably reflect the combined effect of a limited length of the melt column underneath thick lithosphere with small degrees of melting and of the Santa Maria off-axis positioning relatively to the tilted (volatile-rich) plume. Our data also suggest that the association of CO2-rich peridotite melts with oceanic hotspots may be more common than usually thought.

ACKNOWLEDGEMENTS

We acknowledge help by D. Garbe-Schönberg and U. Westernströer during the trace element analyses in Kiel. Stephan Klemme is acknowledged for his patient and quick

help with partition coefficients. This study was funded by a grant of the German Science Foundation (BE4459/1-1) and by Fundação para a Ciência e Tecnologia (Portugal) through the projects EVOLV (PTDC/CTE-GIN/71838/2006), Pest-OE/CTE/UI0263/2011 and Pest-OE/CTE/LA0019/201. We also thank J. Habermann and J. Titschack for help during work in the field. We acknowledge the help of V.-H. Forjaz and the Azores Volcanological and Geothermal Observatory during various stays in the Azores and ChB thanks Andreas Stracke and Stephan Klemme for an entertaining field trip. We also acknowledge the help of A. Mohammadi for providing enough well roasted coffee to stand the test of writing this paper in a relatively short time.

REFERENCES

Abdel Monem AA, Fernandez LA, Boone GM (1975) K-Ar-Ages from the eastern Azores group (Santa Maria, Sao Miguel and the Formigas islands). Lithos 8:247-254.

Abouchami W, Galer SJG, Hofmann AW (2000) High precision lead isotope systematics of lavas from the Hawaiian Scientific Drilling Project. Chem. Geol. 169:187-209.

Allègre CJ, Turcotte DL (1986) Implications of a two component marble-cake mantle. Nature 323:123-127.

Anderson MC, Flower MFJ (1982) Petrology and geochemistry of lavas from Santa Maria, Azores; a preliminary study of mantle heterogeneity. 16th annual meeting; North-Central Section, Geological Society of America 14(5):153.

Asimow PD, Dixon JE, Langmuir CH (2004) A hydrous melting and fractionation model for mid-ocean ridge basalts: Application to the Mid-Atlantic Ridge near the Azores. Geochem. Geophys. Geosyst. 5(1):Q01E16. doi:10.1029/2003GC000568.

Beier C, Haase KM, Abouchami W, Krienitz M-S, Hauff F (2008) Magma genesis by rifting of oceanic lithosphere above anomalous mantle: Terceira Rift, Azores. Geochem. Geophys. Geosyst. 9(12):Q12013. doi:10.1029/2008GC002112.

Beier C, Haase KM, Hansteen TH (2006) Magma evolution of the Sete Cidades volcano, São Miguel, Azores. J. Pet. 47(7):1375-1411. doi:10.1093/petrology/egl014.

Beier C, Haase KM, Turner SP (2012) Conditions of melting beneath the Azores. Lithos 144-145:1-12. doi:10.1016/j.lithos.2012.02.019.

Beier C, Stracke A, Haase KM (2007) The peculiar geochemical signatures of São Miguel lavas: metasomatised or recycled mantle sources? Earth. Planet. Sc. Lett. 259(1-2):186-199. doi:10.1016/j.epsl.2007.04.038.

Beier C, Turner SP, Plank T, White W (2010) A preliminary assessment of the symmetry of source composition and melting dynamics across the Azores plume Geochem. Geophys. Geosyst. 11 (1):Q02004. doi:10.1029/2009GC002833.

Beier C, Vanderkluysen L, Regelous M, Mahoney JJ, Garbe-Schönberg D (2011) Lithospheric control on geochemical composition along the Louisville Seamount

Chain. Geochem. Geophys. Geosyst. 12:Q0AM01. doi:10.1029/2011gc003690.

Blundy J, Dalton J (2000) Experimental comparison of trace element partitioning between clinopyroxene and melt in carbonate and silicate systems, and implications for mantle metasomatism. Contrib. Mineral. Petr. 139:356-371.

Blundy JD, Robinson JAC, Wood BJ (1998) Heavy REE are compatible in clinopyroxene on the spinel lherzolite solidus. Earth. Planet. Sc. Lett. 160(3-4):493-504.

Bourdon B, Langmuir CH, Zindler A (1996) Ridge-hotspot interaction along the Mid-Atlantic Ridge between 37°30' and 40°30'N: the U-Th disequilibrium evidence. Earth. Planet. Sc. Lett. 142:175-189.

Bourdon B, Turner SP, Ribe NM (2005) Partial melting and upwelling rates beneath the Azores from U-series isotope perspective. Earth. Planet. Sc. Lett. 239(1-2):42-56. doi:10.1016/j.epsl.2005.08.008.

Brandl PA, Beier C, Regelous M, Abouchami W, Haase KM, Garbe-Schönberg D, Galer SJG (2012) Volcanism on the flanks of the East Pacific Rise: Quantitative constraints on mantle heterogeneity and melting processes. Chem. Geol. 289-299(3-4):41-56. doi:10.1016/j.chemgeo.2011.12.015.

Brey G, Green DH (1977) Systematic study of liquidus phase relations in olivine melilitite + H2O + CO2 at high pressures and petrogenesis of an olivine melilitite magma. Contrib. Mineral. Petr. 61(2):141-162. doi:10.1007/BF00374364.

Cannat M, Briais A, Deplus C, Escartín J, Georgen J, Lin J, Mercouriev S, Meyzen C, Muller M, Pouliquen G, Rabain A, Silva Pd (1999) Mid-Atlantic Ridge - Azores hotspot interactions: along-axis migration of a hotspot-derived event of enhanced magmatism 10 to 4 Ma ago. Earth. Planet. Sc. Lett. 173:257-269.

Class C, Goldstein SL (1997) Plume-lithosphere interactions in the ocean basins: constraints from the source mineralogy. Earth. Planet. Sc. Lett. 150:245-260.

Class C, Goldstein SL, Altherr R, Bachèlery P (1998) The Process of Plume-Lithosphere Interactions in the Ocean Basins-the Case of Grande Comore. J. Pet. 39(5):881-903.

Courtier AM, Jackson MG, Lawrence JF, Wang Z, Lee C-TA, Halama R, Warren JM,

Workman R, Xu W, Hirschmann MM, Larson AM, Hart SR, Lithgow-Bertelloni C, Stixrude L, Chen W-P (2007) Correlation of seismic and petrologic thermometers suggests deep thermal anomalies beneath hotspots. Earth. Planet. Sc. Lett. 264(1-2):308-316. doi:10.1016/j.epsl.2007.10.003.

Courtillot V, Davaille A, Besse J, Stock J (2003) Three distinct types of hotspots in the Earth´s mantle. Earth. Planet. Sc. Lett. 205:295-308.

Dasgupta R, Hirschmann MM (2006) Melting in the Earth's deep upper mantle caused by carbon dioxide. Nature 440:659-662. doi:10.1038/nature04612.

Dasgupta R, Hirschmann MM, McDonough WF, Spiegelman M, Withers AC (2009) Trace element partitioning between garnet lherzolite and carbonatite at 6.6 and 8.6 GPa with applications to the geochemistry of the mantle and of mantle-derived melts. Chem. Geol. 262(1-2):57-77. doi:10.1016/j.chemgeo.2009.02.004.

Dasgupta R, Hirschmann MM, Smith ND (2007) Partial Melting Experiments of Peridotite + CO2 at 3 GPa and Genesis of Alkalic Ocean Island Basalts. J. Pet. 48(11):2093-2124. doi:10.1093/petrology/egm053.

Dasgupta R, Hirschmann MM, Stalker K (2006) Immiscible Transition from Carbonate-rich to Silicate-rich Melts in the 3 GPa Melting Interval of Eclogite + CO2 and Genesis of Silica-undersaturated Ocean Island Lavas. J. Pet. 47(4):647-671. doi:10.1093/petrology/egi088.

Davies GF (1988) Ocean bathymetry and mantle convection; 1. Large-scale flow and hotspots. J. Geophys. Res. B93(9):10,467-410,480.

Dupré B, Allègre CJ (1983) Pb-Sr isotope variation in Indian Ocean basalts and mixing phenomena. Nature 303(5913):142-146.

Elkins LJ, Gaetani GA, Sims KWW (2008) Partitioning of U and Th during garnet pyroxenite partial melting: Constraints on the source of alkaline ocean island basalts. Earth. Planet. Sc. Lett. 265(1-2):270-286. doi:10.1016/j.epsl.2007.10.034.

Elliott T, Blichert-Toft J, Heumann A, Koetsier G, Forjaz V (2007) The origin of enriched mantle beneath Sao Miguel, Azores. Geochim. Cosmochim. Acta 71(1):219-240. doi:10.1016/j.gca.2006.07.043.

Escartín J, Cannat M, Pouliquen G, Rabain A (2001) Crustal thickness of V-shaped ridges south of the Azores: Interaction of the Mid-Atlantic Ridge (36°-39°N) and the Azores hot spot. J. Geophys. Res. 106(10):21,719 - 721,735.

Esenwein P (1929) Zur Petrographie der Azoren. Zeitschrift für Vulkanologie 3(12):128-227.

Féraud G, Kaneoka I, Allègre CJ (1980) K/Ar Ages and Stress Pattern in the Azores: Geodynamic Implications. Earth. Planet. Sc. Lett. 46:275-286.

Féraud G, Schmincke H-U, Lietz J, Gastaud J, Pritchard G, Bleil U (1981) New K-Ar ages, chemical analyses and magnetic data of rocks from the islands of Santa Maria (Azores), Porto Santo and Madeira (Madeira Archipelago) and Gran Canaria (Canary Islands). Bull. Volcanol. 44:359-375.

Fernandes RMS, Bastos L, Miranda JM, Lourenco N, Ambrosius BAC, Noomen R, Simons W (2006) Defining the plate boundaries in the Azores region. J. Volcanol. Geotherm. Res. 156(1-2):1-9. doi:10.1016/j.jvolgeores.2006.03.019.

Galer SJG, Abouchami W (1998) Practical application of lead triple spiking for correction of instrumental mass discrimination. Mineral. Mag. 62A:491-492.

Garbe-Schönberg C-D (1993) Simultaneous determination of thirty-seven trace elements in twenty-eight international rock standards by ICP-MS. Geostandards Newsletters 17:81-97.

Gente P, Dyment J, Maia M, Goslin J (2003) Interaction between the Mid-Atlantic Ridge and the Azores hotspot during the last 85 Myr: Emplacement and rifting of the hot spot-derived plateaus. Geochem. Geophys. Geosyst. 4(10):Q8514. doi:10.1029/2003GC000527.

Govindaraju K (1994) 1994 Compilation of working values and sample description for 383 geostandard. Geostandard. Newslett. 18(Special Issue):331-331.

Grose CJ (2012) Properties of oceanic lithosphere Revised plate cooling model predictions. Earth. Planet. Sc. Lett. 333-334:250-264. doi:10.1016/j.epsl.2012.03.037.

Gudfinnsson GH (2005) Continuous Gradations among Primary Carbonatitic, Kimberlitic, Melilititic, Basaltic, Picritic, and Komatiitic Melts in Equilibrium with Garnet Lherzolite at 3-8 GPa. J. Pet. 46(8):1645-1659. doi:10.1093/petrology/egi029.

Haase KM (1996) The relationship between the age of the lithosphere and the composition of oceanic magmas: Constraints on partial melting, mantle sources and the thermal structure of the plates. Earth. Planet. Sc. Lett. 144:75-92.

Haase KM, Beier C (2003) Tectonic control of ocean island basalt sources on Sao Miguel, Azores? Geophys. Res. Lett. 30(16):1856. doi:10.1029/2003GL017500.

Halliday AN, Lee D-C, Tommasini S, Davies GR, Paslick CR, Fitton JG, James DE (1995) Incompatible trace elements in OIB and MORB and source enrichment in the sub-oceanic mantle. Earth. Planet. Sc. Lett. 133:379-395.

Hammouda T, Laporte D (2000) Ultrafast mantle impregnation by carbonatite melts. Geology 28(3):283-285. doi:10.1130/0091-7613(2000)28<283:UMIBCM>2.0.CO;2.

Hart SR, Dunn T (1993) Experimental cpx/melt partitioning of 24 trace elements. Contrib. Mineral. Petr. 113:1-8.

Hart SR, Hauri EH, Oschmann LA, Whitehead JA (1992) Mantle plumes and entrainment; isotopic evidence. Science 256(5056):517-520.

Hauri EH, Hart SR (1993) Re-Os isotope systematics of HIMU and EMII oceanic island basalts from the South Pacific Ocean. Earth. Planet. Sc. Lett. 114(2-3):353-371.

Herzberg C (2011) Geodynamic Information in Peridotite Petrology. J. Pet. 45(12):2507-2530. doi:10.1093/petrology/egh039.

Herzberg C, Asimow PD (2008) Petrology of some oceanic island basalts: PRIMELT2.XLS software for primary magma calculation. Geochem. Geophys. Geosyst. 9(Q09001) doi:10.1029/2008GC002057.

Hirschmann MM, Stolper EM (1996) A possible role for garnet pyroxenite in the origin of the "garnet signature" in MORB. Contrib. Mineral. Petr. 124(2):185-208.

Hoernle K, Tilton G, Le Bas MJ, Duggen S, Garbe-Schönberg D (2002) Geochemistry of oceanic carbonatites compared with continental carbonatites: mantle recycling of

oceanic crustal carbonate. Contrib. Mineral. Petr. 142:520-542. doi:10.1007/s004100100308.

Hofmann AW (1997) Mantle geochemistry: the message from oceanic volcanism. Nature 385:219-229.

Hofmann AW (2003) Sampling mantle heterogeneity through oceanic basalts: isotopes and trace elements. In: Carlson RW (ed) Treatise on Geochemistry, vol 2. The Mantle and Core. Elsevier, Amsterdam, pp 61-101

Hofmann AW, Farnetani CG, Spiegelman M, Class C (2011) Displaced helium and carbon in the Hawaiian plume. Earth. Planet. Sc. Lett. 312(1-2):226-236. doi:10.1016/j.epsl.2011.09.041.

Humphreys ER, Niu Y (2009) On the composition of ocean island basalts (OIB): The effects of lithospheric thickness variation and mantle metasomatism. Lithos 112(1-2):118-136. doi:10.1016/j.lithos.2009.04.038.

Hunter RH, McKenzie D (1989) The equilibrium geometry of carbonate melts in rocks of mantle composition. Earth. Planet. Sc. Lett. 92:347-356.

Ito G, Mahoney JJ (2005) Flow and melting of a heterogeneous mantle: 1. Method and importance to the geochemistry of ocean island and mid-ocean ridge basalts. Earth. Planet. Sc. Lett. 230:29-46. doi:10.1016/j.epsl.2004.10.035.

Jean-Baptiste P, Allard P, Coutinho R, Ferreira T, Fourré E, Queiroz G, Gaspar JL (2009) Helium isotopes in hydrothermal volcanic fluids of the Azores archipelago. Earth. Planet. Sc. Lett. 281(1-2):70-80. doi:10.1016/j.epsl.2009.02.009.

Johnson CL, Wijbrans JR, Constable CG, Gee J, Staudigel H, Tauxe L, Forjaz V-H, Salgueiro M (1998) 40Ar/39Ar ages and paleomagnetism of Sao Miguel lavas, Azores. Earth. Planet. Sc. Lett. 116(3-4):637-649.

Kelemen PB, Dunn JT (1992) Depletion of Nb relative to other highly incompatible elements by melt/rock reaction in the upper mantle. EOS, Transactions, AGU 73:656-657.

Kogarko L, Kurat G, Ntaflos T (2001) Carbonate metasomatism of the oceanic mantle

beneath Fernando de Noronha Island, Brazil. Contrib. Mineral. Petr. 140:577-587. doi:10.1007/s004100000201.

LaTourrette T, Hervig RL, Holloway JR (1995) Trace element partitioning between amphibole, phlogopite, and basanite melt. Earth. Planet. Sc. Lett. 135(1-4):13-30.

Le Roux V, Dasgupta R, Lee C-TA (2011) Mineralogical heterogeneities in the Earth's mantle: Constraints from Mn, Co, Ni and Zn partitioning during partial melting. Earth. Planet. Sc. Lett. 307(3-4):395-408. doi:10.1016/j.epsl.2011.05.014.

Le Roux V, Lee CTA, Turner SJ (2010) Zn/Fe systematics in mafic and ultramafic systems: Implications for detecting major element heterogeneities in the Earth's mantle. Geochim. Cosmochim. Acta 74(9):2779-2796. doi:10.1016/j.gca.2010.02.004.

Lee C-T, Leeman WP, Canil D, A Li Z-X (2005) Similar V/Sc systematics in MORB and Arc basalts: implications for the oxygen fugacities of their mantle source regions. J. Pet. 46(11):2313-2336. doi:10.1093/petrology/egi056.

Lee C-TA, Luffi P, Plank T, Dalton H, Leeman WP (2009) Constraints on the depths and temperatures of basaltic magma generation on Earth and other terrestrial planets using new thermobarometers for mafic magmas. Earth. Planet. Sc. Lett. 279(1-2):20-33. doi:10.1016/j.epsl.2008.12.020.

Luis J, Miranda J (2008) Reevaluation of magnetic chrons in the North Atlantic between 35°N and 47°N: Implications for the formation of the Azores Triple Junction and associated plateau. J. Geophys. Res. 113:B10105. doi:10.1029/2007JB00557.

Lyubetskaya T, Korenaga J (2007) Chemical composition of Earth's primitive mantle and its variance: 1. Method and results. J. Geophys. Res. 112:B03211. doi:10.1029/2005JB004223.

Madeira P, Kroh A, de Frias Martin AM, Ávila SP (2007) The marine fossils on Santa Maria island: an historical overview. Acoreana 5:59-73.

Madureira P, Mata J, Mattielli N, Queiroz G, Silva P (2011) Mantle source heterogeneity, magma generation and magmatic evolution at Terceira Island (Azores archipelago): Constraints from elemental and isotopic (Sr, Nd, Hf, and Pb) data. Lithos 126:402-

418. doi:10.1016/j.lithos.2011.07.002.

Madureira P, Moreira M, Mata J, Allègre C-J (2005) Primitive neon isotopes in Terceira Island (Azores archipelago). Earth. Planet. Sc. Lett. 233:429-440. doi:10.1016/j.epsl.2005.02.030.

Mallik A, Dasgupta R (2012) Reaction between MORB-eclogite derived melts and fertile peridotite and generation of ocean island basalts. Earth. Planet. Sc. Lett. 329-330:97-108. doi:10.1016/j.epsl.2012.02.007.

Martins S, Mata J, Munhá J, Mendes M, Maerschalk C, Caldeira R, Mattielli N (2010) Chemical and mineralogical evidence of the occurrence of mantle metasomatism by carbonate-rich melts in an oceanic environment (Santiago Island, Cape Verde). Mineralogy and Petrology 99:43-65. doi:10.1007/s00710-009-0078-x.

Mata J, Kerrich R, MacRae ND, Wu C (1998) Elemental and isotopic (Sr, Nd, and Pb) characteristics of Madeira Island basalts: evidence for a composite HIMU - EM I plume fertilizing lithosphere. Canadian Journal of Earth Sciences 35(9):980-997.

Mata J, Moreira M, Doucelance R, Ader M, Silva LC (2010) Noble gas and carbon isotopic signatures of Cape Verde oceanic carbonatites: Implications for carbon provenance. Earth. Planet. Sc. Lett. 291(1-4):70-83. doi:10.1016/j.epsl.2009.12.052.

Mattielli N, Weis D, Scoates JS, Shimizu N, Gregoire M, Mennessier JP, Cottin JY, Giret A (1999) Evolution of Heterogeneous Lithospheric Mantle in a Plume Environment Beneath the Kerguelen Archipelago. J. Pet. 40(11):1721-1744. doi:10.1093/petroj/40.11.1721.

McKenzie D, Bickle MJ (1988) The volume and composition of melt generated by extension of the lithosphere. J. Pet. 29(3):625-679.

McKenzie DAN, O'Nions RK (1995) The Source Regions of Ocean Island Basalts. J. Pet. 36(1):133-159. doi:10.1093/petrology/36.1.133.

Millet M-A, Doucelance R, Baker JA, Schiano P (2009) Reconsidering the origins of isotopic variations in Ocean Island Basalts: Insights from fine-scale study of São Jorge Island, Azores archipelago. Chem. Geol. 265(3-4):289-302. doi:10.1016/j.chemgeo.2009.04.005.

Montelli R, Nolet G, Dahlen FA, Masters G, Engdahl ER, Hung SH (2004) Finite-frequency tomography reveals a variety of plumes in the mantle. Science 303(5656):338-343.

Moreira M, Doucelance R, Kurz MD, Dupre B, Allegre CJ (1999) Helium and lead isotope geochemistry of the Azores Archipelago. Earth. Planet. Sc. Lett. 169(1-2):189-205.

Mourão C, Moreira M, Mata J, Raquin A, Madeira J (2012) Primary and secondary processes constraining the noble gas isotopic signatures of carbonatites and silicate rocks from Brava Island: evidence for a lower mantle origin of the Cape Verde plume. Contrib. Mineral. Petr. 163:995-1009. doi:10.1007/s00410-011-0711-7.

Nowell GM, Kempton PD, Noble SR, Fitton JG, Saunders AD, Mahoney JJ, Taylor RN (1998) High precision Hf isotope measurements of MORB and OIB by thermal ionisation mass spectrometry; insights into the depleted mantle. Chem. Geol. 149(3-4):211-233.

Pertermann M, Hirschmann MM (2003) Partial melting experiments on a MORB-like pyroxenite between 2 and 3 GPa: Constraints on the presence of a pyroxenite in basalt source regions from solidus location and melting rate. J. Geophys. Res. 108(B2):2125. doi:10.1029/2000JB000118.

Pfänder JA, Münker C, Stracke A, Mezger K (2007) Nb/Ta and Zr/Hf in ocean island basalts -- Implications for crust-mantle differentiation and the fate of Niobium. Earth. Planet. Sc. Lett. 254(1-2):158-172. doi:10.1016/j.epsl.2006.11.027.

Philpotts JA, Schnetzler CC (1970) Phenocryst-matrix partition coefficients for K, Rb, Sr and Ba, with applications to anorthosite and basalt genesis. Geochim. Cosmochim. Acta 34(3):307-322.

Pilet S, Baker M, Stolper E (2008) Metasomatized Lithosphere and the Origin of Alkaline Lavas. Science 320(5878):916-919. doi:10.1126/science.1156563.

Prytulak J, Elliott T (2009) Determining melt productivity of mantle sources from 238U-230Th and 235U-231Pa disequilibria; an example from Pico Island, Azores. Geochim. Cosmochim. Acta 73(7):2103-2122. doi:10.1016/j.gca.2009.01.001.

Putirka K (2008) Excess temperatures at ocean islands: Implications for mantle layering and convection. Geology 36(4):283-286. doi:10.1130/G24615A.1.

Regelous M, Hofmann AW, Abouchami W, Galer SJG (2003) Geochemistry of Lavas from the Emperor Seamounts, and the Geochemical Evolution of Hawaiian Magmatism from 85 to 42 Ma. J. Pet. 44(1):113-140. doi:10.1093/petrology/44.1.113.

Ritsema J, Allen RM (2003) The elusive mantle plume. Earth. Planet. Sc. Lett. 207:1-12. doi:10.1016/S0012-821X(02)01093-2.

Rohrbach A, Schmidt MW (2011) Redox freezing and melting in the Earth's deep mantle resulting from carbon-iron redox coupling. Nature 472(7342):209-212. doi:10.1038/nature09899.

Salters VJM, White WM (1998) Hf isotope constraints on mantle evolution. Chem. Geol. 145(3-4):447-460.

Schaefer BF, Turner S, Parkinson I, Rogers N, Hawkesworth C (2002) Evidence for recycled Archaean oceanic mantle lithosphere in the Azores plume. Nature 420:304-307.

Schilling J-G (1975) Azores mantle blob: rare-earth evidence. Earth. Planet. Sc. Lett. 25:103-115.

Schmincke H-U (1973) Magmatic Evolution and Tectonic Regime in the Canary, Madeira, and Azores Island Groups. Geological Society of America Bulletin. 84:633-648.

Searle RC (1980) Tectonic pattern of the Azores spreading center and triple junction. Earth. Planet. Sc. Lett. 51:415-434.

Silveira G, Vinnik L, Stutzmann E, Farra V, Kiselev S, Morais I (2010) Stratification of the Earth beneath the Azores from P and S receiver functions. Earth. Planet. Sc. Lett. 299(1-2):91-103. doi:10.1016/j.epsl.2010.08.021.

Sleep NH (1990) Hotspots and mantle plumes; some phenomenology. J. Geophys. Res. 95(B5):6715-6736.

Sobolev AV, Hofmann AW, Kuzmin DV, Yaxley GM, Arndt NT, Chung S-L, Danyushevsky LV, Elliott T, Frey FA, Garcia MO, Gurenko AA, Kamenetsky VS, Kerr AC, Krivolutskaya NA, Matvienkov VV, Nikogosian IK, Rocholl A, Sigurdsson IA, Sushchevskaya NM, Teklay M (2007) The Amount of Recycled Crust in Sources of Mantle-Derived Melts. Science 316(5823):412-417. doi:10.1126/science.1138113.

Sobolev AV, Hofmann AW, Sobolev SV, Nikogosian IK (2005) An olivine-free mantle source of Hawaiian shield basalts. Nature 434:590-597.

Späth A, le Roex AP, Opiyo-Akech N (2001) Plume-Lithosphere Interaction and the Origin of Continental Rift-related Alkaline Volcanism--the Chyulu Hills Volcanic Province, Southern Kenya. J. Pet. 42(4):765-787. doi:10.1093/petrology/42.4.765.

Stagno V, Frost D (2010) Carbon speciation in the asthenosphere: Experimental measurements of the redox conditions at which carbonate-bearing melts coexist with graphite or diamond in peridotite assemblages. Earth. Planet. Sc. Lett. 300:72-84. doi:10.1016/j.epsl.2010.09.038.

Stein CA, Stein S (1992) A model for the global variation in oceanic depth and heat flow with lithospheric age. Nature 359(6391):123-129.

Stracke A, Bizimis M, Salters VJM (2003) Recycling oceanic crust: Quantitative constraints. Geochem. Geophys. Geosyst. 4(3):Q8003. doi:10.1029/2001GC000223.

Stracke A, Bourdon B (2009) The importance of melt extraction for tracing mantle heterogeneity. Geochim. Cosmochim. Acta 73(1):218-238. doi:10.1016/j.gca.2008.10.015.

Stracke A, Hofmann AW, Hart SR (2005) FOZO, HIMU and the rest of the mantle zoo. Geochem. Geophys. Geosyst. 6:Q05007. doi:10.1029/2004GC000824.

Stracke A, Salters VJM, Sims KWW (1999) Assessing the presence of garnet-pyroxenite in the mantle sources of basalts through combined hafnium-neodymium-thorium isotope systematics. Geochem. Geophys. Geosyst. 1:1-15. doi:10.1029/1999GC000013.

Sweeney RJ, Green DH, Sie SH (1992) Trace and minor element partitioning between

garnet and amphibole and carbonatitic melt. Earth. Planet. Sc. Lett. 113(1-2):1-14.

Turner S, Hawkesworth C, Rogers N, King P (1997) U-Th isotope disequilibria and ocean island basalt generation in the Azores. Chem. Geol. 139(1-4):145-164.

Vogt PR, Jung WY (2004) The Terceira Rift as hyper-slow, hotspot-dominated oblique spreading axis: A comparison with other slow-spreading plate boundaries. Earth. Planet. Sc. Lett. 218:77-90. doi:10.1016/S0012-821X(03)00627-7.

Walter MJ (1998) Melting of garnet peridotite and the origin of komatiite and depleted lithosphere. J. Pet. 39(1):29-60.

Weis D, Frey FA (1996) Role of the Kerguelen Plume in generating the eastern Indian Ocean seafloor. J. Geophys. Res. 101(B6):13831-13849. doi:10.1029/96JB00410.

Weis D, Kieffer B, Maerschalk C, Barling J, de Jong J, Williams GA, Hanano D, Pretorius W, Mattielli N, Scoates JS, Goolaerts A, Friedman RM, Mahoney JB (2006) High-precision isotopic characterization of USGS reference materials by TIMS and MC-ICP-MS. Geochem. Geophys. Geosyst. 7(8):Q08006. doi:10.1029/2006GC001283.

Wessel P, Smith WHF (1991) Free software helps map and display data. EOS 72:441.

Wessel P, Smith WHF (1998) New, improved version of the Generic Mapping Tools released. EOS 79:579.

White R, McKenzie D, O'Nions R (1992) Oceanic Crustal Thickness From Seismic Measurements and Rare-Earth Element Inversions. J. Geophys. Res. 97(B13):19683-19715.

White WM, Hart SR, Schilling JG (1975) Geochemistry of the Azores and the Mid-Atlantic Ridge; 29°N to 60°N. Year Book - Carnegie Institution of Washington 74:224-234.

White WM, Hofmann AW (1982) Sr and Nd isotope geochemistry of oceanic basalts and mantle evolution. Nature 296:821-825.

White WM, Tapia MDM, Schilling J-G (1979) The Petrology and Geochemistry of the Azores Islands. Contrib. Mineral. Petr. 69:201-213.

Widom E, Carlson RW, Gill JB, Schmincke HU (1997) Th-Sr-Nd-Pb isotope and trace element evidence for the origin of the Sao Miguel, Azores, enriched mantle source. Chem. Geol. 140(1-2):49-68.

Yang T, Shen Y, van der Lee S, Solomon SC, Hung S-H (2006) Upper mantle structure beneath the Azores hotspot from finite-frequency seismic tomography. Earth. Planet. Sc. Lett. 250(1-2):11-26. doi:10.1016/j.epsl.2006.07.031.

Zindler A, Hart S (1986) Chemical Geodynamics. Annu Rev Earth Pl Sc 14:493-571.

CHAPTER 7: SUMMARY AND OUTLOOK

This thesis was designed primarily to collect new samples from the two remote western Azores islands, Flores and Corvo, and to subsequently analyse these for the geochemical composition, including novel isotope systems. These oceanic islands are part of the Azores archipelago, but are the only two emerging volcanoes west of the MAR. Most of the previous literature concerning the evolution of the Azores islands focused on the seven eastern islands. Thus, the main conclusions regarding the origin of the mantle plume feeding the volcanism of this archipelago are now further elaborated in this thesis.

A major part of the work conducted during the time of this thesis comprises important information on the petrology and geochemistry of the newly collected samples from Flores and Corvo. This aspect was published in the *Journal of Petrology,* which forms thesis chapter two. In detail, the lavas from Flores and Corvo provide new constraints on the evolution of the Azores archipelago. The major and trace element data from these westernmost islands provide evidence for continuous, polybaric, fractional crystallization from the lithosphere asthenosphere boundary to the crust-mantle boundary. Modelling of the major elements supports polybaric fractionation, thus no long-lived magma chamber is required to explain the most differentiated lavas, which have <3wt % MgO. The Nd-Sr isotope ratios of the Corvo and Flores lavas are similar to those observed amongst the eastern islands of Terceira, Graciosa and western São Miguel, but display a much more restricted range. Trace-element ratios (e.g. Nb/Zr, Ta/Hf, La/Sm) suggest the involvement of an enriched source composition that is not observed in the eastern Azores islands or along the Mid-Atlantic Ridge. This mantle source feature is further investigated in chapter 5 of this thesis. A further conclusion from this paper is that 3-5% melting of an enriched mantle formed the primary melts underneath Flores and Corvo at depths around 80 km and temperatures around 1450°C. The resultant primary melts commenced to fractionate upon entering the lithosphere, potentially undergoing short-term storage at the lithosphere asthenosphere boundary.

The other major aim of this thesis was to analayse otherwise well-characterised samples for non-traditional isotope systems across the entire plateau, which included the analysis of Os, Li, B and O isotopes. It was intended to investigate if and how these data can

further constrain the heterogeneous source of the Azores mantle plume. Thus, in chapter 3 of this thesis, a detailed study on the oxygen isotopic composition of mantle derived olivine crystals is presented. In line with previous observations from other OIB settings such as Hawaii or the Canary islands, it is uniquely evident from the oxygen isotope and mineral chemical data that olivine records crustal assimilation. A clear positive correlation between the forsterite content and the $\delta^{18}O$ composition is best explained by assimilation of hydrothermally altered gabbro sections of the underlying oceanic crust. This study was presented at the Goldschmidt conference in Montreal, Canada in 2012, and was published in *Geology*.

Further to the oxygen isotope study, lithium and boron stable isotopes were analysed on representative, primitive lavas across the Azores islands. The intention was to assess the variability of these isotopic systems and to see if these correlate with the traditional radiogenic isotope systems, such as Sr and Nd. This work forms chapter 4 of the thesis. The major outcome of this study was that there is virtually no correlation between stable and radiogenic isotopes, but the former further support the view obtained from the oxygen isotope data that there is ubiquitous assimilation recorded in the Azores lavas. The fact that the large range observed in Sr and Nd isotopes does not correlate with any of the stable isotopes implies that this range has its origin in intra-mantle processes and does not describe variable contributions from recycled low-T materials to the source of the mantle plume. The Li and B isotope data have been presented at the AGU Fall meeting in San Francisco, USA in 2011. The paper has now been submitted for publication to *Chemical Geology*.

A more detailed study on the radiogenic isotopes of hafnium, lead and osmium was carried out to further decipher the relationships between the mantle sources east and west of the MAR. A preliminary assessment is presented in chapter 5. Even though there are differences in the chemical composition between eastern and western lavas, it is obvious from these data that a common plume source feeds the volcanism on both sides of the ridge. However, simple mixing of a common Azores plume component with the local depleted mantle fails to fully explain the observed isotope-trace element relationships. Differences in Nb/Zr and Ta/Hf between islands east and west of the MAR indicate the presence of an additional mantle component that is largely absent in the east, or, that unusual conditions during partial melting prevail. The latter may promote pronounced fractionation of Zr and Hf from Nb and Ta, respectively. Interestingly, a similar

enrichment of Nb-Ta over Zr-Hf has been observed in MORB from the MAR to the south of the Azores plateau, suggesting that this signature of the high field strength elements may be a feature of the regional north Atlantic mantle or that conditions during partial melting in ridge and plume-related settings can produce these unusual trace element signatures. The authors, with the intention to submit it to *Earth and Planetary Science Letters* in due course, are currently revising this manuscript. It will also be presented to the community during the Goldschmidt conference being held in Florence, Italy in August 2013.

The major outcome from chapter 6 is the evidence of melting of carbonated peridotite, which was found in lavas from the easternmost island from the archipelago, Santa Maria. Since this paper is also published (*Contributions to Mineralogy and Petrology)* and because the contribution of the author of this thesis to this particular manuscript, no further summary is given here.

In summary, this thesis represents a step forward in our understanding of the mante source of lavas from the Azores islands. Particularly, the data presented in chapters 2-5 have made the western Azores lavas among the best-studied of the Azores islands, and even among global OIB.

APPENDIX

ANALYTICAL METHODOLOGY

The methodology described here details the analytical work carried out by the author at Macquarie University, Sydney and the Friedrich-Alexander Universität Erlangen-Nürnberg. For the lead and boron isotope work, the reader is referred to the references given in the method sections of Chapter 4&5, since these analyses were performed by Dr. Sonia Tonarini at the Istituto di Geoscienze e Georisorse-CNR, Pisa, Italy and Dr. Folkmar Hauff at the GEOMAR, Helmholtz Centre for Ocean Research Kiel, Germany, respectively.

Mineral chemistry

Electron microprobe analysis

The mineral analyses were performed at the GeoZentrum Nordbayern, Erlangen using a JEOL JXA8200 electron microprobe. The instrument was operated with an accelerating voltage of 20 kV, a beam current of 20 nA, and a focused electron beam. Counting times were set to 20 and 10 s for peaks and backgrounds respectively for all oxides except NiO (40 and 20 s, respectively). The CaO, NiO and Fo contents of the individual grains are summarized in Table 1 of this appendix. Most grains were measured multiple times on different splits and, as shown by Genske et al. (2012), the olivine crystals appear very homogeneous with the exception of alteration rims that are characterized by lower Fo compositions. However, minerals with any visible alteration were not selected for analysis. The Fo range from individual lavas often exceeds that predicted by crystal-melt equilibrium. This is interpreted to reflect continuous fractionation in magma conduits, where olivines settle and are transported to the surface by more mafic magmas, perhaps without re-equilibrating due to relatively fast magma ascent rates.

Whole-rock chemistry

Major element analysis via XRF

Selected sample cores were cut into ~1 cm slices using a diamond-tipped circular saw where weathered edges were discarded. Samples were then crushed wrapped in plastic bags using a hydraulic press and powdered using an agate mill to obtain fine powder (<50

μm grainsize). Thorough care was taken when cleaning the mill with Milli-Q water and ethanol between samples to avoid cross contamination.

Glass discs for X-Ray fluorescence (XRF) major element analysis were prepared by homogeneously fusing 0.4 g of sample with 2.5 g lithium metaborate flux and ammonium iodide in a Pt crucible at 1000°C. The discs were analysed using a Spectro XEPOS energy dispersive XRF spectrometer at the School of Earth and Environmental Sciences, University of Wollongong. Loss on ignition was determined for each sample at 1050°C for 1.5 hours.

Analyses of international rock standards and samples are listed below in the Appendix. Accuracy of the measured values was generally better than 0.9% and precision of all elements was better than 0.6%. The measured Fe_2O_3 contents were converted to whole-rock FeO_T concentrations by $FeO_T=Fe_2O_3$ x 0.8998.

Trace element analysis Q-ICP-MS

For the trace element analysis approximately 100 mg of sample were weighed into clean 15 mL Savillex Teflon beakers. Sample digestion was carried out using a 1:1 mixture of HF (Merck, suprapur grade) and HNO_3 (Ajax) at 160°C for 24 hours, then dried down and repeated. To fully dissolve any spinel in the samples an HF-HCl-$HClO_4$ mix was added to the digestion procedure for 2 days at 160°C. This step was repeated as necessary. After drying down at 200°C the samples were then further digested in 6N HNO_3 for 24 hours, dried down again, and diluted to 10 mL in 2% HNO_3 with trace HF. 1:1000 dilutions of each sample were then individually spiked with a 15 μL aliquot of a solution of Li, As, Rh, In, Tm and Bi in 2% HNO_3. The samples and standards were analysed on an Agilent 7500c/s Quadrupole Inductively Coupled Plasma Mass Spectrometer (ICPMS) at the GAU, Macquarie University. BCR-2 was used as a calibration standard to correct for instrument sensitivity and drift, and background was measured on the 2% HNO_3 rinse solution. Measured and reference values for standards BIR-1 and BHVO-2 and the sample analyses are shown in the tables of the Appendix.

Radiogenic isotope analysis

Strontium-Neodymium-Hafnium isotopes

Column chemical separation of Sr, Nd and Hf was carried out at GEMOC, Macquarie University using standard methods (e.g. Blichert-Toft, 2001) in order to analyse the radiogenic isotope composition of selected samples.

Whole rock samples and the BHVO-2 standard (~140 mg) were digested in Teflon beakers using concentrated HF and HNO_3. Samples were then dried down and approximately 1 ml of concentrated $HClO_4$ was added, followed by 4 ml 6N HCl and H_2O_2. Samples were dried down again, dissolved in 6N HCl, dried, dissolved in HCl and HF and centrifuged to remove any undissolved residue. Samples were then loaded onto Teflon columns using Biorad® AG50W-X8 (200-400 mesh) cation exchange resin, and eluted using a 2.5N HCl/0.1N HF solution. Hafnium was collected with the matrix after 5.4 ml and Sr after 34.9 ml, followed by Nd. Neodymium was separated from Sm, Ba, La, Ce using a second column (Eichrom® Ln spec resin (50-100μm)). Strontium was collected after 34.9 ml. Hf was separated from the matrix using two further columns (Biorad® AG1-X8 (100-200 mesh) anion exchange resin and AG50W-X8 cation exchange resin).

Isotopic analyses of Sr and Nd were obtained using a Thermo Finnigan Triton thermal ionisation mass spectrometer (TIMS) at the GAU, Macquarie University. Samples for Sr isotope analysis were loaded onto single rhenium filaments and analysed between 1380 and 1430°C. Measured $^{87}Sr/^{86}Sr$ ratios for BHVO-2 and NIST SRM 987 are in good agreement with published values. Ratios were normalised to $^{86}Sr/^{88}Sr = 0.1194$ to correct for mass fractionation. Samples for Nd isotope analysis were loaded onto double rhenium filaments and analysed with an evaporation filament current of 1200-1600 mA and a signal of 0.5-10 V. Reference materials BHVO-2 and JMC 321 were also analysed, producing $^{143}Nd/^{144}Nd$ ratios close to published values. Ratios were normalised to 146Nd/144Nd = 0.7219 to correct for mass fractionation.

Hafnium isotope analyses were obtained using a Nu Instruments 34 multi-collector (MC) ICPMS at the GAU, Macquarie University. Reference materials BHVO-2 and JMC 475 gave $^{176}Hf/^{177}Hf$ values of which were close to published values. Ratios were normalised to $^{176}Hf/^{177}Hf = 0.7325$ to correct for mass fractionation.

Osmium concentration and isotope analysis

For Osmium concentration and isotopic composition of the lavas, 4-5 g of powder was spiked with 0.01642 ppm Os MQ (in house spike at Macquarie University), according to anticipated Os contents in the lavas. These powders were then digested in inverse aqua regia (8 ml 16 N HNO3, 4 ml 12 N HCl) by Carius tube dissolution followed by solvent extraction using CCl4 and micro distillation techniques involving Cr2O3 and H2SO4, as described in more detail elsewhere (Cohen, 1996; Birck et al., 2007). The samples were run on a Thermo Finnigan Triton thermal ionisation mass spectrometer in negative-ion mode (N-TIMS) at the GAU, Macquarie University. The Os samples were loaded onto Pt filaments. Due to the low Os abundance in the samples, total procedural blank (TPB) levels of typically 3 pg or better were achieved so that blank contributions were typically less than 1.1 % on 5 g sample dissolutions. The WPR-1 standard was processed along with unknown samples to monitor chemical separation reproducibility and gave $^{187}Os/^{188}Os = 0.14462 \pm 0.00022$ (2 sd, n = 2) and Os (ppb) = 17.97 ± 0.02 (2sd). These values are in good agreement with published values (e.g. (Correia et al., 2007)). Solutions of the JMC-2 standard run to monitor instrument performance during the course of the study resulted in $^{187}Os/^{188}Os = 0.183447 \pm 0.00004$ (2sd).

Stable isotope analyses

Lithium isotopes

Standard digestion procedures (HF–HNO_3–HCl, concentrated double distilled acids) were performed and followed by single-column chromatographic separation to obtain purified Li cuts of each sample for isotopic analysis. During the digestion, special attention was paid to the formation of fluorides and incomplete decomposition of oxides. Therefore, multiple centrifugation steps were performed and when such residues were observed, another reflux with HCl or HNO3 was added. The method generally follows that described by Seitz et al. (2004) and references therein. Briefly, AG 50W-X8 (200-400 mesh) resin was used for elution of Li in BioRad ® polyprep columns, using a nitric acid–methanol mixture (1M HNO3 - 80% (v/v) methanol) as an eluent. The recovery yield of Li was checked by analysing solutions collected before and after the Li cuts on an Agilent 7500c/s quadrupole (Q-) ICP-MS at GEMOC, Macquarie University, Sydney. More than 99.9 % of Li recovery was typical in the course of our separation procedure. Impurities in the eluted samples are capable of shifting Li isotopic ratios during MC-ICP-

MS analysis, and these were assessed before isotope analysis (e.g. Na/Li ratios << 4 in this study) by Q-ICP-MS analyses. The isotopic analysis of each unknown sample was bracketed by two L-SVEC standard solutions to correct for mass fractionation on the Nu034 Plasma MC-ICP-MS at GEMOC, Macquarie University, Sydney. Additionally, one ACR Li single-element standard solution was measured multiple times as a secondary check on instrument performance (δ^7Li=14.2 ± 0.4 ‰ (2sd, n=19)). Replicates of several samples and international rock standards were undertaken to further evaluate the reproducibility.

Oxygen isotopes on olivine via Laser fluorination

The oxygen isotope analyses were performed on fresh, and optically inclusion-free olivine. The minerals were separated from their rock matrix by crushing, followed by hand separation under a binocular microscope. The resultant olivine separates per lava were rigorously cleaned to remove adhering matrix materials using an ultrasonic bath and MQ-H2O and methanol. After cleaning, these separates were again handpicked for individual grains based on size (>0.5 mm) and appearance. These individual grains were then coarsely crushed in a steel mortar to obtain multiple splits and cleaned again. On average 3-5 smaller splits were then embedded in epoxy mounts for EMPA mineral chemistry. The remaining material (1.9-2.2 mg) was then weighed into a stainless steel sample chamber, along with 4 standards.

δ18O values were determined by laser fluorination using a 25 W- Synrad CO2-laser and F2 as reagent at GeoZentrum Nordbayern. The laser was operated in continuous mode and the energy manually adjusted to allow a reaction process that was as smooth as possible and to avoid any sputtering. The general setup follows that of Sharp (1990). Samples were pre-fluorinated overnight at 0.02 bar F2. F2 pressure during fluorination was 0.1 bar. The entire setup was kept at minimum volume to aid maximum oxygen yields. Visual monitoring of the fluorination during laser heating was aimed at ensuring complete reaction of the minerals and avoiding sample cross contamination. The released oxygen was analyzed for isotopic composition on a ThermoFisher Delta Plus mass spectrometer. During each measurement day, four standard samples (UWG-2, NBS-30) were measured together with the unknowns. The δ18O raw values were corrected by the mean difference of the reference values from the standards (5.8 and 5.1‰, respectively). All oxygen isotope values are given in permil relative to V-SMOW. Reproducibility of

10 replicate samples (i.e. duplicates of the same grain), which would include analytical error as well as sample heterogeneity and impurity, varied between 0.02 ‰ and 0.07 ‰ (1σ; mean 0.06‰ 1σ). Long-term reproducibility of the UWG-2 garnet standard obtained during this study was 5.84 ± 0.07 ‰ (1sd, n = 29). An additional set of data from a nominally homogeneous olivine population from Moroccan xenoliths yielded a mean δ18O value of 5.34 ± 0.08 ‰ (1sd, n = 12), and was used as an external standard.

Although the total variation of our olivine δ18O values is only 0.35 ‰, we remain confident that this range is real. The mean 2sd of our replicates is 0.12, thus the lowest and highest δ18O values measured do not overlap within their errors.

Major & trace elements and Sr-Nd isotope data of lavas from Flores and Corvo (Chapter 2)

Sample no.	C-09-01	C-09-02	C-09-03	C-09-04	C-09-05	C-09-06	C-09-07	C-09-08	C-09-09	C-09-10
island	Corvo	Corvo	Corvo	Corvo	Corvo	Corvo	Corvo	Corvo	Corvo	Corvo
Lat. [°N]	39.6752	39.6766	39.6766	39.6802	39.6802	39.6802	39.6802	39.7128	39.7086	39.7081
Long. [°W]	31.1036	31.1025	31.1025	31.0963	31.0963	31.0963	31.0963	31.1079	31.1038	31.1029
mASL	2	2	4	2	5	2	5	412	430	460
Volcano-stratigraphy	pre-caldera	pre-caldera	pre-caldera	caldera	pre-caldera	pre-caldera	pre-caldera	caldera	pre-caldera	caldera
TAS classification	Alkali Basalt	Tephrite	Alkali Basalt	Basaltic Trachy-andesite	Tephrite	Alkali Basalt	Alkali Basalt	Basaltic Trachy-andesite	Alkali Basalt	Tholeiite Basalt
SiO_2	45.54	47.06	45.48	52.86	44.64	45.15	45.18	48.50	45.11	46.55
TiO_2	2.43	3.10	1.80	1.72	3.34	2.66	1.98	2.97	2.70	1.33
Al_2O_3	13.99	16.33	11.26	18.03	15.15	13.79	12.48	16.34	15.38	7.60
Fe_2O_3	11.33	12.02	9.63	10.02	14.48	12.12	10.71	11.33	12.03	9.10
MnO	0.18	0.22	0.15	0.24	0.20	0.18	0.16	0.19	0.18	0.15
MgO	9.27	4.23	12.25	2.18	5.97	8.76	11.49	3.27	6.70	18.18
CaO	12.06	8.61	14.51	6.11	11.06	11.94	13.90	6.34	11.99	14.92
Na_2O	3.12	5.10	3.32	6.01	3.98	3.28	2.89	4.16	3.64	1.08
K2O	1.17	1.97	0.76	2.54	1.24	1.12	0.45	2.67	1.27	0.37
P_2O_5	0.49	0.84	0.30	0.67	0.55	0.49	0.30	0.94	0.51	0.20
LOI	0.41	0.77	0.28	0.25	0.43	0.35	0.80	2.98	0.14	0.70
Total	99.99	100.25	99.74	100.63	101.04	99.82	100.34	99.69	99.65	100.18
(ppm)										
Sc	32.23	12.82				30.35	42.69	14.30		66.51
V	268.27	213.48	*316.30*	*50.50*	*499.80*	327.34	296.59	171.81	*388.20*	281.68
Cr	456.15	21.87				417.90	697.02	24.01		2529.55
Co	49.13	28.80	*60.80*	*22.10*	*53.80*	50.99	55.03	25.25	*52.70*	76.97
Ni	182.13	11.26	*215.10*		*68.00*	186.38	189.73	17.09	*80.60*	595.42
Cu	161.28	35.06	*128.10*	*7.20*	*56.10*	127.11	95.89	41.96	*55.10*	172.16
Zn	80.98	105.61	*61.20*	*115.10*	*104.50*	82.49	67.58	121.12	*87.10*	64.31
Mo	1.54	2.61	*1.50*	*4.90*	*2.00*	1.76	0.97	2.20	*3.00*	0.51
Rb	26.54	47.96	*16.60*	*69.10*	*29.10*	28.90	10.87	61.49	*31.30*	7.10
Sr	540.65	738.23	*377.80*	*760.70*	*644.50*	560.48	425.54	693.88	*625.00*	271.78
Y	24.90	38.87	*19.30*	*38.60*	*31.70*	25.99	19.96	38.59	*28.20*	16.99
Zr	184.58	306.77	*115.80*	*360.00*	*191.90*	181.47	125.96	346.73	*190.30*	94.56
Nb	64.80	109.74	*34.70*	*121.10*	*63.30*	60.20	35.90	124.35	*64.80*	31.18
Cs	0.28	0.40				0.26	0.37	0.40		0.14
Ba	380.46	629.70	*249.80*	*791.30*	*472.80*	383.54	244.61	573.30	*465.00*	181.88
La	38.00	63.55				36.25	23.49	63.45		17.63
Ce	72.99	122.68	*49.50*	*138.70*	*82.70*	69.15	46.41	118.50	*79.80*	36.61
Pr	8.62	15.26				8.38	5.82	14.23		4.50
Nd	32.82	54.68				32.28	23.26	52.06		18.28
Sm	6.36	10.19				6.38	4.90	9.78		3.95
Eu	2.02	3.14				2.03	1.53	2.88		1.22
Gd	5.71	8.89				5.73	4.62	8.52		3.66
Tb	0.80	1.26				0.81	0.68	1.20		0.47
Dy	4.36	6.67				4.42	3.60	6.31		2.85
Ho	0.79	1.25				0.82	0.69	1.19		0.47
Er	2.14	3.35				2.17	1.78	3.14		1.31
Yb	1.71	2.68				1.72	1.40	2.54		0.98
Lu	0.19	0.34				0.20	0.19	0.33		0.12
Hf	3.81	5.81				3.66	2.97	6.52		2.31
Ta	3.95	6.69				3.64	1.93	7.42		2.20
Pb	2.36	3.30	*0.70*	*4.00*	*1.90*	1.62	1.35	5.10	*1.50*	0.83
Th	4.67	7.71	*4.30*	*12.40*	*7.10*	4.22	2.62	8.59	*7.70*	1.90
U	1.25	1.94	*3.90*	*2.70*	*2.50*	1.02	0.65	2.13	*3.10*	0.52
$^{87}Sr/^{86}Sr$	0.703350	0.703386				0.703432		0.703340		
$^{143}Nd/^{144}Nd$	0.512920	0.512930				0.512922		0.512931		

Sample no.	C-09-11	C-09-12	C-09-13	C-09-14	C-09-15a	C-09-15b	C-09-16	C-09-17.1	C-09-17.2	C-09-18
island	Corvo	Corvo	Corvo	Corvo	Corvo	Corvo	Corvo	Corvo	Corvo	Corvo
Lat. [°N]	39.7137	39.7081	39.7051	39.7009	39.6999	39.6999	39.6753	39.6727	39.6727	39.6736
Long. [°W]	31.1061	31.0983	31.0982	31.0980	31.0985	31.0985	31.1112	31.1215	31.1215	31.1089
mASL	408	555	546	484	482	482	128	5	5	5
Volcano-stratigraphy	caldera	caldera	caldera	caldera	caldera	caldera	VDC	VDC	VDC	pre-caldera
TAS classification	Basaltic Trachy-andesite	Tephrite	Tholeiite Basalt	Alkali Basalt	Alkali Basalt	Basaltic Trachy-andesite	Basaltic Trachyandesite	Trachy-andesite	Picro-basalt	Tephrite
SiO_2	49.81	43.73	46.07	44.49	44.49	44.12	52.57	56.08	41.05	44.56
TiO_2	2.68	2.63	1.50	2.59	2.09	2.01	1.96	1.03	2.99	2.58
Al_2O_3	16.88	18.56	10.12	17.22	13.06	12.62	17.80	18.85	11.76	14.90
Fe_2O_3	10.61	11.78	9.31	11.22	11.37	11.02	9.75	7.99	14.13	12.05
MnO	0.21	0.17	0.14	0.17	0.17	0.16	0.24	0.24	0.17	0.19
MgO	3.70	4.81	15.52	5.66	11.14	11.29	2.50	1.23	10.67	8.08
CaO	6.93	11.57	14.61	12.05	13.08	12.71	5.99	4.16	15.29	12.04
Na_2O	4.95	2.96	1.51	3.15	2.73	3.04	5.46	6.48	1.67	3.55
K2O	2.62	0.90	0.48	1.04	0.53	0.80	2.40	2.99	0.13	1.18
P_2O_5	0.86	0.51	0.25	0.53	0.33	0.31	0.85	0.50	0.17	0.45
LOI	1.07	2.49	0.75	2.01	1.40	1.88	1.45	0.43	2.01	0.75
Total	100.32	100.11	100.26	100.13	100.39	99.96	100.97	99.98	100.04	100.33
(ppm)										
Sc			55.86		48.70			2.71	58.91	28.85
V	*164.00*	*300.20*	263.63	*212.00*	336.43	*298.60*	*34.60*	11.68	624.97	338.31
Cr			1413.69		1069.41			2.04	715.96	226.46
Co	*31.70*	*46.90*	59.40	*42.00*	69.25	*52.50*	*23.00*	7.45	72.48	52.53
Ni	*5.50*	*45.80*	356.05	*48.70*	298.04	*223.70*		0.89	95.90	150.61
Cu	*19.50*	*96.60*	114.30	*145.90*	174.27	*127.40*	*7.50*	7.73	53.84	121.19
Zn	*98.00*	*92.20*	53.55	*78.30*	87.45	*66.40*	*133.40*	131.10	115.05	82.98
Mo	*3.30*	*1.50*	0.70	*2.00*	1.00	*0.90*	*3.30*	3.31	4.67	1.93
Rb	*58.90*	*14.80*	9.66	*20.50*	4.43	*11.10*	*73.40*	54.11	2.59	28.66
Sr	*735.20*	*677.60*	292.81	*668.40*	605.89	*385.20*	*852.40*	770.35	572.89	592.95
Y	*37.90*	*27.20*	16.44	*29.10*	25.64	*24.10*	*56.00*	41.66	20.20	24.95
Zr	*329.20*	*179.90*	98.39	*201.20*	159.56	*119.10*	*512.00*	590.64	84.84	176.95
Nb	*112.80*	*58.70*	30.17	*63.60*	51.90	*34.00*	*203.70*	200.37	11.63	61.80
Cs			0.09		0.14			0.13	0.03	0.29
Ba	*568.20*	*469.80*	191.09	*478.40*	333.38	*268.60*	*703.00*	1157.55	109.57	381.32
La			19.27		31.32			106.18	18.38	36.24
Ce	*121.40*	*75.60*	37.05	*74.60*	59.58	*44.50*	*186.10*	190.92	29.37	69.66
Pr			4.65		7.30			20.55	4.45	8.27
Nd			18.50		28.60			65.46	19.35	31.40
Sm			3.89		5.91			10.56	4.67	6.09
Eu			1.21		1.91			3.34	1.51	1.95
Gd			3.65		5.44			8.30	4.53	5.45
Tb			0.50		0.77			1.28	0.62	0.76
Dy			2.87		4.27			6.64	3.60	4.17
Ho			0.50		0.76			1.34	0.59	0.76
Er			1.36		2.05			3.73	1.59	2.04
Yb			1.06		1.59			3.58	1.14	1.61
Lu			0.09		0.21			0.57	0.14	0.18
Hf			2.30		3.51			10.61	2.92	3.52
Ta			1.69		4.02			18.69	0.62	3.58
Pb	*3.70*	*1.70*	0.85	*1.80*	1.62	*3.40*	*6.20*	7.38	0.47	1.68
Th	*11.00*	*6.80*	2.05	*7.30*	3.08	*3.50*	*21.20*	16.71	0.65	4.05
U	*3.10*	*3.00*	0.55	*2.80*	0.77	*3.00*	*3.80*	4.21	0.44	1.10
$^{87}Sr/^{86}Sr$			0.703500							0.703372
$^{143}Nd/^{144}Nd$			0.512938							0.512921

Sample no.	C-09-19	C-09-20	FL-09-01	FL-09-02	FL-09-03	FL-09-04	FL-09-05a	FL-09-06	FL-09-07	FL-09-08
island	Corvo	Corvo	Flores	Flores	Flores	Flores	Flores	Flores	Flores	Flores
Lat. [°N]	39.6718	39.6718	39.4100	39.3955	39.3931	39.3929	39.3928	39.3766	39.3769	39.4354
Long. [°W]	31.1108	31.1108	31.2451	31.2466	31.2587	31.2583	31.2581	31.2351	31.2373	31.2310
mASL	5	5	356	362	11	7	9	140	151	513
Volcano-stratigraphy	VDC	pre-caldera	UVC1	UVC1	BVC	BVC	BVC	BVC	BVC	UVC1
TAS classification	Tephrite	Alkali Basalt	Trachy-basalt	Trachy-basalt	Trachy-basalt	Trachy-basalt	Trachy-basalt	(altered Basalt)	Trachyte	Alkali Basalt
SiO_2	46.82	45.52	47.64	56.79	54.69	53.98	43.98	40.98	62.11	45.69
TiO_2	3.13	2.30	2.21	1.53	1.42	1.39	3.75	1.57	0.62	1.98
Al_2O_3	16.46	12.74	16.31	17.97	18.94	17.32	14.96	8.29	17.95	15.05
Fe_2O_3	11.77	11.32	10.46	6.44	7.17	6.89	11.84	8.78	3.97	10.75
MnO	0.22	0.17	0.19	0.23	0.21	0.23	0.19	0.11	0.19	0.17
MgO	4.29	10.74	6.67	1.78	0.98	1.42	3.94	12.33	0.50	9.77
CaO	8.35	13.21	9.81	4.28	4.27	5.05	9.89	12.32	1.35	12.13
Na_2O	5.59	2.32	3.74	6.31	5.45	5.38	3.25	1.10	6.14	2.57
K2O	1.86	0.88	1.45	3.62	3.81	3.60	1.67	0.37	5.35	0.98
P_2O_5	1.11	0.39	0.61	0.49	0.45	0.47	0.85	0.29	0.14	0.53
LOI	0.05	0.40	1.15	0.83	2.85	4.02	5.99	14.02	1.69	0.63
Total	99.65	99.99	100.24	100.27	100.23	99.75	100.31	100.16	100.01	100.25
(ppm)										
Sc	12.65	41.71	25.38						1.56	
V	184.39	320.63	215.61	*51.00*		*69.30*	*334.00*	*159.00*	8.56	*278.00*
Cr	3.71	624.90	254.61						1.86	
Co	26.79	57.91	38.99	*16.70*	*3.40*	*3.20*	*27.90*	*37.00*	1.92	*58.60*
Ni	3.44	234.93	106.36			*5.10*		*290.30*	0.56	*160.60*
Cu	19.28	91.85	64.25		*11.70*	*10.60*	*6.50*	*136.30*	5.67	*65.10*
Zn	111.06	78.79	94.21	*110.10*	*110.80*	*96.40*	*103.10*	*48.40*	84.91	*69.80*
Mo	3.07	1.41	2.12	*3.40*	*3.00*	*5.00*	*3.90*	*1.30*	0.50	*1.10*
Rb	56.21	23.92	36.43	*83.20*	*100.00*	*100.70*	*39.30*	*22.10*	50.20	*25.30*
Sr	949.15	499.06	665.60	*1001.00*	*642.80*	*648.10*	*874.10*	*220.60*	99.66	*608.70*
Y	42.89	24.78	49.82	*45.70*	*35.70*	*34.80*	*33.60*	*16.50*	14.71	*22.60*
Zr	324.75	166.16	246.49	*428.30*	*409.10*	*410.20*	*229.40*	*92.10*	521.26	*131.40*
Nb	131.35	56.39	81.21	*139.30*	*151.60*	*149.30*	*83.10*	*30.80*	151.24	*47.10*
Cs	0.69	0.23	0.39						0.36	
Ba	612.85	348.96	615.48	*1573.00*	*1167.00*	*1038.00*	*676.00*	*244.10*	1060.82	*528.60*
La	74.30	37.03	72.85						24.46	
Ce	144.36	67.30	95.48	*154.30*	*140.40*	*138.00*	*106.10*	*37.70*	46.90	*58.80*
Pr	17.64	8.42	14.31						5.39	
Nd	62.43	31.98	51.91						18.65	
Sm	11.77	6.28	9.26						3.31	
Eu	3.49	2.00	3.08						1.19	
Gd	10.38	5.71	9.10						2.84	
Tb	1.51	0.82	1.30						0.44	
Dy	7.75	4.37	6.74						2.75	
Ho	1.49	0.81	1.37						0.55	
Er	3.84	2.12	3.51						1.66	
Yb	3.15	1.67	2.66						1.62	
Lu	0.45	0.19	0.39						0.21	
Hf	7.03	3.62	5.12						9.78	
Ta	11.24	4.08	6.59						11.97	
Pb	3.89	1.58	2.17	*6.20*	*6.30*	*6.00*	*2.40*		5.19	*1.70*
Th	10.54	4.01	5.44	*11.80*	*16.60*	*16.10*	*8.20*	*1.10*	6.67	*4.70*
U	2.63	1.01	1.62	*4.10*	*4.50*	*6.00*	*3.70*	*3.10*	1.03	*1.60*
$^{87}Sr/^{86}Sr$	0.703301	0.703410	0.703390							
$^{143}Nd/^{144}Nd$	0.512922	0.512920	0.512943							

Sample no.	FL-09-09	FL-09-10	FL-09-11	FL-09-12	FL-09-13	FL-09-16	FL-09-18	FL-09-19	FL-09-20	FL-09-21
island	Flores	Flores	Flores	Flores	Flores	Flores	Flores	Flores	Flores	Flores
Lat. [°N]	39.4480	39.5198	39.5206	39.5204	39.5204	39.5214	39.4928	39.4985	39.5023	39.5089
Long. [°W]	31.1308	31.2077	31.2132	31.2133	31.2133	31.2115	31.2296	31.2317	31.2316	31.2314
mASL	59	9	2	2	12	55	446	359	303	210
Volcano-stratigraphy	UVC2/3	UVC1	UVC1	UVC1	UVC1	UVC1	UVC1	UVC1	UVC1	UVC1
TAS classification	(altered Basalt)	Alkali Basalt	Trachy-basalt	Tephrite	Tephrite	Tephrite	Trachy-basalt	Tephrite	Basalt	Tephrite
SiO_2	41.74	44.85	44.10	44.31	44.07	43.18	45.41	46.90	44.03	43.77
TiO_2	3.12	3.39	3.48	3.43	3.60	3.84	3.39	3.11	3.61	3.43
Al_2O_3	17.83	15.96	16.82	16.75	17.23	16.77	17.21	16.61	16.19	17.77
Fe_2O_3	13.84	12.43	12.22	12.45	12.57	13.48	11.81	11.24	13.18	12.08
MnO	0.27	0.20	0.20	0.19	0.19	0.18	0.21	0.20	0.19	0.19
MgO	3.36	6.05	4.40	4.83	4.00	4.67	4.24	4.22	5.52	3.41
CaO	5.57	10.33	9.63	10.18	8.49	9.27	6.83	7.88	10.27	6.05
Na_2O	4.32	3.04	3.42	4.11	4.33	4.59	3.29	4.51	2.58	4.01
K2O	1.63	1.45	1.50	1.02	1.66	1.07	1.99	2.06	1.27	2.14
P_2O_5	1.67	1.26	1.28	1.27	1.40	0.65	1.40	1.33	0.86	1.38
LOI	6.36	1.12	2.77	1.31	3.10	1.99	4.13	1.79	2.00	5.33
Total	99.71	100.08	99.82	99.85	100.64	99.69	99.91	99.85	99.70	99.56
(ppm)										
Sc	12.85	21.88	22.06			21.93		16.67	23.32	
V	100.08	268.36	262.38	*312.60*	*288.00*	388.31	*160.00*	211.49	336.30	
Cr	3.03	108.90	44.88			22.62		12.99	42.12	
Co	22.64	36.62	35.77	*32.90*	*32.00*	45.37	*27.00*	22.72	40.61	
Ni	2.57	46.63	23.83	*17.50*	*8.30*	42.43		7.18	30.61	
Cu	18.74	50.79	39.86	*25.80*	*16.10*	49.95	*18.40*	27.45	46.73	
Zn	103.14	110.47	110.57	*95.00*	*102.70*	110.34	*98.20*	100.43	104.36	
Mo	1.09	1.25	0.59	*2.40*	*3.10*	1.74	*4.30*	2.23	1.87	
Rb	28.06	23.85	33.67	*7.20*	*34.50*	10.11	*49.30*	46.95	27.43	
Sr	653.82	965.38	948.36	*995.40*	*902.30*	870.75	*887.80*	955.66	866.46	
Y	41.63	35.56	36.09	*35.30*	*34.80*	33.29	*53.60*	42.48	33.59	
Zr	303.82	252.31	269.76	*238.50*	*243.90*	267.46	*307.40*	321.58	224.57	
Nb	103.55	84.24	81.02	*70.90*	*72.80*	78.15	*86.80*	97.00	66.45	
Cs	0.22	0.11	0.16			0.11		0.20	0.19	
Ba	1078.99	678.62	603.42	*589.30*	*625.90*	526.67	*864.10*	755.50	464.37	
La	53.33	57.86	59.87			48.38		68.39	44.67	
Ce	111.48	115.51	121.90	*106.20*	*112.90*	94.81	*137.40*	139.01	87.06	
Pr	15.52	14.83	14.98			12.18		18.04	11.23	
Nd	60.77	56.83	60.11			45.13		68.32	44.82	
Sm	12.38	11.06	11.45			8.91		12.95	9.05	
Eu	4.63	3.86	3.70			2.88		4.43	3.16	
Gd	11.05	9.52	10.08			7.97		11.05	8.08	
Tb	1.59	1.36	1.42			1.13		1.57	1.15	
Dy	7.91	6.51	6.90			5.74		7.75	5.75	
Ho	1.48	1.18	1.26			1.04		1.43	1.06	
Er	3.66	2.91	3.11			2.64		3.47	2.63	
Yb	2.80	2.08	2.28			1.97		2.57	1.90	
Lu	0.39	0.14	0.27			0.24		0.35	0.25	
Hf	5.96	5.10	5.51			5.27		6.19	4.59	
Ta	7.72	7.51	4.61			5.89		7.47	5.76	
Pb	3.21	4.38	3.11	*2.80*	*2.80*	2.12	*1.30*	2.91	1.99	
Th	7.39	5.51	6.06	*8.00*	*8.50*	5.26	*12.10*	6.49	4.04	
U	1.90	1.28	1.37	*3.10*	*1.60*	1.16	*3.70*	1.73	0.91	
$^{87}Sr/^{86}Sr$	0.703510							0.703500	0.703549	
$^{143}Nd/^{144}Nd$	0.512911							0.512902	0.512899	

Sample no.	FL-09-23	FL-09-25	FL-09-26	FL-09-28	FL-09-29	FL-09-30	FL-09-32	FL-09-34	FL-09-35	FL-09-36
island	Flores	Flores	Flores	Flores	Flores	Flores	Flores	Flores	Flores	Flores
Lat. [°N]	39.5149	39.5149	39.5149	39.5093	39.5093	39.4753	39.4581	39.4376	39.4376	39.4288
Long. [°W]	31.2281	31.2281	31.2281	31.2190	31.2190	31.2567	31.2645	31.2429	31.2429	31.2467
mASL	100	92	95	312	312	80	6	190	195	240
Volcano-stratigraphy	UVC1	UVC1	UVC1	UVC1	UVC1	UVC2/3	UVC2/3	UVC2/3	UVC2/3	UVC1
TAS classification	Alkali Basalt	Alkali Basalt	Alkali Basalt	Tephrite	Tephrite	Tephrite	Trachy-basalt	Trachybasalt	Trachy-basalt	Trachy-basalt
SiO_2	46.71	45.76	47.42	43.65	43.88	44.95	44.89	45.20	45.98	48.13
TiO_2	1.76	1.97	1.82	3.52	3.46	3.24	2.79	2.80	2.77	1.80
Al_2O_3	15.74	15.66	16.00	16.68	16.71	16.21	15.30	15.53	15.66	15.58
Fe_2O_3	11.11	12.04	11.14	12.61	12.53	11.45	12.09	12.28	12.21	10.53
MnO	0.17	0.17	0.17	0.19	0.18	0.22	0.18	0.18	0.18	0.18
MgO	8.79	7.75	7.57	3.94	4.22	3.51	7.91	7.61	7.84	7.31
CaO	11.15	12.25	11.80	9.88	10.15	10.05	10.02	9.95	9.75	9.84
Na_2O	2.61	3.35	2.77	4.17	4.02	4.71	4.36	4.03	3.85	4.47
K2O	0.61	0.36	0.62	1.63	1.62	2.08	1.30	1.25	1.30	1.39
P_2O_5	0.43	0.36	0.43	1.29	1.16	0.79	0.70	0.70	0.70	0.41
LOI	1.09	0.66	0.38	2.08	1.80	2.95	0.31	0.15	0.54	0.59
Total	100.17	100.33	100.12	99.64	99.73	100.16	99.85	99.68	100.78	100.23
(ppm)										
Sc	30.84	34.37	32.99	21.38		17.02	22.89			24.91
V	206.82	245.11	218.72	237.61	*245.10*	288.18	248.54	*284.10*	*303.30*	191.60
Cr	366.84	389.77	232.38	52.78		60.78	419.29	*397.10*		390.81
Co	46.18	47.80	43.84	35.36	*19.00*	33.23	45.59	*55.70*	*49.30*	40.54
Ni	175.20	139.23	112.94	23.87	*20.30*	19.08	147.25	*109.40*	*110.50*	169.50
Cu	63.90	98.04	80.54	40.32	*28.60*	61.97	54.27	*44.30*	*44.70*	74.14
Zn	74.30	87.09	77.62	102.67	*99.80*	86.55	90.54	*89.20*	*85.80*	86.30
Mo	0.82	0.38	0.97	0.25	*1.20*	2.42	2.35	*2.70*	*2.60*	1.98
Rb	10.09	2.41	11.01	39.07	*37.20*	50.93	28.99	*30.90*	*34.80*	32.11
Sr	446.45	436.34	484.13	965.32	*952.70*	873.95	767.65	*735.10*	*744.10*	453.70
Y	21.83	24.78	25.14	35.20	*33.50*	30.75	26.76	*27.40*	*27.90*	25.81
Zr	118.22	110.59	119.68	254.06	*232.40*	266.39	221.39	*214.10*	*217.90*	192.33
Nb	33.43	33.03	34.68	83.64	*70.40*	93.39	72.36	*63.60*	*64.60*	59.01
Cs	0.04	0.02	0.10	0.30		0.49	0.30			0.31
Ba	310.32	314.13	307.44	566.01	*560.90*	574.62	495.09	*486.90*	*519.30*	571.90
La	22.33	23.09	24.52	55.58		54.72	42.09			33.13
Ce	45.60	43.66	47.86	113.05	*98.80*	106.76	80.52	*74.00*	*78.20*	64.76
Pr	5.93	5.80	6.22	14.36		13.34	9.71			7.66
Nd	23.93	23.46	24.92	55.16		46.80	36.80			28.86
Sm	4.95	4.93	5.15	10.87		8.48	7.09			5.58
Eu	1.82	1.79	1.87	3.72		2.69	2.40			2.04
Gd	4.66	4.83	4.94	9.24		7.29	6.12			5.03
Tb	0.67	0.67	0.72	1.32		1.04	0.85			0.71
Dy	3.74	4.00	4.03	6.37		5.31	4.54			4.06
Ho	0.69	0.73	0.76	1.15		1.00	0.81			0.74
Er	1.84	2.01	2.03	2.82		2.56	2.16			2.08
Yb	1.46	1.55	1.61	1.99		2.07	1.68			1.71
Lu	0.16	0.20	0.18	0.26		0.28	0.22			0.23
Hf	2.43	2.46	2.48	4.97		5.15	4.26			3.61
Ta	2.30	2.31	2.28	7.40		7.20	5.97			4.61
Pb	0.94	0.88	0.92	2.08	*1.30*	2.56	2.15	*2.10*	*2.40*	1.71
Th	1.89	1.73	1.92	5.17	*7.80*	6.06	4.59	*7.60*	*6.70*	3.63
U	0.55	0.31	0.54	1.00	*4.20*	1.52	1.24	*1.70*	*3.10*	1.09
$^{87}Sr/^{86}Sr$	0.703268		0.703309				0.703434			
$^{143}Nd/^{144}Nd$	0.512948		0.512941				0.512916			

Sample no.	FL-09-37	FL-09-38	FL-09-39	FL-09-41	FL-09-42	FL-09-44	FL-09-47	FL-09-54	FL-09-55	FL-09-58
island	Flores	Flores	Flores	Flores	Flores	Flores	Flores	Flores	Flores	Flores
Lat. [°N]	39.4292	39.4285	39.4277	39.4226	39.4244	39.4457	39.4436	39.4789	39.4725	39.4224
Long. [°W]	31.2494	31.2512	31.2563	31.2417	31.2399	31.1829	31.1488	31.1567	31.1480	31.1634
mASL	266	284	333	460	472	565	312	260	170	350
Volcano-stratigraphy	UVC1	UVC1	UVC2/3	UVC2/3	UVC2/3	UVC2/3	UVC1	UVC1	UVC1	UVC1
TAS classification	Trachy-basalt	Trachy-basalt	Alkali Basalt	Alkali Basalt	Alkali Basalt	Trachyte	Tephri-phonolite	Tephrite	Trachy-basalt	Alkali Basalt
SiO_2	46.88	46.70	45.82	46.35	44.80	59.07	53.66	46.92	46.71	45.13
TiO_2	2.39	2.50	2.36	1.82	2.24	1.29	1.96	3.06	3.64	2.97
Al_2O_3	16.58	16.30	13.61	13.59	14.63	19.82	16.86	17.01	15.80	15.49
Fe_2O_3	11.38	11.55	11.56	10.74	11.42	5.34	9.65	10.43	12.72	11.85
MnO	0.17	0.20	0.17	0.17	0.18	0.14	0.25	0.18	0.20	0.19
MgO	3.93	5.76	7.03	10.50	9.30	0.88	1.01	3.52	4.45	6.42
CaO	10.68	10.36	11.00	11.61	10.77	3.35	5.32	8.86	9.47	10.38
Na_2O	3.93	4.08	2.38	3.16	2.78	6.84	7.28	4.68	3.93	2.78
K2O	1.19	1.45	1.15	1.14	1.09	3.81	2.48	2.22	1.92	0.78
P_2O_5	0.58	0.76	0.58	0.46	0.64	0.44	0.73	0.71	0.73	0.65
LOI	1.89	0.38	1.82	0.01	1.92	1.27	1.35	2.20	0.22	3.11
Total	99.60	100.04	100.00	99.55	99.77	100.08	100.55	99.79	99.79	99.75
(ppm)										
Sc	25.58	22.96		35.52	33.01			13.09		29.25
V	244.52	252.99	*186.40*	252.17	253.13	*34.50*	*60.40*	231.55		326.76
Cr	53.02	140.64		671.26	572.03			7.34		197.43
Co	33.14	35.37	*59.50*	51.75	48.64	*14.30*	*20.10*	25.46		43.53
Ni	29.78	66.53	*146.30*	245.59	209.31		*1.50*	9.41		82.37
Cu	41.08	56.26	*70.90*	96.15	93.46	*2.20*	*1.90*	36.34		95.35
Zn	97.62	93.18	*76.50*	68.00	76.44	*94.00*	*124.10*	92.79		89.81
Mo	2.40	2.43	*0.70*	1.89	1.35	*2.30*	*2.90*	2.14		1.98
Rb	25.92	34.38	*19.50*	32.64	27.71	*75.20*	*64.60*	59.11		5.40
Sr	549.77	697.89	*618.40*	555.57	626.85	*796.30*	*863.70*	974.80		726.21
Y	29.03	30.09	*25.50*	24.00	25.48	*53.00*	*46.20*	32.65		30.59
Zr	183.26	200.43	*162.90*	158.19	160.09	*355.40*	*406.70*	253.57		249.28
Nb	51.66	77.41	*56.30*	57.94	61.18	*114.00*	*107.10*	82.47		85.21
Cs	0.35	0.47		0.43	0.20			1.36		0.17
Ba	540.47	584.76	*545.50*	467.09	527.96	*2157.00*	*789.50*	658.33		489.70
La	34.49	42.75		33.22	36.86			45.33		50.62
Ce	69.07	83.99	*67.30*	64.34	70.65	*122.70*	*133.70*	86.60		98.43
Pr	8.64	10.28		7.75	8.67			10.90		12.26
Nd	34.23	39.58		29.35	33.08			41.65		43.92
Sm	6.86	7.55		5.65	6.33			8.10		8.10
Eu	2.49	2.63		1.90	2.17			2.71		2.55
Gd	6.51	6.57		5.08	5.62			6.96		6.97
Tb	0.96	0.93		0.74	0.81			0.98		1.01
Dy	5.16	4.93		3.95	4.20			5.08		5.12
Ho	1.01	0.90		0.75	0.79			0.94		0.97
Er	2.67	2.43		1.99	2.07			2.45		2.46
Yb	2.19	1.91		1.64	1.67			1.90		1.97
Lu	0.31	0.26		0.21	0.21			0.26		0.26
Hf	3.95	3.73		3.08	3.10			4.71		4.85
Ta	2.96	6.18		4.06	4.30			6.83		6.26
Pb	1.82	1.88	*0.80*	1.51	1.60	*4.80*	*4.60*	2.79		2.09
Th	3.86	4.16	*6.60*	3.58	3.55	*10.60*	*11.20*	4.24		5.24
U	1.17	1.16	*3.20*	0.97	0.94	*4.00*	*2.40*	1.11		1.12
$^{87}Sr/^{86}Sr$		0.703370		0.703330	0.703370					0.703535
$^{143}Nd/^{144}Nd$		0.512922		0.512920	0.512929					0.512905

Sample no.	FL-09-59	FL-09-60	FL-09-63	FL-09-64	FL-09-65	FL-09-69
island	Flores	Flores	Flores	Flores	Flores	Flores
Lat. [°N]	39.4094	39.4123	39.4005	39.3834	39.4039	39.4529
Long. [°W]	31.1602	31.1569	31.1659	31.1706	31.2292	31.1860
mASL	278	321	122	120	550.00	644
Volcano-stratigraphy	UVC1	UVC1	UVC1	UVC1	UVC2/3	UVC2/3
TAS classification	Tephrite	Trachyte	Trachy-basalt	Alkali Basalt	Trachy-andesite	Trachy-basalt
SiO_2	44.53	60.99	47.11	46.35	56.69	45.07
TiO_2	3.47	0.78	2.80	2.65	1.34	2.28
Al_2O_3	15.80	18.35	16.97	15.68	20.05	16.72
Fe_2O_3	12.68	4.52	10.73	11.27	6.72	11.76
MnO	0.19	0.18	0.19	0.17	0.18	0.20
MgO	6.45	0.36	5.38	7.64	0.83	5.73
CaO	10.75	0.90	10.57	9.29	1.75	9.83
Na_2O	3.34	6.74	3.89	3.46	6.73	3.66
K2O	1.37	5.43	1.23	1.41	3.80	1.36
P_2O_5	1.01	0.17	0.69	0.60	0.44	0.86
LOI	0.67	1.09	0.81	1.77	2.54	2.40
Total	100.26	99.51	100.37	100.29	101.07	99.86
(ppm)						
Sc	27.04		21.64	27.95		
V	310.33		256.55	244.12		
Cr	115.74		96.64	308.81		
Co	42.03		33.39	43.94	*1.50*	
Ni	56.86		45.20	138.38		
Cu	56.63		66.86	65.53		
Zn	103.19		89.85	86.89	*98.90*	
Mo	0.41		2.25	1.53	*2.60*	
Rb	32.28		55.07	34.82	*74.50*	
Sr	915.27		808.73	542.19	*469.00*	
Y	34.39		30.52	30.29	*64.30*	
Zr	228.13		262.28	243.28	*441.00*	
Nb	72.73		103.51	66.10	*124.60*	
Cs	0.16		0.87	0.25		
Ba	539.85		560.80	424.75	*2075.00*	
La	46.92		55.46	39.67		
Ce	95.08		105.26	75.25	*140.10*	
Pr	12.49		12.72	10.01		
Nd	48.53		44.09	37.02		
Sm	9.64		7.97	7.36		
Eu	3.39		2.48	2.42		
Gd	8.26		6.60	6.62		
Tb	1.16		0.94	0.96		
Dy	5.67		4.83	5.05		
Ho	1.00		0.88	0.94		
Er	2.49		2.32	2.42		
Yb	1.71		1.85	1.95		
Lu	0.22		0.25	0.25		
Hf	4.20		4.66	4.73		
Ta	5.64		8.01	4.94		
Pb	1.84		2.31	1.85	*3.50*	
Th	3.52		5.35	4.53	*13.90*	
U	0.78		1.24	1.14	*3.50*	
$^{87}Sr/^{86}Sr$	0.703502					
$^{143}Nd/^{144}Nd$	0.512895					

Table DR1: Single olivine grain analyses, sampled from Azores lavas. (Chapter 3)

Table DR1: Single olivine grain analyses, sampled from Azores lavas.

sample	Island	CaO [wt %]	NiO [wt %]	Fo [%]	sd	$\delta^{18}O$ [‰]	sd	n=	$T_{(ol\text{-}liq)}$ °C	$\delta^{18}O_{(Fo89)}$ [‰]	$\delta^{18}O_{(Fo93)}$ [‰]	$^{87}Sr/^{86}Sr_{(lava)}$	$^{143}Nd/^{144}Nd_{(lava)}$
C-01 ol 1	Corvo	0.34	0.22	87.1	0.3	5.14	0.03	1	1341	5.18	5.27	0.703350	0.512920
C-05 ol 1	Corvo	0.29	0.10	85.7		5.17	0.02	2	1327	5.24	5.33		
C-06 ol 1	Corvo	0.40	0.30	88.7	0.0	5.19	0.03	1	1357	5.20	5.29	0.703432	0.512922
C-06 ol 2	Corvo	0.36	0.25	89.7	0.1	5.18	0.02	1	1366	5.17	5.26	0.703432	0.512922
C-06 ol 4	Corvo	0.35	0.27	90.0	0.2	5.16	0.03	1	1370	5.14	5.23	0.703432	0.512922
C-06 ol 5	Corvo	0.36	0.20	89.7	0.2	5.24	0.01	1	1367	5.22	5.31	0.703432	0.512922
C-06 ol 6	Corvo	0.36	0.22	90.0	0.3	5.22	0.02	1	1370	5.20	5.29	0.703432	0.512922
C-07 ol 1	Corvo	0.25	0.11	79.6	0.1	4.99	0.02	2	1267	5.20	5.29		
C-07 ol 2	Corvo	0.27	0.10	78.9	0.2	4.90	0.07	2	1260	5.13	5.22		
C-07 ol 3	Corvo	0.25	0.10	78.5		5.04	0.01	1	1257	5.28	5.37		
C-07 ol 4	Corvo	0.38	0.23	88.8		5.21	0.06	2	1358	5.21	5.30		
C-13 ol 2	Corvo	0.41	0.18	89.2	0.3	5.25	0.01	1	1362	5.24	5.33	0.703500	0.512938
C-13 ol 1	Corvo	0.28	0.14	86.3		5.14	0.01	1	1334	5.20	5.29	0.703500	0.512938
C-18 ol 3	Corvo	0.37	0.19	87.6	0.4	5.24	0.01	1	1346	5.27	5.36	0.703372	0.512921
AZF-01 ol 1	Faial	0.19	0.08	77.2	0.2	4.84	0.02	1	1244	5.10	5.19		
AZF-01 ol 2	Faial	0.20	0.10	80.5	0.6	4.95	0.01	1	1276	5.14	5.23		
F/FG-28 ol	Faial	0.22	0.12	81.2	0.5	4.96	0.02	1	1283	5.13	5.22	0.703875	0.512768
AZP-09 ol 1	Pico	0.17	0.11	77.4	0.2	4.98	0.01	1	1246	5.24	5.33	0.703524	0.512957
AZP-09 ol 3	Pico	0.20	0.16	82.1	0.0	5.12	0.01	1	1292	5.27	5.36	0.703524	0.512957
AZP-17 ol 2	Pico	0.20	0.12	79.1	0.4	5.04	0.02	1	1262	5.26	5.35		
AZP-38 ol 2	Pico	0.25	0.26	85.9	0.3	5.15	0.02	1	1329	5.22	5.31	0.703704	0.512926
AZP-47 ol 2	Pico	0.23	0.19	81.5	0.2	4.96	0.01	1	1286	5.13	5.22	0.703793	0.512919
P25 ol 1	Pico	0.19	0.13	78.9	0.5	5.00	0.04	1	1260	5.23	5.32	0.703840	0.512827
P29 ol 1	Pico	0.25	0.14	82.9	0.2	5.01	0.03	1	1299	5.15	5.24	0.703800	0.512813
Pico Ank ol 2	Pico	0.31	0.15	87.1		5.12	0.01	1	1342	5.16	5.25		
SJ-11 ol 1	São Jorge	0.24	0.20	83.7	0.1	5.12	0.01	1	1307	5.24	5.33		0.512851
SJ-6 ol 1	São Jorge	0.25	0.19	84.5	0.2	5.08	0.08	1	1316	5.18	5.27	0.703937	
S10 ol 1	São Miguel	0.22	0.12	78.7	0.4	4.91	0.14	1	1259	5.14	5.23	0.704362	0.512774
S3 ol 1	São Miguel	0.28	0.30	88.1	0.3	5.18	0.01	1	1351	5.20	5.29	0.704524	0.512685
S7 ol 1	São Miguel	0.30	0.31	88.2	0.3	5.24	0.01	1	1352	5.26	5.35	0.704443	0.512785
SM129 ol 1	São Miguel	0.25	0.20	84.5	0.4	5.15	0.05	2	1316	5.25	5.34	0.705338	0.512699
Gr UWG2						5.84	0.07	29					
Bio NBS 30						5.09	0.06	31					

Table 2: Single clinopyroxene grain analyses, sampled from lavas across the Azores islands. (Chapter 3)

Table 2: Clinopyroxene mineral analyses. Wo, En and Fs componets where calculated stoichiometrically.

	SiO2	TiO2	Al2O3	Cr2O3	FeO	Fe2O3	MgO	MnO	CaO	Na2O	K2O	NiO	Total	Mg #	Cr #	Wo	En	Fs	d18O	sd
AZF-01 cpx-1_1	47.76	1.83	7.04	0.21	4.87	1.70	13.76	0.09	20.82	0.56	0.00	0.02	98.47	0.83	0.02	0.39	0.51	0.10	5.36	0.00
AZF-01 cpx-1_2	47.79	1.90	7.08	0.19	5.29	1.48	13.76	0.08	20.59	0.56	0.00	0.00	98.57	0.82	0.02	0.38	0.51	0.11	5.36	0.00
AZP-09 cpx-1_3	47.84	1.93	6.94	0.16	5.47	1.59	14.15	0.15	19.70	0.60	0.02	0.00	98.39	0.82	0.02	0.37	0.52	0.11	5.21	0.02
AZP-09 cpx-2_1	49.02	1.38	5.71	0.93	5.18	0.77	14.49	0.10	20.31	0.59	0.00	0.02	98.41	0.83	0.10	0.36	0.53	0.11	5.10	0.01
AZP-09 cpx-2_2	46.56	2.45	7.39	0.41	4.43	2.32	13.42	0.16	20.61	0.62	0.00	0.08	98.22	0.84	0.04	0.39	0.51	0.09	5.10	0.01
AZP-09 cpx-2_3	46.75	2.46	7.63	0.42	4.71	1.69	13.63	0.10	20.53	0.57	0.02	0.04	98.37	0.84	0.04	0.38	0.52	0.10	5.10	0.01
AZP-13 cpx-1_1	46.91	2.33	6.82	0.15	5.27	2.81	13.18	0.16	20.09	0.75	0.00	0.04	98.23	0.82	0.01	0.40	0.49	0.11	5.28	0.02
AZP-13 cpx-1_2	48.00	2.01	6.51	0.14	6.16	2.08	13.46	0.20	19.90	0.72	0.00	0.03	98.99	0.80	0.01	0.38	0.49	0.13	5.28	0.02
AZP-47 cpx-2_1	47.39	2.00	6.49	0.32	4.64	2.84	13.95	0.17	19.91	0.70	0.01	0.00	98.13	0.84	0.03	0.39	0.52	0.10	5.34	0.02
AZP-47 cpx-2_2	47.50	1.97	6.80	0.30	4.62	2.46	14.11	0.12	20.12	0.62	0.00	0.00	98.39	0.84	0.03	0.38	0.52	0.10	5.34	0.02
AZP-48 cpx-1_1	49.46	1.21	4.50	0.56	4.44	1.62	15.40	0.15	20.51	0.41	0.00	0.00	98.09	0.86	0.08	0.39	0.52	0.08	5.42	0.02
AZP-48 cpx-1_2	52.35	0.64	2.64	0.57	4.18	0.00	16.59	0.09	21.13	0.38	0.00	0.00	98.57	0.86	0.13	0.38	0.54	0.09	5.42	0.02
AZP-48 cpx-2_1	51.15	1.33	3.06	0.22	5.84	0.33	15.44	0.16	21.17	0.35	0.01	0.06	99.07	0.82	0.05	0.41	0.49	0.10	5.34	0.01
AZP-48 cpx-2_2	51.28	1.27	3.14	0.23	6.01	0.16	15.50	0.13	21.08	0.35	0.00	0.04	99.19	0.82	0.05	0.40	0.49	0.11	5.34	0.01
AZP-48 cpx-2_3	51.03	1.31	3.40	0.12	6.45	0.06	15.25	0.11	20.51	0.46	0.00	0.04	98.74	0.81	0.02	0.38	0.50	0.12	5.34	0.01
C-13 cpx-1_1	52.60	0.44	2.19	0.68	3.28	0.00	17.27	0.12	21.56	0.29	0.02	0.00	98.46	0.90	0.17	0.40	0.54	0.06	5.24	0.02
C-13 cpx-1_2	52.33	0.51	2.37	0.70	3.33	0.00	17.05	0.11	21.80	0.23	0.03	0.04	98.51	0.90	0.17	0.40	0.54	0.06	5.24	0.02
C-13 cpx-1_3	52.39	0.47	2.50	0.84	3.34	0.00	16.63	0.04	21.65	0.27	0.02	0.04	98.19	0.87	0.18	0.38	0.54	0.08	5.24	0.02
C-13 cpx-2_1	52.20	0.57	2.85	0.55	3.69	0.00	16.86	0.12	21.27	0.37	0.01	0.00	98.49	0.89	0.11	0.38	0.55	0.07	5.29	0.01
C-13 cpx-2_2	52.15	0.63	2.84	0.54	3.59	0.00	16.86	0.08	21.30	0.33	0.00	0.01	98.32	0.88	0.11	0.38	0.55	0.07	5.29	0.01
C-13 cpx-2_3	52.31	0.55	2.77	0.56	3.32	0.00	16.78	0.12	21.55	0.29	0.00	0.03	98.27	0.88	0.12	0.38	0.55	0.07	5.29	0.01
C-13 cpx-2_4	52.08	0.59	2.84	0.64	3.41	0.00	16.96	0.08	21.45	0.31	0.00	0.03	98.41	0.89	0.13	0.39	0.55	0.06	5.29	0.01
C-13 cpx-3_1	52.43	0.55	2.91	0.48	3.45	0.00	17.00	0.10	21.75	0.24	0.00	0.03	98.94	0.89	0.10	0.39	0.54	0.07	5.27	0.02
C-13 cpx-3_2	52.46	0.41	2.28	0.66	2.94	0.39	17.33	0.06	21.64	0.30	0.00	0.09	98.53	0.91	0.16	0.41	0.54	0.05	5.27	0.02
C-13 cpx-3_3	52.77	0.47	2.29	0.61	3.03	0.00	17.39	0.04	21.53	0.28	0.00	0.07	98.47	0.90	0.15	0.39	0.55	0.06	5.27	0.02
C-18 cpx-2_1	48.81	1.41	6.88	0.08	4.44	1.02	14.40	0.13	21.61	0.35	0.01	0.03	99.08	0.85	0.01	0.39	0.52	0.09	5.39	0.02
C-18 cpx-2_2	48.29	1.46	7.27	0.12	4.38	1.31	14.18	0.10	21.39	0.39	0.01	0.06	98.82	0.85	0.01	0.38	0.53	0.09	5.39	0.02
C-18 cpx-2_3	48.45	1.51	7.13	0.11	4.65	0.98	14.21	0.13	21.43	0.37	0.01	0.00	98.87	0.84	0.01	0.38	0.52	0.10	5.39	0.02
C-18 cpx-2_4	49.22	1.40	6.50	0.18	4.53	0.84	14.76	0.10	21.58	0.33	0.00	0.00	99.35	0.85	0.02	0.39	0.52	0.09	5.39	0.02
C-18 cpx-3_1	48.46	1.43	6.95	0.11	4.74	0.45	14.21	0.13	21.38	0.35	0.01	0.00	98.17	0.84	0.01	0.37	0.53	0.10	5.24	0.07
C-18 cpx-3_2	49.06	1.33	6.33	0.11	4.77	0.33	14.59	0.09	21.42	0.32	0.02	0.02	98.35	0.85	0.01	0.38	0.53	0.10	5.24	0.07
C-18 cpx-3_3	48.58	1.35	6.81	0.10	4.06	1.20	14.56	0.09	21.57	0.33	0.00	0.00	98.53	0.86	0.01	0.39	0.53	0.08	5.24	0.07
C-5 cpx-1_1	48.60	1.29	6.26	0.18	4.02	1.48	14.51	0.08	21.68	0.32	0.00	0.05	98.33	0.87	0.02	0.40	0.52	0.08	5.42	0.09
C-5 cpx-1_2	48.34	1.36	6.44	0.26	3.59	2.01	14.44	0.13	21.79	0.35	0.01	0.00	98.51	0.88	0.03	0.40	0.53	0.07	5.42	0.09
C-6 cpx-1_1	48.86	1.58	5.43	0.33	5.03	1.53	14.26	0.14	21.08	0.48	0.00	0.05	98.60	0.83	0.04	0.40	0.50	0.10	5.22	0.08
C-6 cpx-1_2	48.50	1.78	6.00	0.30	5.51	0.58	13.89	0.07	21.21	0.44	0.01	0.00	98.23	0.82	0.03	0.39	0.50	0.11	5.22	0.08
C-6 cpx-1_3	49.19	1.60	5.56	0.38	5.67	0.38	14.32	0.11	20.98	0.44	0.00	0.02	98.61	0.82	0.04	0.38	0.51	0.11	5.22	0.08
C-6 cpx-2_1	53.21	0.44	2.10	0.59	2.95	0.00	17.18	0.12	21.68	0.28	0.00	0.02	98.57	0.88	0.16	0.37	0.55	0.08	5.17	0.01
C-6 cpx-3_1	50.48	0.94	4.46	0.54	3.96	0.32	15.61	0.12	21.74	0.31	0.01	0.00	98.45	0.88	0.07	0.39	0.53	0.08	5.23	0.02
C-6 cpx-3_3	50.66	0.87	4.14	0.80	4.36	0.04	15.44	0.12	21.70	0.32	0.01	0.03	98.49	0.86	0.11	0.39	0.53	0.08	5.23	0.02
C-6 cpx-5_1	49.44	1.31	5.56	0.10	4.43	1.26	14.78	0.13	21.57	0.36	0.00	0.10	98.90	0.86	0.01	0.40	0.51	0.09	5.40	0.15
C-6 cpx-5_2	49.18	1.32	5.47	0.04	4.48	1.04	14.67	0.11	21.67	0.32	0.00	0.00	98.19	0.85	0.00	0.41	0.51	0.09	5.40	0.15
C-7 cpx-1_1	47.73	1.90	6.65	0.22	4.88	1.41	13.63	0.11	21.57	0.40	0.00	0.02	98.36	0.83	0.02	0.40	0.50	0.10	5.32	0.02
C-7 cpx-1_2	48.36	1.63	6.05	0.20	5.00	1.15	14.01	0.09	21.48	0.36	0.01	0.00	98.23	0.83	0.02	0.40	0.50	0.10	5.32	0.02
C-7 cpx-1_3	47.87	1.84	6.30	0.25	4.93	1.64	13.59	0.15	21.43	0.45	0.00	0.02	98.32	0.83	0.03	0.41	0.49	0.10	5.32	0.02
C-7 cpx-2_1	49.87	1.41	5.18	0.28	5.62	0.15	14.40	0.14	21.52	0.41	0.00	0.02	98.96	0.82	0.04	0.39	0.50	0.11	5.39	0.02
Pico Ank cpx-2_1	52.58	0.60	2.60	0.67	4.04	0.00	16.58	0.13	21.59	0.41	0.00	0.08	99.26	0.88	0.15	0.39	0.53	0.07	5.30	0.01
Pico Ank cpx-2_2	51.14	0.91	3.92	0.64	4.80	0.09	15.70	0.15	20.96	0.46	0.00	0.06	98.83	0.85	0.10	0.37	0.53	0.09	5.30	0.01
Pico Ank cpx-3_1	52.56	0.42	2.09	0.82	3.75	0.00	16.37	0.08	21.66	0.42	0.00	0.04	98.20	0.87	0.21	0.39	0.53	0.08	5.37	0.03
SM129 cpx-1_1	48.32	2.21	5.21	0.05	7.07	1.00	13.61	0.15	20.56	0.42	0.00	0.01	98.51	0.77	0.01	0.40	0.46	0.14	6.85	0.02
SM129 cpx-1_2	48.40	2.26	5.32	0.09	6.95	1.41	13.66	0.15	20.52	0.44	0.00	0.12	99.18	0.78	0.01	0.40	0.46	0.13	6.85	0.02
SM129 cpx-2_1	46.59	2.75	6.17	0.00	6.40	2.94	13.13	0.19	20.26	0.48	0.00	0.00	98.62	0.79	0.00	0.41	0.46	0.13	5.49	0.03
SM129 cpx-2_2	47.30	2.47	5.69	0.00	6.31	2.50	13.31	0.15	20.54	0.48	0.00	0.05	98.55	0.79	0.00	0.41	0.46	0.12	5.49	0.03

Full chemical charaterisation of Azores lavas analysed for Hf-Pb-Os isotopes, including unpublished data of 4 samples from the MAR. (Chapter 5)

	FL-09-01	FL-09-20	FL-09-23	FL-09-26	FL-09-32	FL-09-38	FL-09-41	FL-09-42	FL-09-58	FL-09-59	FL20	FL8
Island	Flores	Flores	Flores	Flores	Flores	Flores	Flores	Flores	Flores	Flores	Flores	Flores
Long [°W]	31.245	31.232	31.228	31.228	31.265	31.251	31.242	31.240	31.164	31.160	31.170	31.170
Lat [°N]	39.410	39.502	39.515	39.515	39.458	39.428	39.423	39.424	39.422	39.409	39.483	39.433
SiO2 [wt.%]	47.64	44.03	46.71	47.42	44.89	46.70	46.35	44.80	45.13	44.53	48.25	46.33
TiO2 [wt.%]	2.21	3.61	1.76	1.82	2.79	2.50	1.82	2.24	2.97	3.47	2.18	2.64
Al2O3 [wt.%]	16.31	16.19	15.74	16.00	15.30	16.30	13.59	14.63	15.49	15.80	13.60	15.53
Fe2O3 [wt.%]	10.46	13.18	11.11	11.14	12.09	11.55	10.74	11.42	11.85	12.68	10.78	12.06
MnO [wt.%]	0.19	0.19	0.17	0.17	0.18	0.20	0.17	0.18	0.19	0.19	0.17	0.19
MgO [wt.%]	6.67	5.52	8.79	7.57	7.91	5.76	10.50	9.30	6.42	6.45	9.17	8.45
CaO [wt.%]	9.81	10.27	11.15	11.80	10.02	10.36	11.61	10.77	10.38	10.75	11.93	10.00
Na2O [wt.%]	3.74	2.58	2.61	2.77	4.36	4.08	3.16	2.78	2.78	3.34	2.76	3.22
K2O [wt.%]	1.45	1.27	0.61	0.62	1.30	1.45	1.14	1.09	0.78	1.37	1.50	1.36
P2O5 [wt.%]	0.61	0.86	0.43	0.43	0.70	0.76	0.46	0.64	0.65	1.01	0.38	0.69
Sc [ppm]	25.4	23.3	30.8	33.0	22.9	23.0	35.5	33.0	29.2	27.0	32.0	22.3
V [ppm]	215.6	336.3	206.8	218.7	248.5	253.0	252.2	253.1	326.8	310.3	291.9	241.3
Cr [ppm]	254.6	42.1	366.8	232.4	419.3	140.6	671.3	572.0	197.4	115.7	427.4	385.0
Co [ppm]	39.0	40.6	46.2	43.8	45.6	35.4	51.7	48.6	43.5	42.0	44.9	44.1
Ni [ppm]	106.4	30.6	175.2	112.9	147.3	66.5	245.6	209.3	82.4	56.9	131.3	147.1
Cu [ppm]	64.3	46.7	63.9	80.5	54.3	56.3	96.1	93.5	95.4	56.6	85.6	59.7
Zn [ppm]	94.2	104.4	74.3	77.6	90.5	93.2	68.0	76.4	89.8	103.2	69.6	81.4
Rb [ppm]	36.4	27.4	10.1	11.0	29.0	34.4	32.6	27.7	5.4	32.3	37.0	33.3
Sr [ppm]	665.6	866.5	446.5	484.1	767.6	697.9	555.6	626.8	726.2	915.3	521.3	701.3
Y [ppm]	49.8	33.6	21.8	25.1	26.8	30.1	24.0	25.5	30.6	34.4	21.3	23.0
Zr [ppm]	246.5	224.6	118.2	119.7	221.4	200.4	158.2	160.1	249.3	228.1	181.4	212.3
Nb [ppm]	81.2	66.4	33.4	34.7	72.4	77.4	57.9	61.2	85.2	72.7	50.2	60.9
Cs [ppm]	0.4	0.2	0.0	0.1	0.3	0.5	0.4	0.2	0.2	0.2	0.4	0.3
Ba [ppm]	615.5	464.4	310.3	307.4	495.1	584.8	467.1	528.0	489.7	539.8	425.7	485.8
La [ppm]	72.9	44.7	22.3	24.5	42.1	42.8	33.2	36.9	50.6	46.9	28.2	35.8
Ce [ppm]	95.5	87.1	45.6	47.9	80.5	84.0	64.3	70.7	98.4	95.1	58.9	72.9
Pr [ppm]	14.3	11.2	5.9	6.2	9.7	10.3	7.7	8.7	12.3	12.5	7.4	8.8
Nd [ppm]	51.9	44.8	23.9	24.9	36.8	39.6	29.4	33.1	43.9	48.5	28.5	34.4
Sm [ppm]	9.3	9.0	4.9	5.1	7.1	7.6	5.6	6.3	8.1	9.6	5.6	6.6
Eu [ppm]	3.1	3.2	1.8	1.9	2.4	2.6	1.9	2.2	2.5	3.4	1.8	2.3
Gd [ppm]	9.1	8.1	4.7	4.9	6.1	6.6	5.1	5.6	7.0	8.3	5.4	6.0
Tb [ppm]	1.3	1.2	0.7	0.7	0.8	0.9	0.7	0.8	1.0	1.2	0.8	0.9
Dy [ppm]	6.7	5.7	3.7	4.0	4.5	4.9	3.9	4.2	5.1	5.7	4.4	4.9
Ho [ppm]	1.4	1.1	0.7	0.8	0.8	0.9	0.8	0.8	1.0	1.0	0.8	0.8
Er [ppm]	3.5	2.6	1.8	2.0	2.2	2.4	2.0	2.1	2.5	2.5	2.1	2.2
Yb [ppm]	2.7	1.9	1.5	1.6	1.7	1.9	1.6	1.7	2.0	1.7	1.7	1.8
Lu [ppm]	0.4	0.1	0.2	0.2	0.1	0.1	0.2	0.2	0.3	0.0	0.3	0.3
Hf [ppm]	5.12	4.59	2.43	2.48	4.26	3.73	3.08	3.10	4.85	4.20	4.09	4.53
Ta [ppm]	6.59	5.76	2.30	2.28	5.97	6.18	4.06	4.30	6.26	5.64	2.79	3.42
Re [ppb]												
Os [ppb]								0.0673			0.0362	0.0718
Pb [ppm]	2.17	1.99	0.94	0.92	2.15	1.88	1.51	1.60	2.09	1.84	3.20	2.57
Th [ppm]	5.44	4.04	1.89	1.92	4.59	4.16	3.58	3.55	5.24	3.52	3.45	4.19
U [ppm]	1.62	0.91	0.55	0.54	1.24	1.16	0.97	0.94	1.12	0.78	0.93	1.40
87Sr/86Sr	0.703390	0.703549	0.703268	0.703309	0.703434	0.703370	0.703330	0.703370	0.703536	0.703502	0.703320	0.703460
143Nd/144Nd	0.512943	0.512899	0.512948	0.512941	0.512916	0.512922	0.512920	0.512929	0.512905	0.512895	0.512997	0.512978
ε Nd	5.95	5.09	6.05	5.91	5.42	5.54	5.50	5.68	5.21	5.01	7.00	6.63
206Pb/204Pb	19.57	19.73	19.57	19.55	19.64	19.58	19.53	19.52	19.71	19.67	19.53	19.02
207Pb/204Pb	15.61	15.62	15.61	15.61	15.62	15.61	15.61	15.61	15.62	15.62	15.62	15.60
208Pb/204Pb	39.26	39.52	39.27	39.23	39.35	39.31	39.25	39.24	39.45	39.57	39.17	38.79
176Hf/177Hf	0.283046	0.283038	0.283053	0.283069	0.283024	0.283033	0.283037	0.282997	0.282957	0.283024		
ε Hf	6.58	6.29	6.82	7.39	5.80	6.12	6.26	4.84	3.43	5.80		
187Os/188Os								0.129170			0.132984	0.141800
Nb/Zr	0.33	0.30	0.28	0.29	0.33	0.39	0.37	0.38	0.34	0.32	0.28	0.29
Nb/Ta	12.33	11.54	14.54	15.24	12.12	12.53	14.26	14.24	13.62	12.89	18.01	17.81
Zr/Hf	48.18	48.92	48.55	48.32	52.00	53.78	51.32	51.62	51.37	54.32	44.39	46.90
Ta/Hf	1.29	1.25	0.94	0.92	1.40	1.66	1.32	1.39	1.29	1.34	0.68	0.76

	C-09-01	C-09-06	C-09-18	C-09-20	C2	AZG-03-07	AZG-03-08	AZG-03-28	T18	T2	T6	AZT-03-11
Island	Corvo	Corvo	Corvo	Corvo	Corvo	Graciosa	Graciosa	Graciosa	Terceira	Terceira	Terceira	Terceira
Long [°W]	31.104	31.096	31.109	31.111	31.104	28.042	28.024	27.589	27.320	27.320	27.320	27.157
Lat [°N]	39.675	39.680	39.674	39.672	39.675	39.040	39.035	39.009	38.550	38.800	38.800	38.480
SiO2 [wt.%]	45.54	45.15	44.56	45.52	47.55	45.17	45.64	46.24	48.07	49.65	47.22	46.95
TiO2 [wt.%]	2.43	2.66	2.58	2.30	2.91	3.10	3.19	3.27	2.69	2.93	3.02	3.02
Al2O3 [wt.%]	13.99	13.79	14.90	12.74	17.47	15.80	16.49	16.89	15.05	15.09	14.06	13.81
Fe2O3 [wt.%]	11.33	12.12	12.05	11.32	11.66	11.48	11.02	10.55	11.63	11.69	12.24	11.95
MnO [wt.%]	0.18	0.18	0.19	0.17	0.20	0.16	0.17	0.15	0.18	0.20	0.18	0.17
MgO [wt.%]	9.27	8.76	8.08	10.74	5.11	8.17	7.84	7.02	7.94	5.54	8.70	8.25
CaO [wt.%]	12.06	11.94	12.04	13.21	9.50	10.70	9.17	10.50	10.14	8.65	10.47	10.51
Na2O [wt.%]	3.12	3.28	3.55	2.32	3.59	2.42	2.55	2.86	3.12	4.07	3.11	3.21
K2O [wt.%]	1.17	1.12	1.18	0.88	1.76	0.82	1.26	1.08	1.10	1.48	0.96	0.93
P2O5 [wt.%]	0.49	0.49	0.45	0.39	0.67	0.45	0.54	0.46	0.65	1.18	0.89	0.85
Sc [ppm]	32.2	30.3	28.8	41.7	18.5	33.0	32.4	27.2	25.7	20.0	26.1	27.6
V [ppm]	268.3	327.3	338.3	320.6	247.8	356.0	338.4	334.8	271.0	226.9	261.8	257.1
Cr [ppm]	456.1	417.9	226.5	624.9	46.1	334.1	413.2	221.5	273.8	123.6	267.2	300.7
Co [ppm]	49.1	51.0	52.5	57.9	33.1	48.5	45.9	42.2	39.4	24.4	41.5	40.9
Ni [ppm]	182.1	186.4	150.6	234.9	31.8	136.8	166.8	108.2	131.6	55.3	123.4	115.7
Cu [ppm]	161.3	127.1	121.2	91.9	45.9	39.3	44.4	28.3	50.2	24.4	44.0	35.5
Zn [ppm]	81.0	82.5	83.0	78.8	90.7	89.7	95.1	89.2	85.2	101.1	87.9	95.1
Rb [ppm]	26.5	28.9	28.7	23.9	46.8	9.2	23.6	23.0	25.7	31.9	20.4	19.0
Sr [ppm]	540.6	560.5	593.0	499.1	739.8	589.7	520.3	638.9	505.5	631.0	543.2	528.5
Y [ppm]	24.9	26.0	24.9	24.8	29.9	25.9	29.4	25.6	29.5	42.7	33.1	32.0
Zr [ppm]	184.6	181.5	176.9	166.2	266.3	237.3	268.8	224.4	185.6	263.6	182.0	178.0
Nb [ppm]	64.8	60.2	61.8	56.4	88.6	42.4	50.0	40.7	41.5	59.4	40.8	37.0
Cs [ppm]	0.3	0.3	0.3	0.2	0.7	0.0	0.2	0.2	0.2	0.1	0.1	0.2
Ba [ppm]	380.5	383.5	381.3	349.0	631.2	334.5	338.7	302.6	388.6	746.2	512.2	495.7
La [ppm]	38.0	36.2	36.2	37.0	48.7	32.1	35.2	26.5	28.5	47.1	31.1	34.9
Ce [ppm]	73.0	69.1	69.7	67.3	96.0	69.0	75.4	58.2	62.2	106.2	71.3	79.0
Pr [ppm]	8.6	8.4	8.3	8.4	11.8	8.6	9.7	7.5	7.9	13.9	9.5	10.2
Nd [ppm]	32.8	32.3	31.4	32.0	44.4	33.7	38.7	30.3	33.3	58.8	41.0	44.2
Sm [ppm]	6.4	6.4	6.1	6.3	8.3	6.7	7.7	6.4	7.2	12.3	9.0	10.1
Eu [ppm]	2.0	2.0	1.9	2.0	2.7	2.1	2.4	2.1	2.4	3.9	3.3	3.8
Gd [ppm]	5.7	5.7	5.5	5.7	7.6	6.2	7.0	6.0	7.2	11.8	8.8	9.7
Tb [ppm]	0.8	0.8	0.8	0.8	1.2	0.9	1.0	0.9	1.1	1.8	1.3	1.4
Dy [ppm]	4.4	4.4	4.2	4.4	6.1	4.7	5.4	4.7	5.9	9.1	6.8	7.5
Ho [ppm]	0.8	0.8	0.8	0.8	1.1	0.9	1.0	0.8	1.1	1.6	1.2	1.3
Er [ppm]	2.1	2.2	2.0	2.1	2.9	2.3	2.6	2.2	2.8	4.1	3.0	3.3
Yb [ppm]	1.7	1.7	1.6	1.7	2.4	1.9	2.1	1.8	2.3	3.1	2.3	2.6
Lu [ppm]	0.2	0.2	0.2	0.2	0.4	0.3	0.3	0.3	0.3	0.5	0.3	0.4
Hf [ppm]	3.81	3.66	3.52	3.62	5.62	4.49	6.09	5.02	4.23	5.91	4.27	4.59
Ta [ppm]	3.95	3.64	3.58	4.08	5.00	2.47	2.99	2.39	2.46	3.63	2.43	2.52
Re [ppb]									0.2525		0.2611	
Os [ppb]	0.0755		0.1233	0.0541					0.1476		0.0107	
Pb [ppm]	2.36	1.62	1.68	1.58	2.75	1.66	1.76	1.46	1.64	2.05	1.12	1.15
Th [ppm]	4.67	4.22	4.05	4.01	6.47	2.86	3.23	2.47	2.50	3.59	2.15	2.16
U [ppm]	1.25	1.02	1.10	1.01	1.64	0.77	0.88	0.77	0.74	1.20	0.68	0.71
87Sr/86Sr	0.703350	0.703432	0.703372	0.703410	0.703380	0.703647		0.703373	0.703551	0.703565	0.703483	0.703455
143Nd/144Nd	0.512920	0.512922	0.512921	0.512920		0.512897	0.512927	0.512962	0.512900	0.512960	0.512915	0.512981
ε Nd	5.50	5.54	5.52	5.50		5.06	5.65	6.32	5.11	6.28	5.40	6.69
206Pb/204Pb	19.78	19.65	19.77	19.75	19.70	19.32	19.57	19.90	19.74	19.88	19.38	19.62
207Pb/204Pb	15.63	15.62	15.63	15.62	15.59	15.63	15.62	15.63	15.54	15.63	15.51	15.59
208Pb/204Pb	39.48	39.35	39.45	39.45	39.35	39.18	39.21	39.33	38.99	39.31	38.69	39.08
176Hf/177Hf	0.282996	0.283037	0.283040	0.283039								
ε Hf	4.81	6.25	6.36	6.33								
187Os/188Os	0.128360		0.136976	0.124850					0.125575		0.138753	
Nb/Zr	0.35	0.33	0.35	0.34	0.33	0.18	0.19	0.18	0.22	0.23	0.22	0.21
Nb/Ta	16.41	16.55	17.25	13.81	17.73	17.15	16.75	16.99	16.84	16.38	16.80	14.67
Zr/Hf	48.41	49.62	50.33	45.85	47.41	52.83	44.13	44.68	43.86	44.62	42.62	38.79
Ta/Hf	1.04	0.99	1.02	1.13	0.89	0.55	0.49	0.48	0.58	0.61	0.57	0.55

	AZT-03-116	AZT-03-12	AZT-03-16	AZF-03-11	AZF-03-41	F/CA-6	F/CP-18	F/FG-28	AZP-03-09	AZP-03-10	AZP-03-23	AZP-03-38
Island	Terceira	Terceira	Terceira	Faial	Faial	Faial	Faial	Faial	Pico	Pico	Pico	Pico
Long [°W]	27.177	27.158	27.164	28.997	28.764	28.730	28.730	28.730	28.300	28.500	28.200	28.400
Lat [°N]	38.464	38.444		38.778	38.794	38.550	38.550	38.550	38.600	38.500	38.500	38.600
SiO2 [wt.%]	46.75	46.95	46.66	47.29	47.15	47.20	48.06	47.17	46.87	44.42	45.54	46.63
TiO2 [wt.%]	3.68	3.88	3.00	3.08	3.35	2.55	2.60	2.65	2.97	3.53	3.59	2.69
Al2O3 [wt.%]	13.84	13.92	15.64	16.87	15.95	15.20	16.16	15.82	15.81	17.15	16.66	13.32
Fe2O3 [wt.%]	13.45	13.79	12.06	10.78	12.28	10.72	10.34	10.82	11.86	12.03	12.68	11.13
MnO [wt.%]	0.21	0.21	0.18	0.16	0.17	0.15	0.15	0.16	0.17	0.16	0.18	0.16
MgO [wt.%]	6.09	5.45	5.67	5.47	5.89	9.73	7.83	8.13	7.12	6.60	5.79	10.42
CaO [wt.%]	9.69	9.48	10.59	10.07	10.64	10.76	9.30	9.58	9.35	10.30	9.67	11.00
Na2O [wt.%]	3.33	3.65	3.55	3.51	3.23	2.96	3.96	3.46	3.37	2.93	3.64	3.05
K2O [wt.%]	1.20	1.29	1.00	1.46	1.19	1.01	1.55	1.55	1.26	0.76	1.01	1.04
P2O5 [wt.%]	1.17	1.31	0.45	0.56	0.48	0.39	0.50	0.46	0.58	0.58	0.68	0.42
Sc [ppm]	14.9	23.3	24.3	22.7	25.1	28.6	23.5	24.5	22.3	22.5	21.3	29.8
V [ppm]	181.3	287.3	175.3	249.8	266.5	251.6	232.1	246.7	216.2	256.6	252.7	239.0
Cr [ppm]	8.6	64.0	51.3	53.8	71.9	410.3	219.5	206.4	174.4	130.7	65.1	564.4
Co [ppm]	20.6	31.4	41.3	32.0	39.1	45.4	38.7	41.0	42.1	44.2	36.4	47.5
Ni [ppm]	11.0	27.8	31.2	40.3	52.9	167.7	110.5	108.0	102.2	75.7	44.0	197.6
Cu [ppm]	20.4	22.6	31.3	29.1	26.3	47.1	42.2	38.8	32.1	25.6	28.6	41.0
Zn [ppm]	115.4	118.4	100.6	94.3	109.3	70.4	76.6	78.0	111.5	106.6	118.2	91.8
Rb [ppm]	27.0	27.2	20.1	31.7	26.6	23.6	39.3	34.4	32.5	14.1	17.6	22.6
Sr [ppm]	782.3	535.6	568.9	747.2	650.6	551.9	669.0	717.2	587.0	781.1	722.8	545.1
Y [ppm]	38.8	42.7	28.5	28.5	30.1	23.2	25.3	24.7	30.9	30.5	33.4	24.4
Zr [ppm]	327.7	216.2	190.2	250.7	254.6	191.1	264.4	254.8	286.6	281.4	304.5	204.7
Nb [ppm]	61.6	48.4	36.9	46.5	45.7	35.0	46.0	46.7	50.3	50.9	57.5	36.6
Cs [ppm]	0.1	0.2	0.2	0.3	0.3	0.2	0.3	0.3	0.3	0.1	0.2	0.2
Ba [ppm]	389.8	756.5	305.0	397.7	343.1	287.3	425.5	436.9	368.3	303.4	361.4	271.0
La [ppm]	49.3	49.0	29.1	37.7	36.0	22.5	32.9	31.6	37.3	38.3	41.3	28.5
Ce [ppm]	104.5	111.9	60.4	82.2	78.7	50.1	69.7	67.1	80.2	85.9	92.5	59.5
Pr [ppm]	12.9	14.2	8.0	10.0	9.7	6.6	8.9	8.5	9.9	10.5	11.2	7.8
Nd [ppm]	52.2	61.3	33.1	40.5	39.7	27.1	34.6	33.8	40.1	43.0	45.4	32.0
Sm [ppm]	11.5	13.6	7.7	8.7	8.9	5.8	6.8	6.8	8.9	9.5	9.8	7.2
Eu [ppm]	3.7	4.8	2.5	2.8	2.9	1.9	2.2	2.2	2.8	3.1	3.1	2.3
Gd [ppm]	10.7	12.9	7.6	7.9	8.4	5.7	6.4	6.3	8.2	8.8	9.1	6.8
Tb [ppm]	1.6	1.8	1.1	1.2	1.2	0.9	1.0	1.0	1.2	1.3	1.3	1.0
Dy [ppm]	8.6	9.8	6.6	6.4	6.9	4.8	5.3	5.2	6.8	7.1	7.4	5.5
Ho [ppm]	1.6	1.7	1.2	1.2	1.3	0.9	0.9	0.9	1.2	1.3	1.3	1.0
Er [ppm]	4.0	4.3	3.1	3.0	3.2	2.2	2.4	2.4	3.2	3.2	3.4	2.5
Yb [ppm]	3.3	3.3	2.7	2.5	2.7	1.8	2.0	1.9	2.7	2.7	2.9	2.1
Lu [ppm]	0.5	0.5	0.4	0.3	0.4	0.3	0.3	0.3	0.4	0.4	0.4	0.3
Hf [ppm]	7.91	5.40	5.06	6.05	6.48	4.36	5.75	5.54	6.68	6.88	7.02	5.13
Ta [ppm]	3.89	3.15	2.48	3.02	3.14	2.04	2.65	2.64	3.25	3.48	3.71	2.40
Re [ppb]						0.1495	0.0425					
Os [ppb]						0.0164	0.0125					
Pb [ppm]	2.45	1.59	3.10	2.75	1.86	1.88	3.46	3.10	1.90	1.55	2.00	1.80
Th [ppm]	4.70	3.03	2.32	3.46	3.19	2.45	3.90	3.73	3.71	3.46	3.75	2.54
U [ppm]	1.58	0.92	0.68	1.06	1.01	0.76	1.05	1.14	1.21	1.14	1.27	0.80
87Sr/86Sr	0.703591	0.703420	0.703492	0.703840	0.703722	0.703770	0.704012	0.703875	0.703524	0.703535	0.703500	0.703704
143Nd/144Nd	0.512997	0.512982	0.512993	0.512881	0.512879	0.512927	0.512797	0.512768	0.512957	0.512963	0.512976	0.512926
ε Nd	7.01	6.71	6.93	4.73	4.71	5.64	3.10	2.54	6.23	6.34	6.59	5.62
206Pb/204Pb	19.98	19.65	20.03	19.62	19.62	19.12	19.11	19.02	19.75	20.01	19.87	19.83
207Pb/204Pb	15.62	15.60	15.63	15.65	15.63	15.61	15.66	15.62	15.55	15.64	15.63	15.65
208Pb/204Pb	39.25	39.13	39.32	39.33	39.36	38.89	39.06	38.79	39.21	39.51	39.31	39.44
176Hf/177Hf												
ε Hf												
187Os/188Os						0.110191	0.130577					
Nb/Zr	0.19	0.22	0.19	0.19	0.18	0.18	0.17	0.18	0.18	0.18	0.19	0.18
Nb/Ta	15.86	15.35	14.89	15.39	14.56	17.11	17.32	17.71	15.48	14.62	15.49	15.25
Zr/Hf	41.42	40.07	37.62	41.41	39.28	43.83	45.99	45.98	42.90	40.90	43.37	39.89
Ta/Hf	0.49	0.58	0.49	0.50	0.48	0.47	0.46	0.48	0.49	0.51	0.53	0.47

	AZP-03-47	P25	P26	P29	P4	P5	PK91 P10	PK91 P14	PK91 P23	PK91 P27	PK91 P7	PK92-SJ6
Island	Pico	Pico	Pico	Pico	Pico	Pico	Pico	Pico	Pico	Pico	Pico	Sao Jorge
Long [°W]	28.300	28.400	28.400	28.400	28.400	28.400	28.400	28.400	28.400	28.400	28.400	28.080
Lat [°N]	38.500	38.450	38.450	38.510	38.500	38.500						
SiO2 [wt.%]	47.76	47.07	46.84	49.74	47.26	48.03	46.75	46.28	47.95	46.64	47.64	45.90
TiO2 [wt.%]	3.05	2.77	2.64	2.21	2.49	2.49	2.63	3.10	2.66	2.69	2.66	2.98
Al2O3 [wt.%]	16.25	14.92	13.58	14.57	13.70	14.49	13.85	15.35	14.70	13.40	14.46	13.81
Fe2O3 [wt.%]	11.40	11.09	11.41	10.33	11.03	10.88	11.93	12.14	10.95	11.35	11.41	12.16
MnO [wt.%]	0.16	0.16	0.16	0.17	0.16	0.16	0.16	0.16	0.16	0.16	0.15	0.17
MgO [wt.%]	6.06	8.24	10.83	8.16	10.36	9.63	10.20	9.03	7.99	10.87	10.12	10.20
CaO [wt.%]	9.30	11.11	11.00	9.17	10.66	10.48	11.28	10.52	11.11	10.96	10.66	11.06
Na2O [wt.%]	3.69	3.43	3.02	4.12	2.94	3.13	2.62	3.00	3.59	2.94	2.78	2.59
K2O [wt.%]	1.52	1.18	1.01	1.59	0.96	1.01	0.91	0.87	1.19	0.96	0.76	0.98
P2O5 [wt.%]	0.59	0.47	0.41	0.45	0.37	0.40	0.40	0.46	0.46	0.41	0.36	0.45
Sc [ppm]	20.3	27.8	29.8	23.4	28.2	26.3	26.0	28.0	27.0	33.2	29.3	31.4
V [ppm]	218.0	266.5	250.7	185.3	248.2	242.3	230.0	245.0	251.0	263.2	241.7	275.3
Cr [ppm]	122.1	289.9	512.8	439.0	391.0	344.8	367.0	222.0	256.0	684.9	392.4	482.8
Co [ppm]	34.3	40.8	48.1	36.5	47.0	43.5	52.0	53.0	44.0	50.7	49.4	51.8
Ni [ppm]	63.5	115.9	206.4	140.3	220.0	180.1	154.0	134.0	100.0	242.2	201.9	227.8
Cu [ppm]	26.4	58.1	54.5	45.0	53.5	51.4	41.0	32.0	56.0	66.2	56.1	83.2
Zn [ppm]	106.5	78.8	79.1	91.4	78.0	79.5	87.0	98.0	89.0	89.8	96.5	95.5
Rb [ppm]	33.6	27.3	23.5	38.9	22.3	23.9	20.4	19.2	25.5	21.2	17.1	19.9
Sr [ppm]	715.5	624.2	546.5	546.8	524.5	526.9	522.0	597.0	580.0	542.2	505.0	589.0
Y [ppm]	29.3	26.5	24.6	28.4	23.6	24.8	27.0	29.0	28.7	26.9	25.2	27.8
Zr [ppm]	304.9	222.4	209.0	296.5	199.0	201.2	202.0	229.0	222.0	213.4	202.4	226.9
Nb [ppm]	48.2	43.1	38.6	52.4	36.4	37.6	35.1	38.0	39.7	40.1	34.4	44.3
Cs [ppm]	0.3	0.2	0.2	0.3	0.2	0.2				0.2	0.2	0.2
Ba [ppm]	389.3	315.1	265.0	405.0	260.3	271.2	286.0	227.0	303.0	274.1	209.8	278.0
La [ppm]	40.5	27.9	24.0	33.1	24.0	23.3	28.0		30.8	26.8	22.0	30.3
Ce [ppm]	90.0	60.7	53.5	70.4	53.2	52.1	60.9		65.8	56.9	47.2	64.7
Pr [ppm]	10.6	8.0	7.1	9.0	6.5	6.9				7.3	6.2	8.3
Nd [ppm]	42.9	32.5	29.4	34.5	26.7	28.3	31.8		33.6	30.6	26.1	34.0
Sm [ppm]	9.2	6.8	6.3	7.0	5.8	6.0	6.7		7.1	6.7	5.9	7.3
Eu [ppm]	2.9	2.2	2.1	2.2	1.9	2.0	2.2		2.3	2.1	1.9	2.3
Gd [ppm]	8.5	6.6	6.1	6.7	5.7	6.0				6.3	5.7	6.8
Tb [ppm]	1.2	1.0	0.9	1.0	0.9	0.9	1.0		1.0	0.9	0.8	0.9
Dy [ppm]	7.0	5.4	5.1	5.7	4.7	5.0				4.9	4.5	5.2
Ho [ppm]	1.3	1.0	0.9	1.0	0.9	0.9				0.8	0.8	0.9
Er [ppm]	3.2	2.5	2.3	2.7	2.2	2.4				2.3	2.1	2.5
Yb [ppm]	2.8	2.0	1.9	2.3	1.8	1.9	2.2		2.4	1.8	1.6	1.9
Lu [ppm]	0.4	0.3	0.3	0.3	0.3	0.3	0.3		0.3	0.1	0.1	0.1
Hf [ppm]	7.64	5.07	4.76	6.10	4.34	4.62	4.75		5.21	4.70	4.36	5.18
Ta [ppm]	3.47	2.43	2.21	2.97	2.16	2.13	2.44		2.69	2.67	2.26	3.08
Re [ppb]		0.2196	0.0767	0.1792	0.1086	0.0428						
Os [ppb]		0.0127	0.0197	0.0350	0.0228	0.0369	0.0045	0.0076	0.0095	0.0297	0.0229	
Pb [ppm]	2.60	2.20	1.79	2.96	1.57	1.75	5.00	3.00	6.00	1.89	1.45	1.98
Th [ppm]	3.87	2.95	2.51	3.92	2.36	2.46	2.85		3.19	2.66	2.18	3.06
U [ppm]	1.23	0.93	0.80	1.24	0.78	0.79	1.21		0.85	0.76	0.72	0.95
87Sr/86Sr	0.703793	0.703840	0.703803	0.703800	0.703788	0.703756	0.703759	0.703632	0.703828	0.703719	0.703521	0.703937
143Nd/144Nd	0.512919	0.512827	0.512813	0.512813	0.512818	0.512887	0.512879		0.512870		0.512931	
ε Nd	5.48	3.69	3.41	3.41	3.51	4.86	4.70		4.53		5.72	
206Pb/204Pb	19.69	19.67	19.65	19.71	19.59	19.54	19.62		19.76	19.48		
207Pb/204Pb	15.64	15.59	15.58	15.59	15.57	15.56	15.56		15.57	15.56		
208Pb/204Pb	39.39	39.15	39.09	39.19	39.00	38.95	38.82		39.18	38.92		
176Hf/177Hf										0.282993	0.283017	0.282994
ε Hf										4.69	5.54	4.73
187Os/188Os		0.126312	0.126703	0.124930	0.138634	0.120120	0.138850	0.129570	0.128110	0.127090	0.125840	
Nb/Zr	0.16	0.19	0.18	0.18	0.18	0.19	0.17	0.17	0.18	0.19	0.17	0.20
Nb/Ta	13.89	17.70	17.42	17.64	16.86	17.67	14.39		14.76	15.02	15.22	14.37
Zr/Hf	39.90	43.88	43.94	48.61	45.91	43.59	42.53		42.61	45.38	46.41	43.84
Ta/Hf	0.45	0.48	0.47	0.49	0.50	0.46	0.51		0.52	0.57	0.52	0.60

	SJ30	SJ31b	SM0104	SM0116	SM0121	SM0129	SM0133	SM0136	SM0145	SM0155	SM0161	SM0169
Island	Sao Jorge	Sao Jorge	Sao Miguel	Sao Miguel	Sao Miguel	Sao Miguel	Sao Miguel	Sao Miguel	Sao Miguel	Sao Miguel	Sao Miguel	Sao Miguel
Long [°W]	28.080	28.080	25.500	25.500	25.500	25.200	25.500	25.500	25.500	25.500	25.500	25.500
Lat [°N]	38.600	38.600	37.500	37.500	37.500	37.900	37.500	37.500	37.500	37.500	37.500	37.800
SiO2 [wt.%]	45.53	43.63	46.71	46.09	45.36	46.88	47.09	46.85	47.06	45.20	45.36	46.38
TiO2 [wt.%]	3.37	4.12	2.98	3.55	3.10	3.95	3.40	3.17	3.53	3.14	3.59	3.01
Al2O3 [wt.%]	14.88	15.58	14.05	14.74	12.60	14.52	13.33	11.89	13.92	12.00	13.05	12.90
Fe2O3 [wt.%]	12.56	13.76	10.94	11.81	11.53	13.36	11.60	11.47	12.12	11.98	12.44	11.83
MnO [wt.%]	0.17	0.17	0.18	0.18	0.17	0.17	0.17	0.17	0.17	0.17	0.18	0.17
MgO [wt.%]	9.70	8.91	7.51	6.85	10.72	4.85	8.60	10.63	8.47	11.11	9.14	8.84
CaO [wt.%]	10.48	10.47	9.96	9.92	11.01	8.18	11.03	11.96	9.26	11.36	10.81	8.93
Na2O [wt.%]	2.87	2.80	2.95	3.08	2.40	3.08	2.83	2.48	3.05	1.85	2.76	2.93
K2O [wt.%]	1.06	1.01	1.80	1.80	1.45	1.91	1.58	1.38	1.87	1.15	1.26	2.32
P2O5 [wt.%]	0.46	0.51	0.69	0.59	0.47	0.58	0.57	0.52	0.61	0.47	0.69	0.44
Sc [ppm]	25.1	24.4	20.2	22.4	30.0	18.8	28.1	28.4		30.5	24.4	17.7
V [ppm]	272.6	313.7	225.7	271.0	294.4	233.9	297.1	261.1		293.6	289.0	178.8
Cr [ppm]	306.5	175.9	344.3	161.6	670.8	134.3	449.5	662.1	439.0	483.5	405.0	321.5
Co [ppm]	52.7	54.5	35.8	40.8	53.2	37.0	44.9	47.4		59.7	47.1	44.8
Ni [ppm]	150.9	105.1	117.0	57.4	247.4	53.1	121.8	197.7	145.0	228.2	138.8	140.9
Cu [ppm]	47.9	32.9	54.8	43.8	96.8	51.4	67.8	87.7		85.4	36.7	55.3
Zn [ppm]	101.3	99.1	100.8	104.4	90.1	122.2	98.7	88.4	113.0	93.0	99.0	91.0
Rb [ppm]	24.6	22.8	39.8	40.9	35.3	78.3	39.0	31.6	45.0	28.1	33.1	60.7
Sr [ppm]	608.4	700.9	785.9	833.4	666.1	660.0	714.6	637.9	714.0	639.7	797.5	551.3
Y [ppm]	26.1	27.6	28.7	26.3	24.6	42.9	28.2	21.7		23.8	25.4	27.2
Zr [ppm]	255.3	258.7	321.2	335.9	215.5	366.8	305.5	237.6	346.0	237.2	247.7	350.2
Nb [ppm]	49.1	50.6	73.5	74.1	49.6	66.8	60.7	56.5		48.6	57.4	61.9
Cs [ppm]	0.2	0.2	0.4	0.3	0.3	4.4	0.2	0.3		0.3	0.3	0.6
Ba [ppm]	267.8	246.9	570.9	501.7	456.1	798.0	517.8	380.7	732.0	394.2	493.7	379.1
La [ppm]	26.4	29.0	50.5	48.8	35.4	61.1	42.5	37.0		34.5	40.9	50.5
Ce [ppm]	59.4	66.6	105.8	102.4	72.9	120.9	88.3	78.9		72.4	86.5	104.4
Pr [ppm]	7.9	8.9	12.9	12.5	9.1	15.9	11.0	9.7		9.1	10.8	12.7
Nd [ppm]	33.2	36.6	51.2	49.2	36.5	63.3	44.1	39.1		36.6	44.3	49.0
Sm [ppm]	7.1	7.8	10.2	9.6	7.5	13.0	8.8	7.9		7.4	9.0	9.8
Eu [ppm]	2.3	2.5	3.0	2.9	2.3	3.9	2.7	2.4		2.3	2.8	2.7
Gd [ppm]	6.9	7.3	8.6	8.1	6.4	11.8	7.5	6.6		6.4	7.6	8.5
Tb [ppm]	1.0	1.1	1.2	1.1	0.9	1.7	1.1	0.9		0.9	1.1	1.3
Dy [ppm]	5.6	5.7	6.4	5.9	4.8	9.4	5.6	4.8		4.7	5.6	6.7
Ho [ppm]	1.0	1.0	1.2	1.1	0.9	1.7	1.0	0.9		0.8	1.0	1.2
Er [ppm]	2.5	2.6	2.9	2.6	2.1	4.4	2.4	2.1		2.1	2.5	3.0
Yb [ppm]	2.0	2.0	2.3	2.1	1.7	3.6	1.9	1.6		1.6	1.9	2.5
Lu [ppm]	0.3	0.3	0.3	0.3	0.2	0.5	0.3	0.2		0.2	0.3	0.3
Hf [ppm]	5.46	6.03	7.59	7.71	5.22	10.03	6.33	6.01		5.09	5.94	9.48
Ta [ppm]	2.87	3.17	4.67	4.72	2.99	4.55	3.64	3.58		3.01	3.65	4.30
Re [ppb]	0.0846											
Os [ppb]	0.0076											
Pb [ppm]	1.57	1.44	2.46	2.22	1.92	3.68	2.04	1.64		1.40	1.80	3.82
Th [ppm]	2.67	2.68	5.81	5.33	3.85	7.28	4.57	3.87		3.79	4.06	7.43
U [ppm]	0.87	1.00	1.38	1.53	1.00	1.78	1.24	1.14		1.01	1.06	1.94
87Sr/86Sr	0.703502	0.703481	0.703534	0.703336		0.705338	0.703274	0.703397	0.704364		0.703604	0.704673
143Nd/144Nd	0.512831	0.512835	0.512900	0.512919		0.512699	0.512919	0.512918	0.512800		0.512906	0.512754
ε Nd	3.76	3.84	5.11	5.48		1.19	5.48	5.46	3.16		5.23	2.26
206Pb/204Pb	19.63	19.82				20.01	19.45					
207Pb/204Pb	15.56	15.62				15.75	15.58					
208Pb/204Pb	39.04	39.27				40.24	39.24					
176Hf/177Hf			0.282987	0.282996	0.282990	0.282787	0.283008	0.283004	0.282872	0.282979	0.282965	0.282825
ε Hf			4.49	4.81	4.60	-2.58	5.23	5.09	0.42	4.21	3.71	-1.24
187Os/188Os	0.200000											
Nb/Zr	0.19	0.20	0.23	0.22	0.23	0.18	0.20	0.24		0.20	0.23	0.18
Nb/Ta	17.11	15.96	15.74	15.71	16.61	14.68	16.69	15.77		16.15	15.73	14.40
Zr/Hf	46.78	42.91	42.31	43.58	41.24	36.57	48.24	39.55		46.56	41.71	36.95
Ta/Hf	0.53	0.53	0.62	0.61	0.57	0.45	0.57	0.60		0.59	0.61	0.45

	SM0171	SM0203	SM0204	SM160501-	SM9704-a	SM9716	SP2	SP8	S1	S10	S19	S3
Island	Sao Miguel	Sao Miguel	Sao Miguel	Sao Miguel	Sao Miguel	Sao Miguel	Sao Miguel	Sao Miguel	Sao Miguel	Sao Miguel	Sao Miguel	Sao Miguel
Long [°W]	25.300	25.700	25.600	25.500	25.700	25.700	25.670	25.670	25.670	25.670	25.670	25.670
Lat [°N]	37.500	37.800	37.800	37.500	37.800	37.800			37.440			
SiO2 [wt.%]	45.40	46.56	44.63	46.17	45.71	48.33	45.53	48.09	45.31	45.12	54.49	46.43
TiO2 [wt.%]	3.83	2.43	3.54	3.49	3.44	3.92	4.07	2.94	4.09	3.76	2.11	3.59
Al2O3 [wt.%]	14.16	12.52	11.84	14.18	12.76	14.69	13.89	13.49	14.11	14.02	14.96	14.22
Fe2O3 [wt.%]	13.09	11.18	13.14	12.01	12.75	13.06	13.59	11.89	13.76	13.07	8.00	12.88
MnO [wt.%]	0.18	0.16	0.17	0.17	0.17	0.16	0.18	0.17	0.17	0.17	0.15	0.17
MgO [wt.%]	7.68	10.42	10.41	6.38	9.81	5.52	7.93	9.10	7.76	8.33	6.38	8.34
CaO [wt.%]	9.30	11.58	11.90	10.76	11.14	8.80	10.36	8.69	10.41	10.81	5.50	9.47
Na2O [wt.%]	2.85	2.67	1.92	3.02	2.55	2.98	3.09	3.17	3.16	2.87	4.26	3.24
K2O [wt.%]	1.86	1.15	1.24	1.47	1.06	2.08	1.69	2.49	1.70	1.75	4.26	1.87
P2O5 [wt.%]	0.66	0.40	0.41	0.52	0.52	0.54	0.59	0.43	0.58	0.66	0.43	0.64
Sc [ppm]	22.4	31.2	35.3	22.2	19.9	19.2	25.0	21.6	24.8	27.5	13.4	21.2
V [ppm]	285.6	262.0	320.8	298.7			299.1	230.9	289.8	313.0	129.3	260.7
Cr [ppm]	182.8	787.8	577.7	211.3	670.0	152.0	297.5	358.1	269.9	315.0	223.1	280.8
Co [ppm]	47.4	50.3	57.5	41.9	48.6	40.0	49.1	51.6	47.3	50.4	27.3	46.3
Ni [ppm]	122.7	211.9	113.9	77.1	185.0	95.0	103.2	158.8	94.5	112.3	151.1	149.1
Cu [ppm]	46.6	86.2	27.1	95.3	25.9	28.1	79.9	75.9	67.4	82.4	40.5	67.7
Zn [ppm]	118.3	89.7	99.2	109.7	82.6	99.5	116.7	101.5	112.5	109.1	96.9	116.1
Rb [ppm]	46.1	33.3	35.5	20.6	22.6	55.3	47.3	67.8	45.6	45.8	83.1	51.4
Sr [ppm]	844.5	527.2	549.9	732.9	615.0	624.0	766.3	536.6	761.0	759.4	497.7	819.3
Y [ppm]	34.0	25.8	25.8	26.6	23.2	38.8	30.6	27.9	30.9	28.0	29.2	31.0
Zr [ppm]	359.6	176.8	252.7	304.9	207.0	389.0	345.9	377.7	330.6	331.8	452.0	373.7
Nb [ppm]	65.0	40.9	42.9	68.1	45.7	62.4	74.4	72.7	70.7	68.8	87.4	77.9
Cs [ppm]	0.4	0.4	0.4	0.3	0.1	0.2	0.4	0.6	0.3	0.3	0.5	0.5
Ba [ppm]	540.6	410.8	372.6	483.9	359.0	487.0	486.8	353.2	494.0	485.1	767.4	530.8
La [ppm]	50.9	28.0	32.2	45.5	30.5	59.1	42.3	44.8	41.8	42.1	58.5	47.5
Ce [ppm]	117.9	57.8	67.7	91.0	64.6	112.0	92.6	93.1	91.8	89.8	118.7	101.7
Pr [ppm]	13.4	7.3	8.6	11.1	8.0	13.6	12.1	11.6	12.1	11.6	14.6	13.2
Nd [ppm]	53.6	29.5	35.1	43.8	33.5	53.0	48.8	43.7	49.0	46.2	54.0	51.8
Sm [ppm]	10.7	6.4	7.4	8.7	7.1	10.5	9.9	8.5	10.0	9.1	9.7	10.2
Eu [ppm]	3.2	2.0	2.3	2.6	2.2	3.0	3.1	2.4	3.1	2.9	3.0	3.2
Gd [ppm]	8.9	5.9	6.6	7.5	6.6	9.8	8.9	7.6	9.0	8.2	8.3	9.1
Tb [ppm]	1.3	0.9	1.0	1.1	0.9	1.3	1.3	1.2	1.4	1.2	1.3	1.4
Dy [ppm]	6.6	4.9	5.1	5.7	5.0	7.7	6.8	6.0	6.9	6.3	6.4	6.9
Ho [ppm]	1.2	0.9	0.9	1.0	0.9	1.4	1.2	1.1	1.2	1.1	1.1	1.2
Er [ppm]	2.9	2.2	2.2	2.6	2.2	3.7	2.9	2.7	3.0	2.7	2.8	3.0
Yb [ppm]	2.2	1.8	1.7	2.0	1.7	3.1	2.3	2.2	2.3	2.1	2.3	2.3
Lu [ppm]	0.3	0.3	0.2	0.3	0.2	0.4	0.3	0.3	0.3	0.3	0.3	0.3
Hf [ppm]	7.55	4.37	5.68	6.98	5.36	8.99	7.58	7.82	7.76	6.99	8.64	8.04
Ta [ppm]	3.92	2.47	2.72	4.23	3.04	4.18	4.27	4.09	4.25	3.97	4.71	4.48
Re [ppb]							0.7233	0.2708	0.3474	0.3803		0.3590
Os [ppb]							0.0226	0.0580	0.0252	0.0173		0.0797
Pb [ppm]	2.80	1.85	1.42	2.30	1.93	3.46	2.66	3.91	2.66	2.90	4.80	3.04
Th [ppm]	5.25	3.33	3.95	5.80	3.67	6.98	4.57	6.43	4.54	4.84	7.27	5.04
U [ppm]	1.35	0.89	1.03	1.63	1.08	1.59	1.27	1.77	1.25	1.27	1.89	1.44
87Sr/86Sr	0.704497		0.704264	0.703627	0.703743	0.706210	0.704220	0.704785	0.704255	0.704362	0.704990	0.704524
143Nd/144Nd	0.512783	0.512923	0.512812	0.512910	0.512887	0.512678	0.512729	0.512650	0.512739	0.512774	0.512620	0.512685
ε Nd	2.83	5.56	3.39	5.31	4.86	0.78	1.78	0.23	1.97	2.65	-0.35	0.92
206Pb/204Pb		19.50	19.69		19.65	20.16	19.75	19.79	19.72	19.81	19.99	19.76
207Pb/204Pb		15.59	15.68		15.63	15.80	15.66	15.67	15.65	15.71	15.74	15.67
208Pb/204Pb		39.23	39.75		39.51	40.43	39.39	39.87	39.74	39.97	40.16	39.88
176Hf/177Hf	0.282867		0.282897	0.282978	0.282986							
ε Hf	0.25		1.31	4.17	4.45							
187Os/188Os							0.133381	0.134128	0.135279	0.141963		0.135171
Nb/Zr	0.18	0.23	0.17	0.22	0.22	0.16	0.22	0.19	0.21	0.21	0.19	0.21
Nb/Ta	16.59	16.57	15.76	16.12	15.03	14.93	17.41	17.77	16.63	17.34	18.57	17.37
Zr/Hf	47.61	40.48	44.52	43.68	38.62	43.27	45.64	48.31	42.61	47.45	52.30	46.47
Ta/Hf	0.52	0.57	0.48	0.61	0.57	0.46	0.56	0.52	0.55	0.57	0.54	0.56

	S7	PK91 S4	PK92-S36	PK92-S41	DR21-3	DR17-3	DR22-6	DR29-1
Island	Sao Miguel	Sao Miguel	Sao Miguel	Sao Miguel	MAR	MAR	MAR	MAR
Long [°W]	25.670	25.670	25.670	25.670	30.267	31.518	30.025	29.846
Lat [°N]					38.49	37.838	39.039	39.432
SiO2 [wt.%]	45.83	43.58	47.62	46.91	51.3	49.09	52.28	51.84
TiO2 [wt.%]	3.96	3.64	3.81	3.18	2.14	1.28	1.66	1.59
Al2O3 [wt.%]	15.15	13.85	14.71	14.14	15.88	16.1	15.18	15.91
Fe2O3 [wt.%]	13.51	13.36	12.93	11.70	10.61	8.51	10.4	10.31
MnO [wt.%]	0.17	0.18	0.17	0.17				
MgO [wt.%]	6.69	8.11	6.86	8.32	5.77	8.46	6.66	6.76
CaO [wt.%]	9.52	12.95	9.31	11.72	11	14.04	11.19	10.8
Na2O [wt.%]	3.42	2.87	2.95	2.83	3.53	2.42	2.58	2.82
K2O [wt.%]	1.88	1.21	1.90	1.42				
P2O5 [wt.%]	0.69	0.51	0.52	0.55				
Sc [ppm]	20.5	29.0	20.0	27.0	25.3	36.45	31.29	31.23
V [ppm]	282.5	312.0	280.0	277.0	230.31	223.38	268.85	214.47
Cr [ppm]	126.7	183.0	156.0	342.0	110.99	325	93.8	273.71
Co [ppm]	43.5	54.0	50.0	44.0	31.05	37.98	37.79	35.89
Ni [ppm]	67.9	94.0	119.0	11.0	52.23	117.05	55.03	112.84
Cu [ppm]	58.4	68.0	68.0	52.0	45.57	67.83	44.54	53.06
Zn [ppm]	120.3	90.0	99.0	85.0	90.95	53.93	70.37	65.83
Rb [ppm]	46.8	30.2	48.9	33.4	17.56	16.14	14.96	13.44
Sr [ppm]	882.6	683.0	634.0	673.0	326.82	258.38	237.34	255.44
Y [ppm]	32.7	30.3	38.7	29.9	24.55	19.1	23.8	20.03
Zr [ppm]	368.9	193.0	322.0	236.0	156.97	82.44	119.01	109.96
Nb [ppm]	78.9	41.9	55.2	52.6	29.45	24.83	27.2	24.11
Cs [ppm]	0.4	0.5	0.4	0.5	0.19	0.21	0.16	0.15
Ba [ppm]	532.4	381.0	461.0	436.0	230.68	224.3	212.18	162.92
La [ppm]	48.9	31.0	46.2	37.9	19.77	14.2	16.92	14.84
Ce [ppm]	105.4	64.7	100.0	78.9	41.7	28.06	35.51	30.91
Pr [ppm]	13.8				5.33	3.49	4.49	3.96
Nd [ppm]	54.6	36.0	48.8	40.0	21.96	14.2	18.35	16.32
Sm [ppm]	10.8	8.0	9.4	8.3	4.88	3.25	4.14	3.7
Eu [ppm]	3.3	2.6	2.9	2.6	1.57	1.11	1.35	1.23
Gd [ppm]	9.6				4.92	3.41	4.34	3.79
Tb [ppm]	1.4	1.1	1.3	1.1	0.76	0.54	0.69	0.6
Dy [ppm]	7.3				4.37	3.23	4.11	3.46
Ho [ppm]	1.2				0.88	0.67	0.86	0.7
Er [ppm]	3.1				2.4	1.87	2.37	1.94
Yb [ppm]	2.4	2.2	2.7	2.4	2.08	1.68	2.12	1.69
Lu [ppm]	0.4	0.3	0.4	0.3	0.31	0.25	0.31	0.25
Hf [ppm]	7.79	4.87	7.59	5.66	3.57	1.95	2.87	2.56
Ta [ppm]	4.49	2.87	4.12	3.68	1.55	1.28	1.56	1.41
Re [ppb]								
Os [ppb]					0.0110	0.0070	0.0040	0.0080
Pb [ppm]	2.79	6.00	8.00	4.00	1.69	0.77	1.2	1.22
Th [ppm]	4.95	2.95	6.03	4.12	2.45	1.97	2	1.79
U [ppm]	1.38	1.75	1.50	1.42	0.78	0.55	0.57	0.54
87Sr/86Sr	0.704443	0.703928	0.705360	0.703687	0.703372	0.703212	0.703434	0.703335
143Nd/144Nd	0.512785				0.51295	0.51299	0.51296	0.51296
ε Nd	2.87							
206Pb/204Pb	19.80	19.57	20.11	19.49	19.64	19.14	19.45	19.42
207Pb/204Pb	15.66	15.58	15.75	15.55	15.62	15.59	15.62	15.61
208Pb/204Pb	39.80	39.31	40.29	39.13	39.12	38.78	39.15	39.04
176Hf/177Hf								
ε Hf								
187Os/188Os					0.205337	0.329336	0.388548	0.5278517
Nb/Zr	0.21	0.22	0.17	0.22	0.19	0.3	0.23	0.22
Nb/Ta	17.59	14.60	13.40	14.29	19.00	19.40	17.44	17.10
Zr/Hf	47.34	39.63	42.42	41.70	43.97	42.28	41.47	42.95
Ta/Hf	0.58	0.59	0.54	0.65	0.43	0.66	0.54	0.55

Supplemental table 1 - Santa Maria: (Chapter 6)

Comprehensive major element, trace element and Sr-Nd-Pb isotope ratios of the Santa Maria lavas. Samples marked in italics were measured at Activation laboratories (Canada) for major and trace elements, all other samples were measured in Erlangen for major elements and at the University of Kiel for trace elements as described in the main text. In cases where only V, Cr, Co, Ni, Cu, Zn, Rb, Sr, Y, Zr, Nb, Ba are available as trace elements, these were measured by XRF as described in the main text. Fe_2O_3 values in bold are calculated from FeO^T electron microprobe measurements (Fe_2O_3=1.1113 * FeO).

Supplemental Table 1: Comprehensive major element, trace element and Sr-Nd-Pb isotope ratios of the Santa Maria lavas. Samples marked in italics were measured at Activation laboratories (Canada) for major and trace elements, all other samples were measured in Erlangen for major elements and at the University of Kiel for trace elements as described in the main text. In cases where only V, Cr, Co, Ni, Cu, Zn, Rb, Sr, Y, Zr, Nb, Ba are available as trace elements, these were measured by XRF as described in the main text. Fe_2O_3 values in bold are calculated from FeOT electron microprobe measurements

Sample	Locality	WR/GL	Lat [°N]	Long [°W]	SiO_2 [wt.%]	TiO_2 [wt.%]	Al_2O_3 [wt.%]	$Fe_2O_3^T$ [wt.%]	MnO [wt.%]	MgO [wt.%]	CaO [wt.%]	Na_2O [wt.%]	K_2O [wt.%]	P_2O_5 [wt.%]	SO_3 [wt.%]	Cl [wt.%]	F [wt.%]	LOI	Total
MA09-001	Praia	WR	36.952	25.102	53.40	1.61	19.07	7.14	0.16	1.95	5.08	4.67	4.16	0.53				0.76	98.53
MA09-002	Anjos	WR	37.005	25.160	43.90	2.24	11.60	11.53	0.15	12.60	12.69	1.77	1.01	0.34				1.01	98.84
MA09-004	Anjos	WR	37.009	25.148	43.30	2.18	11.51	11.70	0.17	13.83	11.90	2.01	0.61	0.35				1.23	98.79
MA09-005	Barreiros	WR	36.957	25.094	42.60	2.40	13.99	12.34	0.16	10.01	12.17	3.23	0.62	0.47				1.28	99.27
MA09-006	Ponta da Malbusca	WR	36.931	25.065	42.70	2.55	14.17	12.43	0.19	9.92	10.95	3.58	1.12	0.51				0.66	98.78
MA09-009	Ponta da Malbusca	WR	36.932	25.066	42.70	2.42	14.29	12.77	0.20	9.71	11.05	4.18	0.77	0.53				0.72	99.34
MA09-010A	Castelo	GL	36.929	25.018	44.17	2.76	16.80	**13.52**	0.22	4.38	11.10	4.63	2.47	0.55	0.02	0.11	0.07		100.80
MA09-010B	Castelo	GL	36.929	25.018	44.50	2.75	17.03	**13.72**	0.22	4.33	10.97	4.09	2.54	0.55	0.02	0.11	0.08		100.91
MA09-012	Castelo	GL	36.929	25.016	43.54	2.77	17.00	**13.65**	0.21	4.30	11.42	5.08	2.41	0.55	0.02	0.10	0.11		101.16
MA09-013	Castelo	GL	36.929	25.016	43.70	2.76	17.05	**13.85**	0.22	4.25	11.17	4.97	2.46	0.55	0.02	0.11	0.07		101.18
MA09-014	Castelo	WR	36.930	25.017	43.60	2.48	14.67	12.04	0.20	8.84	9.97	4.13	1.23	0.54				1.54	99.24
MA09-015	Castelo	WR	36.930	25.018	44.10	2.52	14.77	12.46	0.20	7.56	10.20	4.75	1.14	0.59				0.94	99.23
MA09-016	Lourenco	GL	36.986	25.049	45.65	2.36	18.24	**13.12**	0.22	3.32	9.36	5.24	2.75	0.56	0.02	0.12	0.11		101.07
MA09-019	Pico Alto	WR	36.979	25.091	42.50	2.39	12.75	12.85	0.18	11.89	12.54	2.18	0.53	0.31				0.10	98.22
MA09-023	Praia	WR	36.953	25.095	44.00	3.70	16.76	14.23	0.15	3.87	8.84	1.97	1.61	0.58				4.07	99.78
MA09-027	Vila do Porto	WR	36.945	25.151	43.70	2.72	14.85	12.37	0.15	8.83	11.94	1.97	1.23	0.40				1.10	99.26
MA09-031	Vila do Porto	WR	36.945	25.151	44.10	2.84	16.30	12.37	0.16	6.28	11.79	2.69	1.58	0.47				0.64	99.22
MA09-032A	Vila do Porto	WR	36.944	25.151	49.50	1.74	18.04	9.39	0.15	3.66	6.84	3.70	3.04	0.58				2.67	99.31
MA09-042	Lagoinhas Top	WR	37.008	25.088	43.10	2.45	13.52	12.19	0.17	11.53	11.34	3.09	0.57	0.45				0.93	99.34
MA09-043	Lagoinhas	WR	37.013	25.083	45.10	2.59	14.38	12.12	0.17	8.46	11.83	2.73	1.15	0.34				0.55	99.42
MA09-046	Lagoinhas	WR	37.011	25.083	44.80	3.23	14.89	13.06	0.18	4.96	12.06	1.61	0.55	0.57				3.45	99.36
MA09-047	Lagoinhas	WR	37.011	25.085	41.20	2.44	12.83	12.35	0.18	12.98	11.57	2.51	1.37	0.43				1.10	98.96
MA09-048	Lagoinhas	WR	37.011	25.086	41.00	2.45	12.75	12.25	0.17	12.72	12.52	2.05	1.20	0.44				1.78	99.33
MA09-049	Lagoinhas Top	WR	37.010	25.086	42.40	2.54	12.96	12.90	0.18	11.65	11.64	3.19	0.60	0.52				0.69	99.27
MA09-050	Lagoinhas Top	WR	37.010	25.087	42.40	2.53	13.01	13.00	0.18	11.34	11.75	3.21	0.48	0.54				0.85	99.29
MA09-057	Monte Gordo	GL	37.001	25.135	43.71	2.56	16.77	**12.60**	0.21	5.35	13.18	4.27	2.02	0.55	0.02	0.09	0.07		101.40
MA09-063	Monte Gordo	GI	37.001	25.134	44.37	2.12	17.83	**12.22**	0.23	3.84	10.19	5.55	2.86	0.55	0.02	0.19	0.10		100.07
MA09-075	Cavacas	WR	36.958	25.078	43.10	2.64	12.12	13.15	0.17	13.32	12.13	1.56	1.03	0.32				0.69	100.23
MA09-079	Barreiros	WR	36.955	25.080	42.60	2.19	12.98	11.83	0.17	12.81	12.07	2.63	0.45	0.39				0.97	99.09
MA09-081	North of Malbusca	WR	36.953	25.072	43.20	2.43	12.43	13.52	0.18	11.80	11.38	1.29	0.92	0.33				1.86	99.34
MA09-086D	Malbusca	WR	36.948	25.082	43.20	2.48	13.23	12.03	0.18	11.21	11.24	3.05	0.97	0.47				0.54	98.60
MA09-089	Praia East	WR	36.945	25.084	44.90	2.35	15.18	11.41	0.19	7.94	9.72	3.67	1.25	0.50				2.51	99.62
MA09-093	Barreiros	WR	36.957	25.093	42.60	2.21	13.19	11.85	0.17	11.95	12.26	2.42	1.05	0.40				0.58	98.68
MA09-094	Barreiros	WR	36.957	25.094	42.70	2.37	13.91	12.16	0.17	9.87	11.95	3.56	0.54	0.48				1.32	99.03
MA09-101	Ponta da Malbusca	WR	36.930	25.063	43.30	2.51	13.53	12.32	0.19	11.70	10.73	2.76	1.26	0.46				0.68	99.44
MA09-103	Ponta da Malbusca	GL	36.929	25.063	44.74	2.84	16.13	**13.52**	0.19	5.09	11.97	4.15	1.84	0.55	0.02	0.07	0.06		101.17
MA09-105	Ponta da Malbusca	WR	36.931	25.063	41.20	2.16	12.36	12.78	0.17	13.38	11.43	2.51	0.66	0.45				2.27	99.37
MA09-106	North of Malbusca	WR	36.944	25.062	44.10	2.69	14.82	12.43	0.20	7.14	10.35	3.98	0.76	0.59				1.42	98.48
MA09-107	Rio do Farropo	WR	36.958	25.088	49.40	2.37	8.87	13.96	0.10	7.83	11.29	0.99	0.91	0.16				3.09	98.97
MA09-108	Barreiros	WR	36.954	25.087	42.30	2.33	13.57	11.88	0.18	11.51	11.74	3.32	0.52	0.46				0.67	98.48
MA09-114	Castelo	WR	36.930	25.017	43.80	2.48	14.81	12.07	0.20	7.88	9.91	3.45	2.28	0.56				1.87	99.31
MA09-116A	Ponta da Malbusca	WR	36.930	25.063	42.40	2.55	13.07	12.75	0.17	11.85	11.09	2.38	0.68	0.50				1.57	99.01
MA09-116B	Ponta da Malbusca	GI	36.930	25.063	44.60	2.87	16.41	**14.25**	0.22	4.70	11.24	3.82	1.97	0.55	0.02	0.07	0.08		100.80
MA09-117	Ponta da Malbusca	WR	36.930	25.063	43.30	2.33	14.05	11.95	0.20	9.73	10.82	3.47	1.16	0.49				1.63	99.13
MA09-118B	Ponta da Malbusca	GL	36.930	25.063	44.26	2.13	17.67	**12.64**	0.22	4.29	11.06	5.24	2.71	0.55	0.02	0.12	0.11		101.02
MA09-119	Rio do Farropo	WR	36.959	25.088	49.40	1.21	19.21	8.57	0.22	2.78	5.61	4.53	3.70	0.36				3.30	98.89
MA09-121A	Praia	GL	36.946	25.085	45.26	3.45	16.67	**15.07**	0.25	3.64	9.09	4.28	2.63	0.55	0.02	0.13	0.12		101.16
MA09-121B	Praia	GI	36.946	25.085	45.17	3.48	16.44	**14.12**	0.21	4.04	10.17	4.46	2.36	0.55	0.02	0.12	0.14		101.28
MA09-122	Malbusca	WR	36.944	25.080	42.60	2.33	13.25	12.74	0.19	11.54	11.38	3.08	0.63	0.50				1.10	99.34
SMA09-006	Praia	WR	36.952	25.106	43.80	3.15	16.62	10.87	0.20	4.44	11.94	2.91	1.29	0.62				3.45	99.29
SMA09-011	Praia	WR	36.953	25.100	45.40	2.79	12.00	14.78	0.10	6.55	11.90	0.96	0.39	0.45				4.24	99.56
SMA09-012	Praia	WR	36.952	25.108	43.20	3.27	15.00	11.73	0.14	6.81	11.39	2.13	0.75	0.62				4.60	99.64
SMA09-015	Praia	WR	36.951	25.109	42.30	3.31	14.66	13.22	0.18	7.64	12.35	1.75	0.76	0.49				3.09	99.75
SMA09-037	Pico Facho	WR	36.952	25.122	42.60	2.26	13.28	12.56	0.19	11.21	11.42	3.64	0.62	0.54				0.93	99.25
SMA09-040	Pico Facho	WR	36.946	25.134	42.50	2.24	14.00	12.61	0.21	9.61	11.54	3.95	1.47	0.58				0.86	99.57
SMA09-049	Vila do Porto	WR	36.940	25.141	43.80	3.31	17.24	12.29	0.20	5.21	9.56	3.85	1.93	0.67				1.71	99.77
SMA09-051	Vila do Porto	WR	36.944	25.144	42.20	3.43	15.87	12.83	0.19	6.93	10.80	3.15	1.79	0.69				1.66	99.54
SMA09-058	Pico Facho	WR	36.944	25.133	41.30	3.42	14.67	13.36	0.19	7.58	12.35	2.40	1.30	0.61				2.20	99.38
SMA09-059	Pico Facho	WR	36.948	25.133	41.90	2.21	14.20	12.61	0.21	9.20	10.95	4.00	0.93	0.64				2.80	99.65
SMA09-097	Praia	WR	36.957	25.107	42.50	2.37	13.38	12.40	0.17	10.41	11.77	3.92	0.72	0.61				0.93	99.18
SMA09-109	Praia	WR	36.953	25.102	48.90	2.43	17.45	8.94	0.10	4.38	8.94	2.65	2.76	0.54				2.65	99.74

Sample	Sc	V	Cr	Co	Ni	Cu	Zn	Mo	Rb	Sr	Y	Zr	Nb	Cs	Ba	La	Ce	Pr	Nd	Sm	Eu	Gd	Tb	Dy	Ho	Er	Tm	Yb	Lu	Hf	Ta	Pb	Th	U
MA09-001	4.06	62.3	14.2	16.5	31.5	14.4		3.29	147	715	32.4	485	111	1.95	1093	74.6	133	13.7	48.0	7.96	2.40	7.15	1.02	5.47	1.05	2.90	0.416	2.74	0.403	9.20	6.78	6.38	14.1	2.53
MA09-002	40.64	283	723	62.0	296	59.3		1.63	21.9	494	17.9	169	37.8	0.275	347	26.9	55.4	6.67	27.0	5.50	1.78	5.14	0.728	3.79	0.673	1.68	0.219	1.35	0.189	3.95	2.31	1.71	3.01	0.768
MA09-004		278	703	64	288		87		7	474	23	164	33		353																			
MA09-005		274	521	54	229		89		9	648	28	195	44		452																			
MA09-006	26.43	265	472	55.9	206	55.3		3.07	18.1	781	24.7	258	62.0	0.635	642	41.2	81.0	9.47	37.5	7.48	2.39	6.92	0.986	5.14	0.922	2.29	0.300	1.87	0.265	5.48	3.66	2.52	4.84	1.20
MA09-009		255	484	54.0	197		88	4.00	16.0	754	31.0	203	60.0		638																			
MA09-010A	33.38	272	514	60.3	259	70.0		2.15	34.8	604	23.5	171	45.1	0.376	472	29.8	60.1	7.24	29.8	6.36	2.09	6.16	0.903	4.83	0.873	2.18	0.286	1.75	0.247	3.93	2.57	1.85	3.19	0.830
MA09-010B																																		
MA09-012																																		
MA09-013																																		
MA09-014	21.65	223	410	46.3	145	49.4		3.40	24.3	965	26.0	270	68.5	0.621	806	49.1	96.5	10.9	42.4	8.09	2.59	7.42	1.040	5.38	0.950	2.39	0.314	1.95	0.273	5.46	3.79	3.02	4.82	1.31
MA09-015	22.03	243	413	47.2	146	49.1		3.12	14.2	993	26.4	271	68.8	0.953	827	49.8	97.7	11.1	43.0	8.26	2.63	7.55	1.063	5.45	0.964	2.42	0.319	1.97	0.279	5.47	3.81	3.69	4.90	1.22
MA09-016																																		
MA09-019	35.86	300	572	66.9	238	58.3		1.57	15.6	533	20.7	160	30.4	0.449	338	21.4	45.7	5.75	24.6	5.56	1.85	5.45	0.812	4.37	0.781	1.93	0.251	1.55	0.218	3.97	1.86	1.51	2.19	0.587
MA09-023		337	67	48	137		95		31	622	30	258	85		672																			
MA09-027		321	234	52	160		95		27	588	26	196	41		410																			
MA09-031	22.08	306	88.3	46.3	75.8	97.2		2.40	40.8	728	23.5	226	53.3	0.413	523	37.8	77.4	9.21	36.8	7.30	2.38	6.68	0.953	4.92	0.883	2.19	0.287	1.78	0.249	5.01	3.23	2.36	4.19	1.059
MA09-032A	6.17	87.2	37.9	18.3	21.3	16.6		2.12	78.8	855	31.1	467	102	0.524	814	71.8	137	15.2	55.2	9.31	2.84	8.10	1.15	6.03	1.12	3.03	0.421	2.78	0.402	9.03	6.32	5.54	9.12	1.46
MA09-042	30.15	276	594	57.9	260	58.4		2.27	27.8	651	23.8	219	52.0	0.440	506	36.5	73.3	8.68	34.9	7.04	2.26	6.56	0.938	4.95	0.884	2.23	0.290	1.79	0.251	4.82	3.03	0.91	3.87	0.980
MA09-043	31.16	284	282	50.6	152	90.2		1.93	25.8	527	24.0	196	35.6	0.286	347	25.3	54.5	6.81	28.9	6.37	2.12	6.29	0.929	5.02	0.904	2.26	0.297	1.81	0.254	4.72	2.15	1.85	2.68	0.760
MA09-046		330	421	51	125		109		7	816	35	261	64		525																			
MA09-047	29.21	269	635	64.3	289	60.0		1.99	52.0	618	21.3	183	42.9	0.312	438	29.2	60.7	7.40	30.9	6.46	2.11	6.11	0.880	4.60	0.812	1.98	0.251	1.53	0.213	4.20	2.51	2.03	2.99	0.823
MA09-048		279	647	67	278		89		36	581	25	178	37		490																			
MA09-049	29.43	276	587	60.9	271	66.6		2.65	24.0	724	23.2	201	49.2	0.787	517	36.5	74.4	8.94	36.4	7.46	2.39	6.94	0.985	5.02	0.872	2.13	0.269	1.60	0.222	4.56	2.82	2.32	3.52	0.842
MA09-050	29.38	272	606	61.2	265	60.9		2.52	14.4	714	23.3	199	48.7	0.874	571	36.4	74.4	8.93	36.5	7.45	2.41	6.94	0.982	5.04	0.880	2.13	0.273	1.62	0.225	4.53	2.80	2.24	3.55	0.880
MA09-057																																		
MA09-063																																		
MA09-075		317	800	66	344		93		28	504	25	171	30		521																			
MA09-079		269	794	64	304		87		5	541	40	171	36		517																			
MA09-081		315	714	77	330		102		24	316	28	168	31		502																			
MA09-086D	28.76	259	712	56.0	267	64.9		2.81	18.0	682	24.1	235	55.4	0.532	504	36.9	74.1	8.78	35.2	7.17	2.31	6.72	0.965	5.07	0.905	2.25	0.295	1.81	0.253	5.15	3.30	2.40	4.23	1.041
MA09-089	20.73	214	370	44.2	150	41.8		4.12	14.3	858	26.9	351	78.4	0.773	556	55.9	108	11.9	44.7	8.17	2.54	7.38	1.047	5.42	0.992	2.54	0.345	2.20	0.311	7.15	4.92	3.83	7.16	2.37
MA09-093	34.93	276	696	58.9	303	74.5		1.81	24.1	549	23.4	175	40.1	0.235	429	28.4	56.7	7.08	29.4	6.23	2.05	6.03	0.885	4.74	0.868	2.18	0.289	1.79	0.253	4.08	2.37	1.89	2.94	0.782
MA09-094	32.01	283	471	55.9	230	51.0		2.04	7.3	692	24.9	211	50.0	0.423	497	34.0	68.7	8.27	33.7	6.98	2.27	6.61	0.965	5.09	0.923	2.32	0.304	1.89	0.265	4.62	2.87	2.42	3.59	0.810
MA09-101	28.65	262	658	59.7	292	62.8		3.39	35.1	651	25.9	284	56.0	0.421	411	38.6	78.8	9.32	37.3	7.49	2.39	7.00	1.016	5.34	0.961	2.44	0.327	2.03	0.287	5.97	3.47	2.60	4.51	1.30
MA09-103																																		
MA09-105	29.44	250	706	66.9	343	43.6		2.06	11.2	605	22.0	172	41.0	0.401	431	28.7	58.7	7.18	29.7	6.27	2.04	5.97	0.867	4.58	0.826	2.05	0.268	1.65	0.232	3.93	2.36	1.81	3.02	0.805
MA09-106		261	432	56	134		95	4	38	899	34	289	76		604																			
MA09-107		260	1996	52	453		71		21	254	19	149	24		285																			
MA09-108		278	514	56	183		84	4	9	633	30	191	44		479																			
MA09-114	21.58	224	391	45.0	140	46.5		3.08	62.1	955	26.0	266	68.9	0.580	791	48.3	95.0	10.9	41.9	8.06	2.57	7.37	1.040	5.34	0.957	2.42	0.317	1.99	0.280	5.39	3.80	3.85	4.91	1.29
MA09-116A	28.74	258	624	60.9	274	61.5		2.43	16.3	631	25.1	245	48.9	0.194	369	33.6	70.2	8.53	34.8	7.19	2.30	6.72	0.977	5.17	0.927	2.35	0.309	1.91	0.270	5.29	3.00	2.06	3.69	1.02
MA09-116B																																		
MA09-117	27.71	256	546	51.7	190	52.6		2.97	24.7	733	27.0	269	61.3	0.679	539	41.0	80.7	9.28	36.4	7.23	2.32	6.86	1.004	5.40	0.993	2.56	0.350	2.22	0.317	5.65	3.68	3.92	4.92	1.15
MA09-118B																																		
MA09-119	3.99	60.8	26.5	14.0	15.9	10.4		3.77	112	959	25.3	435	93.0	1.20	980	66.6	119	12.2	41.6	6.85	2.19	6.01	0.873	4.69	0.891	2.45	0.356	2.36	0.342	7.19	5.79	6.50	10.0	2.08
MA09-121A																																		
MA09-121B																																		
MA09-122		255	620	65	288		99		7	675	30	200	46		546																			
SMA09-006		336	117	53	77		103		27	817	35	238	89		588																			
SMA09-011		351	690	55	249		91		11	470	32	186	41		407																			
SMA09-012		309	163	54	210		111		14	924	32	269	80		606																			
SMA09-015		382	464	62	232		93		10	745	30	213	55		513																			
SMA09-037	27.93	259	609	55.9	239	52.0		2.27	12.9	756	24.5	186	50.7	0.522	589	38.0	73.9	8.73	34.8	6.98	2.26	6.61	0.945	4.99	0.899	2.28	0.301	1.85	0.266	4.14	2.86	2.83	3.59	0.780
SMA09-040		231	519	54	182		90		41	817	31	202	52		654																			
SMA09-049		273	15	37	31		106		44	832	38	332	92		631																			
SMA09-051		315	81	46	60		120		48	833	35	331	93		521																			
SMA09-058		348	199	48	87		115		34	712	34	288	76		377																			
SMA09-059		233	417	48.0	160	110	90	3.00	15.0	891	33.0	203	55.0		741																			
SMA09-097		252	607	52	218	53	91	2.00	5	788	29	203	51		624																			
SMA09-109		217	286	29	158		82		70	778	27	284	80		725																			

Supplemental Table 1: Continued

Sample	Locality	WR/GL	Lat [°N]	Long [°W]	SiO_2 [wt.%]	TiO_2 [wt.%]	Al_2O_3 [wt.%]	$Fe_2O_3^T$ [wt.%]	MnO [wt.%]	MgO [wt.%]	CaO [wt.%]	Na_2O [wt.%]	K_2O [wt.%]	P_2O_5 [wt.%]	LOI	Total	Sc	V	Cr
SM 1	Vila do Porto harbour	WR	36.945	25.152	44.20	2.66	15.49	11.68	0.17	6.73	12.25	2.03	1.47	0.46	2.03	99.17	22	318	90
SM 2	Vila do Porto harbour	WR	36.945	25.152	43.53	2.66	15.34	12.01	0.16	6.75	11.50	2.23	1.50	0.47	2.54	98.69	21	307	100
SM 7	Baía dos Cabestrantes	WR	36.999	25.172	44.60	3.97	14.84	13.90	0.19	4.88	10.29	2.65	2.04	0.66	1.16	99.18	20	389	
SM 8	Baía dos Cabestrantes	WR	36.999	25.172	45.40	3.14	16.82	12.10	0.17	4.47	9.87	3.29	1.78	0.62	2.56	100.22	14	311	
SM 9	N of the airoport (quarry)	WR	36.988	25.166	43.74	1.87	11.98	11.19	0.16	15.41	9.57	2.02	0.55	0.28	2.25	99.02	23	204	1090
SM 10	N of the airoport (quarry)	WR	36.988	25.166	44.26	1.80	11.44	11.19	0.16	15.94	9.70	2.24	0.57	0.28	2.02	99.59	24	204	1150
SM 12	Campo quarry	WR	36.947	25.136	42.66	2.17	13.54	12.46	0.20	10.29	11.01	3.43	0.84	0.57	3.67	100.84	24	238	470
SM 15	Campo quarry	WR	36.947	25.136	42.62	2.15	13.67	12.47	0.20	9.70	11.66	3.84	1.30	0.61	1.48	99.71	24	237	480
SM 16	Baía dos Anjos	WR	37.005	25.161	45.08	2.89	16.46	12.39	0.17	5.12	11.69	2.48	1.58	0.51	1.64	100.02	20	333	30
SM 19	Baía dos Anjos	WR	37.005	25.161	44.05	3.08	15.62	12.36	0.17	6.20	11.47	2.55	1.56	0.51	1.66	99.24	22	339	20
SM 20	Baía dos Anjos	WR	37.006	25.164	45.31	3.17	16.30	12.39	0.20	5.40	8.96	3.66	1.80	0.80	2.42	100.41	17	253	50
SM 22	ENE of Santana	WR	36.986	25.145	43.04	2.38	13.41	12.28	0.20	11.12	11.95	3.19	1.60	0.53	0.93	100.63	27	279	590
SM 23	N of the airoport	WR	36.990	25.173	45.20	2.87	15.55	12.00	0.17	6.15	12.18	2.70	1.70	0.49	1.60	100.61	23	329	80
SM 29	Saramago	WR	36.904	25.127	43.57	2.09	13.35	12.52	0.22	9.63	11.08	4.06	1.35	0.63	1.27	99.76	25	249	520
SM 30	Trevina	WR	36.992	25.118	43.12	2.37	13.34	12.22	0.19	11.37	11.80	3.02	0.68	0.52	2.05	100.67	27	283	580
SM 32	Ribeira do Engenho	WR	36.981	25.110	42.62	2.40	12.63	12.76	0.18	11.70	11.38	3.47	0.61	0.51	1.18	99.44	26	270	600
SM 33	S of Brejo	WR	36.959	25.105	42.38	2.31	13.18	12.26	0.19	10.51	11.49	3.52	0.76	0.57	1.93	99.10	26	254	580
SM 35	NW of Malbusca	WR	36.950	25.078	43.08	2.34	12.94	12.36	0.18	11.02	11.74	3.39	0.55	0.50	1.39	99.49	28	271	550
SM 38	SSE of Malbusca	WR	36.938	25.074	44.31	2.57	14.22	12.05	0.17	7.58	10.24	3.19	0.90	0.57	3.84	99.64	25	274	340
SM 40	Barreiro	WR	36.957	25.093	44.02	2.46	13.41	12.27	0.18	10.69	11.09	3.30	0.67	0.49	1.28	99.86	27	266	820
SM 41	Barreiro quarry	WR	36.957	25.094	43.61	2.16	12.92	12.32	0.18	12.16	11.84	2.59	1.07	0.44	1.02	100.31	32	280	850
SM 42	Barreiro quarry	WR	36.957	25.094	42.20	2.32	13.45	12.17	0.18	10.40	11.75	3.09	0.67	0.49	1.60	98.32	29	271	510
SM 44	Praia Formosa	WR	36.947	25.088	44.96	2.29	14.89	11.52	0.20	7.65	9.38	3.21	1.83	0.52	2.01	98.46	20	218	410
SM 46	Ponta do Castelo	WR	36.929	25.018	41.89	2.14	12.48	12.20	0.17	13.10	11.53	2.15	1.03	0.40	1.39	98.49	29	256	690
SM 47	Ponta do Castelo	WR	36.929	25.018	42.87	2.12	12.44	12.63	0.18	13.23	11.67	2.33	1.16	0.43	0.73	99.79	29	261	720
SM 49	Ponta do Castelo lighthouse	WR	36.930	25.017	43.56	2.41	13.91	11.72	0.19	8.69	9.87	3.73	1.26	0.56	3.13	99.03	20	222	410
SM 50	Maia	WR	36.942	25.014	42.69	2.34	12.50	12.82	0.18	11.94	11.58	3.15	1.12	0.56	0.50	99.38	26	251	860
SM 53	Setadas quarry	WR	36.958	25.067	44.01	2.19	14.84	12.32	0.19	8.90	11.48	3.02	0.50	0.43	1.84	99.72	28	295	380
SM 56	Ribeira do Salto	WR	36.981	25.053	43.39	2.27	13.41	11.79	0.18	11.13	11.13	3.41	0.51	0.44	1.51	99.17	27	262	670
SM 57	S. Lourenço	WR	36.995	25.054	42.24	2.21	12.82	11.72	0.16	13.04	11.50	1.78	0.81	0.35	2.28	98.92	31	270	740
SM 59	*Pico do Facho*	WR	36.952	25.124	42.15	2.14	13.27	12.40	0.20	11.22	11.16	2.99	0.65	0.53	2.71	99.41	24	240	580
SM 60	*Pico do Facho*	WR	36.952	25.124	43.06	2.17	13.53	12.85	0.20	10.88	11.17	3.40	0.83	0.56	2.30	100.95	25	261	560
SM 61	*Pico do Facho*	WR	36.952	25.124	42.36	2.15	13.10	12.46	0.20	11.11	11.22	3.41	0.67	0.54	2.07	99.29	24	244	550
SM 65	LORAN	WR	37.008	25.057	42.71	2.20	12.41	12.38	0.18	13.86	11.16	3.05	0.52	0.45	0.56	99.47	27	271	680
SM 67	Ponta do Malmerendo	WR	36.942	25.161	42.45	2.90	16.16	13.07	0.17	6.17	10.78	2.25	1.69	0.51	3.72	99.88	16	318	
SM 68	Ponta do Malmerendo	WR	36.942	25.106	43.51	2.94	17.00	12.52	0.20	5.04	9.39	3.94	1.93	0.77	2.25	99.49	12	255	30
SM 71	*NE Δ Monte das Flores*	WR	36.000	25.134	44.02	2.11	12.40	11.66	0.16	13.42	11.69	1.98	0.92	0.39	1.51	100.25	29	266	1100

Sample	Co	Ni	Cu	Zn	Mo	Rb	Sr	Y	Zr	Cs	Ba	La	Ce	Pr	Nd	Sm	Eu	Gd	Tb	Dy	Ho	Er	Tm	Yb	Lu	Ta	Th	U	$^{87}Sr/^{86}Sr$	$^{143}Nd/^{144}Nd$	$^{206}Pb/^{204}Pb$	$^{207}Pb/^{204}Pb$	$^{208}Pb/^{204}Pb$
SM 1	47	76	91	80	3	35	928	24	246	0.30	484	36.8	76.3	8.93	35.6	7.32	2.39	6.49	0.940	5.09	0.910	2.32	0.304	1.81	0.271	3.99	4.27	1.21	0.703732	0.512840	19.218	15.586	39.234
SM 2	48	80	83	77	3	38	714	24	246	0.40	493	37.3	77.1	9.04	36.3	7.47	2.37	6.49	0.940	5.04	0.900	2.34	0.307	1.83	0.276	4.17	4.13	1.21					
SM 7	47	43	71	89		48	796	34	368	0.30	551	50.6	106.0	12.7	51.4	10.5	3.29	9.25	1.34	7.23	1.31	3.31	0.428	2.62	0.396	6.22	5.67	1.45					
SM 8	39	26	40	88	5	43	941	27	327	0.50	666	53.3	107.0	12.2	46.7	8.90	2.87	7.56	1.11	5.93	1.07	2.74	0.364	2.20	0.338	6.14	6.29	1.77	0.703638	0.512839	19.150	15.574	39.146
SM 9	72	401	57	65		9	467	16	158	0.30	328	23.1	48.3	5.64	23.0	4.81	1.65	4.36	0.640	3.41	0.590	1.56	0.210	1.26	0.189	2.46	2.46	0.690	0.703752	0.512855	19.071	15.561	39.049
SM 10	74	401	55	59		7	501	15	150	0.30	310	21.6	45.1	5.32	21.6	4.54	1.57	4.24	0.610	3.23	0.570	1.50	0.200	1.16	0.166	2.38	2.32	0.670					
SM 12	53	142	48	68	3	18	729	28	235	0.60	639	47.4	91.5	10.4	40.1	8.05	2.57	7.17	1.06	5.80	1.04	2.74	0.373	2.29	0.357	4.30	4.52	1.28	0.703638	0.512889	19.786	15.607	39.374
SM 15	52	145	46	68	4	42	828	28	225	0.50	629	46.8	90.7	10.2	39.1	7.98	2.51	7.11	1.04	5.65	1.03	2.72	0.363	2.23	0.348	4.21	4.53	1.21					
SM 16	45	73	75	84	3	37	783	29	265	0.30	513	44.5	87.4	10.6	42.3	8.65	2.75	7.90	1.13	6.03	1.08	2.81	0.360	2.14	0.329	4.45	4.36	1.10	0.703681	0.512871	19.202	15.574	39.192
SM 19	50	63	81	90	3	37	751	25	262	0.30	495	43.9	91.2	10.7	41.6	8.28	2.66	7.29	1.04	5.52	0.980	2.48	0.321	1.86	0.280	4.81	4.85	1.41	0.703742	0.512835	18.345	15.570	38.311
SM 20	38	39	30	96	5	42	877	36	452	0.40	579	64.0	133.0	15.5	60.5	11.5	3.47	9.76	1.38	7.50	1.37	3.57	0.475	2.92	0.454	7.14	6.79	2.32					
SM 22	61	193	55	68	4	48	754	27	247	0.50	596	45.6	90.6	10.4	40.7	8.40	2.68	7.72	1.10	5.79	1.04	2.75	0.356	2.14	0.328	4.58	4.69	1.36	0.703554	0.512908	17.536	15.493	37.217
SM 23	45	82	65	79	4	42	782	29	256	0.30	531	40.6	82.3	9.61	38.1	7.98	2.52	7.03	1.01	5.38	0.960	2.51	0.329	1.89	0.287	4.37	4.35	1.20					
SM 29	52	161	49	75	5	28	986	34	282	1.20	826	64.0	120.0	13.2	49.9	9.66	2.97	8.33	1.23	6.80	1.27	3.41	0.457	2.84	0.456	5.52	6.42	1.68	0.703509	0.512901	19.526	15.581	39.102
SM 30	59	153	38	53	4	33	747	26	229	1.50	649	42.5	83.3	9.71	38.7	7.93	2.54	7.28	1.06	5.60	0.980	2.56	0.331	1.99	0.303	4.20	4.15	1.00					
SM 32	65	224	63	77	3	12	660	23	243	0.50	537	38.1	78.0	9.18	37.1	8.00	2.54	7.22	1.02	5.35	0.910	2.27	0.284	1.68	0.247	4.01	4.02	0.990	0.703611	0.512880	19.322	15.575	39.097
SM 33	63	188	71	76	3	12	790	26	235	0.50	596	45.9	90.4	10.4	41.0	8.31	2.65	7.38	1.05	5.61	0.980	2.54	0.331	1.94	0.281	4.34	4.56	1.11					
SM 35	62	193	44	68	4	10	652	25	237	0.70	507	38.0	76.8	9.10	36.7	7.73	2.51	7.17	1.07	5.50	0.950	2.46	0.323	1.89	0.276	4.03	3.87	1.01					
SM 38	45	103	47	67	3	19	784	27	257	0.60	640	45.3	87.3	10.3	40.1	7.96	2.53	7.16	1.06	5.77	1.05	2.77	0.376	2.34	0.371	4.61	4.15	1.07					
SM 40	60	236	56	64	3	14	623	25	237	0.80	446	36.2	74.0	8.73	35.1	7.51	2.40	7.04	1.01	5.38	0.970	2.52	0.325	1.98	0.304	4.07	3.91	1.04	0.703591	0.512877	19.284	15.565	39.064
SM 41	69	302	65	68	2	26	553	31	203	0.20	456	36.6	64.5	7.97	32.5	7.03	2.26	6.77	1.01	5.54	1.01	2.68	0.357	2.13	0.326	3.23	2.96	0.880	0.703613	0.512885	19.437	15.586	39.160
SM 42	60	213	66	70	3	10	624	25	228	0.50	448	35.6	72.9	8.57	34.8	7.52	2.42	7.07	1.03	5.61	0.990	2.55	0.343	2.05	0.305	3.78	3.65	0.950					
SM 44	47	127	41	79	8	49	773	29	423	0.60	541	60.1	116.0	12.8	47.3	8.95	2.77	7.64	1.11	6.03	1.10	2.94	0.397	2.41	0.362	6.71	7.43	2.36					
SM 46	68	262	63	66	3	27	514	24	182	0.30	396	30.5	62.0	7.36	30.3	6.72	2.13	6.38	0.93	5.06	0.910	2.34	0.308	1.85	0.274	3.30	3.14	0.920	0.703757	0.512874	19.077	15.576	39.023
SM 47	72	275	65	69	3	31	534	24	184	0.30	408	30.0	60.9	7.35	29.7	6.50	2.10	6.24	0.93	5.03	0.900	2.28	0.300	1.79	0.277	3.25	3.14	0.880					
SM 49	48	127	47	76	5	24	878	27	303	0.60	763	51.4	102.0	11.5	44.4	8.77	2.80	7.74	1.13	5.88	1.04	2.60	0.353	2.18	0.334	5.08	5.03	1.51					
SM 50	64	258	68	73	3	29	610	23	208	0.40	437	32.8	67.6	8.15	34.0	7.44	2.34	6.73	0.980	5.09	0.890	2.21	0.287	1.73	0.266	3.46	3.24	0.980	0.703636	0.512891	19.515	15.602	39.287
SM 53	55	111	35	56	3	74	654	25	229	0.80	499	33.7	70.0	8.30	33.3	6.99	2.25	6.49	0.970	5.33	0.960	2.52	0.334	2.09	0.325	3.72	3.27	0.980					
SM 56	59	193	47	58	2	25	596	24	213	0.50	430	31.6	66.2	7.95	32.3	6.98	2.20	6.44	0.960	5.25	0.950	2.52	0.336	2.05	0.310	3.43	3.04	0.820					
SM 57	63	254	64	63	2	19	532	22	195	0.20	313	26.1	55.3	6.76	28.5	6.34	2.05	6.17	0.890	4.80	0.870	2.25	0.303	1.85	0.271	3.04	2.75	0.850					
SM 59	57	169	52	63	3	36	768	26	219	0.50	587	43.0	84.8	9.68	38.2	7.77	2.48	7.05	1.03	5.60	1.01	2.66	0.358	2.14	0.318	4.03	4.10	1.05	0.703534	0.512900	19.727	15.608	39.348
SM 60	57	172	55	67	4	29	769	26	218	0.50	639	43.2	84.8	9.58	37.7	7.60	2.46	7.09	1.03	5.59	1.00	2.66	0.359	2.22	0.334	4.06	4.24	1.07					
SM 61	56	170	42	68	3	33	718	26	214	0.50	583	43.4	84.9	9.64	38.0	7.73	2.47	6.97	1.03	5.66	0.990	2.62	0.363	2.19	0.324	3.99	4.16	1.02					
SM 65	70	275	34	67	3	9	583	22	205	0.40	419	31.6	65.0	7.78	32.4	6.86	2.24	6.37	0.940	4.92	0.850	2.22	0.292	1.69	0.248	3.41	3.20	0.860	0.703627	0.512869	19.197	15.561	38.982
SM 67	49	35	34	84	3	32	780	28	251	0.20	552	37.5	79.1	9.53	38.6	8.33	2.64	7.67	1.12	6.00	1.05	2.73	0.372	2.25	0.338	4.29	3.69	0.960					
SM 68	37	45	33	90	5	49	1002	34	367	0.70	689	58.8	119.0	13.8	54.0	10.7	3.34	9.03	1.32	7.21	1.27	3.35	0.451	2.76	0.426	6.34	6.18	1.83	0.703691	0.512869	19.405	15.588	39.285
SM 71	61	321	70	61	2	24	531	24	187	0.30	392	29.7	57.7	7.37	30.5	6.56	2.17	6.23	0.930	4.94	0.890	2.36	0.309	1.79	0.258	3.03	2.91	0.810	0.703590	0.512894	19.212	15.580	39.057

Supplemental table 2 - Santa Maria: (Chapter 6)

Comparison of standard trace element measurements from Kiel and Activation laboratories compared to values from Govindaraju (1994) and to GEOREM certified values from the GEOREM database (http://georem.mpch-mainz.gwdg.de).

Supplemental Table 2: Comparison of standard trace element measurements from Kiel and Activation laboratories compared to values from Govindaraju (1994) and to GEOREM certified values from the GEOREM database (http://georem.mpch-mainz.gwdg.de).

Sample	USGS W-2A Measured Measured by Activation laboratories	USGS W-2A Certified Govindaraju (1994)	BHVO-2 Preferred values from GEOREM database	BHVO-2 Measured (n=2) Measured University of Kiel	BCR-2 Preferred values from GEOREM database	BCR-2 Measured (n=2) Measured University of Kiel	JA-2 Preferred values from GEOREM database	JA-2 Measured (n=2) Measured University of Kiel	AGV-2 Preferred values from GEOREM database	AGV-2 Measured (n=2) Measured University of Kiel
SiO_2 [wt.%]	52.48	52.4								
TiO_2 [wt.%]	1.073	1.06								
Al_2O_3 [wt.%]	15.57	15.4								
FeO* [wt.%]										
Fe_2O_3* [wt.%]	10.89	10.7								
MnO [wt.%]	0.166	0.163								
MgO [wt.%]	6.4	6.37								
CaO [wt.%]	11.07	10.9								
Na_2O [wt.%]	2.23	2.14								
K_2O [wt.%]	0.63	0.626								
P_2O_5 [wt.%]	0.15	0.13								
SO_3 [wt.%]										
Cl [wt.%]										
F [wt.%]										
LOI										
Total	100.659	99.889								
Sc	36	36	32.0	31.8	33.0	33.5	18.4	19.3	13.0	13.0
V	259	262	317	314	416	414	122	125	122	121
Cr	90	92	280	275	18.0	18.2	450	402	16.0	20.3
Co	42	43	45.0	45.3	37.0	38.3	27.0	29.9	16.0	16.1
Ni	60	70	119	121	18.0	12.6	134	145	20.0	19.1
Cu	110	110	127	127	21.0	19.2	27.9	28.7	53.0	51.7
Zn	80	80	103	104	127	129	65.0	60.2	86.0	87.4
Mo			4.00	3.90	250	261	0.590	0.570	2.26*	2.02
Rb	18	21	9.11	9.19	46.9	47.2	71.0	68.8	66.3	68.8
Sr	198	190	396	393	340	341	250	243	661	665
Y	20.3	24	26.0	25.4	37.0	35.0	18.1	16.3	19.0	19.3
Zr	97	94	172	171	184	189	112	109	230	236
Nb	8	7.9	18.1	17.8	12.6	12.1	9.00	8.75	14.5	13.7
Cs			0.110	0.102	1.10	1.16	4.90	4.64	1.20	1.18
Ba	181	182	131	131	677	673	315	305	1130	1120
La	11.3	10	15.2	15.3	24.9	25.2	16.1	15.3	37.9	38.4
Ce	23.4	23	37.5	37.5	52.9	53.4	34	32	68.6	70.2
Pr	-	-	5.35	5.29	6.70	6.79	3.70	3.58	7.84	8.18
Nd	12	13	24.5	24.5	28.7	28.8	14.2	13.9	30.5	30.9
Sm	3.09	3.3	6.07	6.05	6.58	6.59	3.10	2.99	5.49	5.54
Eu	1.01	1	2.07	2.04	1.96	1.94	0.910	0.865	1.53	1.51
Gd	-	-	6.24	6.09	6.75	6.70	3.00	2.98	4.52	4.82
Tb	0.64	0.63	0.920	0.948	1.07	1.08	0.480	0.479	0.640	0.671
Dy	3.76	3.6	5.31	5.28	6.41	6.39	2.90	2.87	3.47	3.51
Ho	0.79	0.76	0.980	0.965	1.28	1.29	0.61	0.58	0.650	0.664
Er	2.11	2.5	2.54	2.42	3.66	3.52	1.70	1.62	1.81	1.79
Tm	0.33	0.38	0.330	0.321	0.54	0.51	0.260	0.241	0.260	0.252
Yb	2.07	2.1	2.00	1.98	3.38	3.37	1.68	1.62	1.62	1.67
Lu	0.29	0.33	0.274	0.277	0.50	0.50	0.250	0.243	0.247	0.249
Hf	2.3	2.6	4.36	4.39	4.90	4.90	2.93	2.76	5.00	5.17
Ta	0.52	0.5	1.14	1.14	0.74	0.77	0.700	0.640	0.870	0.833
Pb			1.60	1.71	11.0	10.4	19.3	19.4	13.2	13.7
Th	2.24	2.4	1.22	1.18	5.70	5.80	5.00	4.63	6.10	6.06
U	0.57	0.53	0.403	0.409	1.69	1.66	2.20	2.15	1.86	1.88

*Mo value from Jochum K.P., Stoll B., Herwig K., Amini M., Flanz M., Kreuzburg B., Kuzmin D., Willbold M., Enzweiler J. Geostandards and Geoanalytical Research 32 (1) [2008] 5-26 An automated iridium-strip heater for LA-ICP-MS bulk analysis of geological samples